UNIVERSITÉ PARIS-EST

École des Ponts ParisTech

同濟大學 TONGJI UNIVERSITY

Thèse

soumise pour l'obtention du grade de
Docteur de l'Université Paris-Est
Ecole Doctorale Sciences, Ingénierie et Environnement (SIE)

par

Qiutong LI

Noise reduction mechanism analyses and effect predictions of nearly-enclosed barriers in urban rail transit

---

Spécialité : *Structures et Matériaux*

Soutenue le 19 juin 2020 devant un jury composé de :

Prof. Tianxing WU	Shanghai Jiao Tong University	Rapporteur
Prof. Weikang JIANG	Shanghai Jiao Tong University	Rapporteur
Prof. Dongxing MAO	Tongji University	Examinateur
Prof. Songliang LIAN	Tongji University	Examinateur (Président du Jury)
A/Prof. Li LI	Tongji University	Examinateur
Prof. Denis DUHAMEL	Ecole des Ponts ParisTech	Directeur de thèse
Prof. Honore YIN	Ecole des Ponts ParisTech	Co-directeur de thèse
Prof. Yanyun LUO	Tongji University	Co-directeur de thèse

Abstract

Due to the rapid urbanization in China, urban rail transit (URT) systems have entered a phase of quick expansion. However, it also brings serious noise and vibration pollution along lines. As one of the most important noise reduction measures, sound barrier can effectively reduce noise pollution of URT systems. The acoustic performance of a noise barrier in urban rail transit is not only dependent on the geometry of the noise barrier and sound absorption properties of absorptive panels, but also directly dependent on the characteristics of urban rail transit noise. Wheel-rail noise is the main component of urban rail transit noise, which is broadband noise and often regarded as incoherent line sources. Nowadays, most of the studies on noise barriers in urban rail transit neglected the influence of the incoherent characteristics of noise sources, and rarely considered the multiple reflections between vehicle bodies and noise barriers, the reflections by the top of viaducts and the sound insulation performances of sound panels. As a result, the researches on noise barriers in urban rail transit were not targeted.

Nearly-enclosed noise barrier is generally considered to be the best type for reducing urban rail transit noise. In recent years, on account of its high insertion loss, the limited practical applications of nearly-enclosed noise barrier performed an excellent role for reducing urban rail transit noise. However, because of municipal fire protection requirements, an opening on the top of nearly-enclosed barriers is required. Urban rail transit noise could overflow from the top opening after multiple reflections in the interior of the noise barriers, resulting in the acoustic performances of the noise barriers usually lower than the predicted results. In this context, new requirements are put forward for the design and the research of nearly-enclosed noise barriers in urban rail transit. Therefore, acoustic designs of nearly-enclosed noise barriers in urban rail transit need to be further deepened.

Based on the imperfections of the researches on near-enclosed noise barriers in urban rail transit mentioned above, the following studies were conducted by using scale model tests, numerical simulations and in-situ field measurements:

1. The acoustic performance of a noise barrier by different kinds of sources were studied by conducting scale model tests combined with numerical simulations. It could be found that the insertion loss of a noise barrier by incoherent line sources was overestimated by using two-dimensional boundary element method (2-D BEM). Since

urban rail transit noise is always simplified as incoherent line sources, using 2.5-dimensional boundary element method (2.5-D BEM) to do numerical simulation is more in line with the incoherent characteristics of urban rail transit noise.

2. A 1:20 scale model of a reflective nearly-enclosed noise barrier in urban rail transit was established. In this model, the viaduct structure and vehicle body were built, and therefore the multiple reflections between the vehicle body and the noise barrier were considered. The scale models considering and not considering sound transmission of panels were established, respectively. By using scale model tests, the sound insulation performances of panels were studied. It can be found that the use of the PC sheets could not insulate sound perfectly, leading to a significant reduction of the reflective nearly-enclosed noise barrier performance.

3. A 2.5-D BEM model of the nearly-enclosed noise barrier in urban rail transit was established and verified by scale model tested results. By using 2.5-dimensional boundary element method, the model considered the actual geometric boundary conditions and the characteristics of urban rail transit noise. In the model, the ground was considered as a completely reflective surface, the viaduct structure was built to consider the reflection by the top of the viaduct. The vehicle body structure was also built, and hence the multiple reflections between the vehicle body and the noise barrier was considered. According to the characteristics of wheel-rail noise, the sound source was considered as incoherent line sources at the positions of wheel-rail interactions.

4. Due to the sound absorption characteristics of nearly-enclosed noise barriers in urban rail transit in reality, a 2.5-dimensional BEM model of nearly-enclosed noise barriers in urban rail transit including sound absorptive boundaries was established by conversing acoustic impedance at each calculated frequency. Taking a typical absorptive nearly-enclosed noise barrier in urban rail transit as an instance, the noise reduction mechanism of the nearly-enclosed noise barrier was analyzed by using numerical simulations of this model combined with in-situ field measured results.

5. In view of the deficiencies in the noise reduction effect of nearly-enclosed noise barriers in urban rail transit, the 2.5-dimensional boundary element method was applied to optimize the noise reduction effect of the absorptive nearly-enclosed noise barrier. According to the noise source characteristics and spectrum of urban rail transit, several optimal plans to effectively improve the noise reduction effect of the absorptive nearly-enclosed noise barrier in urban rail transit were picked out.

Abstract (French)

En raison de l'urbanisation rapide de la Chine, le système de transport ferroviaire Urbain (URT) est entré dans une phase d'expansion rapide. Mais il peut également engendrer une forte pollution sonore et vibratoire le long des voies ferrées. En tant que l'une des mesures de réduction du bruit les plus importantes, la barrière antibruit peut réduire efficacement la pollution sonore dans les systèmes de transport ferroviaire Urbain. La performance acoustique d'une barrière antibruit dans le transport ferroviaire urbain dépend non seulement de la géométrie de la barrière antibruit et des propriétés d'absorption sonore des panneaux absorbants, mais aussi directement des caractéristiques du bruit du transport ferroviaire urbain. Le bruit de contact roue/rail est la principale composante du bruit du transport ferroviaire urbain, qui est un bruit à large bande et souvent considéré comme des sources de lignes incohérentes. Aujourd'hui, la plupart des études sur les barrières antibruit dans le transport ferroviaire urbain ont négligé l'influence des caractéristiques incohérentes des sources de bruit, et ont rarement pris en compte les multiples réflexions entre les caisses de véhicules et les barrières antibruit, les réflexions par le haut des viaducs et les performances d'isolation acoustique des panneaux acoustiques. Par conséquent, la recherche sur les barrières antibruit du transport ferroviaire urbain n'est pas ciblée.

On considère généralement qu'une barrière antibruit presque fermée est le meilleur type pour réduire le bruit du transport ferroviaire urbain. Au cours des dernières années, en raison de la perte d'insertion élevée, les applications pratiques limitées de la barrière antibruit presque fermée ont joué un excellent rôle dans la réduction du bruit du transport ferroviaire urbain. Cependant, en raison des exigences municipales de protection contre les incendies, une ouverture est requise au-dessus de la barrière antibruit presque fermée. Après plusieurs réflexions à l'intérieur de la barrière antibruit, le bruit du transport ferroviaire urbain débordera de l'ouverture supérieure, ce qui entraînera des performances acoustiques de la barrière acoustique généralement inférieures à celles prévues. Dans ce contexte, de nouvelles exigences ont été avancées pour la conception et la recherche de la barrière acoustique presque fermées dans le transport ferroviaire urbain. Par conséquent, la conception acoustique du transport ferroviaire urbain de la barrière antibruit presque fermée doit être approfondie.

Compte tenu des imperfections des recherches sur les barrières antibruit presque fermées dans le transport ferroviaire urbain mentionnées ci-dessus, les études suivantes ont été

menées à l'aide de tests de modèles à l'échelle réduite, de simulations numériques et de mesures sur le terrain :

1. Les performances acoustiques des barrières antibruit pour différents types de sources ont été étudiées en effectuant des essais sur modèles réduits combinés à des simulations numériques. Il a pu être constaté que la perte d'insertion d'une barrière antibruit par des sources linéaires incohérentes a été surestimée en utilisant la méthode de l'élément de frontière bidimensionnel (2-D BEM). Étant donné que le bruit des transports ferroviaires urbains est toujours simplifié en tant que sources linéaires incohérentes, l'utilisation de la méthode de l'élément de frontière de 2,5 dimensions (2.5-D BEM) pour effectuer une simulation numérique est plus conforme aux caractéristiques incohérentes du bruit des transports ferroviaires urbains.

2. Un modèle à l'échelle 1:20 d'une barrière antibruit réfléchissante presque fermée dans le transport ferroviaire urbain a été établi. Dans ce modèle, la structure du viaduc et la caisse du véhicule ont été construites et, par conséquent, les réflexions multiples entre la caisse du véhicule et la barrière antibruit ont été prises en compte. Les modèles à l'échelle réduite avec et sans prise en compte de la transmission sonore des panneaux sont établis respectivement. En utilisant des tests sur maquette, les performances d'isolation sonore des panneaux ont été étudiées. Il peut être constaté que l'utilisation de films PC ne peut pas parfaitement isoler le son, ce qui réduit considérablement les performances de la barrière antibruit presque fermée.

3. Un modèle BEM 2.5-D de la barrière antibruit presque fermée dans le transport ferroviaire urbain a été établi et vérifié par des résultats testés par modèle à l'échelle réduite. La méthode des éléments de frontière à 2,5 dimensions est utilisée pour considérer les conditions aux limites géométriques réelles et les caractéristiques du bruit des transports ferroviaires urbains. Dans le modèle, le sol est considéré comme une surface entièrement réfléchissante et la structure du viaduc est conçue pour prendre en compte la réflexion au sommet du viaduc. La structure de caisse du véhicule a également été construite, et par conséquent les réflexions multiples entre la caisse du véhicule et la barrière antibruit ont été considérées. Selon les caractéristiques du bruit de roulement, la source sonore était considérée comme des sources linaires incohérentes aux positions des interactions entre les roues et les rails.

4. En raison des caractéristiques d'absorption sonore des barrières antibruit presque fermées dans le transport ferroviaire urbain en réalité, un modèle BEM à 2,5 dimensions des barrières antibruit presque fermées, y compris les limites d'absorption acoustique, a été établi en convertissant l'impédance acoustique à chaque fréquence calculée. Prenant comme exemple une barrière antibruit presque fermée dans le transport ferroviaire urbain, le mécanisme de réduction du bruit de la barrière antibruit presque

fermée a été analysé à l'aide de simulations numériques de ce modèle combinées à des résultats mesurés sur le terrain.

5. Compte tenu des déficiences dans l'effet de réduction du bruit des barrières antibruit presque fermées dans le transport ferroviaire urbain, la méthode de l'élément de frontière de 2,5 dimensions a été appliquée pour optimiser l'effet de réduction du bruit de la barrière antibruit presque fermée. Selon les caractéristiques et le spectre de fréquences de la source de bruit du transport ferroviaire urbain, plusieurs schémas d'optimisation sont proposés pour améliorer efficacement l'effet de réduction du bruit de la barrière antibruit presque fermée.

Contents

1 Introduction

1.1 Noise pollution and abatement for urban rail transit systems

Due to the rapid urbanization in China, Urban rail transit (URT) systems have entered a phase of rapid expansion. According to the China Association of Metros, by the end of 2018, there had been 185 URT lines constructed and put into operation in 35 cities in China, with a total operation length of about 5,761km. Among all operational lines, underground lines account for 75.6% with a length of 4354km, whereas elevated lines account for 22.4% with a length of 1288km. In terms of construction cost, duration and operation maintenance, the latter have advantages over the former. However, due to their exposure to the environment, the vibration and noise pollution generated by elevated lines has become an urgent and serious environmental problem in urban areas. And the environmental quality of urban spaces is gradually degraded with the increased number of lines. If this problem cannot be sufficiently solved, the development and use of the land space along the lines will be severely affected[1, 2].

The approaches to tackle this noise pollution can be classified by the positions: source controls, propagation process controls and receiver protections. They can also be classified by active and passive controls: the first one belongs to active control methods, whereas the last two belongs to passive control methods. To absorb the vibration energy generated by the wheel-rail interaction and divert the energy from the viaduct, different kinds of low vibration wheels and track structures are commonly used in the construction[3–6]. Besides, tuned mass dampers(TMDs) employed in the construction of the viaduct is another common way to reduce structural-borne vibration, but the noise reduction effect was found to be slight[7–11]. To protect the receiver positions where people work or live, the performance of windows to insulate the noise outside is usually enhanced by the use of double-layer glass and rubber seal materials. Receiver protections are often considered as supplementary approaches in projects concerning the technology of noise reduction for urban rail transit. Another effective way to control urban rail traffic noise in the propagation process is noise barriers[12–15]. Noise barriers installed in-between source and receiver positions are of interest to our studies.

1.2 Noise barriers

In general, noise barriers are built on the side of viaducts to reduce urban railway traffic noise pollution. In the presence of a noise barrier, sound pressure at a given receiver position is propagated from three pathways: the diffraction over the top edge of the barrier, the transmission through the barrier and the multiple reflections between the vehicle structure and the barrier. The sound transmitted through the barrier in level is commonly 10 dB lower than that propagated in the other two ways. And the barrier performance is therefore primarily limited by the multiple reflections and the diffraction sound over the top. Absorptive treatments are often required to contribute to reductions in multiple reflections. With the help of absorptive treatments, the diffraction sound is thought of as the main component of the sound pressure at the receiver position. The diffraction sound is thought to depend largely on its height as well as the relative distance between the source, the barrier, and receiver positions.[16]. The simplest way to improve the acoustic performance of an urban railway barrier is to increase the height. However, aesthetic problems and safety reasons usually prevent the rail transportation authorities from erecting very high barriers. To improve the performance, devices installed on the top of the barrier are sometimes introduced instead of increasing the height. Another difficulty lies in the unalterable relative distance from the source to barriers on elevated lines since the predominant source for urban railway traffic is located at the place of wheel-rail interaction, and the barrier position, varying with changes of width of the viaduct, remains basically unchanged. Based on the geometry diffraction theory, there is another relationship between the strength of the diffracted field and frequency. Noise barriers are more effective at high frequencies than at low frequencies, which presents problems since urban rail transit noise mainly occurs at low- and mid-frequencies. Besides, there is also a close relationship between the acoustic performance of barriers and environmental factors, such as ground effect, atmospheric turbulence, air absorption, refraction by wind and temperature gradient profiles[17, 18]. To achieve a noise reduction effect of barriers on site during the operation of a real urban rail transit system, all factors must be taken into account.

1.2.1 Barrier shape

The acoustic performance of a noise barrier was predominately enhanced by the increased height to meet the requirement of low noise around residential buildings in the early stage. Then the limitation of the height for aesthetic reasons gave birth to different cost-effective designs and materials for barrier construction. New barrier profiles were successively proposed. Some of them shown in Figure 1.1.

K. Fujiwara et al.[19] used the boundary element numerical modelling method to study the insertion loss of rectangular, T-shape and cylindrical edged noise barriers with rigid,

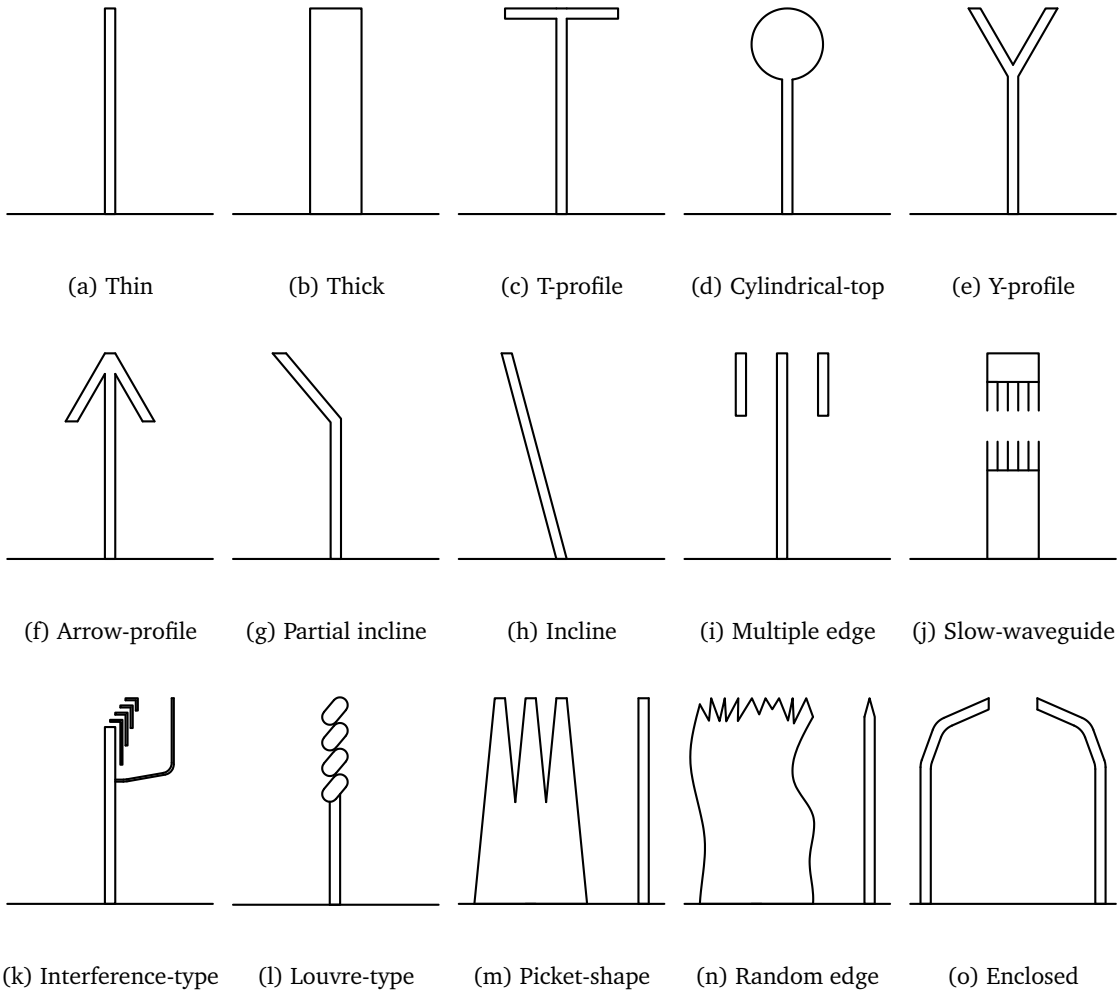

Fig 1.1.: Different shapes of barriers in the literature

absorbing and soft surfaces. From the results, the T-shape with a soft upper surface was the most efficient design, which produced a marked increase in mean insertion loss over that of a straight barrier of 8.3 dB. They also made a parametric investigation and found the width of cap affected insertion loss the most. D.C. Hothersall et al.[20] found the T-shape noise barrier performed more efficiently than the Y- and arrow-profiles in most conditions. By scale model testing, D.N. May and M.M. Osman[21] investigated a number of relatively novel noise barriers including thin, wide, T-shape, cylindrically topped, corrugated, inclined, Y-shape, arrow-shape and picket-shape, and some of them were treated with absorptive materials. They found that the improvement in insertion loss over that of a conventional barrier was positive for all the kinds of tested barriers, except for the picket types of which the excess attenuations were -6 to -1 dB(A). The greater increase with the T-profile reflective barrier was explained theoretically as the limited opportunity for sound pressure doubling to occur at the end of the T. They also found that T-shape absorptive top barriers with cap width of 0.6 m or more and of small cap thickness were the most effective in reducing highway noise. Z. Venckus et al.[22] measured the sound attenuations of inclined-type barriers with

slope angles of $90°$, $120°$, $150°$ and $180°$(the usual straight type) on the basis of methodical recommendations stated in the standard ISO 11821:1997. They found in the range of low frequencies(100-315 Hz) the barrier with a slope angle of $120°$ was the most effective, whereas high frequency sound waves(2000-5000 Hz) were most effectively reduced by using the usual straight noise barrier. G. R. Watts[23] tested the acoustical performance of T-shape, multiple edge and double barriers in full scale. He found that the average improvement of insertion loss for tested 2-meter-high barriers over a simple reflective straight barrier of identical overall height ranged from 1.4 to 3.6 dB(A), depending on detailed design. He also concluded that multiple edge and T-shape barriers showed consistent improvements in insertion loss, whereas double barriers provided large gains where significant diffraction occurred at the upper edge of both screens. Among all the tested barriers, the multiple edge barriers could be the most cost-effective method of improving barrier performance. Then a multiple edge noise barrier profile was constructed at three sites adjacent to the M25 motorway and measurements were taken by his team[24]. The results showed that the acoustical performance could be significantly improved by the multiple edge profile, and under favourable conditions the improvement was predicted to be over 3 dB(A).

A random edge profile was proposed by Steve S. T. Ho et al.[25], which lay in the destructive interference to the field diffracted by the top edge. The phase variation of the diffracted sound along a random edge was random and less coherent, enhancing the performance of a conventional barrier. Steve S. T. Ho et al.[25] made laboratory model experiments to study the random edge barriers. The tested results showed that the random edge barriers performed significantly better than the straight barriers, especially at high frequencies above 5 kHz where the insertion loss was 3-7 dB. And the unexplained poorer performance of the jagged-edge barrier at low frequencies was also obtained. A method termed Directive Line Source Model was proposed by P. Menounou et al.[26] to predict the field due to diffraction by straight- and jagged-edge barriers. The predictions were in reasonably good agreement with the tested results from [25]. W. Shao et al.[27] proposed a numerical method based on the diffraction integration of Rubinowicz, and used it to compare the performance of straight and the random edge barriers. They found the efficiency could be better by increasing the jaggedness of the top edge. J. Nicolas and G.A. Daigle[28] proposed a slow-waveguide barrier which incorporated a slow-waveguide filter consisting of an open network of rigid strips. The acoustic performance of the slow-waveguide barrier was dependent on the interference between the diffraction field owing to the barrier edge and the propagation field through the waveguide. Experimental results showed that in the frequency range where destructive interference occurred the insertion loss was enhanced, whereas at adjacent frequencies the constructive interference degraded the barrier performance. Another kind of sound-interference-type barrier was proposed by G.R. Watts[29], which was a device added to an existing noise barrier used for screening train and tram noise. By BEM modelling and full-scale tests, the performance of the device was obtained with an estimated gain of 1.9 dB(A) of which 0.7 dB(A) was considered to be due to an interference effect. The remainder was due to the diffraction field owing to the two edges of the device.

Transparent barriers provide optical transparency without compromising the acoustics[12]. However, due to the high cost of the installation and regular cleaning, louvred barriers were designed as alternatives and applied to roadsides. T. Matsumoto et al.[30] investigated the efficiency of noise barriers with horizontal louvres by full scale model experiments. An improvement of 2.5 dB was obtained at a distance less than 15 m from the barrier. G. R. Watts et al.[31] measured and predicted the acoustic performance of vertically louvred noise barriers using a 1/20th scale modelling and a modified Boundary Element Method, respectively. They investigated the angle effect of louvres and found a louvred barrier with the angels at 9° provided the driver with good visibility over the angle range within 30°, while the largest noise shielding efficiency was predicted for louvres at the angle of 30°. C.Wassilieff[32] developed a barrier diffraction theory incorporating the effect of partial sound transmission through a barrier of finite size and used this theory to investigate the noise reduction of picket barriers. The results showed that the performance of the picket barrier can be improved at high frequencies by the supplement of a sound absorbent into the gaps and retained good performance for low-frequency sound.

S.J. Martin and D.C. Hothersall[33] proposed the idea to incorporate median barriers as noise control measures on the central reservation of dual carriageway roads. They used a numerical model simulating the traffic as six incoherent line sources of sound to investigate the performance of the median barriers alone and in conjunction with roadside barriers. The improvement in insertion loss was found to be about 1 dB for the configuration above rigid ground, and 2 dB for grassland. M.R. Monazzam et al.[34] discussed the impacts of different median barrier shapes on a roadside straight reflective barrier by a 2-D BEM method. The calculated median barrier models included the T-shape, the arrow-shape, the Y-shape, the partially inclined, the inclined, the inverse L-shape, the trapezoid-shape, the isosceles-shape and the right triangle-shape. The results showed that the best performance improvement related to the reference barrier was seen in the inclined model, by 1.41 dB(A).

The last profile shown in Figure 1.1 is the enclosed type. Fully-enclosed barriers have been constructed but are used little due to the high cost of construction and provision of sufficient ventilation[12], though they have the best noise shielding efficiency. Besides, a reverberant build-up of noise occurs on the inner surface of fully-enclosed barriers, degrading the acoustic performance. Absorptive treatments can be beneficial for avoiding this. Most enclosed barrier profiles at sites are partially enclosed solutions, such as partially inclined barriers, cantilevered barriers, galleried barriers, etc (see in [12], Figure 11), which perform well without issues of reverberant build-up. X. Wei and Y. Wang[35] studied the performance of enclosed and semi-enclosed barriers by business software called RAYNOISE based on the geometrical diffraction theory, and they found that the semi-enclosed barrier with a 5-meter-wide opening had a good performance, similar to that for the fully-enclosed profile. C. Zhang [36] analyzed the influence of the opening ratio of fully-enclosed barriers to the micro-pressure wave, and the results showed that the strong air pressure in front of vehicles was decompressed appropriately by the existence of an opening.

For urban rail transit systems, there are many barrier types on existing lines in China: conventional straight barriers, T-shape barriers, Y-shape barriers, cylindrical topped barriers, half-enclosed barriers, fully-enclosed barriers, etc. Among them, fully-enclosed barriers are the most effective at reducing URT noise. Li. et al.[37] studied the noise reduction of semi- or fully-enclosed barriers of high speed railways using full-scale modelling. The results showed that the attenuation of a fully-enclosed metal noise barrier with composite sound absorption plates was up to 25 dB(A) at 7.5 m distance from the track central line. However, the space inside an enclosed barrier is quite small when a train passes by. For fire safety, an opening on the top is designed for the fully-enclosed barrier, commonly with a width of 2 meters, so that smoke can be emitted through the opening when fire occurs. Hence, in this thesis we call it the "nearly-enclosed" barrier, one of the prototypes depicted in Figure 1.2. As reviewed above, a number of studies have made clear the importance of "T", "Y" and other top devices in improving the diffraction reduction of barriers, but there is little research as a specific guidance that can be applied to the problems of the nearly-enclosed barrier effect on URT noise. Thus, the barrier shape in this research is the nearly-enclosed profile. A nearly-enclosed barrier constructed on a viaduct can contain almost all sound energy inside the barrier, and therefore is able to acoustically isolate residential buildings and industries from URT noise.

(a) Inside the barrier (b) Outside the barrier

Fig 1.2.: A prototype of a nearly-enclosed barrier located in Ningbo, China

1.2.2 Absorptive treatments

Due to the large vehicle structures in the URT system, secondary reflections pose a problem and thus this issue must be taken into account in this research[38]. The surface of a barrier close to the source, treated with absorptive materials, can be effective against the behaviour of the multiple reflections and enhance barrier performance. By using BEM modelling, K. Fujiwara et al.[19] found that with absorbing surfaces(specific normal impedance $z = 1$) on the top of a T-shape profile, a cylindrical topped profile and a rectangular profile, there were significant improvements of approximate 4 dB over the mean insertion losses of rigid ones. T. Matsumoto et al.[30] investigated the efficiency of highway noise barriers with horizontal louvres by full scale model experiments and concluded that highly absorptive

materials applied to the blade surface was favourable to the reduction of the sound leakage through the apertures of the barrier. D.C. Hothersall et al.[39] used a 1:20 scale modelling to compare the performances of plane screens with rigid and sound-absorbing surfaces(full-scale flow resistivity $\sigma = 110kPa \cdot s/m^2$) for a railway system. They found the insertion loss for rigid barriers was 6-10 dB lower than those for similar barriers with complete sound-absorbing surfaces.

Absorptive treatments act not only to minimize the reflection sound between the source and the barrier surface but also to reduce the diffracted sound into the shadow zone[40]. For highways, absorptive treatments may only be needed to prevent the multiple reflections of two parallel barriers or large vehicles driven close to the barrier. For URT systems, it is necessary to treat the inner surface with absorptive materials in order to avoid the build-up of noise inside nearly-enclosed barriers. There are many absorptive materials on the market, with fibre porous materials being employed more in traffic projects. Generally, the absorbing capacity of a material is determined by the sound absorption coefficient α which is defined as a ratio of absorbed energy to incident energy, noting the amount of sound being absorbed by a material[41, 42],

$$\begin{aligned} \alpha &= 1 - |C_r|^2 \\ C_r &= \frac{z - \rho_0 c_0}{z + \rho_0 c_0} \end{aligned} \tag{1.1}$$

where C_r is the sound pressure reflection coefficient, z is the specific normal surface impedance, ρ_0 is air density and c_0 is sound speed in air. Average values of some acoustic absorptive materials that have been used in traffic systems[43] are presented in Table 1.1.

Tab 1.1.: Absorption coefficients of some acoustic absorptive materials

Material	Octave band frequency in Hz						
	125	250	500	1k	2k	4k	8k
$80kg/m^3$ rock wool, thickness $t = 50mm$	0.22	0.60	0.92	0.90	0.88	0.88	0.88
$40kg/m^3$ rock wool, $t = 50mm$	0.23	0.59	0.86	0.86	0.86	0.86	0.86
$40kg/m^3$ mineral wool, $t = 50mm$ glued to wall, untreated surface	0.15	0.70	0.60	0.60	0.85	0.90	0.90
$70kg/m^3$ mineral wool, $t = 50mm$ $300mm$ in front of wall	0.70	0.45	0.65	0.60	0.75	0.65	0.65
$3.4kg/m^2$ mineral fibre, $t = 20mm$, $50mm$ cavity	0.20	0.56	0.82	0.87	0.70	0.53	-
Fibre absorber, mats of porous flexible fibrous web fabric, self-extinguishing	0.07	0.07	0.2	0.41	0.75	0.97	-
Foam ceramsite concrete	0.06	0.34	0.74	0.97	0.93	0.74	-
Cement sawdust acoustical panel, $t = 50mm$	0.14	0.52	0.47	0.44	0.68	0.69	-

The absorption coefficient α gets closer to 1 with the increased absorbed energy and $\alpha = 1$ therefore means that the incident sound is totally absorbed with no reflections.

Besides, the absorption coefficient α is dependent on the incident sound frequency. It can be seen from Table 1.1 that the porous sound-absorbing materials are effective at high frequencies, while for low-frequency sound the absorption coefficients are quite low. Moreover, porous absorptive materials have high costs and require long-term and time-consuming maintenance. Because of these reasons, researchers seek better alternatives.

In the 1990s, K. Fujiwara et al.[19] modelled a "soft" surface on the top of T-, cylindrical, and rectangular barriers and an improvement of 7.5 dB over the mean insertion loss of similar rigid barriers was obtained. The "soft" surface is defined as the specific impedance being approximate to zero, where sound pressure releases completely. When propagating to the "soft" surface, the incident sound wave has a destructive interference with the wave reflected, with anti-phase characteristics. Consequently, the "soft" surface produces a secondary source that counteracts the incident energy, rather than dissipating the energy as heat. Based on this concept, T. Okubo and K. Fujiwara[44, 45] designed a noise barrier with an acoustically soft cylindrical edge. The soft obstacle was referred to as a "Waterwheel cylinder" where open ended tubes were arranged radially. By theoretical and experimental analysis in a 2-D sound field, they found the noise shielding efficiency was strongly dependent on the depth of the tube and sound frequency. Hence, the results they obtained showed a strong frequency dependence of the noise shielding efficiency, with an improvement of more than 10 dB in a certain frequency range, but a visible decrease in another range.

A similar design to the soft cylindrical edge is the profiled single noise barriers covered with quadratic residue diffusers (QRD). The profiled diffusers invented by Schroeder[46] were first designed to diffuse rather than absorb sound, and were widely used in places where high sound quality was required[47, 48]. The unexpectedly high absorption of a poorly constructed QRD was measured at low frequency by Fujiwara and Miyajima[49, 50] afterwards. Subsequently, Kuttruff[51], Mechel[52] tried to explain the absorption efficiency and discussed the way to transform the QRD into a better absorber. T. WU et al.[53] used two methods to predict the absorption efficiency of the profiled structure and verified the predictions by experimental results. They also optimized the profiled diffuser for absorbing low frequency noise. M.R. Monazzam and Y.W. Lam[54] investigated the acoustic performance of variously shaped noise barriers with QRD tops by using 2-D BEM modelling. They concluded that T-shape barriers covered with a QRD tuned to 400 Hz were the most efficient model for traffic noise, especially for low frequency noise.

Although materials and structures for sound absorption can be found in a lot of the literature, a product which can be used in practical engineering is still sought.

1.2.3 A prototype of nearly-enclosed barriers

The nearly-enclosed prototype consists of several separate elements, each 2 meters long. Figure 1.3 shows a schematic cross-section of one element. Each element is composed of several parts: two open-cell aluminium panels located on the inner surface of two flanges and one on the two sides of the safe passage, and two separated arched parts fixed on two sides of the viaduct with a top opening of two meters in width. Each of the two arched parts is an assembly of two sound absorption panels, a PMMA sheet, a PC sheet and a welded steel framework. The absorption panels, jagged and filled with $48kg/m^3$ glass wool, have a thickness of $60mm$. The transparent PMMA sheet with a thickness of $15mm$ is set between two absorption panels for reducing drivers' fatigue. According to the mass law shown in [16], the transmission loss across the PMMA sheet remains above 20 dB (bulk density of PMMA $1.18kg/m^3$, air density $1.21kg/m^3$ and sound speed $343m/s$). It is therefore reasonable to believe that the PMMA sheets have a high quality of sound insulation. In addition, a PC sheet with a thickness of $6.5mm$ is connected to the top absorbing panel, aiming to offer more flexibility to the shape rather than a highly efficient sound insulation capability. The shape of the barrier is designed as an arch to keep sound from propagating out of the barrier.

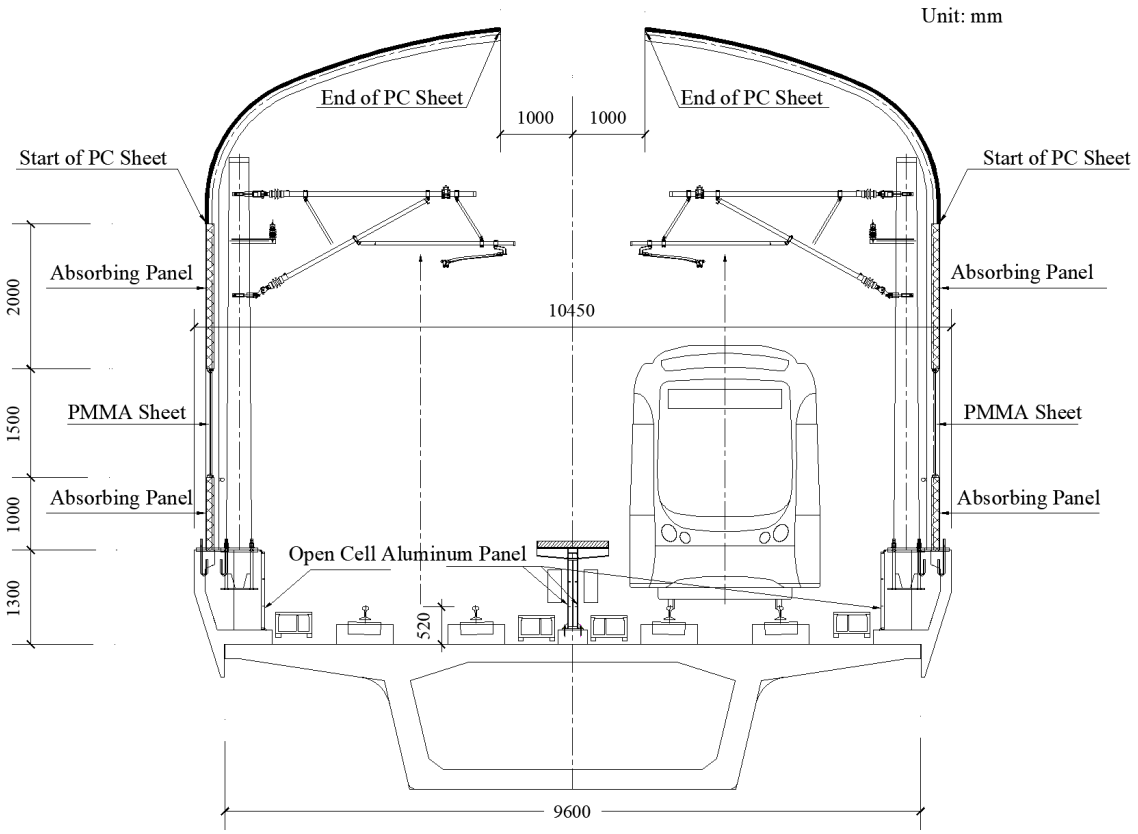

Fig 1.3.: Cross section of the nearly-enclosed barrier on a viaduct in Ningbo, China

As the predominant source of urban railway system noise is the railway rolling noise, it is better to select highly efficient absorptive sound panels close to the location of wheel/rail interactions. For this reason, the open-cell aluminium panels are adopted for absorbing rolling noise since its noise reduction coefficient (NRC) is more than 0.75. Each of the panels located on the two flanges is made up of a 4-mm-thick open-cell aluminium foam panel, a 50-mm-thick cavity and a 1.5-mm-thick backboard. The panel on the centre consists of two aluminium foam panels and cavities on both sides, and a partition board in the middle, which is designed to absorb the rolling noise emitted from trains passing by in both directions.

1.3 Research issues and objectives of this chapter

1.3.1 Research issues

Multiple reflections between two axisymmetric parts and between the extremely high barrier and the vehicle surface significantly degrade the barrier performance. S. Slutsky and H.L. Bertoni[55] developed a program, called BarrierX, to investigate the performance of parallel reflective barriers on the roadside. The results showed that this kind of barrier could severely degrade the anticipated single barrier insertion loss and that absorptive treatments could be beneficial. Watts[56] found that a reflecting wall with a 2m height fixed on the source side could result in a reduction of 4 dB(A) in the insertion loss of a sound barrier of the same height. More pertinent to our study, the acoustical domain bounded by a nearly-enclosed barrier can be considered as a room with a door or an open duct, and then the sound field within such a domain can be dominated by acoustic resonances. Under the influence of this effect, high pressure amplitudes may be observed at the resonant frequencies leading to a significant degradation of barrier performance. In the parametric investigation of the performance of multiple edge highway noise barriers, D.J. Oldham and C.A. Egan[14] observed the acoustic resonance in the air in the gap between an edge and the barrier face resulted in a negative relative insertion loss for the configurations involving reflective edges located on the source side of the barrier. In parallel with this development, Yang et al.[57] firstly proposed the resonance effect of the trapped modes to explain the deterioration in performance of a conventional barrier due to the reflecting surface.

To solve the multiple reflections and the peak sound pressures governed by the resonance, S. Slutsky and H.L. Bertoni[55] found a relatively small angles of tilt(less than 15 degrees) could restore almost all of the single barrier insertion loss. A tilted barrier was then proposed[34, 58] as a solution, with a slope of ten degrees gaining the best profit, and a wave-trapping barrier was proposed[57] effective in reducing the deterioration at peak frequencies. Furthermore, absorptive materials were employed on the surface of reflective barriers near the source and were able to reduce the deterioration with high efficiency[59].

From the prototype of the nearly-enclosed barrier shown in Figure 1.3, it can be seen that there are absorptive panels with two kinds of absorptive materials: open-cell aluminium and mineral wool. One research issue is to understand if these absorptive materials sufficiently reduce the multiple reflections and acoustic resonance.

Another important issue is the efficiency of the sound insulation property of transparent materials that is required to achieve suitable acoustical performance. From Figure 1.3, it can be seen that there are two arched parts on the top made of 6.5-mm-thick PC panels. The transparent panels are utilized to allow in natural light and reduce limitation of drivers' views[31]. However, it cannot be confirmed that the transparent panels are used without compromise to acoustic performance. Generally, the sound insulation property of a material is usually evaluated by an acoustic physical term[60] i.e., transmission loss known as TL which is defined as 20 times the logarithm of the ratio of the acoustic pressure associated with the incident wave and that of the transmitted wave. In this thesis, the transmission losses of PC and PMMA sheets will be taken into account.

1.3.2 Objectives of this chapter

To know the performance of nearly-enclosed barriers in terms of reducing URT noise, the characteristics of urban rail transit noise sources should be studied first. Then the existing assessment systems for urban rail transit noise are discussed in terms of whether they are effective for URT noise. Since environmental factors must be taken into consideration before evaluating the acoustic performance of a noise barrier, ground effects, atmosphere absorption, refraction by temperature and wind gradient and turbulence effect are respectively reviewed. Hence the scope of each environmental factor contributing to the performance of a noise barrier will be identified. Given these scopes, the research methods of this thesis are then discussed and determined.

1.4 Urban rail transit noise

There are many noise sources in an urban rail transit system, such as rolling noise, aerodynamic noise, pantograph noise, curve squeal, brake screech, structural-borne noise from bridges and ground-borne noise[61]. The predominant source varies with increased train speed. When a train speed is less than 50km/h, the source radiated from the power system is of the most importance; With the train speed increasing, the predominant source turns out to be the rolling noise which radiates from the rail and the wheel vibration caused by the roughness at the location of the contact patch. Finally, the aerodynamic noise becomes the focus when the speed is over 200km/h. However, D.J. Thompson[62] thought for residents living adjacent to high speed lines, wheel-rail noise could be a significant source.

But anyhow, the rolling noise is still the most important when the speed of a train is about 50-80km/h. Rolling noise is addressed in the following section.

1.4.1 Source characteristics

Source position

H.J.A. Van leeuwen[63] compared railway noise prediction models by country in Europe. He found the position of the source was at the centre of the track in all models except for two models from the United Kingdom in which the sources were located on the near side rail and on the centre of the two tracks. However, the source positions were assumed at different heights above the railhead: 0m representing the source at the rail-wheel contact, 0.5 m and 0.8 m representing the source at a height of the axle and 2m representing the source at almost half of the vehicle height. In this thesis, the position of wheel/rail noise is determined at the railhead of each rail.

Source type and directivity

Y. Wang and J. Sun[64] thought the urban rail transit source was always assumed as a line source with a finite length but at the near field it could be addressed as a line source with a infinite length. S. Peters[65] found that the approximation of wheel/rail noise modelled by a line of incoherent dipole sources had good agreement with measured results. D. Hohenwarter[66] conducted measurements at receiver positions close to different trains with different speeds. He found that most of the measured trains radiated sound with dipole characteristics. He used a combination of monopole and dipole source characteristics and found the radiation of the train source was characterised by the ratio 15% monopole and 85% dipole component. P.A. Morgan et al.[67] found that modifying monopole sources to exhibit dipole characteristics became more important as the height of a noise barrier increased. X. Zhang[68] found that the model of perpendicular dipole pair could properly explain the measured specified directivity characteristics of wheel/rail vibration noise. In this thesis, incoherent line sources with monopole source characteristics are selected to model urban rail transit noise.

Frequency contents

X. Zhang[68] found that the frequency characteristics of the rolling noise increased with the train speed, like the predominant source. When a train ran at a low speed, the rolling noise was at low and mid- frequency, whereas mid- and high frequency sound waves could be

generated by a running train with a relative high speed. D.J. Thompson[62] thought that the rolling noise had quite a board frequency spectrum, with the highest levels occurring from 800-2500 Hz. Y. Liu et al.[69] found that the highest levels for the wheel noise was about 1000-2000Hz(high frequencies), while for the rail noise they occurred at 500-1000 Hz(low and mid- frequencies). The rolling noise had a significant frequency content at 500-1000 Hz, which was contributed to more by the rail vibrations. G. Zhai et al.[70] found that the rolling noise is mainly at mid- and high frequencies, with the highest levels at 500-1000 Hz. Y. Zhu et al.[71] considered the rolling noise was in the frequency range of 250-1000 Hz. Y. Xu[72] and H. Liu et al.[73] measured the noise source of Line Batong and Line Fangshan in Beijing, respectively. And they found the highest A-weighted levels occurred in the one-third octave band of 630 Hz and 500 Hz, respectively. Q. Wang et al.[74] thought the source frequency characteristics varied significantly under different operations, as shown in Table 1.2. T. Bai et al.[75] thought the light rail transit system radiated noise mainly from 200 Hz to 2000 Hz. P. Liu and Y. Yang[76] measured the ground lines of Line One in Shanghai and found the principal component in A-weighted level was at 200-1600 Hz. In this thesis, the frequency contents of wheel/rail noise will be analyzed by in-situ measurements.

Tab 1.2.: One-third octave bands where the highest levels occur for urban transit system noise under different operations

	Speed up out of stations	At a constant speed between stations	Slow down entering stations
Ground lines	200 Hz	125 Hz	200 Hz
Elevated lines	63 Hz	63 Hz	63 Hz

1.4.2 Noise indicators

To assess the impact of the urban rail transit noise on the environment, France, Germany, Poland and Switzerland consider day-time and night-time A-weighted equivalent level limits($L_{\mathrm{Aeq},6-22h}$, $L_{\mathrm{Aeq},22-6h}$)[77] as noise indicators, and so does China (GB 3096-2008). Portugal uses the END standards L_{den}[1] and L_{night}[2], while the Netherlands only applies the indicator L_{den}. Sweden applies $L_{\mathrm{Aeq},24h}$ as the indicator, with an addition of L_{max}. The legal limit values of the above-mentioned countries are quite different owing to the different definitions of zones, the different purpose of the limit and the complexity of the legislation behind these limits[77]. Nevertheless, in most cases the limit values of noise exposure in urban areas are 55 dB(A) for night time (22:00-06:00) and 70 dB(A) for day time (06:00-22:00) in Europe, as well as in China. For lower values than 55 dB(A), road traffic noise tends to be the dominant source disturbing sleep instead[61]. Moreover, the additional benefit over the presented limits is quite small with a considerable cost of noise abatement.

[1] Day-evening-night noise level is the A-weighted, L_{eq} (equivalent noise level) over a whole day, but with a penalty of +10 dB(A) for night-time noise (22:00-07:00) and +5 dB(A) for evening noise (19:00-23:00).
[2] Night noise level is the A-weighted, L_{eq} over the 8 hour night period of 23:00-07:00 hours.

When considering the noise indicators that assess the impact of urban rail transit noise, it can seen that the A-weighted long-term averaged level L_{Aeq} is widely used in many countries, although with a lack of consideration of the urban rail traffic operations and a severe underestimation of low frequency noise. For instance, $L_{\text{Aeq},22-6h}$ is the averaged level for night-time noise(22:00-6:00). However, urban trains are well-served by broadly fixed timetables and do not run all through the night. Moreover, the passing in and out of an urban train can cause a startle effect by an abrupt increase in the time history of the noise level, and the startle effect can be considerably disturbing. Given the insensitivity of $L_{\text{Aeq},22-6h}$ to the abrupt increase, it is not appropriate to apply the L_{Aeq} as a noise indicator for the urban rail transit system. For this reason, a few authorities in the UK apply other limits like L_{Amax}[3] and L_{Ax}[78].

On the other hand, the use of A-weighting is not acceptable for the assessment of urban railway noise. As discussed above, the rolling noise is the predominant source of urban railway noise, often with a broad peak from 800 to 2500 Hz[62]. Besides, there are many other sources like curve squeal, brake screech and bridges with primary frequency ranges occurring in special situations only, shown in Table 1.3. For a train running on viaducts, structural vibrations of the bridge can produce rumbles which mainly concentrate at low frequencies, while trains operating on the ground or underground can cause ground-borne noise, mainly at low frequencies as well. Since low frequency noise is absorbed less by the air and ground than high frequencies, structural and ground-borne noise can easily disturb residents at very far distances. Therefore, urban railway noise, involving low frequency noise radiating from the structures of viaducts, barriers and related connections, is not acceptably assessed by A-weighted indicators.

Tab 1.3.: Dominant frequency range of noise sources (other than rolling stock noise) in urban rail transit systems

Special Situation	Curve Squeal	Brake Screech	Bridge
Frequency Range	Pure tone, high frequency (up to 10 kHz)	Pure tone, high frequency (during braking)	Low frequency

In recent years, many researchers[79–86] have concluded that A-weighting underestimates the annoyance produced by low-frequency noise, even at low volume levels. Despite the masking effects[87, 88] of higher level components in complex sound environments, the weaknesses of A-weighting have been identified as well. Sonoko Kuwano et al.[79] made experiments on ten sound sources with specific frequency components to compare A-weighting with the indicators of loudness (LLs by Stevens' method, LLz by Zwicker's method). They concluded that A-weighting was not suitable for noise sources with prominent low-frequency or high-frequency components. N. Broner and H.G. Leventhall[80] reviewed many complaints of low frequency noise and found the fact in all the cases that dB(A) criteria unbalanced the low frequency region(< 100 Hz) and the corresponding annoyance

[3] A-weighted maximum sound level.

was much greater than the expectations. K. Persson and M. Björkman[87] conducted a lab experiment to assess the relative annoyance of low frequency noise and reference noises at the same dB(A) levels and found that the dB(A) unit made an underestimation for a broadband continuous low frequency noise of 3 dB for levels around 65 dB(Lin) and of 6 dB for levels around 70 dB(Lin). They[82] also demonstrated by sound exposure experiments that A-weighting underestimated annoyance for frequencies below about 200 Hz. U. Landstrom et al.[83] conducted experiments of sound exposure to 100 and 1000 Hz tones or broadband noise in a sound chamber. Their results showed that A-weighting overestimated low frequency tones but underestimated low frequency band noise with respect to tolerance levels during work. M. Pawlaczyk-Łuszczyńska et al.[84] studied 145 male workers exposed to low frequency noise(LFN) and broadband noise(BBN) at the comparable A-weighted levels, and their feelings were collected by a questionnaire survey. They found LFN was rated significantly more annoying than BBN, representing a higher annoyance to human well-being. H.G. Leventhall[85] summarized the strong dependence of annoyance on low frequency noise and the inadequacy of A-weighted levels for low frequency noise which leads to incorrect decisions by regulatory authorities. He called on regulatory authorities to pay attention to low frequency noise and develop specific assessments. As a consequence, A-weighting is no longer acceptable for the assessment of URT noise and other available indicators need to be taken into account.

The available alternatives can be generally divided into two groups: the indicators used infrequently and the indicators specifically modified to low frequency noise. In the first group, B-, C-, D- weightings are commonly considered to be substituted for the A-weighting, the weighted values being shown in Figure 1.4. It can be seen that compared with B- and C- weighting, the weighted values of A-weighting are extremely low at low frequencies. N. Broner and H.G. Leventhall[80] used a psycho-physical magnitude estimation technique to determine an acceptable indicator of low frequency noise annoyance. Ten noise measures were considered and it was concluded that B-weighting was the most suitable indicator in predicting the annoyance. The Swedish national board of health and welfare and royal board of building[89, 90] firstly recommended a comprehensive assessment, including both dB(A) and dB(C), of noise annoyance. The difference between dB(A) and dB(C) contains a large proportion of low frequency energy, which is a more suitable predictor for low frequency noise. A. Kjellberg et al.[91] used multiple and logistic regression analyses to study the dependence of noise annoyance on L_{Aeq} and the dB(C)-dB(A) difference. They found that the dB(C)-dB(A) difference made a significant contribution to the full awareness of noise annoyance. However, they also found that the dB(C)-dB(A) difference could exceed 15dB in spite of the noise without low-frequency characteristics. As a result, the dB(C)-dB(A) difference still has some limitations in assessing low-frequency noise. Besides, B.M. Shield and J.P. Roberts[78] studied the noise annoyance of the Docklands Light Railway (DLR) and suggested the maximum permitted L_{Ax} or L_{Amax} together with L_{Cmax} was preferred as suitable indicators of community annoyance response.

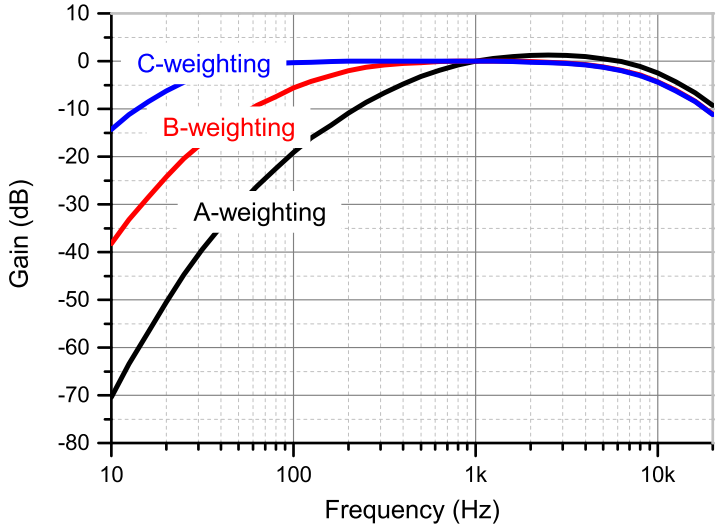

Fig 1.4.: A-, B- and C-weightings in the frequency range from 10 Hz to 20 kHz

In the second group, N. Broner and H.G. Leventhall[80] discussed the acceptabilities of four modified PNdBs[4] proposed by different researchers[92–94] by a psycho-physical magnitude estimation technique. They found the PNdB proposed by [94] gave the highest correlation with noise annoyance. However, the calculations of the modified PNdB were rather laborious compared with the weighting network measures[94]. Later, they [81] proposed another indicator, the Low Frequency Noise Rating (LFNR) curves, for the evaluation of low-frequency noise annoyance complaints, based on the Noise Rating (NR) curves formerly proposed by ISO for the general assessment of acceptable noise levels in buildings. They also validated the LFNR curves by laboratory experiments combined with filed annoyance data.

Overall, the alternatives either underestimate the low-frequency noise or are complicatedly calculated, which is not suitable for assessing urban rail transit noise. To accurately assess the low frequency component and to fully understand the frequency characteristics, so far, the most popular solution is one-third octave spectrum analysis, which is highlighted in this research. The one-third octave spectrum has been recommended by Polish, Swedish and German researchers when concerning the exposure to low frequency noise in general environments[95–97]. With no weighted values for low frequency noise, it is intuitive to observe the frequency components. In this thesis, A-weighting and one-third octave spectrum analysis are chosen to assess urban rail transit noise.

[4]Perceived noise decibel

1.5 Environmental factors

Generally, sound propagation in the environment is not as perfect as analysis which is governed by several wave phenomena like geometrical spreading, ground effect (reflection, absorption & diffraction), diffraction effect of obstacles, atmospheric turbulence, air absorption and refraction by wind & temperature gradient profiles[98]. Due to the complexity of sound propagation outdoors and the interactions with several wave phenomena, many specialists and scholars cannot capture all of the relevant physics and usually focus on a few of the important factors which play vital roles in actual circumstances to obtain a finite resolution. Therefore, a large number of different analytical and numerical models specific to particular realistic situations based on the former source of uncertainty have been proposed successively over the last few years. Rufin Makarewicz[99] proposed a simple model of outdoor noise propagation concerning the important factors above and came to the conclusion that the influence of wind speed profiles becomes important close to the shadow zone apart from those affecting factors. As the purpose of this research is the noise reduction effect of barriers on an urban railway bridge, in this section we throw more light on the mechanisms of other important factors in the modelling process. The details about the acoustic characteristics of the barrier will be presented in the next sections.

1.5.1 Ground effect

For a homogeneous atmosphere, the acoustical problem radiated from a point source above the ground was first proposed by Sommerfeld[100], and then solved with various assumptions and approximations by many researchers due to the difficulties in solving the Sommerfeld integrals. Theoretically, they are classified into two groups: the first group[101–108] is based on the ray tracing theory, represented by an incorporation of a direct sound field between the source and the receiver, a reflected field on the ground and a surface wave sound field. The second group has been proposed and developed by P.Filippi and D. Habault[109, 110], represented by using the layer potentials. Assuming a homogenous isotropic level ground surface with its characteristic impedance Z_g, based on an image source distribution, sound pressure at the receiver propagated from a point source above the ground is given as,

$$p = A_d \frac{e^{ikr_d}}{r_d} + Q\, A_r \frac{e^{ikr_r}}{r_r} \tag{1.2}$$

where (A_d, r_d) and (A_r, r_r) are the amplitudes and the distances between the source and the receiver for the direct field and the reflected field, respectively. Q is the reflection coefficient which is given by the plan wave reflection coefficient C_r and an asymptotic expansion $S_r(\omega)$,

$$Q = C_r + S_r(\omega)(1 - C_r) \tag{1.3}$$

where C_r is always represented by the normal surface impedance and the incident grazing angle,

$$C_r = \frac{Z_g \cos(\theta) - \rho_0 c_0}{Z_g \cos(\theta) + \rho_0 c_0} \tag{1.4}$$

where ρ_0 is the air density and c_o denotes the sound speed in air.

However, the acoustic problem above the homogenous ground is idealistic and unrealistic as in most of situations the ground is mixed with two or more kinds of surfaces. The discontinuity of the ground resulted in a prompt development of technology in solving the sound propagation over multi-impedance ground. The approaches respectively proposed by K.B. Rasmussen[111] and Durnin and Bertoni[112] were both based on Green's theorem, using Rayleigh approximations and Kirchhoff approximations to obtain the analytical solutions. On the other hand, given the excessive computing time, De Jong[113] proposed a semi-empirical model and several approximate extensions[114–116] were then put forward to improve the accuracy in certain geometries involving near-grazing angles and at low frequencies.

Considering the ground effect on sound propagation, the characteristic impedance of a ground surface is of great importance, regardless of its continuity or discontinuity. Basically there are three kinds of stable models: phenomenological models chiefly developed by J.F. Hamet and M. Bérengler[117] and by D.K. Wilson[118], microstructural models primarily developed by C. Zwikker and C.W. Kosten[119], by K. Attenborough[120], by A. Biot[121] and by J. F. Allard[122], and an empirical Delany-Bazley model[123]. Attenborough[124] claimed at the International Congress on Acoustics in 2004 that "the Delany-Bazley model has proved remarkably successful for predicting outdoor ground effects". And there is no doubt that till now this model is the most commonly used in engineering. The success of this model is not only in coming to accurate solutions, but also in considering only one parameter - airflow resistivity σ - to measure. The expressions of the characteristic impedance and the wave number obtained by Delany and Bazley[123] are,

$$\begin{aligned} Z_c &= \rho_0 c_0 \left[1 + 9.08 \left(\frac{f}{\sigma}\right)^{-0.75} - \mathrm{i}11.9 \left(\frac{f}{\sigma}\right)^{-0.73}\right] \\ k &= \frac{\omega}{c_0} \left[1 + 10.8 \left(\frac{f}{\sigma}\right)^{-0.70} - \mathrm{i}10.3 \left(\frac{f}{\sigma}\right)^{-0.59}\right] \end{aligned} \tag{1.5}$$

where ω is the angular frequency. Examples of flow resistivity values for ground material can be found in literature [125, 126]. In 2005, G. Taraldsen[127] found the Delany-Bazley model could be deduced from Darcy's law, highlighting its theoretical basis.

The case in this thesis is the sound propagation from the wheel-rail source to the receiver over a concrete viaduct which can be assumed as acoustically rigid($Z_g \to \infty$). The height of the

viaduct is approximately 10 meters. The ground will be assumed acoustically rigid($Z_g \to \infty$) unless the receiver is positioned close to the ground. Hence, the reflection coefficient Q equals 1 and sound pressure at the receiver is therefore contributed to equally by the direction field and the reflection field.

1.5.2 Atmosphere absorption

When sound waves travel in the air, sound energy can be absorbed by viscosity effects, thermal diffusion, and other behaviours by relaxation and dissipation processes of the air. The absorption of air is basically given by a function of sound frequency, temperature, humidity, and air pressure on the day of tests. ISO 9612-1 1996[128] states the calculations of the attenuations due to atmospheric absorption A_{atm}. Figure 1.5 shows the results for different temperatures and relative humidities. It can be seen that the attenuations are all less than 0.05 dB for the source-receiver distance within 100 meters, in the frequency range of 63-8000 Hz. Hence, in this area the atmosphere absorption can be ignored. According to this, the area close to the urban rail transit studied in this thesis is limited to within 50 meters.

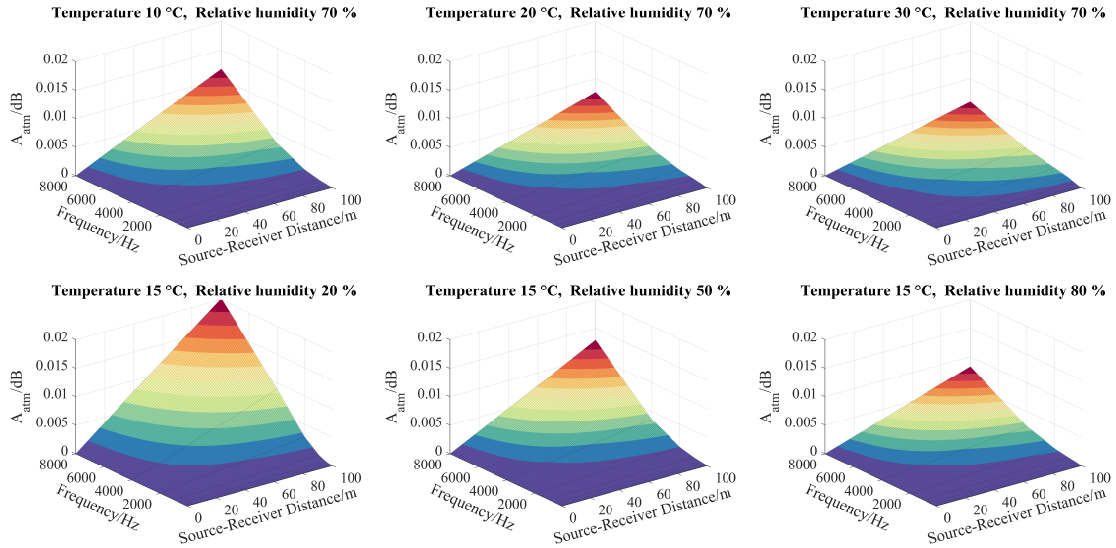

Fig 1.5.: The attenuation of atmosphere absorption varies with frequency and distance

1.5.3 Refractions by wind and sound-speed gradients

The behaviour of sound propagation in an inhomogeneous media is quite different. Delaroche[129] and Arago[130] firstly found through experiments that sound could be measured louder downwind than upwind from a source. Then, with important contributions of Stokes[131], Reynolds[132], Rayleigh[133] and Barton[134] to atmospheric acoustics, a correct qualitative explanation was found. Stokes found sound waves propagated upwind

bend upward, and Reynolds found that sound rays bend upward when the temperature decreases with height. Afterwards, Rayleigh formulated the refraction law due to wind velocity to describe sound propagation in moving media. Barton, Kornhauser[135] and many other researchers pointed out Rayleigh's mistake and presented their corrections, contributing to the development of measuring acoustics in an inhomogeneous atmosphere.

Consider a wind with a velocity vector in the atmosphere. The vertical component of velocity is commonly much less than the horizontal component, thus the value is assumed to be zero[136]. Hence, an effective approximation c_{eff} was introduced by Rayleigh[133] to consider the wind effect on sound speed, which is given as,

$$c_{\text{eff}} = c + \mathbf{s} \cdot \mathbf{v} = c + v \cos\psi \tag{1.6}$$

where $\mathbf{s}$ is the unit vector tangential to the ray path, ψ is the angle between the direction of sound wave and the horizontal component of wind vector $\mathbf{v}$. The effective sound speed has been applied successfully into the solution procedures of many analytical and numerical models in the presence of upwind/downwind and crosswind. Afterwards, K.M. Li et al.[137] found that the use of the effective speed profile was sufficiently accurate in simulating sound propagation upwind, while for the downward case the errors in the phase of propagating modes increased significantly with frequency, which was a severe limitation in the use of the effective speed profile at high frequencies in practical applications. Later, along with the development of mathematics, the wind effect was considered explicitly in many acoustic models instead of using the parameter of the effective sound speed. Models were developed to describe the sound propagation in inhomogeneous media, using normal-mode solution[137–139], residue series solution[140], fast-field program[141, 142], parabolic equation[143, 144], finite-difference time-domain solution[145–147] and Gaussian beams[148]. E. Premat and Y. Gabillet[149] proposed a Meteo-BEM method for predicting outdoor sound propagation above unlevel ground and applied to the case of a sound barrier at long range. The Meteo-BEM method was derived using results from BEM and normal-mode solution. The predictions were finally validated by experimental results.

Based on ray tracing theory, since the wind velocity and temperature vary with height in the near-ground atmosphere, the ray of a sound wave can be bent as an arc of a circle. In a realistic situation, the natural wind velocity in Ningbo is commonly less than 10 m/s (except for those during typhoons). Even though the wind caused by high-speed railway trains is violent and increases with the train speed, R. Li et al.[150] found that the maximum wind velocity at a position 3.5m away from one side of a 200-km/h train is also less than 10m/s. Since the speed of sound in air is $313.3 m/s$ (T=0°C), the wind velocity is not comparable and therefore, sound propagation will only be considered in a calm atmosphere in this thesis. Besides the refraction due to wind velocity stratification, sound propagation in the open air

is dependent on the temperature gradient. To simplify this, in many cases, the sound speed in in-homogeneous air was approximated by a linear function of height,

$$c(z) = c_0(1 + az) \tag{1.7}$$

where c_0 denotes the sound speed at the height $z = 0$, and a is called the normalized sound speed gradient[151]. When sound speed increases with height($a > 0$), sound waves bend downward and generate a second reflected wave before arriving at the far receiver, while an acoustic shadow zone far from a source can be produced by the negative gradient of sound speed($a < 0$).

In this thesis, the source, supported by a viaduct, is located about 10 meters above the ground($z_s = 10m$). To understand the effect of the in-homogeneous linear system to sound propagation in our case, an analytical model proposed by T. Hidaka et al.[151] is utilized. In the model, the in-homogeneous atmosphere was assumed still, with a linear sound velocity profile. The homogenous impedance ground was considered by the Delany-Bazley empirical model. The height of the receiver is 1.2 m to simulate human ears. According to the diurnal variation of sound velocity gradient measured by Geiger[152], the sound speed gradients in our case are chosen as 0.00005, 0.0001, 0.00015. Since the receiver positions are limited to within 50 meters from the source, the excess attenuations (defined in [151]) at the source-receiver distance R of 10 m, 25 m and 50 m are calculated, as shown in Figure 1.6. It can be seen that the excess attenuation for each case is less than 2 dB in the frequency range of 50-5000 Hz. Because of these little effects, the atmosphere where sound propagates is assumed temporarily homogeneous in this thesis.

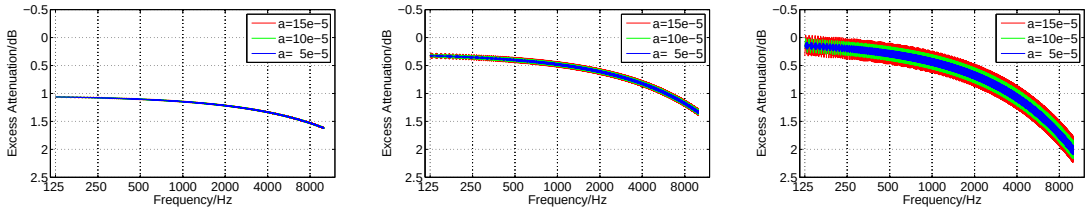

(a)$R = 10m$ (b)$R = 25m$ (c)$R = 50m$

Fig 1.6.: Effect of the change in sound speed gradient for three source-receiver distances(asphalt: $\sigma = 2 \times 10^7 Pa \cdot s \cdot m^{-2}$)

1.5.4 Turbulence

Another phenomenon of irregular air motions characterized by winds is the atmospheric turbulence which leads to scattering of sound energy, fluctuation of refracted waves and interferences between direct waves and reflected waves. It is evidently a challenge to represent atmospheric turbulence in an analytical model due to its random characteristics. Computational fluid dynamic modelling(CFD)[136] is an excellent tool to reveal the kine-

matic behaviour of turbulence. Since the area we are interested is by short distances from the barrier, where the turbulence has little influence on the sound propagation of urban rail transit noise, this thesis will not consider it in the modelling.

1.6 Research methods

1.6.1 Acoustic performance assessments

Many countries have established guidance standards for in-situ experiments[153–155]. ISO 10847-1997[153] proposes that barrier performance in a field test can be represented by the difference in sound pressure levels at specified receiver positions before and after the installation of a barrier, provided that the relevant parameters remain unchanged. This is referred to as "insertion loss" or "attenuation". ISO 10847-1997 also proposes that naturally occurring railway traffic, principally the passenger train, should be used as the sound source equivalence for the "before" and "after" measurements.

However, there are no global standards for receiver positions, a state of affairs which produces vagueness. ISO 10847-1997 proposes that there are only two conditions: semi free-field conditions, and reflecting surfaces. These conditions constitute a very general characterization of the open space behind barriers. In China's standard HJ/T 90-2004[154], receivers are defined as being located in the area which is the most sensitive to the noise. TB/T 3050-2002[156] defines the area sensitive to noise as residential buildings, schools, hospitals and other areas which require strong protection from noise. However, under different meteorological conditions, the shapes of areas are vulnerable to noise change. The standard is thus useful for getting a project accepted, but can be useless as a guide for designers who want to find the best barrier for a particular site. In China, in consequence, these standards have to be supplemented with other standards[156–159] for different receiver positions. The receiver position stated in TB/T 3050-2002, which is concerned with railway lines and used for the investigation of railway boundary noise in GB/T 12525-1990[157], directs a receiver position 30 meters from the nearest track centre and 1.2 m above the mean rail head height of the nearest track in the relevant area. GB/T 5111-2011[158], which is concerned with railway vehicle noise, directs that receivers be located 7.5 m away from lines and at heights of 1.5 m and 3.5 m. HJ 453-2008[159], which is concerned with testing the noise intensity of railway traffic, directs that the receiver be placed 7.5 m away from the source and at a height of 1.5 m. Thus, these given positions can be identified as alternative receivers in the case of comparing barrier performance with different shapes.

Seeking to clarify receiver positions in field experiments, the European Committee for Standardization (ECS) recently made recommendations for the measurement of sound

attenuation of given noise barriers at given sites in given meteorological conditions. The ECS's standard, CEN/TS 16272-7: 2015[155], recommends nine locations to place the receivers, forming a grid, in order to measure the attenuation of a given noise barrier at a given site including given meteorological conditions. They are placed specifically at a distance of 7.5 m, 12.5 m and 25 m away from lines and at a height of 3.5 m, 6.0 m and 9.0 m. This standard is a useful source of comparison of the noise attenuation capacities of different types of barrier at the same site under the same meteorological conditions. However, although there are many researchers at work on the in-situ measurement of insertion loss in railway noise barriers[16, 153–160], very few base themselves on this European standard. In consequence, there are no universally accepted receiver positions for the evaluation of barrier performance. This circumstance may be leading to uncertainty with respect to the noise reduction capacities of barriers presently available.

As the most common descriptor for assessing barrier performance, the equivalent continuous A-weighted sound pressure level[153–155] was introduced to calculate the attenuation of a barrier. The ISO standard[153] minimally requires field measurements of equivalent A-weighted sound levels, with and without a barrier, for all receiver positions, producing a single-number attenuation rating. Chinese[154] and European[155] standards also adopt the latter as an evaluation indicator. However, it is impossible to assess the performance of barriers at different sound frequencies using this single-number rating. In addition, A-weighting tends to devalue the effects of low frequency noise, making its suitability for the evaluation of noise barrier performance dubious. Since barriers are mostly erected on the elevated sections of lines, while relevant sound emissions are mainly concentrated at low frequencies[161], A-weighting is not a useful guide.

In this thesis, the receiver positions and the assessment indicators will be discussed by a field test of a simple barrier before introducing the in-situ measurements for a nearly-enclosed barrier.

1.6.2 In-situ measurements

A number of studies have made clear the importance of "T", "Y" and other top devices in improving the diffraction reduction of barriers but there is little research as specific guidance that can be applied to the problems of nearly-enclosed barriers. Previous studies[162–166] on nearly-enclosed barriers mostly used scale measurements and numerical modelling methods to evaluate the efficiency. Most numerical methods they used are the Ray Tracing Method with software Cadna/A and Statistical Energy Analysis(SEA) based on VAone, although the Boundary Element Method(BEM) is widely used in the prediction of barrier efficiency[15, 167–169]. The attenuations were predicted typically over 20 dB(A). Hence, nearly-enclosed barriers are applicable to many urban lines in different cities. However, little is known about nearly-enclosed barriers through in-situ measurements. Coincidentally,

a fully-enclosed sound barrier was built on the Shenzhen-Maoming Railway line for the first time in China. X. Wu et al.[170] used indirect field measurements to assess its performance. The results showed that when the train speed was not higher than $132km/h$, the attenuation generated by the fully-enclosed barrier could be on average 16-18 dB at different distances and heights from the railway line, with broadband frequency characteristics. Therefore, it seems necessary to carry out in-situ measurements in a real situation in order to assess the actual noise reduction performance for URT noise.

1.6.3 Numerical modelling calculations

In terms of numerical methods, the greatest advantage compared with analytical methods is that numerical methods can deal with more complex geometries of structures in the actual engineering. As typical numerical methods to solve acoustic problems, the finite element method (FEM) and the boundary element method (BEM) play an important role. Actually the BEM consists of applying a FEM discretization to a boundary integral equation formulation of a problem[171], which only discretizes the boundary domains of the studied regions (curves in 2D problems and surfaces in 3D problems). Hence, the dimension of an acoustic problem is effectively reduced by one by using BEM modelling which is more efficient than FEM modelling. Besides, in cases where the domain is infinite and exterior to the boundary, this advantage of the BEM modelling is more noticeable. Moreover, the accuracy of the BEM solution is much higher than that of the FEM solution[172]. Therefore, BEM modelling is a good method for general acoustic field problems.

In BEM modelling, the railway noise source is typically assumed to be an incoherent line source, but to predict the barrier performance within an acceptable computational time, a coherent line source (2-D BEM) or a one-point source facing the receiver (3-D BEM) is always considered as the alternative in the numerical calculations. Compared with the computational cost of 2-D BEM calculations, the cost of 3-D calculations significantly increases due to the sophisticated matrix computations. Furthermore, because the element size must be less than one-sixth the sound wavelength, the cost for higher frequency calculations is considerably high, even in two dimensions. The calculation time also depends on other parameters, such as the frequency range of interest and the absorptive surface treatments. The long calculation time is the main problem when solving 3-D BEM models, especially for barriers with complicated tops, and the calculations are often conducted using a 2-D BEM approach[15, 20, 173, 174](with coherent line sources). In the early years, D.C. Hothersall et al.[20] discussed the 2-D BEM model of T-profile and associated noise barriers based on the results obtained from experimental modelling and field measurements. They found that the predicted results were not applicable to the incoherent line source, but the relative performances of different barrier shapes would be similar. I. Takashi et al.[15] studied the performance of road traffic noise barriers with various shapes and surface conditions using only a 2-D BEM method. When studying the efficiency of low-height noise

reduction devices applied on the roadside, M. Baulac et al.[173] carried out 1:10 scale model measurements to confirm the effectiveness. They found good agreement between the 2D theoretical results and the 3D scale model measurements. Moreover, F. Koussa et al.[174] studied the acoustic performance of conventional and low-height gabion noise barriers using a 2-D BEM model and scale model measurements. The agreement of the results of the two methods was satisfactory.

However, using 2-D BEM models for researching railway/road traffic noise was found to be inappropriate because the results obtained for these cases were noticeably different. P. Jean et al.[175] emphasised the importance of source type on the assessment of noise barriers. Using the Fourier-like transformation proposed by [176], they found that the barrier attenuation was overestimated if coherent line sources were considered, whereas the efficiency of a cap on the top of a straight barrier was underestimated with coherent line sources. Later, with the help of a BEM program that they compiled, their team[177] obtained the real performance of a T-shaped absorbing cap with road traffic noise conditions on the ground. They found that the results of cap efficiency for a coherent line source were different from those for an incoherent line source. For the highest frequencies, the efficiency was proportional to the path difference. They also found the slantwise propagation effects on the barrier attenuation for a point source when the source-receiver distance was not perpendicular to the barrier with a simple analytical formula. However, to date, there has been little research that can clarify the slantwise effects of the distance between the source and receiver along the barrier $|z_s - z_r|$ (in the third direction perpendicular to the cross-section plane, it will be given as "longitudinal distance" for clarity) on the performance of barriers with arbitrary shapes.

To reduce the computational time of 3-D BEM calculations, D. Duhamel[176, 178] proposed a 2.5-D method in which the results obtained for coherent line sources can be transformed via Fourier-like transformations to those corresponding to incoherent point or line sources. Using this method, many articles have predicted the performance of acoustic screens for incoherent point (or line) sources in different applications. Forssen et al.[179] compared the results predicted by a 2.5-D BEM method and the results obtained from an in situ measurement, which showed reasonable agreement. S. Sakamoto et al.[169] and M. Hiroe et al.[180] employed a Fourier-like transformation in a 2-D finite-difference time-domain analysis to study the noise shielding effect of eaves/louvres attached to building facades and the propagation of sound from surface railways. The calculation method was validated by the experimental results. Based on the above successful experiences, the present study continues to use this 2.5-D method to compare the results of different types of sources to predict the performance of urban railway noise barriers.

1.6.4 Scale modelling tests

The predictions must be validated by the measurement results obtained from outdoor in situ[177, 179] or scaled laboratory tests[169, 173, 174, 180]. In situ measurements may be time consuming and it is difficult to find a real environment as simple as the numerical model(rigid barrier, rigid flat ground, no reflecting obstacles, ...), even if background noise can be rejected using controlled signals (like ESS, MLS) and the intrinsic characteristics of noise barriers can be measured in situ with a given reproducibility[181]. However, performing large-scale measurements requires extremely large anechoic laboratories that are not easy to build and run. Hence, only a few studies[182–185] related to in situ measurements have been published.

Because of the difficulties in conducting in situ measurements discussed above, a measurement method in which small-scale model tests are used instead offers a reliable alternative for predicting barrier performance. Many articles[186–188] have used the scale modelling method to understand the propagation of road/railway traffic noise to the surrounding environment, and the scaled measurement method has been widely employed in the study of noise barrier performance[21, 31, 189–192]. Based on the invariance of the speed of sound in air, the performance of real barriers in the field can be imitated by the results of scale models, which is possible when the measured frequency range is increased by the same scale factor to the typical range of interest for the urban railway traffic noise. The scaled approach is perfectly suited for our research because we focus on comparing different source types to evaluate the performance of a simple barrier on the ground and a double-straight barrier on a viaduct, which are assumed to be rigid throughout. In addition, it is known that the impedance of surfaces must be scaled with complicated computations, not as that of an acoustic rigid surface, which is infinite. Such surfaces with absorptive treatments are not considered in the scale modelling tests in this thesis.

Various sound sources, such as air-jet and electro-acoustic sources, laser-generated acoustic pulses and electric sparks, have been used during the measurement process, depending on the scale-modelling application. G.R. Watt et al.[31] used an air-jet whistle activated by an air supply at 10 atmospheres to simulate an omni-directional point source. Among the different source types that are able to provide these characteristics, spark discharge in air is an interesting solution. Many studies have presented the characteristics of the spark discharge, which can be regarded as an adjustable acoustic source for scale model measurements[173, 188, 190, 193]. For researching the propagation of explosions and sonic booms conveniently in the laboratory, Q. Qin et al.[194] investigated the characteristics of acoustical shock waves associated with a focused pulsed laser beam. Aiming at modelling incoherent point sources, our approach is to use scaled outdoor experiments and several point sound sources. The sound radiated simultaneously by several miniature loudspeakers with uncorrelated white noises can easily be considered to be that of incoherent point

sources. Such an approach can validate the prediction results not only for the one-point source but also for the incoherent point sources, thus providing a new avenue for predicting the results for an incoherent line source.

1.7 Conclusion

Aiming to understand the performance of nearly-enclosed barriers in terms of reducing urban rail transit noise, the source characteristics of URT noise were discussed at first. The main noise source of urban rail transit is wheel-rail noise of which the frequency range is concentrated at low- and mid-frequency. A-weighted indicators are not acceptable due to the underestimation of low-frequency components, whereas time-equivalent single ratings are not acceptable due to the discontinuous operation time of the urban rail transit. Spectrum analysis with linear weighted characteristics is not only intuitive to realize the predominant frequency components, but also does not underestimate low frequencies.

There are several wave phenomena besides noise abatements affecting the noise propagation from the URT noise source to receiver positions. These effects are presented in detail. In spite of its significance to sound fields, the road surface will be assumed acoustically rigid in the case of this study. After a thorough discussion of atmosphere absorption, refractions by wind and sound-speed gradients and turbulence, these effects on the noise propagation of the case of this study will be ignored provided that the receiver positions are limited to within 50 meters from the source and the frequency range of interest is 50-5000 Hz.

There are four research methods utilized in this study. The second chapter identified and solved the issue in the indicators for assessing the acoustic performance of noise barriers which was similar to those for assessing the urban rail transit noise, before conducting the in-situ measurements. Then, to understand the source characteristics of URT noise and assess the performance of a prototype of a nearly-enclosed barrier, a series of in-situ measurements were conducted and are detailed in Chapter 3. Subsequently, a comparison between scale model tests and 2.5-D BEM modelling calculations was made respectively for a conventional barrier in Chapter 4 and a totally reflective nearly-enclosed barrier in Chapter 5, in order to validate the numerical simulated results. Then the 2.5-D BEM calculations were used to model the configurations of in-situ measurements, as described in Chapter 6. Finally the acoustic performance of the nearly-enclosed prototype could be evaluated. Optimization of nearly-enclosed barriers was also made by using the 2.5-D BEM calculations, as presented in Chapter 7.

2 Study on in-situ measurement methods of urban rail transit noise barriers

2.1 Introduction

This chapter aims to shed light on the in-situ measurement of insertion loss in urban rail transit noise barriers. In order to measure in-situ the performance of a prototype of a nearly-enclosed barrier in terms of reducing urban rail transit noise, the improved in-situ measurement method is introduced. Based on relevant standards and sound diffraction theory, an improved arrangement of receiver positions is put forward and a current indicator is taken into account as a supplement to the A-weighting method. Utilizing these improved techniques, we designed and carried out an in-situ measurement of a simple straight barrier located near an urban rail transit test line. During the measurement, the receiver positions based on sound diffraction theory and those recommended by relevant norms in Section 1.6.1 were compared. And the differences between A-weighted measured results and the additional evaluating indicators were investigated. In this chapter, the improved in-situ measurement methods were introduced and described at first. Then according to these methods, an in-situ measurement of a simple straight barrier near an urban rail transit test line was designed and implemented. The measured results processed by the A-weighting single rating method and the additional indicator were compared and discussed. The improved in-situ measurement method was finally determined and prepared to measure the acoustic performance of a nearly-enclosed prototype in the next chapter.

2.2 Improved methods

2.2.1 Rearrangement of receiver positions based on the diffraction theory

In order to compare the insertion loss values of different types of barrier at the same site under given meteorological conditions, it is quite important to offer an approach to determine the receiver positions in the full-scaled experiment of barrier performance. In the case of noise barriers, receiver positions are located on the opposite side of the sound source.

Tab 2.1.: Rearrangement of receiver positions based on diffraction theory

	Distance from the nearest track centre	
	$\leq$ 17 meters	$\geq$ 17 meters
Height above the mean rail head of the nearest track	Bright zone in near field	Bright zone in far field
	Transition zone in near field	Transition zone in far field
	Shadow zone in near field	Shadow zone in far field

In accordance with diffraction theory[195], the open area behind the barrier can be divided into three zones: a bright zone where all frequencies transmit directly, a transition zone where low and middle frequencies bend around the barrier during the direct transition of high frequencies, and a shadow zone where, as a result of the vibration and the diffraction, only low-frequency sounds are transmitted. Since the noise reduction effects of barriers vary substantially by zone, and variations are a function of frequency[196], in-situ measurements of insertion loss for all frequencies in each zone are necessary. Depending on distance of receiver from sound source, the acoustic energy produced by the source will behave quite differently. In far field, the spherical shape of the sound waves can be reasonably approximated as a plane-wave, with no curvature[197]. It is important to understand this difference, and place the receiver positions in near field and far field separately when taking measurements. Generally, a far field acoustic begins two wavelengths from the sound source, and extends outward to infinity.The frequency range of interest determined in Chapter 1 is 50-5000 Hz. Hence in the case of urban rail transit noise barriers, the start of the far field is at least around 17 meters[197]. Receiver positions should therefore better be placed less and greater than 17 meters, respectively. It is considered that receiver positions represent barrier performance at all the acoustic areas given above. A conservative estimate is that six positions meet the requirements (see Table 2.1).

The prescribed receiver positions are shown in Figure 2.1, where the height of barrier above the rail head height is 2m. Different shadows based on diffraction theory show that for Chinese standards (indicated by triangles) all receiver positions are located in the shadow zone in near field, with the exception of the receiver in TB/T 3050-2002, which is located in the shadow zone in far field. All nine positions specified by CEN/TS 16272-7:2015 (indicated by circles) cover four of the acoustic areas. M1-1, M2-1 and M2-2 represent the performance in the shadow zone in near field, M3-1, M3-2 and M3-3 represent the performance in the shadow zone in far field, M1-2 and M2-3 represent the performance in the transition zone in near field, while M1-3 represents the performance in the bright zone in near field. In addition, the sound pressure distribution of the whole of the open space behind the barrier is mapped by the nine grid positions, enabling visualization of the noise reduction effect of a barrier. The grid-form method is thus instructive for improving the arrangement.

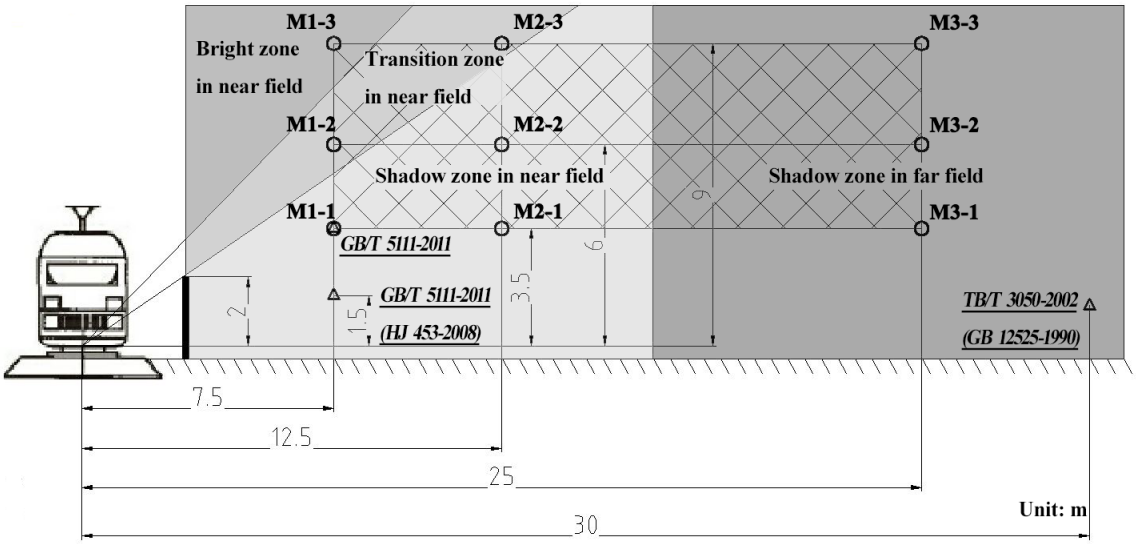

Fig 2.1.: Comparison of receiver positions prescribed according to the standards[153–159]

By considering the actual need of the engineering application in urban railway transit systems, the receiver positions have to be rearranged in terms of the changeable locations of the acoustic areas. For instance, if a barrier is installed on a bridge it is difficult to reach the bright zone. Hence there is no necessity to place receivers at M1-3, M2-3 and M3-3 unless there are tall residential buildings close to the lines. If the sensitive areas are located far from the lines, receivers at M3-1, M3-2 and M3-3 can be placed around the sensitive area instead. When the height of the tested barrier is very low, the boundary dividing the shadow zone and the transition zone must be lower than shown in Figure 2.1. This means that receiver M1-1 can be located in the transition zone in near field, resulting in no receiver positions in the shadow zone in near field close to the barrier. If the shape is near to fully-enclosed, the receiver M1-3 should also probably be located in the shadow zone in near field, resulting in no receiver positions in the bright zone. In consequence, receiver positions need to be rearranged in all the acoustic areas as possible.

2.2.2 Relevant evaluating indicators

The ISO standard[153] recommends octave-band or one-third-octave-band sound pressure levels as indicators when it is necessary to obtain frequency characteristics of barrier insertion loss. Since the dominant frequency components are easily recognizable from one-third-octave-band analysis, this method has been adopted by low frequency noise standards of Polish, Swedish and German in general environment[95–97]. This has implications for the placement of barriers in areas proximate to urban main road traffic. It appears that such noise makes a smaller contribution to reported annoyance than might be inferred from the objective or physical dominance of the noise[198]. In such a case, it is unnecessary to analyze in-situ experimental results by employing one-third-octave-band analysis. The

same applies with railway noise barriers, since it is well known that rolling stock noise is the predominant component of urban railway noise and that the latter is normally within a rather broad frequency range of 800Hz to 2500Hz[62]. There are many other sources of noise, such as curve squeal, brake screech and bridges. The acoustic characteristics[199] of these are shown in Table 1.3. When a train crosses a viaduct, the low-frequency rumble noise induced is a significant annoyance for those in the station and residents in the vicinity, even at considerable distances. This is because lower frequency noise travels farther than higher frequency noise[197]. When sound barriers are installed on a viaduct, the additional low-frequency noise which radiates from the viaduct, the barrier and their related connectors cannot be neglected. One-third-octave-band analysis must be deployed here, since it produces data helpful to the attenuation of such low-frequency noise.

However, in the interests of reliability and applicability, real site testing is necessary. In our view, it is advisable to design an in-situ insertion loss experiment for railway noise barriers based on standards and our findings. This way, it is possible to compare the results of different analysis methods and to offer practicable suggestions.

2.3 Experiment design and implementation

To validate the reliability, rationality as well as the usability of the improved methods as mentioned above, it is necessary to design an in-situ experiment of an urban rail transit noise barrier. The results of different measurement methods and different evaluation indicators are compared. Finally, the reasonable and feasible suggestions are put forward.

The experiment object is a commonly straight barrier, placed at ground level close to the tested urban rail transit line on Jiading Campus, Tongji University. The length of the barrier was 10 meters and its height above the track was 1.5 meters, which is relatively lower than other railway noise barriers. Since the barrier could be removed during the period of experiment, utilizing the direct measurement method[153], sound pressures at receiver positions were tested by microphones before and after barrier installation. The noise source in the experiment was naturally occurring railway traffic: two-carriage passenger trains, each 22 meters in length. Since the experiment sites were located in the middle of the lines, the noise induced by trains in brake mode could not be considered. The trains travelled at 40km/h as they passed the test field.

The circles in Figure 2.2 indicate the directed receiver grid formation. Applying the improved methodology, it was evident that M1-2 and M1-3 could not be located in the transition zone, on account of the low profile of the barrier. The attenuation property of receiver M1-1, located far from the barrier and close to the transition zone in near field, might underestimate the performance of the barrier in the shadow zone in near field. Moreover,

since the barrier was installed at the ground line, it proved possible to choose the receiver above ground at 1.2m to simulate pedestrian hearing. Thus receiver positions were better reset close to the barrier and to the ground. In consideration of the low profile, it was possible, by applying the grid-formation criteria of the standards, to determine receiver positions. These are indicated by crosses in Figure 2.2. They were at a distance from the nearest track centre of 3.3m, 9m and 18m and at a height above the mean rail head of the nearest track of 1.2m, 1.8m and 2.5m, respectively. As per the discussion above, the receiver positions in our experiment were set in four areas of the open space behind the barrier. P1-1, P2-1, P2-2 and P2-3 are represented in the shadow zone in near field. P3 is represented in the shadow zone in far field. P1-2 is represented in the transition zone in near field. P1-3 is represented in the bright zone in near field.

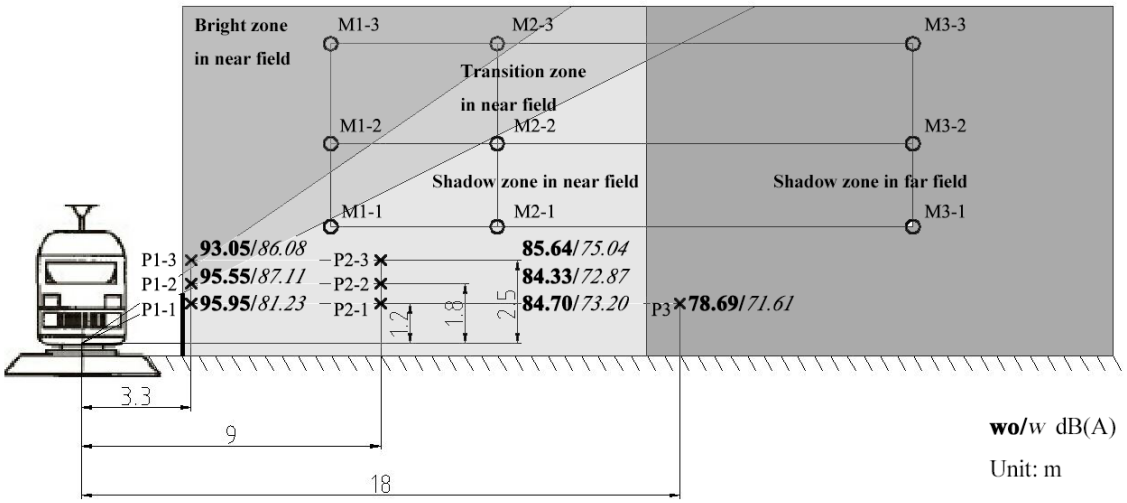

Fig 2.2.: Configurations of the in-situ experiments with the straight barrier on the ground line (frequency range: 20-20 kHz)

The microphones at each receiver position were omnidirectional and protected by wind-screens. Corresponding frequency responses ranged from 20Hz to 20kHz. The sampling frequency of the sound pressure signals was intended to be 51.2kHz, based on the Nyquist Theorem. To avoid message distortion, this was more than twice the maximum frequency component of the audio frequency (20-20kHz). The experiments on the “before” and “after” sites were conducted on sunny days only a few days apart. Meteorological conditions were not significantly different and thus were not measured. However, an acoustic amplifier, an electrical charge amplifier, sound pressure collecting equipment, an A/D data collection card and a computer running a data collecting program were prepared. These instruments met the requirements of EN 61672-1 and the microphones complied with IEC 61672 class 1. Pressure signals at all receiver positions were recorded simultaneously and, to ensure the statistical representativeness of the sample, train-passing data for each distance was obtained by taking at least 10 measurements.

2.4 Results

2.4.1 Signal processing procedure

According to the relevant standards[153, 155, 157], the equivalent continuous A-weighted sound pressure level can be represented as follow,

$$L_{\mathrm{pAeq,T_{pass}}} = 10\log_{10}\left[\frac{1}{T_p}\int_{t_1}^{t_2}\frac{p_A^2(t)}{p_0^2}dt\right] = 10\log_{10}\left[\frac{1}{N}\sum_{n=1}^{N}\frac{p_A^2(n)}{p_0^2}\right] \tag{2.1}$$

where T_p is the train pass-by time interval, p_A is the A-weighted instantaneous sound pressure, and p_0 is the reference sound pressure ($20\mu Pa$). During the post-processing procedure, the sound pressure signals were first filtered by the bandpass of audio frequency range and A-weighting filter, and then, by utilizing the time interval of the train's passing, the equivalent continuous A-weighted sound level $L_{\mathrm{pAeq,T_{pass}}}$ was obtained. Since the valid pressure signals at each position were measured at least 10 times, equivalent levels had to be expressed as an average. The formula for the averaging method is:

$$L_{\mathrm{Aeq}} = 10\log_{10}\frac{1}{n}\sum_{i=1}^{n}10^{0.1L_{AE,i}} \tag{2.2}$$

where L_{Aeq} is the sound level used to calculate the noise attenuation of the barrier, and $L_{AE,i}$ is the ith pass-by level computed by Equation (2.1). Hence, it was easy to obtain the attenuation single-number rating for barrier performance. The C-weighted level and the 1/3 octave band level was acquired in the same way, producing an effective supplement to the A-weighting method. However, for the sake of simplification, the attenuation of each 1/3 octave band was obtained by calculating the ratio of sound energy in the field with and without the barrier. This is given by

$$Att(f_{oct}) = 10\log_{10}\left(\frac{\sum_i^N p_{\mathrm{wo}}^2(f_i)}{\sum_i^N p_{\mathrm{w}}^2(f_i)}\right) \tag{2.3}$$

where $p(f)$ is the sound pressure with respect to a certain frequency, calculated by applying the Fast Fourier Transform formula. f_{oct} is the central frequency of the 1/3 octave band.

2.4.2 Urban rail transit noise characteristics

To reach an assessment of barrier performance, the experimental results of the sound pressure level at all receiver positions on the "before" and "after" measurement will be illustrated first. This is in order to comprehend the characteristics of railway noise at a speed of 40km/h. In Figure 2.2, the bold numbers denote the continuous equivalent A-weighted sound pressure level (L_{Aeq}) at all receiver positions before the installation of the barrier. The

Tab 2.2.: Comparison between L_{Aeq} and maximum value of 1/3 octave band on the "before" site

Receiver Position	P1-1	P1-2	P1-3	P2-1	P2-2	P2-3	P3
L_{Aeq}(20Hz-20kHz)(dB/A)	95.95	95.55	93.05	84.70	84.33	85.64	78.69
800 Hz of 1/3 octave band (dB)	96.76	96.24	93.75	84.88	84.69	85.64	79.02
Absolute difference	0.81	0.69	0.70	0.18	0.36	0.00	0.33

italicized numbers denote L_{Aeq} on the "after" site. It can be seen that before the installation of the barrier, L_{Aeq} at P1-1 was marginally higher than P1-2 and higher than P1-3. Since the P1-1 and P1-2 positions were much closer to the track, the results confirmed that rolling stock noise produced by wheel-rail contact vibrations, could be a predominant component of railway traffic noise. However, P1-1 level was significantly lower than P1-2 and P1-3 around 5dB(A) after the barrier was installed, indicating that the barrier was able to suppress rolling stock noise effectively. Performance of the barrier was particularly good in the shadow zone in near field. At the receiver-source distance of 9m, the levels of each of the three receiver positions were almost the same on the "before" site, whereas the P2-3 level was much higher than P2-1 and P2-2 on the "after" site. With increase of receiver-source distance, L_{Aeq} showed a tendency to decrease at the same height, regardless of the installation of the barrier: P1-1>P2-1>P3 (L_{Aeq}), P1-2>P2-2 (L_{Aeq}) and P1-3>P2-3 (L_{Aeq}). Interestingly, in contrast to the "before" site, the downward trend of the A-weighted level near the ground became slower on the "after" site.

By one-third octave analysis, SPLs at all receiver positions on the "before" site in Figure 2.3(a) show that the dominant frequency range of railway noise was quite wide: five 1/3 octave bands of 400 Hz, 500 Hz, 630 Hz, 800 Hz and 1000 Hz, which are given relatively small weights by A-weighting[200]. Moreover, the maximum values at all receiver positions were, coincidently, all at 800 Hz, and the differences between the L_{Aeq}s and the maximum values at all the positions were no more than 1 dB (Table 2.2). Therefore, without one-third-octave-band analysis, the continuous equivalent A-weighted sound pressure level could present almost the same level as that of the predominant component. This indicated that A-weighting was suitable to describe the annoyance induced by railway noise. On the "after" site (Figure 2.3(b)), sound levels in the dominant range of railway noise were roughly consistent with the levels at low frequencies, which were reduced considerably by the barrier. In order to understand the importance of low frequency noise, the difference between C- and A- weightings has been considered as a predictor since it indicates the amount of low frequency energy in the noise[85]. If the difference is greater than 15 dB, there is a potential for low frequencies. In Table 2.3, we see that the differences between A-weighted and C-weighted levels at all positions were as large as 6 dB. Although the differences were not too large, it is noteworthy that low frequency noise played the same significant role as the middle and high frequencies on the "after" site. This should not be neglected in the future attenuation research.

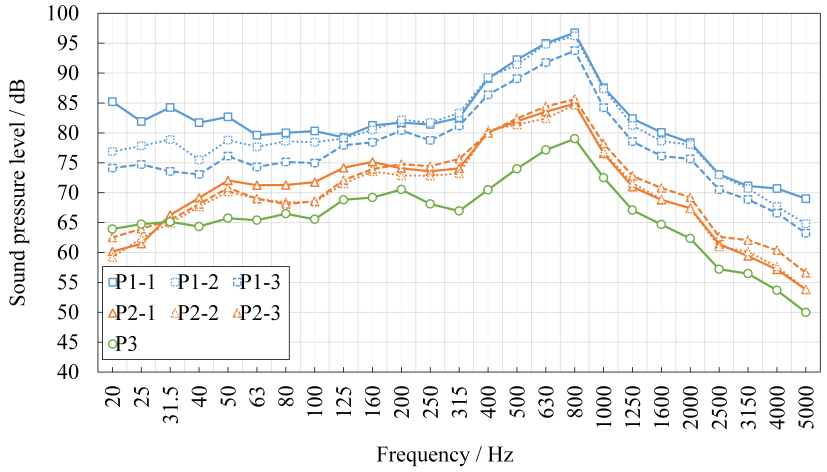

(a) On the “before” site

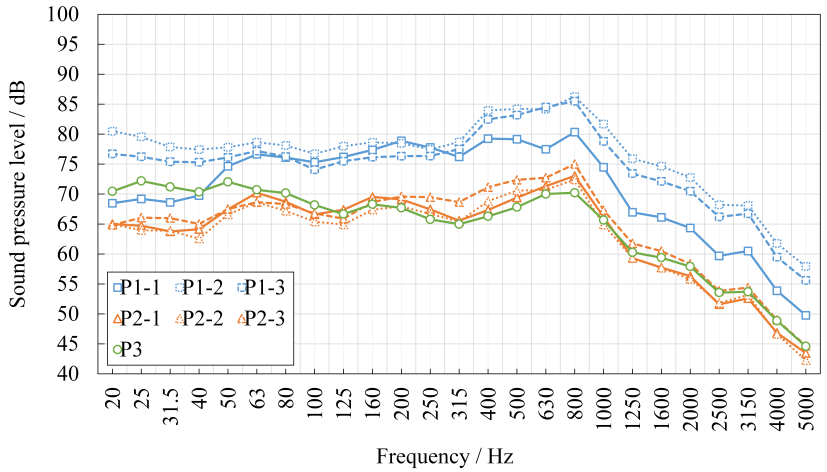

(b) On the “after” site

Fig 2.3.: Sound pressure levels in the one-third-octave band at all receiver positions

2.4.3 Insertion loss in different acoustic areas

Insertion loss, also called attenuation, is defined[153] as the difference in sound levels at a specified receiver position before and after the installation of a barrier. Using the results of SPLs at all the receiver positions analyzed above, barrier attenuation was obtained and listed in Table 2.4. It appears that the barrier varied in effectiveness depending on where the receiver position was located. Of the seven positions, the attenuations in the shadow zone in near field (P1-1, P2-1, P2-2 and P2-3) were the highest, being at least 10 dB(A). The next were in the transition zone in near field (P1-2) and in the shadow zone in far field (P3). The lowest was in the bright zone in near field (P1-3). Hence the area in the shadow zone in near field appears to be the major area of competence for the noise reduction effect of the barrier. Since the difference between the maximum and the minimum values of the attenuations (P1-1 and P1-3) was around 7 dB(A), it is evident that a single measurement point cannot provide a comprehensive presentation of barrier performance. In other words, the significant

Tab 2.3.: Differences between A-weighted and C-weighted SPL at all positions on the “after” site

P1-3	**P2-3**	
2.88dB	3.73dB	
P1-2	**P2-2**	
3.06dB	4.09dB	
P1-1	**P2-1**	**P3**
4.73dB	4.38dB	6.15dB

Tab 2.4.: Attenuations in L_{Aeq} at all receiver positions (frequency range: 20Hz-20 kHz)

P1-3	**P2-3**	
6.97dB(A)	10.60dB(A)	
P1-2	**P2-2**	
8.44dB(A)	11.46dB(A)	
P1-1	**P2-1**	**P3**
14.72dB(A)	11.50dB(A)	7.08dB(A)

difference between these attenuations is attributable to variation among receiver positions. These must be taken into account when evaluating the acoustic performance of barriers.

For comprehension of the frequency characteristics of the attenuation, the attenuations in the one third octave band from 20Hz to 5000 Hz are computed and shown in Figure 2.4. The barrier performed well in the dominant frequency range of these five bands, especially in the shadow zone in near field (P1-1, P2-1, P2-2 and P2-3). From Figure 2.4, we can see that the difference in the attenuations between receiver P1-1 and other receivers in the shadow zone in near field (P2-1, P2-2 and P2-3) were concentrated mainly in the dominant range of railway noise and low frequencies below 50Hz. Attenuations at all receiver positions were as high at the frequencies above the dominant range. However, the attenuations in the range of low frequencies were ultra-low, and, below the band of 100 Hz, even negative. Among all the receiver positions, the maximum of excess attenuation was 7.4 dB in the band of 20Hz at receiver P3. Ground effect and diffraction of low frequencies at the top of the barrier might be the cause of negative values of attenuation located primarily in the shadow zone in far field (P3), the transition zone in near field (P1-2) and the bright zone in near field (P1-3). In summary, the barrier performed quite well in the range of mid and high frequencies, but relatively badly at low frequencies.

2.5 Discussion

By utilizing the grid-form method, attenuation at the recommended positions could be estimated by known results. It appears that the maximum value of attenuation at all recommended positions can be located at receiver M1-1 and M1-2. As receiver M1-1 is close to the boundary between the transition zone and the shadow zone, based on diffraction

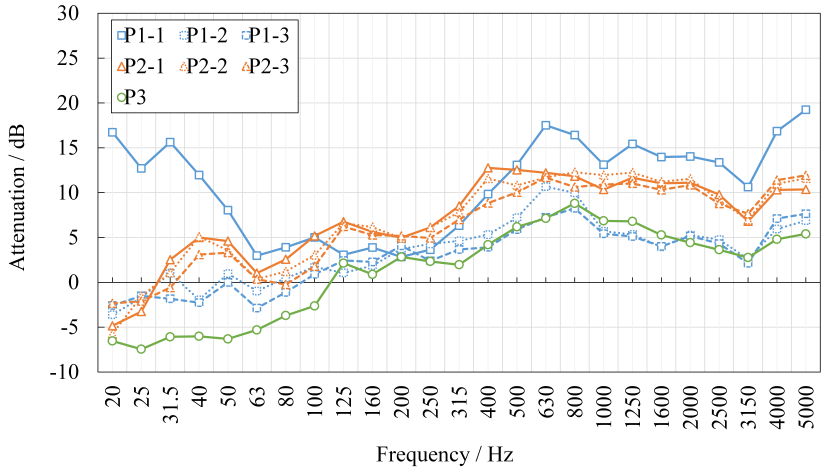

Fig 2.4.: Attenuations in the one-third-octave band at all receiver positions (20Hz-5000Hz)

theory, the attenuation at receiver M1-1 must be a little lower than that at receiver P1-2, which is located in the transition zone in near field. In the same way, attenuation at receiver M2-1 must be a little lower than that at receiver P2-3. It follows that maximum attenuation in the shadow zone in near field is no more than 10 dB(A). Compared with the experimental results in section 3, the attenuations at the recommended positions definitely underestimate the performance of the barrier. As such, the recommended receiver positions seem to be higher than the evaluation requirement, and hence unsuited to low-height barriers. With the rearrangement of receiver positions much closer to the barrier and to the ground, the attenuations in L_{Aeq} in the bright zone, the transition zone and in the shadow zone in near and far field can be demonstrated more completely and distinguished more clearly. In consequence, it would be better to rearrange receiver positions to suit the actual need of the barrier.

Using one-third-octave-band analysis, the predominant frequency range of railway noise can be identified. Moreover, the frequency characteristics of the attenuation can also be recognized: The barrier performed well at the predominant frequency range of railway noise but relatively poorly at low frequencies and at frequencies below 100Hz in particular. It is of interest to note that there is considerable variation in attenuation even in the same frequency band. Although A-weighting is inapplicable here, the single-number rating can be still utilized as a railway noise indicator. Overall, the A-weighting method is inadequate to the analysis of the performance of railway noise barriers. However, a combination of A-weighting method and one-third-octave analysis can rectify the problem.

2.6 Conclusion

Based on diffraction theory, an improved method for the arrangement of receiver positions have been proposed here for the in-situ measurement railway noise barrier insertion loss. The method is capable of optimizing the performance of railway noise barriers in all the areas behind barriers. Our in-situ investigation of insertion loss with low-height barriers validates the claim that this method is more effective than CEN/TS 16272-7. The A-weighted SPL led to the overrating of the railway noise barrier performance with respect to the SPL. We conclude that one-third-octave band analysis provides superior frequency domain results, and is a good supplement to the A-weighting method. The one-third-octave-band values seem to provide a better general description of barrier performance than do A-weighted results.

However, there may be some limitations in the study of this chapter. The tested line in this chapter is a ground line, which is not sufficient to highlight the importance of low-frequency noise. Future research in the thesis will seek to rectify this through experiments on elevated line sections. Nevertheless, to the extent that our study indicates how to achieve railway noise barrier performance from the measurement of sound pressure levels by the improved arrangement of receiver positions and one-third-octave analysis, it is a step toward better understanding.

3 In situ measurement of an absorptive nearly-enclosed noise barrier prototype on an existing line in the urban rail transit system

3.1 Introduction

As mentioned in the last chapter, A-weighted equivalent pass-by level is always referred to as an exact indicator to assess the performance of a noise barrier since it is a typical single rating to reflect the response of the human ear to noise. But for URT noise it is unsuitable because it has a considerable underestimation for low frequencies. When a train is passing by, significant structural noise is radiated from the viaduct. The great energy of the structural noise is concentrated in the low frequencies, doing harm to human health, although we cannot hear it clearly. Through the findings from the experimental results presented in the last chapter, using A-weighted single rating as a evaluation indicator could highlight the importance of the rolling noise(commonly thought to be at mid- and high frequencies), but at a significant expense of structural noise(at low frequencies). Hence, as an effective alternative, one-third octave spectrum was used by many studies[13, 56, 167, 173, 201] to analyze frequency characteristics of the efficiency. It is better than the single rating because we can use it to identify the frequency range of URT noise, and the range of barrier performance.

In this chapter, the performance of a nearly-enclosed barrier prototype meant to attenuate URT noise for the surroundings is measured in situ on an existing line. Firstly, the measurement preparations were introduced, including the selection of the measurement sites, the arrangement of receiver positions according to the conclusion obtained from Chapter 2 and the train speed measurement method. Then after the implementation, measured sound pressure levels and their dependences on the train speeds were investigated. Speed corrected results were then used to describe the characteristics of the elevated rail transit noise. Finally, the accurate performance of the nearly-enclosed prototype in terms of reducing the elevated rail transit noise was evaluated by speed corrected results and 1/3 octave spectra.

3.2 Preparatory work

3.2.1 Selection of measurement sites

Many large cities in China have developed large numbers of metro lines in the past few years. Nevertheless, since most metro lines are built underground, only a few sites in urban areas are required to employ noise barriers on elevated structures. One prototype is constructed on the elevated section of Metro 1 in Ningbo, China, between the stations Liangzhu and Lugang. It is a typical nearly-enclosed prototype with a length of 420m. In this chapter, this prototype was selected as the research object.

The environment is relative noisy along the line. The site is next to a four-lane road which separates the highly protected area from the lines (see Figure 3.1), with many cars and trucks passing by. On the other side of the site there is a river between factories and the metro lines. Given the complexity of the environment, it is essential to pay attention to the influence of background noise during the measurement. As the research purpose in this chapter is to evaluate the noise reduction effect of a nearly-enclosed barrier at a site, the difference in level at a given receiver between the site without and with the barrier can be regarded as the attenuation induced by the barrier, only when the tested source prevails over other surrounding sources which have no relation to the barrier. Accordingly, the background noise emitted by surrounding sources should be as low as possible. So, the difference in level between the background noise and signals should be sufficiently large. ISO 10847-1997[153] states that the level of background noise should be 10dB or more below those obtained from measured signals. And if the difference is between 4dB and 9dB, a correction should be applied to the measurement results. Calculated by A. Jolibois et al. in [16], the minimum difference in level was 9dB when the error on the attenuation was less than 0.5dB.

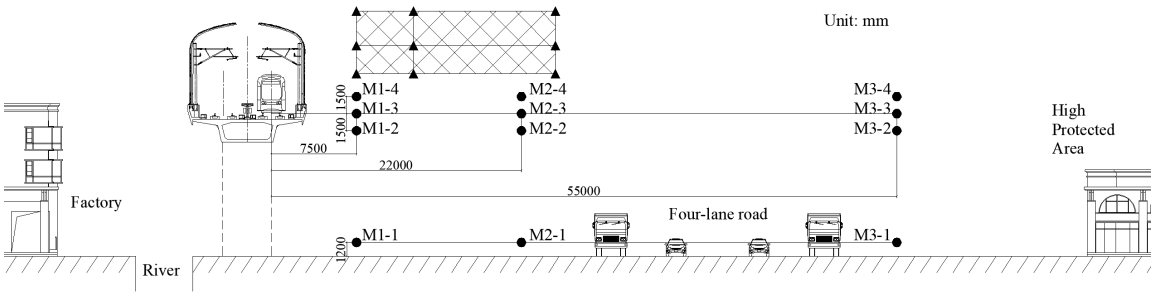

Fig 3.1.: The configuration of the site with the nearly-enclosed prototype

Although the traffic noise of passing cars and trucks could not be prevented during the measurement, one could seek to select the site where the level caused by the passing by of a train was considerably higher. Hence the train speed on the measurement site was required to be as high as possible, since pass-by level varies strongly with the train speed[16, 202, 203]. Based on these considerations, a site was finally selected that was close to the midpoint of the length of the barrier. The source in the measurement is the naturally occurring railway noise. The passenger trains have six cars, each with a length of 19 meters. In addition, the train would not brake during the measurement since the site was located between two stations. For this reason, the brake mode of the trains would not be considered and discussed in the case of this chapter though there is a correlation between railway noise levels and brake mode[204].

In addition to background noise, track structures also have a major influence on the emission of railway traffic noise, and therefore would bias the evaluation of a barrier's effect. On the selected site, Floating Slab Tracks (FSTs) have been constructed on the viaduct. Designed to isolate the rail system vibrations transferring to the supporting foundations and surrounding areas, it is theoretically and experimentally proved that FSTs can effectively reduce structure-borne noise radiated from the viaduct[205–207]. The structural noise of viaducts is concentrated at low frequencies, so that the measured attenuations at low frequencies in this case must be overestimated compared with those for the barrier itself. On the other hand, the rolling noise might also be influenced by the FSTs. Since most of the rail vibration energy is isolated by the FSTs, it may react on the rail vibration. And therefore it will make some contributions to the emission of rolling noise. As a consequence, the employment of the FSTs not only reduces a lot the structural noise radiated from the viaduct, but also increases a little the rolling noise. In order to observe the degree of the bias to the performance of the nearly-enclosed barrier, for the low-frequency structural noise it seems necessary to measure sound pressure in the vicinity of the viaduct structure during each pass-by. If the attenuations at this location at the low frequencies were measured higher than the numerical predictions obtained from a model of only consideration to the employment of the nearly-enclosed barrier, the measured overestimation would be due to the employment of FSTs. For the rolling noise, another possibility would have been to measure the vibration of rails during the tests. In the context of the FST effect, when each train was passing by with the same speed, the vibration acceleration levels of the rails at the site with the barriers must be higher than those at the site without barriers. If they were almost at the same levels, the effect of FSTs on the rolling noise was small enough to be ignored. In addition, this measurement technique for measuring the vibration acceleration of rails plays an important role in the calculation of train speed as well, since the rolling noise has a strong dependence on the train speed. It has been shown that an auxiliary microphone can be placed very close to the tracks to determine the speed of the tram during the pass-by in [16], and more details of this technique in our measurement will be presented in Section 3.3.1.

Aiming at measuring the difference in level at a given receiver with and without the nearly-enclosed barrier, another measurement site, at which there is no barrier installed on the viaduct but several correlated environmental factors (background noise, train type, bridge type, track type...) as well as the train speed being almost identical to the aforementioned site, was required since it is impossible to remove the nearly-enclosed prototype during the measurement. Considering the requirements of environment in the surroundings and the practical reality, the site was chosen between the station Gaoqiao and the station Liangzhu of Metro 1 in Ningbo, on which the measurements were performed with the same type of vehicles and the same type of viaduct structures. To distinguish these two sites, we use a site without a barrier and a site with a barrier to describe them afterwards. However, the difference between these two sites is not only the presence or absence of the barrier, but the type of the track. Thus the measured attenuation in the case of this chapter would be the combination effect of both the barrier and the FSTs. Reasonable explanations will be given in Section 3.3.1 to properly reduce the bias induced by the FSTs.

3.2.2 Measurement method

Arrangement of receiver positions

In this chapter, the interest of the research is to evaluating the performance regarding the noise reduction effect of the nearly-enclosed barrier for the surroundings when trains pass by, typically for the highly protected area far away from the lines(shown in Figure 3.1). As stated in the ISO and European norms[153, 155], the measured receiver positions are recommended to be at three heights above the track and at three horizontal distances from the source(marked with triangles in Figure 3.1), forming a grid, so as to present the acoustic performance of a barrier on the bright zone, transition zone, and shadow zone behind it, respectively. Chapter 2 showed that this gridded measurement technique could offer a set of data to map sound pressure distribution of the whole of the open space behind a barrier, and therefore enabled the visualization of the acoustic performance[208]. However in the case of this chapter, the bright and transition zone behind the nearly-enclosed prototype are too high to reach and the highly protected areas are mostly in its shadow zone. Moreover, the microphones cannot be fixed stably since disturbances are frequent and unavoidable at the top of such a high support. Thus, as a compromise between the gridded receiver arrangement and the in-situ situation, some of the receivers were positioned below the height of the track instead. In terms of residential buildings located far from the lines, the farthest receivers were considered to be placed much closer to them than recommended. The mid vertical array of receivers was positioned at a horizontal distance from the source of 22 metres to avoid the pass-by noise of cars and trucks on the road lanes.

Based on these considerations, the receiver positions were eventually determined and are marked by dots in Figure 3.1. The name of each receiver begins with "M". The first number represents the column number which is smaller as the receiver gets closer to the source, whereas the second number indicates the row number which is larger as the receiver gets closer to the ground. A symbol like "M1-" "M-1" which will be seen in later sections designates, for example, all the receivers in the first column or the first row, respectively. In terms of the distance between source and receiver("source-receiver distance" in short), the receiver M1-3, located at a distance from the nearest track centre of 7.5m and at the height of the mean railhead of the nearest track, can be affected the most significantly by the rail traffic noise due to its location being much closer to the source than others. However, the flange of the viaduct structure is higher than the source, which can be regarded as a block prevent the noise. In these circumstances, the receiver which has the biggest benefit from the barriers may be another one rather than M1-3. To avoid the barrier effect of the flange and assess the effect of the nearly-enclosed prototype more purely, receiver M1-4, located at a height above the mean railhead of 1.5m, was selected to measure. Receiver M1-2 was considered to be measured close to the viaduct at a height below the mean railhead of 1.5 m in order to observe the bias of the structural noise radiated from the viaduct already pointed out in Section 3.2.1. Receiver M1-1 was placed 1.2m above the ground corresponding to the ears of pedestrians. In addition, the farthest receiver M3-1 was placed 55m away horizontally from the nearest track. Based on the gridded measurement technique, a section at a distance horizontally from the nearest track of 22m between the vertical section M1- and M3- was chosen to measure in order to study the propagation law of railway traffic noise exposure more precisely. In summary, we have twenty-four different configurations of measurements depending on twelve receiver positions at sites with and without a barrier.

Sound pressure signals were recorded by twelve B&K microphones (Type 4189, the corresponding response frequency ranges from 20Hz to 20kHz) that were omnidirectional and protected by windscreens, as shown in Figure 3.2(a). The signals were sampled at 51.2kHz based on the Nyquist Theorem, more than twice the maximum frequency component of the audio frequency(20-20kHz), to avoid message distortion. In addition, the microphones were mounted in the grazing position on the standing poles due to signal contamination caused by the microphone safety grid[190]. Moreover, the omnidirectional characteristics could also be improved in the grazing position though the sensitivity was higher in the normal position.

Speed measurement from vibration signals

Train speed is one of the important parameters which influences the pass-by sound pressure level, and its value is required to be as high as possible to ensure the pass-by levels are much higher than the background noise. It is well known that train speed can be measured by the

(a) The microphones (b) The piezoelectric acceleration sensor

Fig 3.2.: Part of the apparatus used on the site with a barrier during the measurement

length of a train and the duration of its pass-by. However, due to the presence of barriers the general method to measure speed is worthless. One approach, as detailed in [16], is to use an extra microphone close to the track to calculate speed by the formula $v = d/\Delta t$ with Δt the time intervals between the passage of the first and the last bogie, and d the distances between the corresponding bogies. Instead of measuring sound pressure during the train pass-by by an extra microphone, a similar technique to obtain the time history of the pass-by is introduced which is to measure the vertical acceleration level of the rail ($AL_{eq,T}$). And thanks to this measurement technique, we can also investigate the effect of the FSTs on the rolling noise. Nevertheless, the rail acceleration measurement is difficult to implement since the acceleration sensor cannot be placed on the rail during traffic operation. To solve this problem, the night before the day of formal measurements but after the end of the traffic operation, the acceleration sensor was adhered to the tested rail foot. It was connected to a data acquisition system that uploaded signals to the network. In this way, the data would be downloaded from the network on the measurement day in order to monitor the vertical vibration of the rail during the period of traffic operation. The acceleration signals were recorded by a piezoelectric acceleration sensor shown in Figure 3.2(b), of which the maximum measurement acceleration is limited to $500g$. The signals were sampled at 5120 Hz based on the Nyquist Theorem. The each record was started automatically two seconds ahead of a trigger from the bump generated by the first bogie pass-by, and lasted for 30 seconds. We also guaranteed that the records of vibration signals and the recordings of sound pressure signals were in sync.

3.2.3 Implementation

The measurements at the sites without and with a barrier were conducted on sunny days six days apart; the meteorological conditions were not significantly different between the two measurement days and thus were not measured in our work. Due to a limitation on the number of apparatus, four microphones were fixed on a long upright pole to simultaneously measure sound pressure at the same horizontal distance from the source but different vertical distances, e.g. at the same time measuring sound pressure at receiver M1-4, M1-3, M1-2 and M1-1(shown in Figure 3.2(a)). Then this pole was moved farther from the source, to record sound at the other two horizontal distances. All the measurements were performed only for the duration of trains passing through the measured cross-section. The start point and end point of each sound record were determined manually at first (by the observation of the naked eye), which was the moment when the train nose travelled close to the measured cross-section and the time when the tail of the train had already left for several seconds, respectively. The pass-by duration of each record was subsequently shortened by the measured results of rail vibration accelerations. All the measurements at each horizontal distance were repeated 10 times or more to ensure the statistical representativeness of the sample. In addition, all the apparatus including an acoustic amplifier, an electrical charge amplifier, sound pressure collecting equipment and an A/D data collection card met the requirements of EN 61672-1 and the microphones complied with IEC 61672 class 1.

3.3 Measured results and discussion

It is easy to imagine that during the measurement, trains passed through the measured section with different speeds, but the difference between two train speeds was not too large. However, despite this, since the train speed has a great influence on the sound pressure level of rolling noise, the differences cannot be ignored. Hence the speed dependence will be studied before assessing the acoustic performance of the nearly-enclosed prototype. By the dependence curve, A-weighted equivalent level at each receiver for different speeds $L_{Aeq,pass}(V)$ will be adjusted to those for a reference speed $L_{\mathrm{Aeq,pass}}(V_{\mathrm{ref}})$, and the evaluation of the acoustic performance for the nearly-enclosed prototype in the realistic environment will be more precise. In this section, the speed-corrected attenuation for each receiver will be calculated in order to present a global view of the barrier effect, including that in the near and far field. To understand the frequency characteristics of the URT noise and the attenuation of the barrier, one-third octave analysis will also be carried out.

3.3.1 $L_{\mathrm{Aeq,pass}}$ and its train speed dependence

Train speed calculation

As mentioned previously, the train speed for each record was calculated through the measured time histories of rail vibration acceleration level $AL_{\mathrm{eq,T}}$. To identify the pass-by of every bogie, the recorded signals were averaged at $100ms$ intervals. Two examples of the time histories for $AL_{\mathrm{eq,T}}$ are shown in Figure 3.3. It can be seen that the acceleration level increased gradually in the first few seconds, and then increased sharply for five to six seconds. Finally the acceleration level decreased back to the level as high as those in the first few seconds. This variation trend of acceleration level presents a vivid description of a train approaching the measured section, passing through and leaving. In the period of the pass-by, one can also notice from Figure 3.3 that there are twelve sharp peaks marked by red circles. The explanation is that when a wheel-rail contact was occurring on the measured section, the rail vertical acceleration level was increasing sharply in response to the force generated by the bogie. Since a standard train on this line has twelve bogies and their locations are fixed on the train, it is reasonable to assume that these peaks are caused by the pass-by of bogies. As the distance between the pass-by of the first and last bogie is $d = 107.6m$(as shown in Figure 3.4), the train speed for each record can be calculated by the formula $V = d/\Delta t$ with the time history of $AL_{\mathrm{eq,T}}$, assuming it is constant. Δt denotes the time period from the first peak to the last one, of which examples are shown in Figure 3.3. The acceleration sensor could detect the bump generated by the passage of a bogie

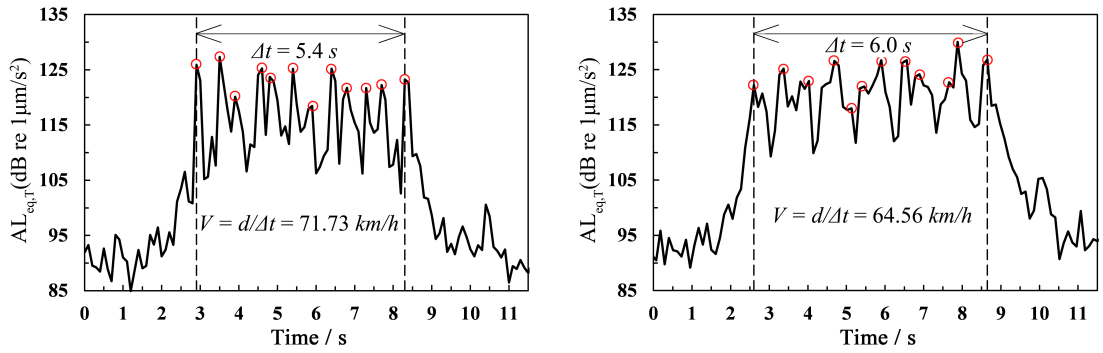

(a) On the site without barrier

(b) On the site with barrier

Fig 3.3.: Examples of time histories for the rail vertical acceleration($AL_{\mathrm{eq,T}}$)

more precisely than the extra microphone. Nevertheless, there was of course uncertainty in the speed measurement. The recorded signals would be averaged at $100ms$ intervals (with a precision of $0.1s$ only), and the duration of the pass-by varied between 5.0 and $7.0s$. Hence the uncertainty in the measurement varied between 2.3% and 2.7%, yielding a precision of $1 - 2km/h$ in the speed, which was acceptable for the purpose of this work.

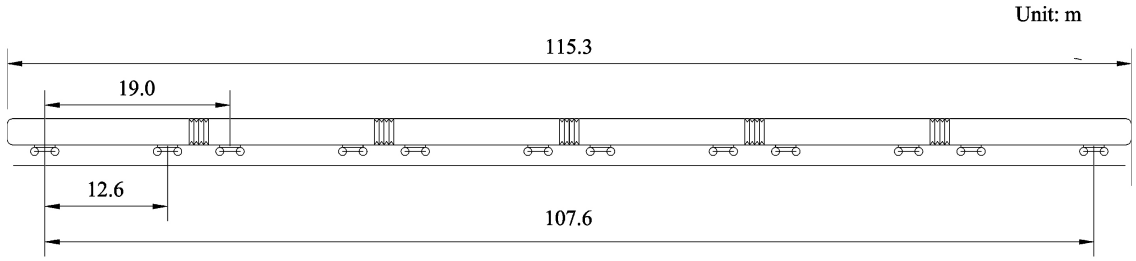

Fig 3.4.: The side view of a simplified standard train on Line 1 in Ningbo, China

Train speed can influence the rolling noise by affecting the wheel-rail interaction, hence it can also influence the vibration of the rail. The relationship between train speed and rail vibration acceleration level is now introduced. By averaging twelve peak values of $AL_{\mathrm{eq,T}}$ for each record, the mean $AL_{\mathrm{eq,T}}$s were plotted as a function of the logarithm of the corresponding train speed, as shown in Figure 3.5. The red circles in Figure 3.5 represent the mean $AL_{\mathrm{eq,T}}$s for the rails at the site without a barrier, whereas the blue crosses represent those at the site with a barrier. It can be seen that the train speed varies between $55km/h$ and $75km/h$ at both sides without and with a barrier, and the $AL_{\mathrm{eq,T}}$ increases with train speed. Besides, it is also obvious that train speeds at the site without a barrier are concentrated in a range above $70km/h$, whereas most of those at the site with a barrier are less than $65km/h$. This is due to the blockage of the nearly-enclosed barrier which can cause the rail traffic to slow. By using the least squares estimation method, two linear regression models are obtained for the relationship between the $AL_{\mathrm{eq,T}}$ and train speed at both sites. In Figure 3.5, the red dotted line represents the regression curve for the site without a barrier, whereas the blue curve is for the site with a barrier. It is noteworthy that these two regression curves almost coincide with each other. In addition, those significant deviations between the regression curves and the measured results are probably due to wheel and rail defects.

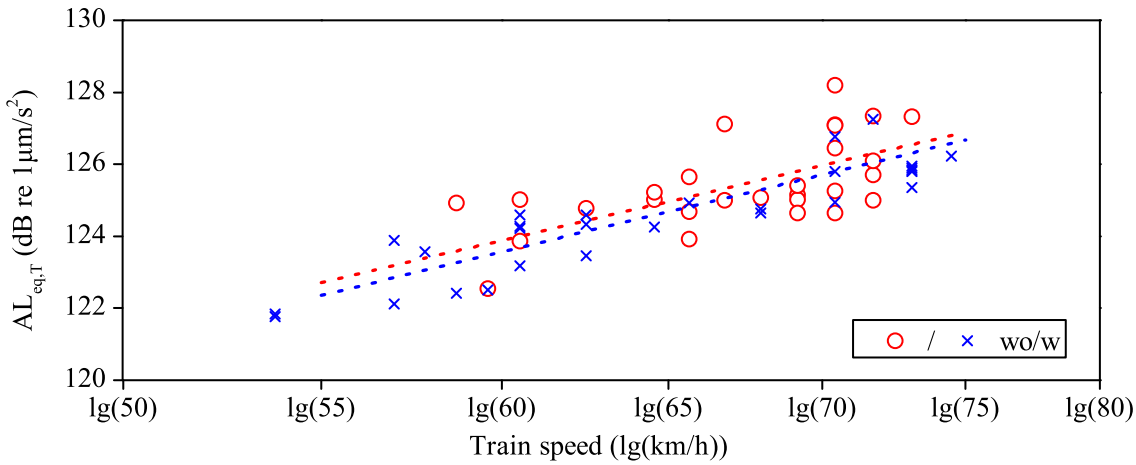

Fig 3.5.: The relationship between $AL_{\mathrm{eq,T}}$ and train speed at both sites

The regression curves also give us an opportunity to study the FST effect on the rolling noise. The FST effect on the $AL_{\mathrm{eq,T}}$ is correlated with several parameters like the type of floating slab, the train speed, etc., and their relationships are difficult to explain by a simple formula[207]. But it is certain that it can insulate the vibration energy from the viaduct structure, resulting in the vibration energy transmitting back to the fastenings, the tracks and the vehicles. Therefore, as introduced in Section 3.2.1, the $AL_{\mathrm{eq,T}}$ for the site with a barrier must be on average higher than that for the site without a barrier when a train is passing by at the same speed. Obviously, it is quite easy to see from Figure 3.5 that with the same speed, the $AL_{\mathrm{eq,T}}$ for the site with a barrier(red dotted curve) is indeed higher than that for the site without a barrier(blue dotted curve), but the difference between them is less than 0.5dB. Hence it is reasonable to believe that the FST has a negligible influence on the rail vibration for all the configurations examined when trains were passing by at speeds from $55km/h$ up to $75km/h$. It is also indicated that the rolling noise at the site with a barrier has little dependence on the FST, which makes it possible to make a comparison of the measured sound pressure levels at both sites.

$L_{\mathrm{Aeq,pass}}$ calculation

The equivalent continuous A-weighted sound pressure level during the train passing by $L_{\mathrm{Aeq,pass}}$ is introduced to estimate the road/rail traffic noise. Although the introduction has been already written in the last chapter, it is referred to and detailed again in this chapter, in order to define the notations with the specifications of this case. According to the relevant norms[153, 155], it is represented by the logarithmic averaging of the sound pressure level over the corresponding time period, as given by

$$L_{\mathrm{Aeq,pass}} = 10\log_{10}\left[\frac{1}{T_p}\int_{t_1}^{t_2}\frac{p_A^2(t)}{p_0^2}dt\right] = 10\log_{10}\left[\frac{1}{N}\sum_{n=1}^{N}\frac{p_A^2(n)}{p_0^2}\right] \tag{3.1}$$

where T_p denotes the duration of a train passing through the measured section, t_1 is the starting time when the first car head enters the measured cross-section and t_2 is the ending time when the last car tail leaves the measured cross-section. $p_{\mathrm{A}}(t)$ denotes A-weighted instantaneous sound pressure at t second, and p_0 is the reference sound pressure (usually $20\mu Pa$). The last term is a discretization, where N denotes the sampling points in the pass-by duration. This discretization equation is employed for the measurement analysis to handle the measured data in this section.

To get a more precise $L_{\mathrm{Aeq,pass}}$, the duration T_p in the equation must be strictly equal to the period of a train pass-by in reality. With the help of the known train speed V calculated in the last section, the duration over which the equivalent level is calculated can be given by $T_p = D/V$ with $D = 115.3m$ the total length of a standard train. Nevertheless, to determine t_1 and t_2 is a technically demanding task. For each record, t_1 is the moment

$\Delta t_1 = d_1/V$ ahead of that for the first bogie pass-by with $d_1 = 3.85m$ whereas t_2 is the moment $\Delta t_2 = d_2/V$ behind that of the last bogie pass-by with $d_2 = 3.85m$. Figure 3.6 presents examples of time histories of A-weighted sound pressure level for receiver M1-4 at both sites, which were recorded at the same time with the examples of $AL_{\mathrm{eq,T}}$ in Figure 3.3. The two dotted lines in each sub-figure represent the starting point and the ending point, respectively. It can be seen from Figure 3.6 that the pass-by level increases considerably when a train is passing through the measured section at the site without a barrier, whereas at the site with a barrier there is a small increase on the pass-by level. These increases are almost synchronous with those for the rail vibration acceleration levels, which can be explained appropriately by a train pass-by. Thus, the measurement technique to measure rail accelerations for determining the time period of a train pass-by is accurate and reasonable, which can be generalized to the in-situ measurements.

Then the truncated time histories of sound pressure between the two dotted lines were filtered by an A-weighting filter in the audio frequency range 20Hz-20kHz, becoming the A-weighted instantaneous sound pressure $p_{\mathrm{A}}\,(t)$. By using Eq ((3.1)), the $L_{\mathrm{Aeq,pass}}$ for each record was finally worked out, of which examples are marked by red lines in Figure 3.6. Obviously, the $L_{\mathrm{Aeq,pass}}$ shows the mean characteristics of the pass-by level in the time history, which can be a good indicator to describe the rail traffic noise. As a consequence, all the measured results at both sites were analyzed by this method.

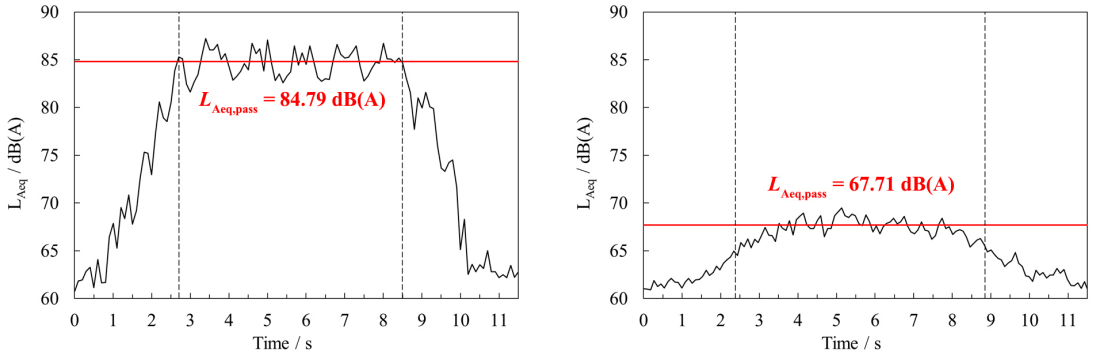

(a) On the site without barrier

(b) On the site with barrier

Fig 3.6.: Examples of time histories for A-weighted level during a train pass-by for receiver M1-4, which were recorded with the examples for $AL_{eq,T}$ in Figure 4 at the same time

The calculation of $L_{\mathrm{Aeq,pass}}$ also give us an opportunity to study the interference of the background noise. As presented in Section 3.2.1, the background noise may have a serious influence on the estimation of the rail traffic noise, particularly for the receivers far from the railway lines since the rail traffic noise declines significantly with source-receiver distance. In this measurement, the distances between source and receiver for M3-1, M3-2, M3-3 and M3-4 are over 55 meters, much larger than those for other receivers. Hence the measured $L_{\mathrm{Aeq,pass}}$ for M3-1, M3-2, M3-3 and M3-4 could be relatively less affected by the train pass-by, but influenced more seriously by the background noise. To make it clear, we made

a comparison between the measured $L_{\mathrm{Aeq,pass}}$ and the background noise for M3-1, M3-2, M3-3 and M3-4 at the sites without and with a barrier, respectively. To be comparable to each other, the $L_{\mathrm{Aeq,pass}}$ was indicated by an average of several records, since the effective measured times for each receiver were at least 10, while the background noise was indicated by $L_{\mathrm{Aeq,bg}}$ for these receivers within 30 seconds during which no trains were passing through the section. The averaging method for $L_{\mathrm{Aeq,pass}}$ is given as,

$$L_{\mathrm{Aeq,pass}} = 10\log_{10}\frac{1}{n}\sum_{i=1}^{n}10^{0.1L_{\mathrm{Aeq,pass},i}} \tag{3.2}$$

where $L_{\mathrm{Aeq,pass},i}$ denotes $L_{\mathrm{Aeq,pass}}$ for the given receiver at the ith time.

The $L_{\mathrm{Aeq,pass}}$s, the $L_{\mathrm{Aeq,bg}}$s and their differences for M3-1, M3-2, M3-3 and M3-4 at the sites without and with a barrier are listed in Table 3.1. One can notice that the differences for each receiver at the site with a barrier are much smaller than those at the site without a barrier. Among all the differences listed, the minimum is 12.36dB(A) for receiver M3-3 at the site with a barrier. On the basis of the previous discussion in Section 3.2.1, if the difference between the measured results and the background noise is more than 9dB, the error on the attenuation of the noise barrier is less than 0.5dB. Therefore, the interference of the background noise for M3-1, M3-2, M3-3 and M3-4 is less than 0.5dB, which is sufficient for the purpose of this chapter. Since the background noise has much smaller influence on other measured receivers, we can conclude that the influence of background noise could be neglected in the following analysis. Furthermore, all the sufficiently large differences between the $L_{\mathrm{Aeq,pass}}$s and the $L_{\mathrm{Aeq,bg}}$s also show our effective control for the road traffic noise during the measurement, and the suitable measured section where the train was passing through with a sufficiently large speed.

Tab 3.1.: Part of the $L_{\mathrm{Aeq,pass}}$s, the $L_{\mathrm{Aeq,bg}}$s and their differences(unit: dB(A))

Site	Receiver	$L_{\mathrm{Aeq,pass}}$	$L_{Aeq,bg}$	Difference
Without a barrier	M3-4	71.47	50.76	20.71
	M3-3	66.04	44.99	21.05
	M3-2	69.65	48.56	21.09
	M3-1	75.07	48.84	26.23
With a barrier	M3-4	60.91	47.16	13.75
	M3-3	56.71	44.35	12.36
	M3-2	60.94	47.72	13.22
	M3-1	60.16	46.84	13.32

Speed dependence

The discussion in the last two subsections and 4.2 indicates that it is reasonable to ignore the influence of the FST effect on the rolling noise and the interference of background noise. In these circumstance, the measured sound pressure for each receiver at the sites without and with a barrier are comparable. Since train speed varies from $55km/h$ to $75km/h$, based on the discussion of the source types in Chapter 1, the rolling noise must be the decisive contribution to the measured $L_{\mathrm{Aeq,pass}}$. Figure 3.7 illustrates the relationship between train speed and the $L_{\mathrm{Aeq,pass}}$ for M1-4 at both sites. It is clear that the $L_{\mathrm{Aeq,pass}}$ increases with train speed at both sites, and the relationship between the $L_{\mathrm{Aeq,pass}}$ and the logarithm of train speed seems to be linear. As there is a prediction formula for the relationship between the rolling noise and the train speed $L_{\mathrm{Aeq}}(V) = 30\log_{10}(V/V_{\mathrm{ref}}) + L_{\mathrm{Aeq}}(V_{\mathrm{ref}})$, that is widely used to extrapolate noise emission of classical trains[202], here we can also perform a similar linear regression model, given as,

$$L_{\mathrm{Aeq,pass}}(V) = \alpha\log_{10}(V/V_{\mathrm{ref}}) + L_{\mathrm{Aeq,pass}}(V_{\mathrm{ref}}) \tag{3.3}$$

where V_{ref} denotes the reference speed and $L_{\mathrm{Aeq,pass}}(V_{\mathrm{ref}})$ is the corresponding reference level.

Assuming that the reference speed equals to 65km/h, the calculated results for the reference level $L_{\mathrm{Aeq,pass}}(V_{\mathrm{ref}})$, the slope α and their uncertainties for each receiver at the site without and with a barrier, are given in Table 3.2. It is noteworthy that the slope α for all the receivers at the site without a barrier are much closer to the value of 30 that is commonly used in the prediction formula for the rolling noise, whereas those for the site with a barrier are nearly 20. It can be concluded that firstly, the measured results at the site without a barrier conform to the typical relationship between the rolling noise and train speed; secondly, the presence of the nearly-enclosed barrier can directly affect the relationship between train speed and the $L_{\mathrm{Aeq,pass}}$ in the surroundings, only reducing the speed dependence of the $L_{\mathrm{Aeq,pass}}$ but maintaining linear characteristics.

The regression model for M1-4 at the site without a barrier is plotted by a red dotted curve in Figure 3.7. The results show that the correlation coefficient R^2 between the measured(the red circles) and predicted results (the red dotted curve) equals 0.85, which is acceptable. Besides, it confirms again that the rolling noise is the principal source of the measured $L_{\mathrm{Aeq,pass}}$ in the surroundings of the rail traffic. Accordingly, the reference level $L_{\mathrm{Aeq,pass}}(V_{\mathrm{ref}})$, when the reference train speed is assumed as 65km/h, can be regarded as the speed-corrected $L_{\mathrm{Aeq,pass}}$ in the next discussion of this measurement. Then the speed-independent attenuation can be estimated by the difference of the speed-corrected $L_{\mathrm{Aeq,pass}}$ for a given receiver between the site without and with a barrier. Table 3.2 also shows the single rating of barrier attenuation for each receiver. The value for the attenuation varies significantly with the receiver position, as well as that for the speed-corrected $L_{\mathrm{Aeq,pass}}$.

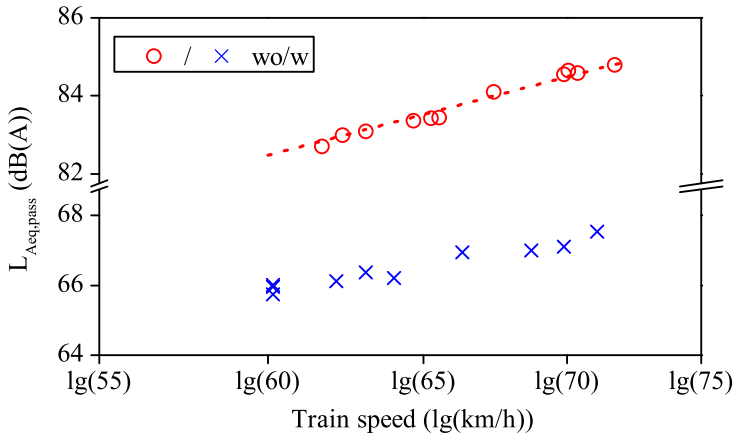

Fig 3.7.: The relationship between $L_{\mathrm{Aeq,pass}}$ for M1-4 and train speed

Tab 3.2.: Speed-corrected $L_{\mathrm{Aeq,pass}}\,(V_{\mathrm{ref}})$ for each receiver at the site with a barrier and the site without a barrier($V_{\mathrm{ref}} = 65km/h$,unit: dB(A))

Receiver	Site type	$L_{Aeq,pass,ref}$	coefficient α	The estimate for attenuation
M1-4	Without a barrier	83.39±0.20	31.60±4.95	16.69±0.40
	With a barrier	66.70±0.20	18.84±3.72	
M1-3	Without a barrier	72.90±0.25	29.21±5.57	11.84±0.47
	With a barrier	61.06±0.22	18.34±4.17	
M1-2	Without a barrier	73.04±0.39	28.54±6.77	8.35±0.60
	With a barrier	64.69±0.20	18.84±3.72	
M1-1	Without a barrier	67.85±0.20	27.10±8.17	6.33±0.67
	With a barrier	61.51±0.12	18.72±3.13	
M2-4	Without a barrier	73.45±0.63	29.18±8.48	10.70±0.96
	With a barrier	62.75±0.33	19.54±5.19	
M2-3	Without a barrier	67.45±0.59	27.51±7.90	9.79±0.95
	With a barrier	57.67±0.36	21.46±5.72	
M2-2	Without a barrier	70.61±0.57	30.56±8.08	8.88±0.85
	With a barrier	61.73±0.28	21.87±4.86	
M2-1	Without a barrier	71.62±0.49	26.98±6.95	9.16±0.84
	With a barrier	62.46±0.35	20.23±5.48	
M3-4	Without a barrier	69.57±0.53	28.34±9.47	8.68±0.69
	With a barrier	60.89±0.16	17.15±3.00	
M3-3	Without a barrier	64.17±0.50	27.54±9.07	8.03±0.95
	With a barrier	56.14±0.45	18.22±5.63	
M3-2	Without a barrier	68.35±0.40	26.59±7.67	7.64±0.85
	With a barrier	60.72±0.45	19.66±5.75	
M3-1	Without a barrier	73.03±0.47	30.69±8.91	12.07±0.72
	With a barrier	60.95±0.25	18.53±3.86	

Since the aim of this chapter is to evaluate the attenuation of the nearly-enclosed prototype for urban rail traffic noise, these variations with the horizontal and vertical source-receiver distance will be discussed in more detail in the next section.

3.3.2 A-weighted single ratings analysis

The speed-corrected $L_{\mathrm{Aeq,pass}}$s obtained for each receiver at both sites are shown in Table 3.2. For the receivers at the site without a barrier, the maximum $L_{\mathrm{Aeq,pass}}$ is 83dB(A) for receiver M1-4, which confirms the prediction in Section 3.2.2 that the receiver located higher than the top of the flange and at the closest horizontal distance among the receivers examined, would be affected the most significantly by the rail traffic noise. As the value is much higher than the limit value (70dB(A)) stated on the Chinese norm GB3096-2008[209], it is absolutely necessary to reduce it by some absorptive or insulative treatments. The second maximum $L_{\mathrm{Aeq,pass}}$ is approximately 73dB(A) for both M2-4 and M3-1. Since M2-4 was located as high as M1-4, it is reasonable that the $L_{\mathrm{Aeq,pass}}$ for M2-4 is relatively higher. However, receiver M3-1, located at the farthest vertical and horizontal source-receiver distance among all the receivers examined, was also affected significantly by the rail traffic noise. Since the interference of background noise to the $L_{\mathrm{Aeq,pass}}$ for M3-1 can be ignored and receiver M3-1 was located the closest to the highly protected area, it is notable that the rail traffic noise had sufficient energy to transmit to the highly protected area about 56 meters away; an effective noise barrier must be designed to reduce the $L_{\mathrm{Aeq,pass}}$ for the highly protected area.

To study the change law of the $L_{\mathrm{Aeq,pass}}$ along with the receiver position more clearly, the speed-corrected $L_{\mathrm{Aeq,pass}}$ for each receiver at both sites are arranged according to the receiver positions in reality, as shown in Figure 3.8. The source is assumed to be located on the left of this figure. The black bars represent the $L_{\mathrm{Aeq,pass}}$ for the given receiver at the site without a barrier, whereas the white bars represent those at the site with a barrier. It can be seen that for the receivers at the site without a barrier, the speed-corrected $L_{\mathrm{Aeq,pass}}$ decreases with the increased horizontal distance in rows M-2, M-3 and M-4, in accordance with the distance-decay law of sound in air. While the opposite trend can be observed in the row M-1 where the receivers were located 1.2 meters above ground. This opposite trend is mainly due to the barrier effect of the viaduct. Since the location of rolling noise was lifted by the viaduct around 10 meters above the ground, there must be a great shadow zone below the viaduct. And the shadow effect must decrease with the increased horizontal distance from the bottom of the viaduct. As a consequence, the measured results for row M-3 accord with the shadow effect caused by the viaduct.

For the receivers at the site with a barrier, the speed-corrected $L_{\mathrm{Aeq,pass}}$s shown in Table 3.2 are all acceptable since they are lower than the limit value 70(A). As observed from the white bars in Figure 3.8, there is a similar pattern to the black bars that the speed-corrected

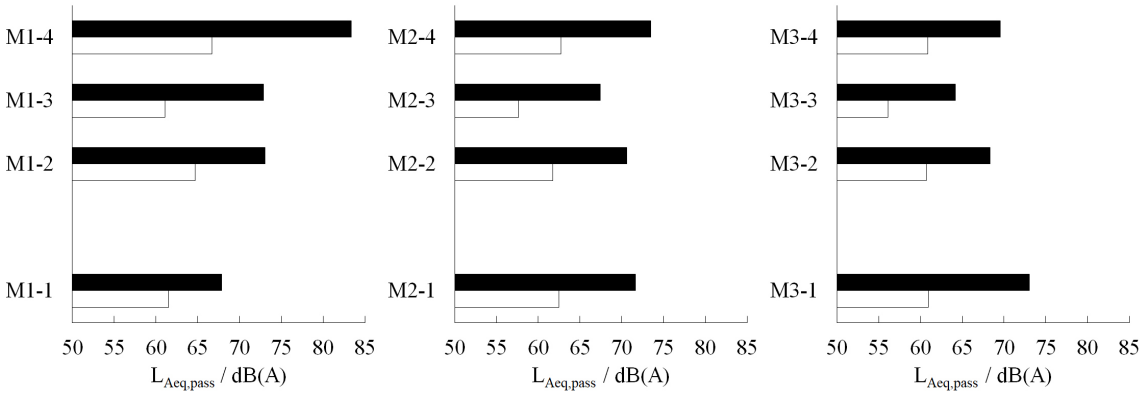

Fig 3.8.: The speed-corrected $L_{\mathrm{Aeq,pass}}$ for each receiver at the sites without and with a barrier(black bars: at the site without a barrier, white bars: at the site with a barrier)

$L_{\mathrm{Aeq,pass}}$ in each row(M-2, M-3 and M-4) decreases with horizontal distance increasing from the source. However, the $L_{\mathrm{Aeq,pass}}$s for the receivers in row M-1 at a level around 61 dB(A) with little difference, which can indicate that at the site with a barrier, the sound pressure level close to the ground was little affected by the rail traffic noise. This variation trend along with the horizontal distance differs completely from the change law in row M-1 at the site without a barrier, from which it can be deduced that the employment of the nearly-enclosed barrier had an effective influence on the $L_{\mathrm{Aeq,pass}}$ for the places close to the ground, reducing the second maximum level(for M3-1) at the site without a barrier to the same as that for M1-1. Hence it can be concluded that the nearly-enclosed barrier was effective in preventing the rail traffic noise from transmitting to the highly protected area.

The estimate of barrier attenuation for each receiver are listed in Table 3.2, which is the difference of the speed-corrected $L_{\mathrm{Aeq,pass}}$ for the given receiver at the site without and with a barrier. The maximum is over 15dB(A) for receiver M1-4 where the $L_{\mathrm{Aeq,pass}}$ is also the highest at the site without a barrier. The second maximum is around 12dB(A) for receiver M1-3 where the $L_{\mathrm{Aeq,pass}}$ is also the second highest at the site without a barrier. For other receivers the attenuation of the nearly-enclosed barrier are less than 10dB(A). To understand the change law along with the source-receiver distance, Figure 3.9 shows the attenuations arranged according to the receiver positions, identical to the arrangement for the $L_{\mathrm{Aeq,pass}}$ in Figure 3.8. It can be seen that with the decreased height above the ground, the attenuation for the receiver in column M1- deceases significantly. The attenuation for M1-1 is only 6.3 dB(A) since the $L_{\mathrm{Aeq,pass}}$ was reduced mainly by the barrier effect of the viaduct rather than the real noise barrier. Again, the attenuation has the same variation trend as $L_{\mathrm{Aeq,pass}}$ that the attenuation decreases with the increased horizontal distance in rows M-4, M-3 and M-2, so does the opposite trend in the row M-1. As a result, in general, the change law of the attenuation along with the receiver position is almost the same as that of the $L_{\mathrm{Aeq,pass}}$ at the site without a barrier. In conclusion, these findings confirm the fact that by the single rating analysis, the nearly-enclosed barrier was indeed effective against the rail traffic noise.

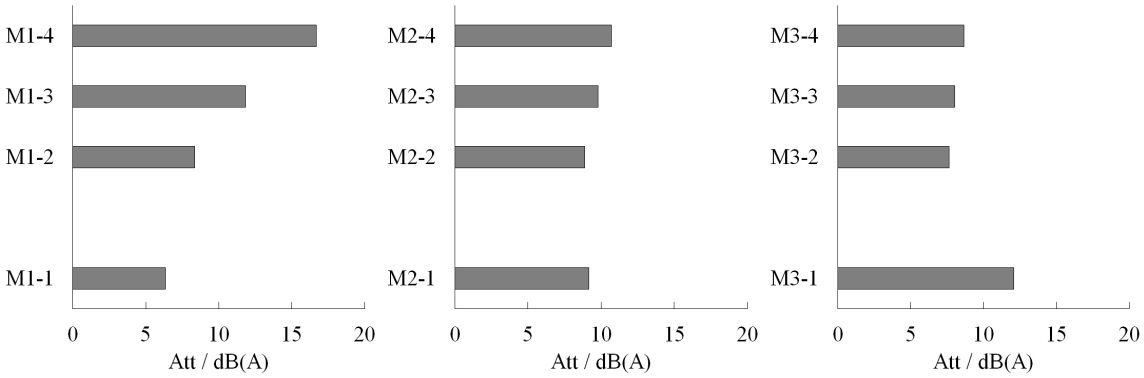

Fig 3.9.: Attenuation in dB(A) for each receiver of the nearly-enclosed barrier

3.3.3 1/3 octave spectra analysis

To understand the frequency characteristics of the rail traffic noise and the barrier performance, one-third octave spectrum analysis method is presented in this section to analyze the measured results. Firstly, combined with the frequency range of interest(50-5000 Hz) in Chapter 1, a comparison between the recorded sound signals and background noise is investigated in order to determine a suitable frequency range for performing the spectrum analysis. Then one-third octave spectrum for each receiver at each site is performed within the determined range. In the end, the barrier attenuation for each receiver is evaluated using one-third octave analysis.

In general, sound pressure in the one-third octave band of f_c is given as,

$$\mathrm{SPL}\left(f_c\right) = 10\log_{10}\int_{f_l}^{f_u}\frac{\left|p_{\mathrm{wo/w}}\left(f\right)\right|^2}{p_0^2}df \tag{3.4}$$

where $p_{\mathrm{wo/w}}\left(f\right)$ denotes the sound pressure at the site without a barrier or at the site with a barrier in the frequency domain, which was calculated from the time history of sound pressure by using the Fast Fourier transform (FFT) method. f_u and f_l denote the upper limit and the lower limit of 1/3 octave band where the central frequency is f_c, respectively. p_0 denotes the reference pressure with the value of $20\mu Pa$ in common.

Sound pressure levels(SPLs) for each receiver at each site were solved in the frequency range from 20Hz to 20kHz. The results of background noise were carried out as well. To know the interference of the background noise, the simplest method is to compare the pressure spectra of background noise with that for M3-1 at the site without and with a barrier, respectively (shown in Figure 3.10), since receiver M3-1 was located at the farthest distance from the source. It can be seen that in each one-third octave band, the SPL for M3-1 at the site without a barrier is higher than that for the background noise except from the band of 20Hz. And at the site with a barrier, the SPL for M3-1 are all higher than the background noise as well. The frequency range stated in the ISO standard 10847-1997 is recommended from

50Hz to 50kHz[153], within which the differences between the measured results and the background noise are all over 10dB. Hence, the error for the attenuation will be less than 0.5dB and it is acceptable to carry out the one-third octave analysis within this range from 50Hz to 5000Hz.

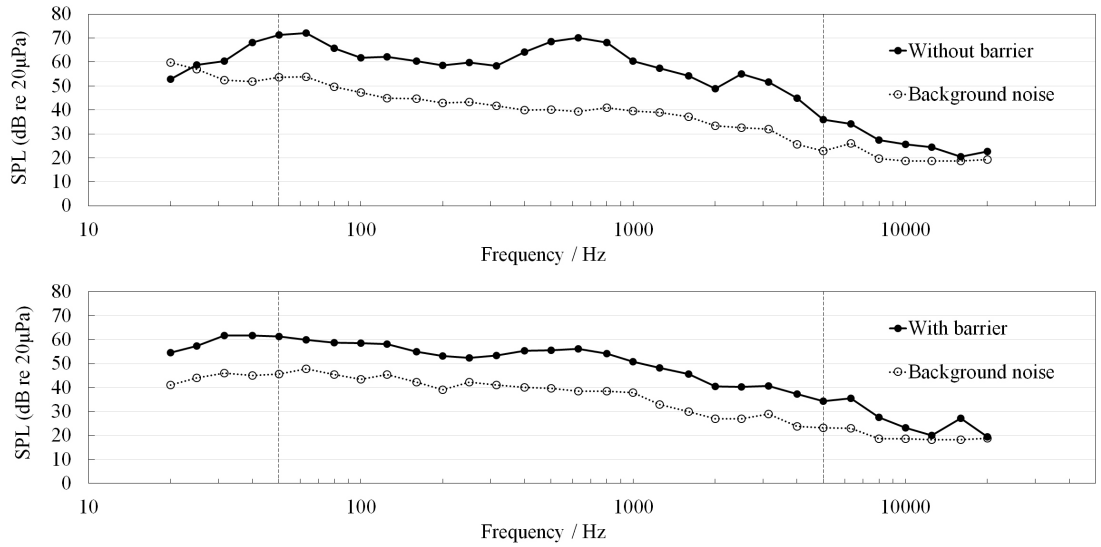

Fig 3.10.: Sound pressure spectra for M3-1 in the frequency range of 20Hz-20kHz(upper: at the site without a barrier; lower: at the site with a barrier)

Sound pressure level

The one-third octave spectra for each receiver at the site without a barrier are shown in Figure 3.11. Each sub-figure presents three curves for the receivers with the same height but different horizontal distances from the source. It can be seen that on the whole, SPL decreases with the increased frequency as usual. However, there is a significant increase in the range of 315-1000Hz regardless of receiver position. And another small increase is from 2000Hz to 4000 Hz for every receiver, except for M1-1 and M1-2. These two ranges are in good agreement with those of peaks measured by Javad S. and Araz H. for rolling noise of the train TM3-51 in the case of a ground track[210]. Coincidentally, Thompson[204] considered the frequency range of rolling noise to be assumed as 100-5000Hz, which covers the range of our measured increases. Hence, it is reasonable to believe that the rolling noise for the train operating on Metro 1 in Ningbo was measured in the frequency range of 315-1000Hz and 2000-4000Hz, with two peaks at 500Hz and 2500Hz, respectively. As observed in Figure 3.11(a)(b), SPL for the rolling noise decreases significantly with the increased horizontal distance from the source, while in Figure 3.11(c)(d) the change of the horizontal distance has little effect on the level of the rolling noise. And with the decreased height of receivers in column M1-, SPL for the rolling noise decreases considerably due to the barrier effect of the viaduct. However, one can notice that SPL for M3-1 in the range of

the rolling noise (2000- 4000Hz) are considerable compared with the other two receivers close to the ground, which confirms the assessment in Section 3.3.2 that M3-1 was indeed affected greatly by the rail traffic noise.

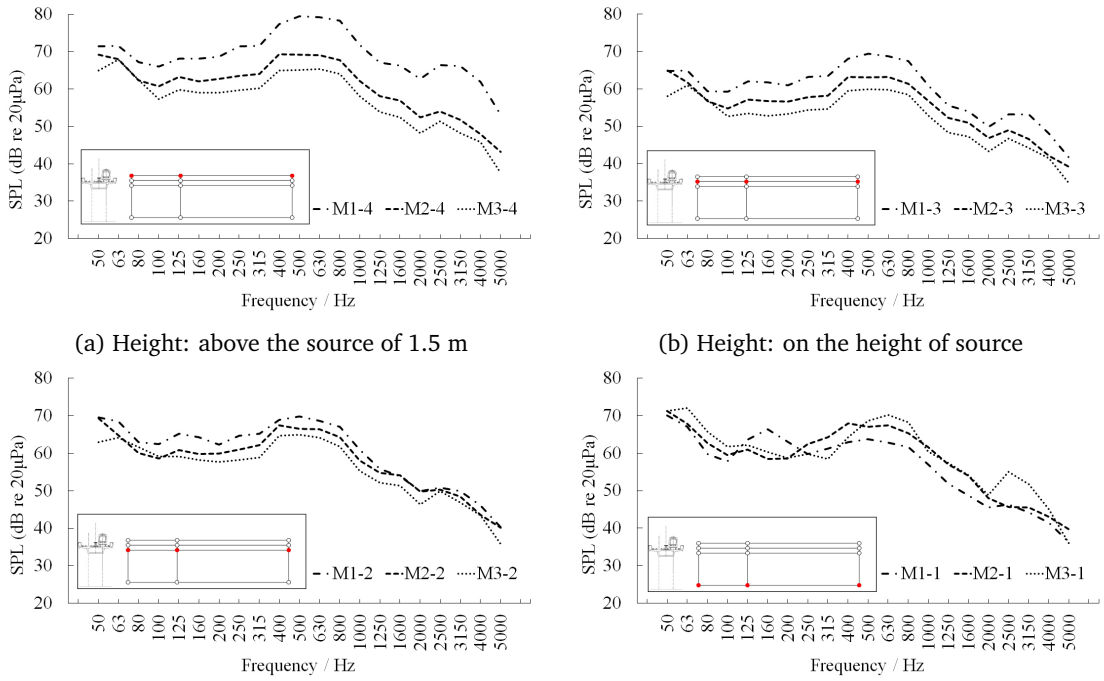

(a) Height: above the source of 1.5 m

(b) Height: on the height of source

(c) Height: below the source of 1.5 m

(d) Height: 1.2 m above the ground

Fig 3.11.: Sound pressure spectra for the receivers at the site without a barrier

Besides observing the rolling noise, we can also see from Figure 3.11 that at 50-200Hz, SPL for each receiver is as high as that for the rolling noise. As introduced in Section 3.2.1, most of the low-frequency noise came from the structural noise of the viaduct generated by the train passing by. Since the low-frequency noise attenuates slower than the high frequencies in air and thus transmits over longer distances, the SPL at low frequencies for each receiver at a given height are almost the same with different horizontal distances. And the levels of the low-frequency noise are even higher than those of the mid frequencies for the rolling noise at the farther distance from the source. Hence the SPL at low frequencies for each receiver are almost identical, with little effect by the change of the source-receiver distance.

Secondly, the one-third octave spectra for each receiver at the site with a barrier are shown in Figure 3.12. On the whole the SPL decreases with the increased frequency as usual. However, it is worthy of note that the two measured increases in the range of 315-1000Hz and 2000-4000Hz in Figure 3.11 do not appear in this figure, which is the most significant difference compared with Figure 3.11. It is indicated that the nearly-enclosed barrier was effective in reducing the exposure to the measured rolling noise, though there is still a small peak in the band of 630Hz at only 2dB. In Figure 3.12, SPL for each receiver is still

very high at low frequencies, which is possibly to observe because the reduction effect of a conventional noise barrier is good for noise at mid- and high frequencies but bad for low-frequency noise. Besides, SPL for each receiver in row M-4 decreases with the increased horizontal distance, whereas in row M-1, SPL for all the receivers are almost identical to each other. It means that with the employment of the nearly-enclosed barrier, the receivers close to the traffic line were still affected a little by the rail traffic noise but those close to the ground were almost unaffected.

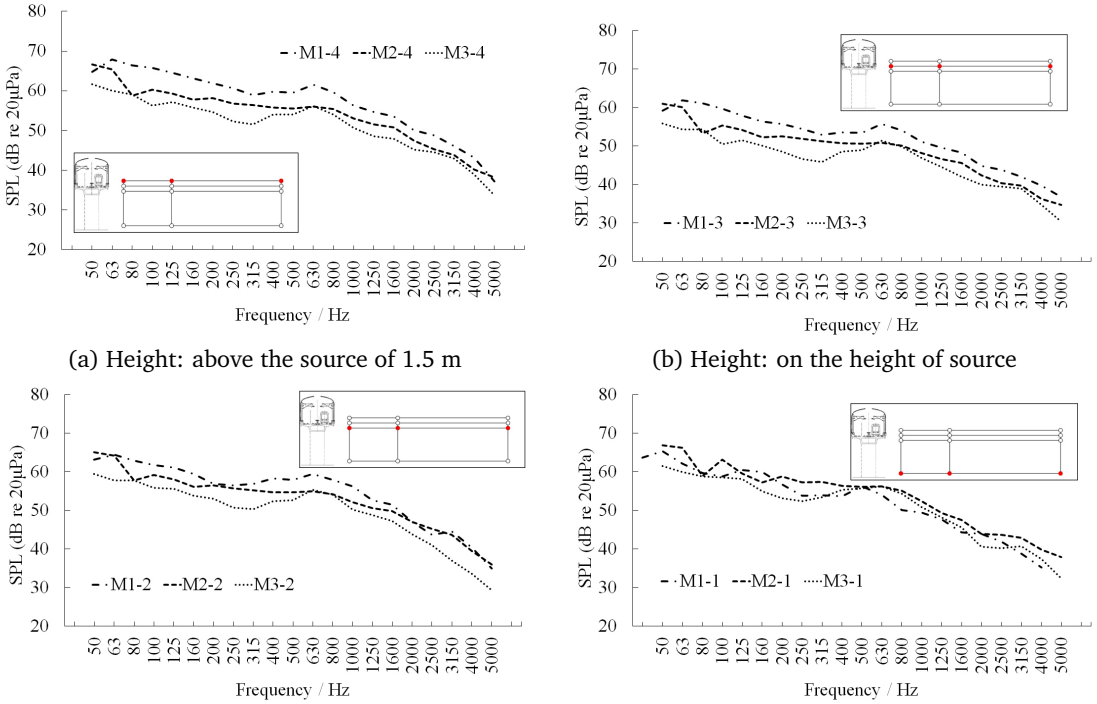

(a) Height: above the source of 1.5 m

(b) Height: on the height of source

(c) Height: below the source of 1.5 m

(d) Height: 1.2 m above the ground

Fig 3.12.: Sound pressure spectra for the receivers at the site with a barrier

As can be seen from the results of the one-third octave analysis for SPL at the site without and with a barrier, the frequency range of measured rolling noise was identified. And the role of the nearly-enclosed barrier was brought into full play for the rolling noise. At the site without a barrier, it is for the whole frequency range that the rail traffic noise affected both the near and far field of the surroundings, whereas at the site with a barrier, the effect of the rail traffic noise was only concentrated at low frequencies. Hence besides the conclusion in Chapter 2, it is emphasized again that the one-third octave analysis must be expected in further studies of rail traffic noise since the A-weighted single rating always devalues the effect of the low-frequency noise, and the dominant frequency range of measured rolling noise cannot be identified by the single rating.

Barrier attenuation

The one-third octave spectra for the barrier attenuation which is expressed by the difference between the SPL for a given receiver at the site without and with a barrier, is supposed to be worked out when the solutions of SPL at both sites are obtained. In order to simplify the calculation method, the attenuation in the band of f_c can be calculated by the ratio of the quadratic sum of sound pressure for a given receiver at the site without and with a barrier, given by,

$$Att\left(f_{\mathrm{c}}\right)=10\log_{10}\left(\frac{\int_{f_{\mathrm{l}}}^{f_{\mathrm{u}}}\left|p_{\mathrm{wo}}^{2}\left(f\right)\right|df}{\int_{f_{\mathrm{l}}}^{f_{\mathrm{u}}}\left|p_{\mathrm{w}}^{2}\left(f\right)\right|df}\right) \tag{3.5}$$

where p_{wo} denotes sound pressure for a given receiver at the site without a barrier and p_{w} denotes sound pressure for a given receiver at the site with a barrier.

By using Equation (3.5), the one-third octave spectra of the barrier attenuation for each receiver position are carried out and shown in Figure 3.13. Due to the multitude of receiver positions, the spectra for the barrier attenuation are also organized by the row number of the receivers. In Figure 3.13, firstly the attenuation in the dominant frequency range of the rolling noise is taken seriously. It can be seen that in the range of 315-1000Hz, the attenuation for all the receivers are sufficiently high, with a maximum value of 20dB at 500Hz for receiver M1-4. And the values for the receivers in column M1- are over 15dB, whereas those for M2- and M3- are over 10dB. It is indicated that the value of the attenuation decreases with the increased horizontal distance, which is in accordance with the change law of SPL for the receivers at the site without a barrier. So, we can conclude that the nearly-enclosed prototype was effective in reducing the rolling noise in the range of 315-1000Hz in both the near and far field. To focus on another frequency range of the rolling noise(2000-4000 Hz), the maximum is also found for receiver M1-4 with the same value of 20dB but at 3150Hz. Unlike those high values in the range of 315-1000Hz, the values for other receivers are less than 10dB, except for M3-1. The attenuation value for M3-1 is 15dB at 2500Hz, less than that for M1-4. Looking back upon the SPL for M3-1 at both sites, we can find the reason that at the site without a barrier the receiver M3-1 was affected seriously by the rolling noise, which was quite different from other receivers in the far field. But at the site with a barrier, the SPL are almost the same in this range, with low values. Hence the variation trend of the attenuation is identical to that of the SPL for the receivers at the site without a barrier. As a consequence, the nearly-enclosed barrier was also sufficiently effective in reducing the rolling noise in the range of 2000-4000Hz in both the near and far field.

Apart from the attenuation in the frequency range of the rolling noise considered previously, in view of the structure-borne noise from the viaduct structure, special attention needs to be paid to the low-frequency noise. At low frequencies, it is obvious that the attenuation at first

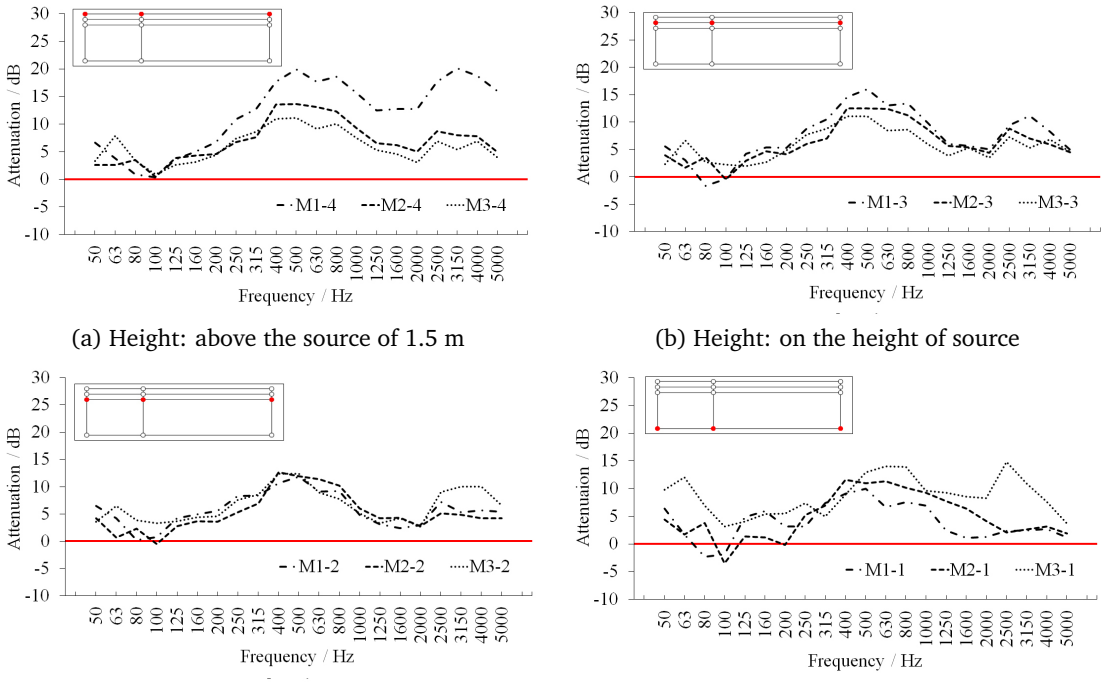

(a) Height: above the source of 1.5 m

(b) Height: on the height of source

(c) Height: below the source of 1.5 m

(d) Height: 1.2 m above the ground

Fig 3.13.: Attenuation spectra for all the receivers examined

decreases with the increased frequency from 50Hz to 100Hz, with a maximum of 12dB at 63Hz for M3-1. Since a conventional noise barrier is ineffective against low-frequency noise, these remarkable low-frequency attenuations are attributed to the FST effect in reducing the structural noise. Then the attenuation increases with the frequency from 100Hz to 200Hz, with a minimum of a negative value at 100Hz. The magnitude of the negative value is less than 5dB, which indicates that the nearly-enclosed barrier had a harmful but not remarkable effect on the low frequencies. As we discussed in a previous article[211], the resonance effect caused by the open air cavity inside a nearly-enclosed barrier resulted in extremely high levels at the resonance frequencies. And with the help of the absorbent treatment, the harmful resonance effect was simply mitigated for the mid- and high frequencies. Hence these negative values at 50-200Hz can be explained by the resonance effect which is caused by the nearly-enclosed barrier.

The following conclusions can be inferred from the one-third octave analysis above: Firstly, the rail traffic noise was identified with two important components: the mid- and high frequency noise in the range of 315-1000Hz and 2000-4000Hz, and the low frequencies at 50-200Hz. Since the train speed was measured to be 55-75km/h, the former component was considered to be caused by the rolling noise, whereas the latter was generated by the structurally borne noise. Secondly, the nearly-enclosed barrier had a sufficient effect on reducing the rolling noise transmitted to the surroundings, leading to the low values of SPL for all the receivers at the site with a barrier. Thirdly, for the structurally borne noise there were significant attenuations to be achieved at 50-80Hz, probably due to the employment of

FSTs rather than the noise barrier. And on the contrary, the nearly-enclosed barrier did harm to the noise reduction at low frequencies, resulting in the negative values of the attenuation at 100Hz, which can be caused by the resonance effect of the open air cavity.

3.4 Conclusion

A prototype of nearly-enclosed noise barrier was implemented on a viaduct on the line of Metro 1, Ningbo, China. The design of the noise barrier as well as its length were chosen essentially to reduce the impact of the traffic noise to meet the requirement of the Chinese norm. A series of pass-by measurements were taken at twelve receiver positions located in the near and far field, at a site without and with a barrier. By using a piezoelectric acceleration sensor on the rail foot, the train speed for each pass-by was measured as well.

First, a positive correlation was found between the pass-by rail vertical acceleration level and speed, with a good agreement between the regression curves at the site without and with a barrier. These results were used to not only calculate train speed for each pass-by, but also eliminate the influence of the FST effect on the rolling noise. Another positive correlation was found between pass-by A-weighted level and speed, in agreement with the prediction formula for the rolling noise. With the help of this correlation for train speed, the pass-by A-weighted level was corrected for each receiver position. It is shown that at the site without a barrier the viaduct attenuated the speed-corrected $L_{\mathrm{Aeq,pass}}$ at the positions below the viaduct, while at the site with a barrier the joint reduction noise effect of the noise barrier and the viaduct resulted in the required levels in the whole field. The nearly-enclosed barrier provides the attenuation with a maximum of 15dB(A), and a minimum of more than 5dB(A).

The frequency characteristics of the rail traffic noise and the effect of the noise barrier was studied as well in this chapter. It is found that the frequency range of the measured rolling noise is 315-1000Hz and 2000-4000Hz, and the pass-by train can induce a significant structural-borne noise of the viaduct in the range of 50-200Hz. The noise barrier provides attenuation in the range of the measured rolling noise, which yields on average an attenuation of more than 15dB. The attenuations at low frequencies come from the effect of the FST.

4 Preliminary investigations of scale model tests and 2.5-D BEM calculations

4.1 Introduction

The main purpose of this chapter is to investigate preliminarily a scale model technique and 2.5-D BEM modelling method on evaluating the acoustic performance of urban rail transit noise barriers. Section 4.2 preliminarily examines the effects of different source types on a simple straight barrier on the rigid ground, with three configurations of source and receiver positions, using a 2.5-D BEM method and an analytical solution. This analysis can provide a preliminary explanation for the comparison of different source types. In Section 4.3, a scale model technique is developed with the help of miniature loudspeakers, and a set of scaled measurements is presented with a short description of the set-up; the results and comparisons between the measured and predicted results are then discussed. Section 4.4 is devoted to the frequency dependence and longitudinal distance dependence of the barrier attenuation for the incoherent point sources, which better characterises the barrier performance in the case of incoherent point or line sources. Some conclusions are then presented in Section 4.5.

4.2 Analytical methods and 2.5-D BEM methods

In this section, our objective is to seek a much closer approximation to the real solution for the sound field due to an incoherent line source in the vicinity of a sound barrier. For simplicity, the time-dependent factor of $e^{-\mathrm{i}wt}$ is understood and omitted from the whole computation process. Suppose that the distance between the source and receiver is R, and therefore, the acoustic field for a free space is $e^{\mathrm{i}kR}/4\pi R$ assuming the customary source term of $-\delta(x-x_s)$[212]. In [212], K.M. Li sorted many different analytical models for calculating the sound diffraction by a thin infinite barrier. Among these models, one of the frequently used exact solutions was selected, which was developed by MacDonald[213], for comparison with the results predicted by the BEM approach for a one-point source. The expression of the sound field in the shadow zone was recast by Bowman and Senior[214]

in the cylindrical polar system due to the original idea solved using the spherical polar coordinate, given as follows:

$$p_D = \frac{\mathrm{i}k\,\mathrm{sgn}(\zeta_1)}{4\pi}\int_{|\zeta_1|}^{\infty}\frac{H_1^{(1)}(kR_1+s^2)}{\sqrt{s^2+2kR_1}}ds + \frac{\mathrm{i}k\,\mathrm{sgn}(\zeta_2)}{4\pi}\int_{|\zeta_2|}^{\infty}\frac{H_1^{(1)}(kR_2+s^2)}{\sqrt{s^2+2kR_2}}ds \tag{4.1}$$

where i is the imaginary number, k is the wave number of the incident wave, $H_1^{(1)}$ is the Hankel function of the first kind. ζ_1 and ζ_2 are the limits of the contour integrals which are determined by,

$$\zeta_{1,2} = \mathrm{sgn}\left(|\theta_s-\theta_r|-\pi\right)\sqrt{k\left(R'-R_{1,2}\right)} \tag{4.2}$$

where R_1 and R_2 are determined by,

$$R_{1,2} = \sqrt{r_s^2+r_r^2-2r_sr_r\cos\left(\theta_s\mp\theta_r\right)+\left(y_s-y_r\right)^2} \tag{4.3}$$

And the shortest source-edge-receiver path can be determined as,

$$R' = \sqrt{\left(r_s+r_r\right)^2+\left(y_s-y_r\right)^2} \tag{4.4}$$

where (r_s,θ_s,y_s) and (r_r,θ_r,y_r) are the cylindrical coordinates of source and receiver, respectively. Note the lack of consideration of the sound reflection induced by the ground because the solution was deduced starting from the assumption of a semi-infinite screen. Generally, sound reflection by the rigid ground or a rigid viaduct is tacitly included in the performance of a sound barrier for road/rail traffic systems. Based on the pertinent theory, the sound reflecting from the surface of the rigid ground or a rigid viaduct can be considered to radiate in terms of an image source located symmetrically with the infinite plane. Likewise, the effect on the receiver side can be described as an image receiver. Consequently, the total sound field influenced by the barrier's diffraction together with the ground's reflection is the summation of four diffracted paths when the surface is fully reflective. This symmetrical method is introduced in the post process of the calculation to allow the solution to approximate that for the case where the noise barrier is on the rigid ground in outdoor situations but not exactly the same because the barrier is semi-infinite in the analysis whereas of finite length in reality.

To model the sound field generated from coherent line, incoherent point and line sources by using a 2.5-D BEM approach, the existing program SAMRAY developed by Duhamel[176, 178] was introduced. The solution for a coherent line source is generally known as a 2-D BEM result that can easily be calculated. Then, via a Fourier-type integration, the solution for a one-point source can possibly be obtained from a series of 2-D results when all the boundaries are assumed to be acoustically rigid[176]. The calculations for incoherent line

sources can also be made by 2-D solutions, which have been discussed in [176]. Note that the solution for an incoherent line source is represented by the density of acoustic potential energy because the source is modelled as a line of uncorrelated point sources perpendicular to the cross-section of the barrier. Based on these discussions, the existing program allows calculating the radiation and the diffraction of sound fields for general 2-D and 2.5-D structures for coherent line, point and incoherent line sources.

4.2.1 Comparisons of the calculated results

Considering the totally reflective ground effect, the comparison of predictions calculated by SAMRAY with the analytical solution is described here for three cases:

1. A source and a receiver located on the totally reflective ground.

2. A source located on the ground, and a receiver 1.0 m above the totally reflective ground.

3. A source 1.0 m above the ground, and a receiver 1.5 m above the totally reflective ground.

Figure 4.1 shows diagrams of the three configurations and the 2-D coordinates of the source and the receiver. The straight barrier was assumed totally reflective as well, with a height of $1.85m$ and a thickness of $0.17m$. To compare the analytical solutions and the BEM results for a one-point source, the barrier attenuation Att_b that is the sound pressure difference between the site without and with a barrier was introduced and given by,

$$Att_b\left(f\right) = 10\log\frac{p_{\mathrm{wo}}^2\left(f\right)}{p_{\mathrm{w}}^2\left(f\right)} \tag{4.5}$$

where $p_{\mathrm{wo}}(f)$ and $p_{\mathrm{w}}(f)$ denote the sound pressure at the given receiver position in the case of the model without and with a barrier, respectively.

Figure 4.2 shows the barrier attenuation as a function of frequency calculated by each analytical or numerical model for each case. Each model was run at 0.1 Hz from 44.7 Hz to 112 Hz and at 1 Hz from 113 Hz to 5623 Hz. The red curves presented in Figure 4.2 represent the analytical solutions for the one-point source used to validate the numerical predictions calculated by SAMRAY. Clearly, the analytical solutions have good agreement with those predicted by the BEM at low frequencies. However, at mid- and high frequencies, the analytical solution becomes much lower, and the variation period becomes much longer. The reason for this result lies in the assumption of the barrier thickness. At the beginning of the analytical calculation, the barrier was assumed to be thin with a thickness of zero. However, in the calculation process of the 2.5-D BEM modelling, the thickness could be

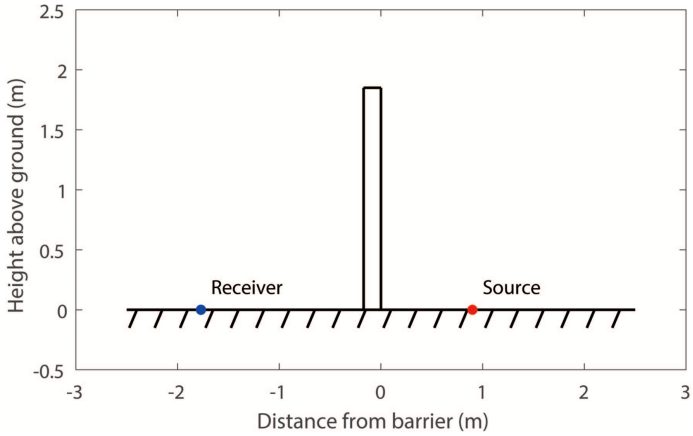

(a) Case 1

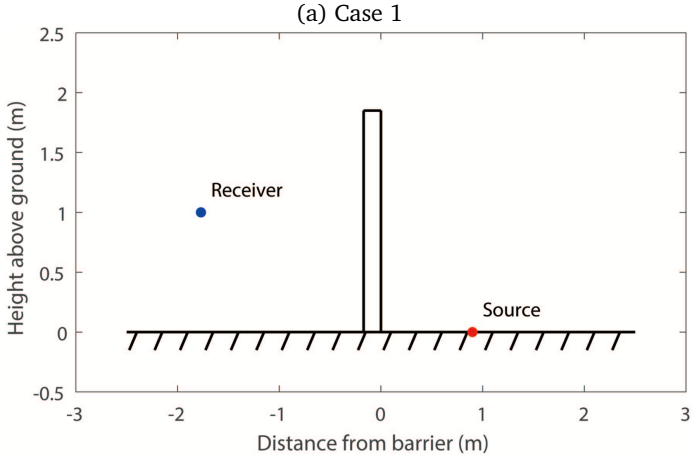

(b) Case 2

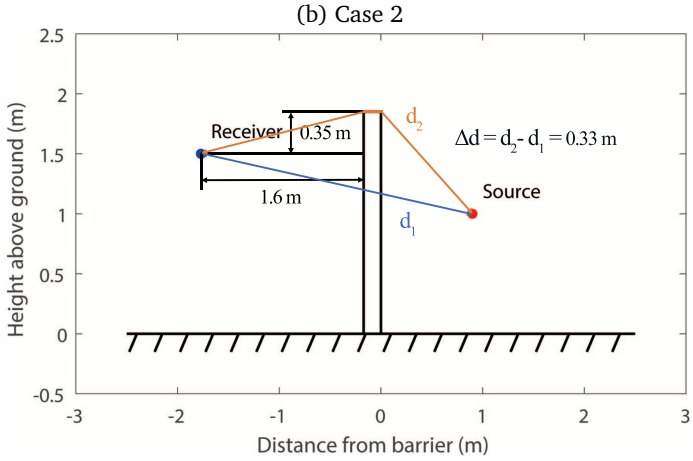

(c) Case 3

Fig 4.1.: Cross-sections of the three configurations calculated in the comparison with the analytical solution

modelled equivalently to that of the actual barrier. Figure 4.3 compares the analytical solution for case 1 with the 2.5-D BEM results predicted for the barrier with different thicknesses. It is clear that the differences between the analytical solution and the BEM results are small at low frequencies, free from the change in thickness. However, with an increase in frequency, the difference is considerably increasing, which is caused by the increased thickness. Thus, it was validated that the results predicted by SAMRAY must be

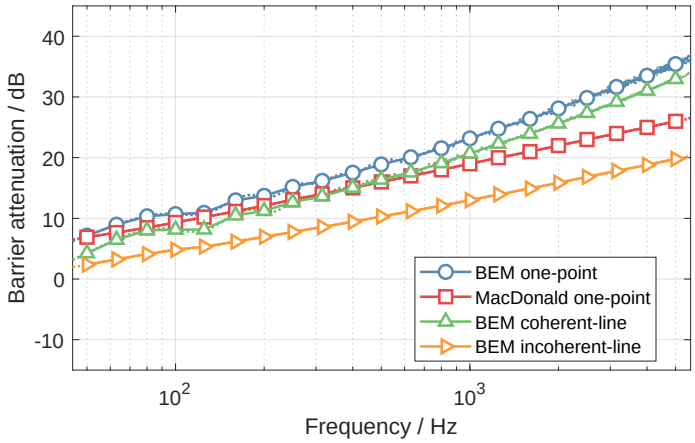

(a) Case 1

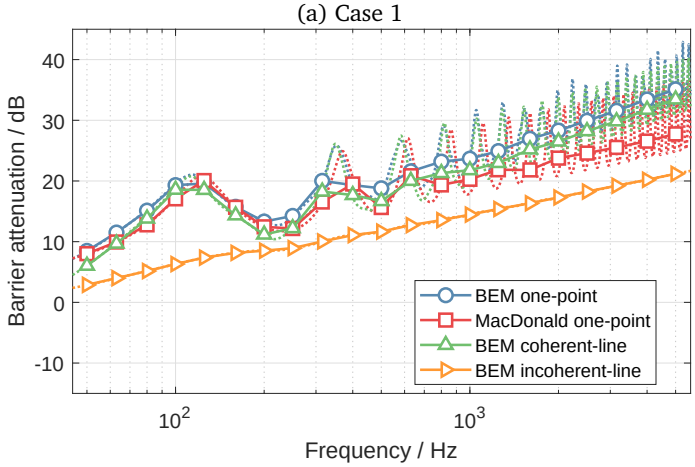

(b) Case 2

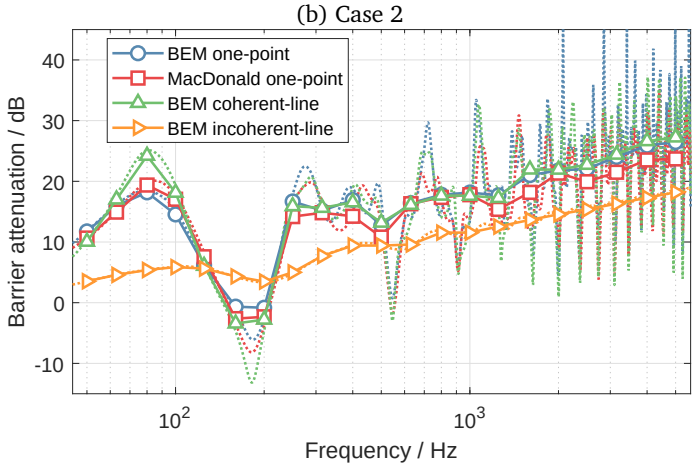

(c) Case 3

Fig 4.2.: Barrier attenuation spectra for the three configurations calculated in the comparison

closer to the actual values due to the consideration of the barrier thickness, particularly for the results at mid- and high frequencies.

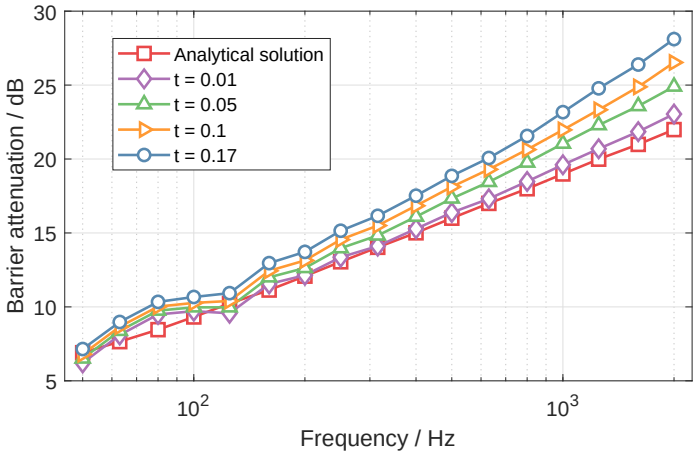

Fig 4.3.: The analytical solution for case 1 compared with the 2.5-D BEM results of the barrier with different thicknesses (units: m)

4.2.2 Ground reflection effects

In case 1 (Figure 4.1(a)), both the source and the receiver are located on the ground such that there is no need to consider the reflection effect in terms of the ground. Without the ground effect, Figure 4.2(a) only shows the component diffracted by the barrier top. As shown, the increase in the barrier attenuation is proportional to the rise of the logarithm of frequency, regardless of the source type. However, in case 2, considering the ground effect on the side of the receiver, the barrier attenuation varies regularly with frequency for the coherent line source and the one-point source. The period of the variation depends on the path difference between the direct way of sound transmission and the reflecting way, which is governed by the height of the receiver above the ground. Furthermore, as shown in Figure 4.2(c), with different heights of the source and the receiver above the ground, the barrier attenuation varies irregularly like a combination of two different periodic variations.

Take for instance the site with the barrier for case 2, Figure 4.4 shows the insertion losses of the straight barrier at the receivers at different heights (h). With the increased height of the receiver, the significantly increased parts of the insertion losses moves from mid- and high frequencies to low frequencies with the decreased values. This change law can be explained by the sound pressures at the receivers on the sites with and without the barrier. On the site without the barrier in case 2, only the receiver has a non-zero height, so there is no path difference between the reflected waves and the direct waves. The superposition of them can only increase the amplitudes of sound pressures at the receivers, without any effects on their spectral characteristics. On the site with the barrier in case 2, Figure 4.5 shows the sound pressures at the receivers at different heights. It can be seen that when the height of the receiver equals zero ($h = 0$), both of the real and the imaginary parts present periodic changes with decreasing amplitudes. when the height of the receiver equals non-zero, both of them present periodic changes in the composition of two simple harmonic waves with decreasing amplitudes (the envelope period is represented by T whereas the

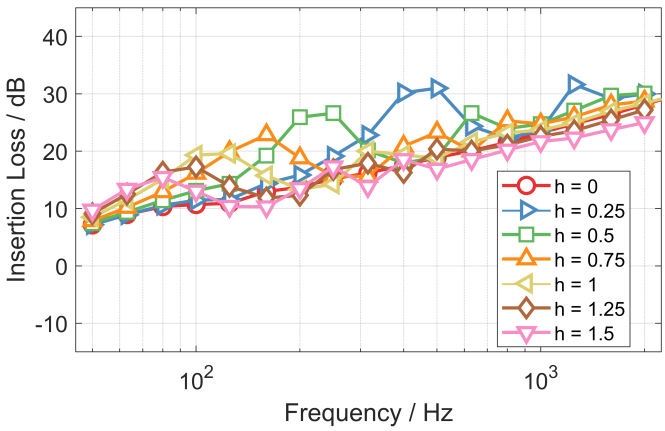

Fig 4.4.: Insertion losses at the receivers at different heights in case 2 (h denotes the height of the receiver, units: m)

high-frequency period by t shown in Figure 4.5). When the height of the receiver equals 0.25 m ($h = 0.25m$), the sound pressure at the receiver appears zero at about 500 Hz and 1300 Hz, resulting in the insertion loss to show considerable peaks in the frequency bands of 500 Hz and 1250 Hz. Therefore, the insertion losses at these two bands are respectively 10 dB and 5 dB higher than those when the height of the receiver equals zero. With the increased height of the receiver, the path difference between the direct and the reflected waves increases, leading to the increase of the absolute value of the frequency difference between the two simple harmonics, and the decrease of the envelope period T. Hence the zero sound pressure appears at lower frequencies and the significantly increased parts of the insertion losses moves to lower frequencies. When the path difference between the direct and the reflected waves increases considerably, the effect of the reflected wave on the direct wave reduces significantly and so does the effect of the reflected wave on the insertion loss. Therefore, it can be observed that there is little difference of the insertion losses between the 1.5-m-high receiver and the 0-m-high receiver, as shown in the red curve and the pink curve in Figure 4.4 .

In case 3, the height of the receiver is 1.5 m whereas the height of the sources equals 1 m. In other words, the ground reflection affects not only the sound pressures on the site with the barrier, but also those on the site without the barrier. Figure 4.6 shows the sound pressures at the receivers at different heights on the site without the barrier. It can be seen that when the height of the receiver equals zero, both of the real and the imaginary parts present periodic changes with unchanged amplitudes. The periods are determined by the path length of the direct wave R. When the height of the receiver is non-zero, both of the real and the imaginary parts present periodic changes in the composition of two simple harmonic waves, with unchanged amplitudes, due to the effect of the ground reflection. Similar with the previous period of the envelope T before, this period T is also inversely proportional to the path difference between the direct and the reflected waves. When the height of the receiver equals 1.5 m ($h = 1.5m$), the sound pressure on the site without the

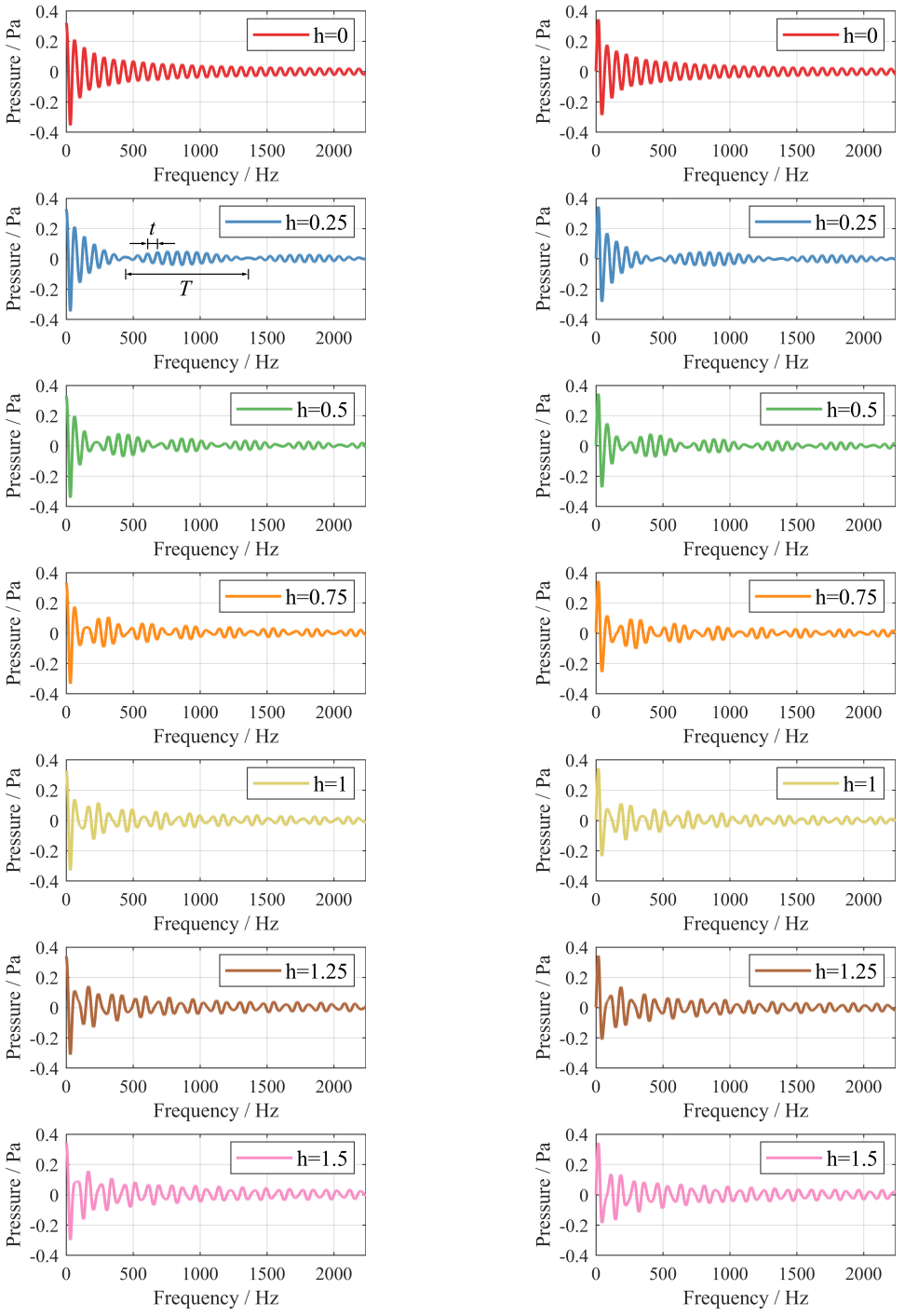

(a) Real parts of sound pressures (b) Imaginary parts of sound pressures

Fig 4.5.: Sound pressures at the receivers at different heights on the site with the barrier, case 2

barrier decreases considerably at about 180 Hz, 550 Hz, 900 Hz, 1250 Hz, 1600 Hz and 2000 Hz, resulting in the decrease of the insertion loss in 160-200 Hz and the frequency bands above 500 Hz. Furthermore, on the site with the barrier, the ground reflection causes the insertion losses to increase at the low frequency band of about 80 Hz (as shown in Figure 4.4). In summary, it can be reasonably interpreted that the insertion loss spectrum at the receiver in case 3 is as follows: the insertion loss first increases and then decreases in the

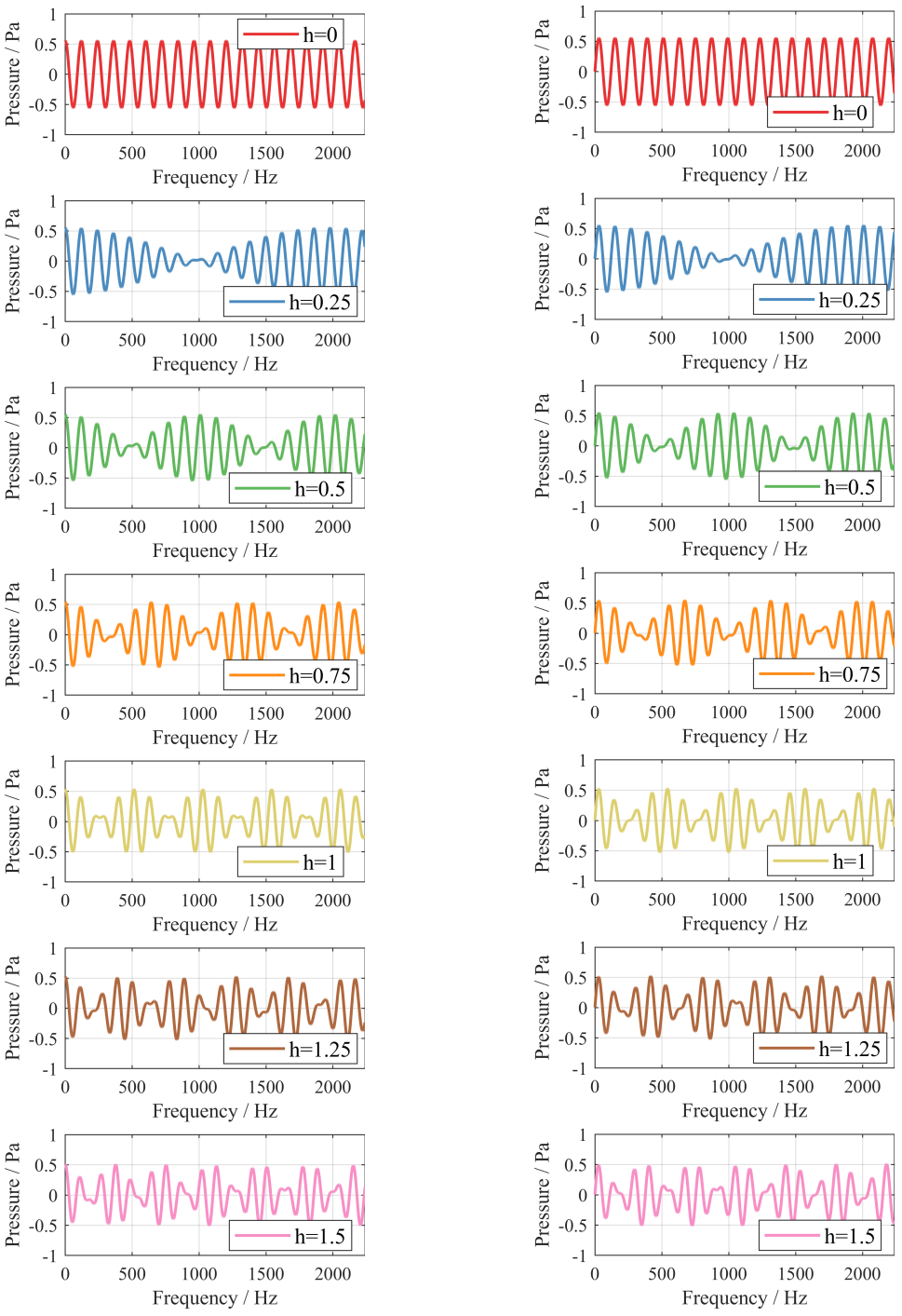

(a) Real parts of sound pressures (b) Imaginary parts of sound pressures

Fig 4.6.: Sound pressures at the receivers at different heights on the site without the barrier, Case 3

low frequency band of 50-100 Hz, with a local maximum at 80 Hz; Then the insertion losses are almost zero in 160-200 Hz; In the band of 250-400 Hz, they are basically consistent with those for case 1 and case 2; Finally, the insertion losses above 500 Hz are significantly lower than those for case 1 and case 2.

As indicated by the discussion above, it can be summarized that on the site without the

barrier, when the height of the source or that of the receiver is non-zero, both of the real and the imaginary parts present periodic changes with unchanged amplitudes, and the periods are determined by the path length of the direct wave; When the height of the source and the receiver are both non-zero, the effect of ground reflection can cause both of the real and the imaginary parts to present periodic changes in the composition of two simple harmonic waves with unchanged amplitudes, and the envelope periods are inversely proportional to the path difference between the direct and the reflected waves. On the site with the barrier, when the height of the source or that of the receiver is non-zero, the effect of ground reflection can cause both of the real and the imaginary parts to present periodic changes in the composition of two simple harmonic waves with decreased amplitudes. The ground reflection caused by the height of the receiver or the source can directly affect the insertion loss since it can cause the change of the spectral characteristics of both the real and the imaginary parts of the sound pressures on the site without and with the barrier. Therefore, the effect of ground reflection on the insertion loss is very significant. Since the viaducts used in urban rail transit are commonly concrete structures, their geometrical surfaces are always approximated as totally reflecting surfaces. Hence the viaduct reflection would be fully considered in the scale model and the numerical model of the nearly-enclosed barrier in the subsequent research.

4.3 Scale modelling tests and 2.5-D BEM calculations

With the assumption of the actual thicknesses of barriers, the 2.5-D BEM prediction results must be much closer to the actual values compared with the analytical solutions. However, the predictions for three cases need to be validated using the scale modelling method. In addition to the three cases for a one-point source discussed in Section 4.2, a case with a double-straight barrier installed on the box girder viaduct(case 4) was introduced to more realistically study the railway noise barrier system. Nevertheless, it remains quite difficult to model the incoherent line source that is commonly used to more closely reflect the traffic noise. Because the incoherent line source can be considered an infinite line of uncorrelated point sources perpendicular to the cross-section, several incoherent point sources were introduced into the test and performed for case 3 and 4. Consequently, the scale model measurement with several point sources was made to not only validate the 2.5-D BEM prediction results for the one-point source but also for the incoherent point sources. Due to the size limitation of the experiment site, the scales of case 1-3 were determined to be 1:10 whereas that of case 4 was 1:20.

4.3.1 Scale modelling tests

The tests for the one-point source were performed in four cases. For the first three, the solid plane barrier remained unchanged, 18.5-cm high and 1.7-cm wide. The site was an

open field on unknown asphalt. To ensure good acoustic reflection to simulate rigid surface conditions, a wood plank with an area of $1.2 \times 1.8m^2$ was placed on the asphalt (shown in Figure 4.7), which was sufficiently large to offer an approximate rigid ground in our scale model test. Figure 4.7 also shows that a layer of sand was inserted to fill the air gap between the plank and the asphalt to eliminate the influence of vibration of the panel and the air cavity resonance effect under the plank surface.

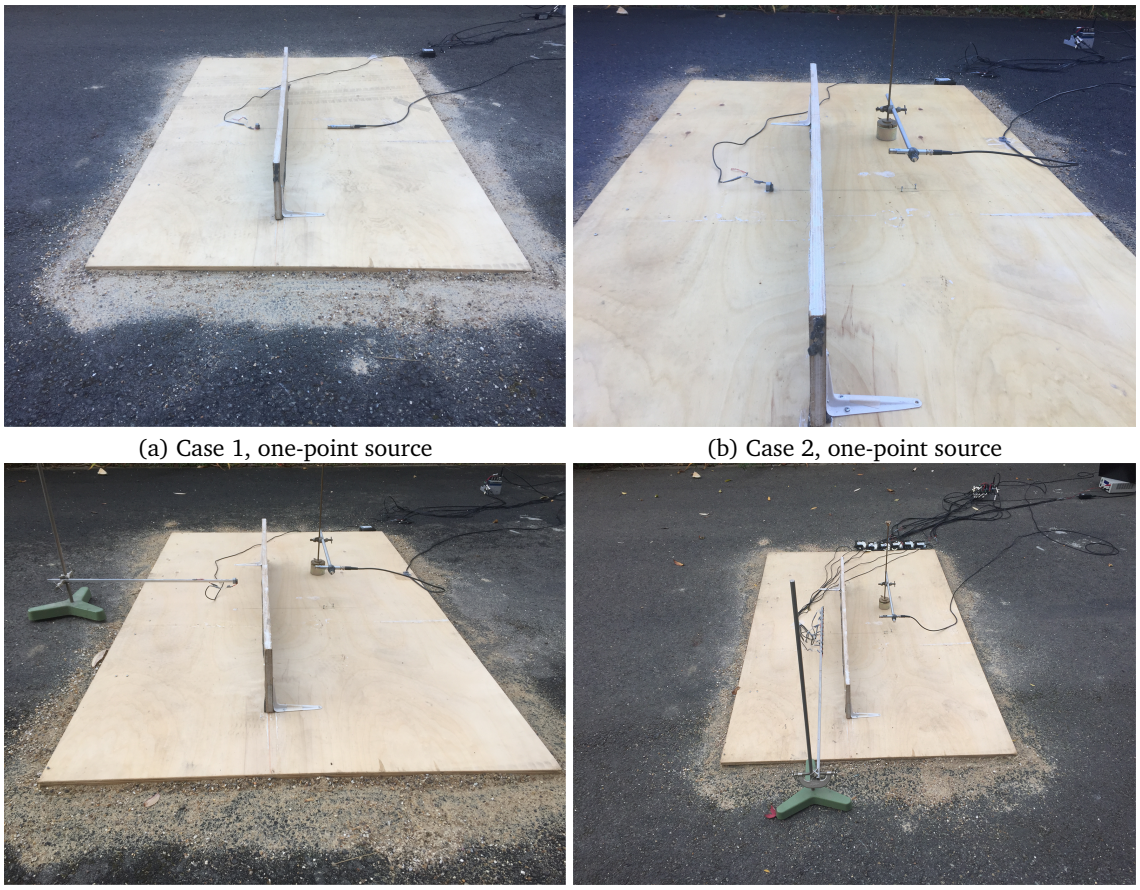

(a) Case 1, one-point source

(b) Case 2, one-point source

(c) Case 3, one-point source

(d) Case 3, incoherent point sources

Fig 4.7.: The scenes of the scale model tests for the former three cases

For case 4, the barriers and the viaducts were made of 9-mm-thick wood panels. The scale model was based on part of the real prototype measured in Chapter 3 and is shown in Figure 4.8(a), with a length of about 6 m. Double-straight barriers with a height of 2.4 cm were located on the box girder viaduct which was 50 cm above the ground supported by discontinuous piers, the gap between each two being about 1 m. The receiver was positioned towards the centre of the model where there was no pier. Figure 4.8(b) shows the cross-section of the real model. Due to the large vehicle structure, secondary reflections pose a problem and thus the train itself had to be taken into account in the scale modelling tests. The T-shape part in the centre of the viaduct was designed as a safe passage. Since the viaduct was the closest reflective surface to the source and it was elevated above the ground, the acoustical characteristic of the ground seemed a lot less important. Hence there was no need to place the wood plank on the asphalt in case 4.

(a) The scene of the scale model

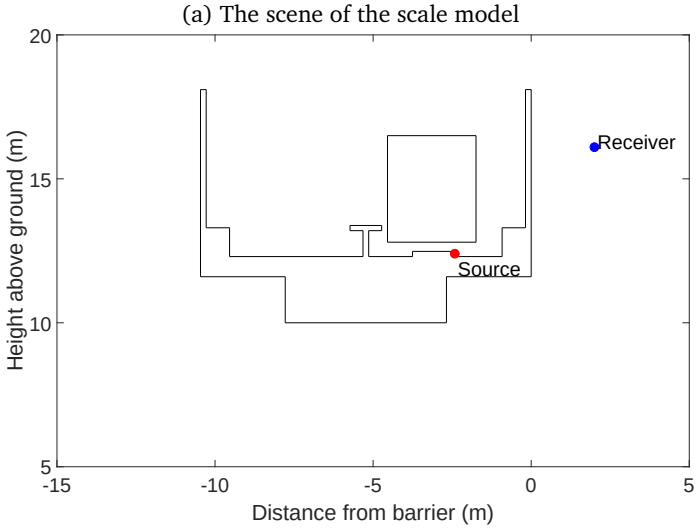

(b) The cross-section with a barrier in the BEM calculation

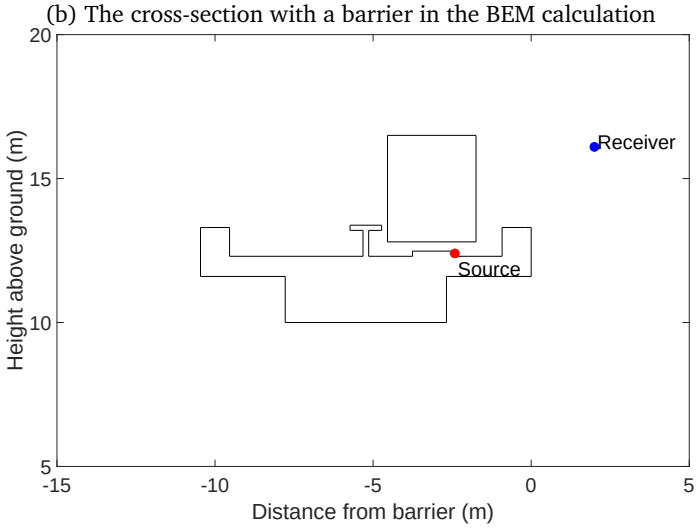

(c) The cross-section without a barrier in the BEM calculation

Fig 4.8.: Configurations of case 4

To evaluate the performance of barriers, it was necessary to prepare the configurations without barriers. For the first three cases only the straight barrier was removed and for case 4 only the double-straight barrier was removed(shown in Figure 4.8(c)). The positions of loudspeakers and microphones were unchanged. To describe the positions of sources and receivers for each case, the horizontal distance to the surface of the barrier was determined as x, the vertical distance to the ground was determined as y and the longitudinal distance to the microphone along the barrier was determined as z. Figures 4.1 and 4.8 show the coordinates for each real model while Table 4.1 illustrates the coordinates for both the real and the scale models. The tests for a one-point source were made at first where the perpendicular from source to receiver meets the barrier($z_r = z_s = 0$). Then the tests for incoherent point sources were made with the increased number of source for case 3 and 4, with other coordinates of loudspeakers and microphones remaining constant. Note that in each case, the height of the receiver was less than that of the barrier, which is a result of the need to keep the receiver well within the shadow zone.

Tab 4.1.: Positions of loudspeakers and microphones in three coordinates(m)

(a) For a one-point source

Real model	Microphone		Loudspeaker		Scale model	Microphone		Loudspeaker	
	x_r	y_r	x_r	y_r		x_r	y_r	x_r	y_r
Case 1	1.6	0.0	0.9	0.0	Case 1	0.16	0.00	0.09	0.00
Case 2	1.6	1.0	0.9	1.0	Case 2	0.16	0.10	0.09	0.10
Case 3	1.6	1.5	0.9	1.0	Case 3	0.16	0.15	0.09	0.10
Case 4	2.0	16.1	2.42	12.4	Case 4	0.10	0.805	0.121	0.62

(b) For incoherent point sources

Real model	Loudspeaker											
	Num	z_s										
Case 3	1						0.00					
	3					-0.35	0.00	0.35				
	12	-2.10	-1.75	-1.40	-1.05	-0.70	-0.35	0.00	0.35	0.70	1.05	1.40	1.75
Case 4	1						0.00					
	4					-19.78	-7.18	0.00	12.60				
	12	-59.34	46.74	-39.56	-26.96	-19.78	-7.18	0.00	12.60	19.78	32.38	39.56	52.16
Scale model	Loudspeaker											
	Num	z_s										
Case 3	1						0.0					
	3					-0.035	0.0	0.035				
	12	-0.21	-0.175	-0.14	-0.105	-0.07	-0.035	0.0	0.035	0.07	0.105	0.14	0.175
Case 4	1						0.0					
	4					-0.989	-0.359	0.0	0.63				
	12	-2.967	-2.337	-1.978	-1.348	-0.989	-0.359	0.0	0.63	0.989	1.619	1.978	2.608

The BEM model assumes omni-directional incoherent point sources, and they were achieved in practice by using miniature loudspeakers (produced by RS PRO, RS Stock Code: 1176047), activated by amplifiers (Viston, AMP 2.2 LN, Art. No. 7102) and a power supply (EA-PS 2042-10B). The sound radiated from the speakers was generated by an output signal module (NI 9263) installed in a NI DAQ system (CDAQ-9174). The effective maximum frequency of

the miniature loudspeaker was up to 20 kHz in the one-third octave band. Together with the recommended frequency range of railway traffic noise in ISO 10847:1997(50-5000 Hz), the measured frequency ranges of case 1-3 were determined 500 Hz - 20 kHz and that of case 4 was 1000 Hz - 20 kHz. Hence the measured results can simulate a 50-2000 Hz emission for case 1-3 and a 50-1000 Hz emission for case 4 in the real size problem.

During the measurement one or more loudspeakers emitted simultaneously random white noise in the same one-third octave band for 10 seconds from the signal output module. In the meantime, sound pressure signals were received by microphones to the signal input module. The ten-second random white noise was based on continuous integrated sound pressure levels so that the barrier end effects had to be limited. To limit end effects, the receiver was positioned towards the centre of the barrier and both barrier ends were filled with mineral wool to absorb the sound diffracted by the ends. Each test was repeated five times.

All the tests were conducted in the same place. The test of each case was done successively for the site with and without the barrier, lasting for about one hour in total. In the duration of the test for each configuration, the effect of humidity and temperature on air absorption of high frequencies was considered unchanged. Since the attenuation of the straight or double-straight barrier that was of our interest was the difference in level between the site with and without barriers, the effect of humidity and temperature could be ignored. Nevertheless, the temperature of tests was measured, as presented in Table 4.2.

Tab 4.2.: Temperature of tests(°C)

	Number of loudspeakers	Configurations	
		Without a barrier	With a barrier
Case 1	1	22.1	21.8
Case 2	1	21.9	22.0
	1	22.3	22.2
Case 3	3	22.2	22.2
	12	22.3	22.5
	1	17.8	17.6
Case 4	4	17.7	17.5
	12	17.8	17.9

4.3.2 Comparisons of test results and the 2.5-D BEM predictions

Predictions were performed for the straight and double-straight barriers using the 2.5-D BEM program SAMRAY. The one-point source in the model was placed in exactly the same position as for the scale model tests. The number of sources defined was initially one for modelling the one-point source, followed by adding sources to reach three or four and

finally reaching twelve sources. The barrier attenuation of the one-point source for each case was calculated by using Eq (4.5). While to yield the results by the combined effect of different incoherent point sources, the barrier attenuation for incoherent point sources was given as,

$$Att_{b,\mathrm{sum}}(f) = 10\log\frac{\sum_{i=1}^{N} p_{\mathrm{wo}}^2(f, z_{si})}{\sum_{i=1}^{N} p_{\mathrm{w}}^2(f, z_{si})} \tag{4.6}$$

where $p_{\mathrm{wo}}(f, z_{si})$ and $p_{\mathrm{w}}(f, z_{si})$ denote the sound pressure at the given receiver position radiated from the source located at z_{si} in the case of the model without and with the barrier, respectively. N denotes the number of incoherent point sources. The barrier attenuations at one-third-octave band frequencies from 50 Hz to 2000 Hz were calculated to be compared for the first three tested results, whereas those from 50 Hz to 1000 Hz were calculated for case 4.

For the one-point source that was perpendicular to the receiver, Figure 4.9 shows plots of the measured and predicted barrier attenuations by the one-third-octave band spectrum for all four cases. The frequency range of the measured spectrum was adjusted in the analysis to be identical to the predicted results. Hence, the frequencies will be given in full scale for clarity. As expected, there are good agreements between the measured results obtained in the scale model tests and those predicted by the 2.5-D BEM approach. However, the measured barrier attenuations are slightly higher than those predicted by the BEM, particularly for high frequencies. This result was considered to be normal and permissible due to the sound absorption of the wood panels and the non-idealised point source in the scale test.

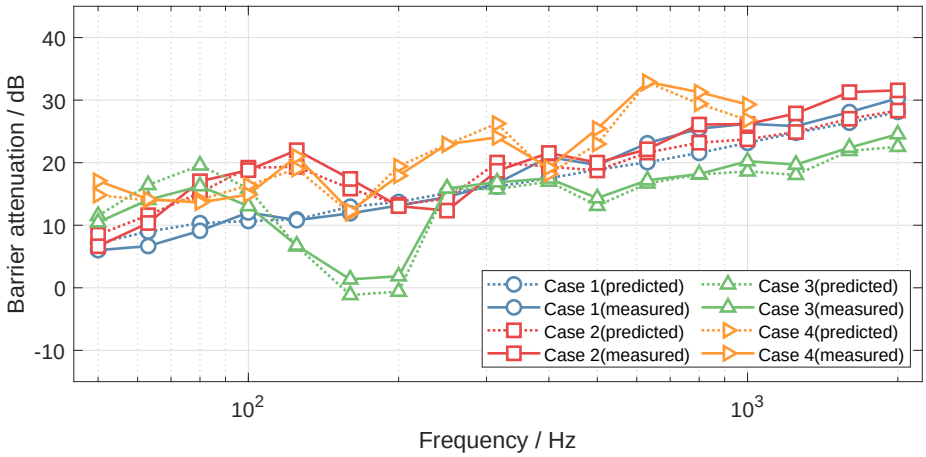

Fig 4.9.: Measured and predicted barrier attenuations for the one-point source

In Figure 4.10, the results for different numbers of loudspeakers in cases 3 and 4 are compared. Here, the simultaneously sound sources were lined up along the length of the barrier, only differing by the longitudinal distance. As shown in Figure 4.10, the measured result for each case in general has a good agreement with the prediction, which indicates

that by using the 2.5-D BEM approach, the predicted barrier attenuations for incoherent point sources are accurate as well. Looking into details, there are discrepancies at peaks(80 Hz and 200 Hz) for case 3, which can be caused by the warping tendency of the wood plank on the ground. It is also clear that all the curves in Figure 4.10(a) are too close to identify each other. This result means that the number of incoherent point sources has little effect on the attenuation of the straight barrier on the ground. Nevertheless, there is no proof that the number effect can be ignored when referring to the barrier attenuation for incoherent point sources.

For the double-straight barrier on the viaduct, as shown in Figure 4.10(b), it is easy to understand that the growth of barrier attenuation seriously fluctuates with frequency for the one-point source. It is surprising that in general the barrier attenuation tends to gradually increase as the number of incoherent point sources increased to four. When the number of sources increased to twelve, the barrier attenuation has a slight decrease at each frequency band compared with those for four-point sources.

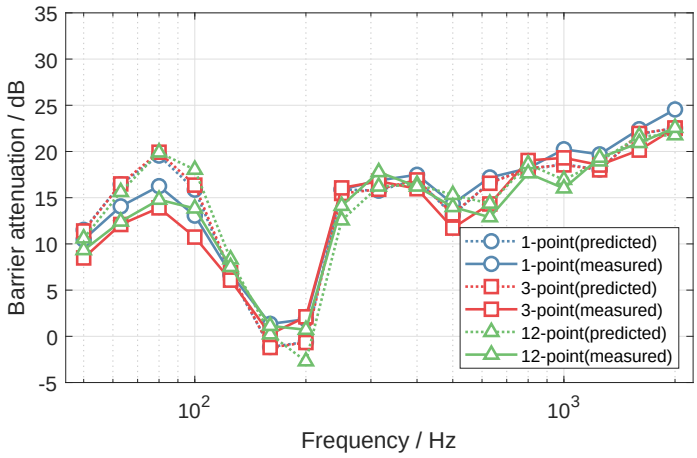

(a) Case 3

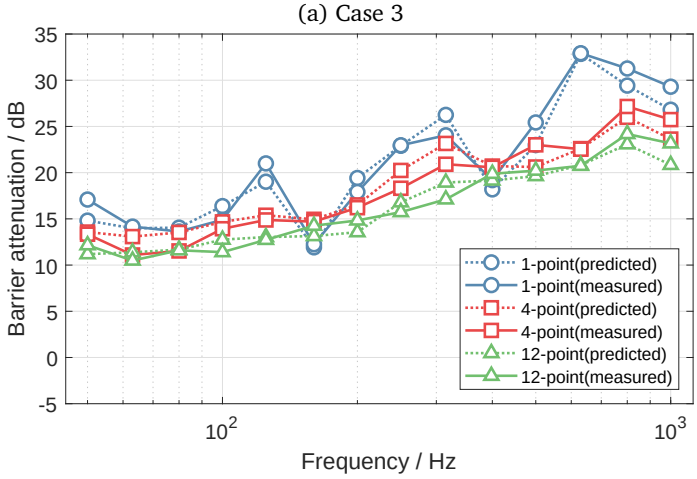

(b) Case 4

Fig 4.10.: Measured and predicted barrier attenuations for incoherent point sources

4.4 Source type effects

4.4.1 Incoherent point sources

To understand the noise reduction mechanism of a barrier in the field radiated by incoherent point sources, the effects of the longitudinal distances between the incoherent point sources and the given receiver (represented by $|z_s - z_r|$) on the spectra of the sound pressures are discussed firstly. Taking for instance the site without the barrier in case 3, the sound pressure spectrum at the given receiver in the field radiated solely by each incoherent point source are shown in Figure 4.11. It can be seen that when the source-receiver longitudinal

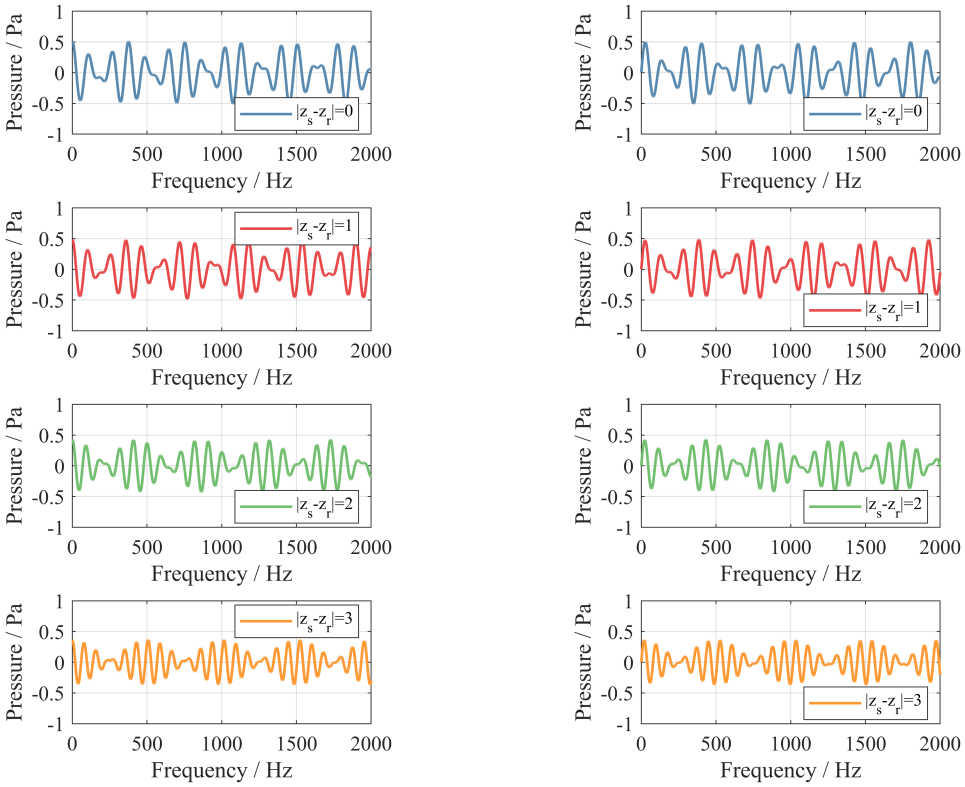

(a) Real parts of sound pressures

(b) Imaginary parts of sound pressures

Fig 4.11.: Sound pressures at the given receivers in the field radiated solely by each incoherent point source on the site without the barrier, case 3 ($|z_s - z_r|$ is the longitudinal distance between the source and the receiver, unit: m)

distance equals zero ($|z_s - z_r| = 0$), since the pressure at the receiver is influenced by the direct and the reflected waves, its spectrum presents periodic changes in the composition of two simple harmonic waves; When the source-receiver longitudinal distance is non-zero ($|z_s - z_r| \neq 0$), with the increase of the longitudinal distance between the source and the receiver, the spectrum still shows a combination of two simple harmonic waves, but the amplitude decreases significantly, from 0.55 Pa ($|z_s - z_r| = 0$) to 0.32 Pa ($|z_s - z_r| = 3$). Meanwhile, the high-frequency period t decreases significantly, whereas the envelope period T increases considerably. These are because the increased longitudinal distance between the

source and the receiver leads to increasing the path length R of the direct and the reflected waves, resulting in the decrease of the amplitude and the high-frequency period t of the pressure spectrum. On the other hand, the increased longitudinal distance also shortens the path difference between the direct and the reflected waves, resulting in the increase of the envelope period T of the pressure spectrum.

On the site with the barrier in case 3, the effect of the longitudinal distance on the sound pressure spectrum is the same as the above discussion, but the effect of the top-diffracted attenuation on the sound pressure spectrum is more significant, resulting in the considerable decrease of the amplitudes. Therefore, it is unnecessary to go into details on the effect of the longitudinal distance.

Then the influence of the longitudinal distance between the source and the receiver on the insertion loss of the barrier is discussed. Figure 4.12 shows the insertion loss spectra at the

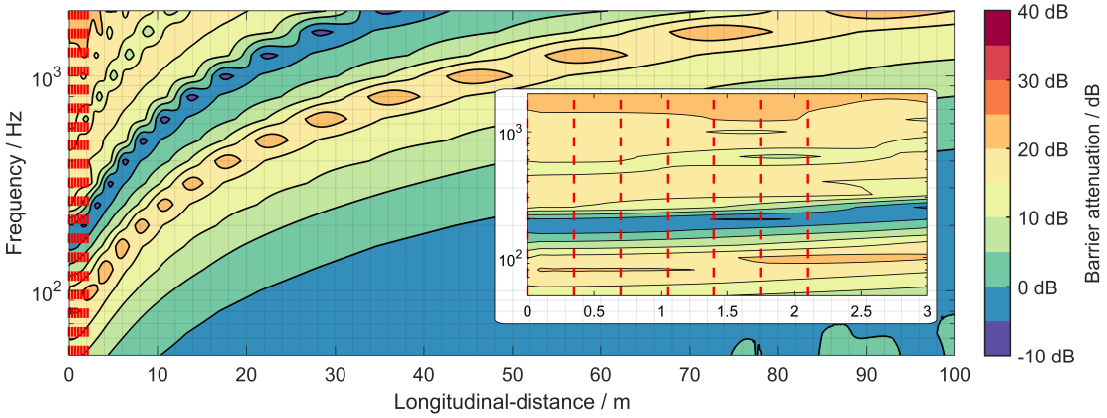

(a) Case 3, the straight barrier on the ground,
source-receiver distance perpendicular to the barrier: 2.67 m

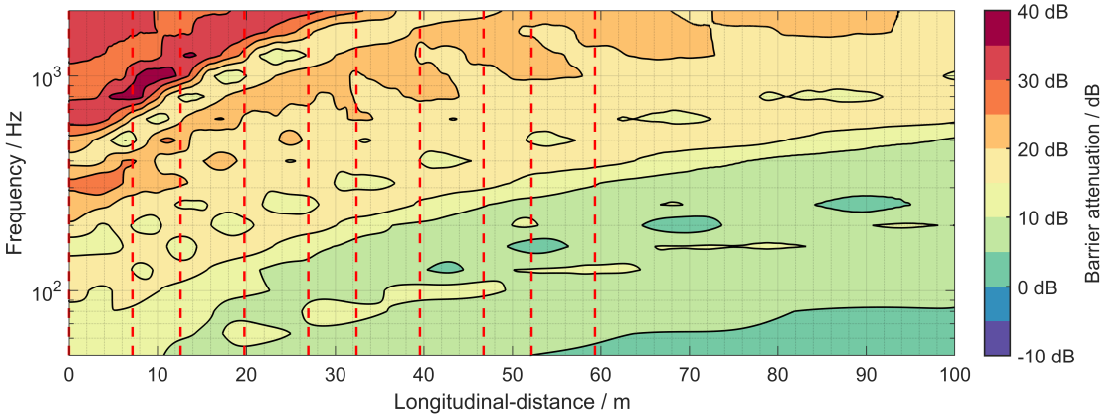

(b) Case 4, the double-straight barrier on the viaduct,
source-receiver distance perpendicular to the barrier: 4.415 m

Fig 4.12.: The relationships between the longitudinal distance and the barrier attenuation spectrum

measured receiver in the field radiated solely by each incoherent point source in case 3

and case 4, respectively. These point sources are positioned 0.1 m apart, within the source-receiver longitudinal distance of 100 m. The x-axis represents the longitudinal distance between the source and the receiver, and the y-axis represents the sound frequency on a log scale. For comparison, the contours for both cases 3 and 4 use the same colourmap. It can be found that the increase of the source-receiver longitudinal distance causes noticeable changes in the insertion loss spectrum. The spectrum of the insertion loss does not completely increase or decrease monotonically, or increase at first and then decrease or decrease at first and then increase, but the low-frequency insertion loss decreases monotonically in the bands lower than 80 Hz, and the rest of the spectrum moves to the higher frequencies. Since the effect of the top-diffracted attenuation on the sound pressure spectrum is more significant on the site with the barrier, this trend of the insertion loss can be mainly attributed to the spectral characteristics of the sound pressure on the site with the barrier: (1) The path length of the direct and the reflected waves increases with the increase of the source-receiver longitudinal distance, and thus the sound pressure amplitude decreases. Due to the narrow characteristics of the 1/3 octave bands at low frequencies, the low-frequency insertion loss spectrum can directly reflect the decrease of the sound pressure amplitude on the site without the barrier. (2) With the source-receive longitudinal distance increase, the envelope period T of the sound pressure spectrum increases and thus the peaks, the valleys and the zero points of both the real and the imaginary parts of the pressure spectrum moves to the higher frequency. Since the 1/3 octave bands at mid- and high frequencies are relatively wider, the mid- and high frequency spectrum can show the mean characteristics of the sound pressure in a certain broad band. Hence the mid- and high frequency spectrum of the insertion loss shows the tendency of the sound pressure spectrum to move to the higher frequency. Meanwhile, this tendency also causes the presences of the local maximums and minimums of the insertion loss regularly, as shown in the closed orange and purple contours in Figure 4.12.

The incoherent characteristics of the field radiated by incoherent point sources lies in the linear superposition of the fields radiated solely by each point source, as shown in Formula 4.6. The discussion above indicates that the spectrum of the insertion loss varies regularly with the source-receiver longitudinal distance (Figure 4.12): the low-frequency insertion loss decreases monotonically, and the rest of the spectrum moves to the higher frequencies. With a linear superposition of such spectra, the insertion loss in the field radiated by the combination of these incoherent point sources must have a mean characteristic. Therefore, the spectrum of the insertion loss becomes smooth, which is related to the number of the incoherent point sources and the maximum source-receiver longitudinal distance. Take for instance the spectrum of the insertion loss in case 3 tends to smooth with the increase of the maximum source-receiver longitudinal distance when the number of point sources is unchanged, as shown in Figure 4.13(a). On the other hand, when the maximum source-receiver longitudinal distance is unchanged, the spectrum of the insertion loss also tends to smooth with the increased number of point sources, as shown in Figure 4.13(b).

As observed above that in case 3, the measured insertion loss spectrum in the field ra-

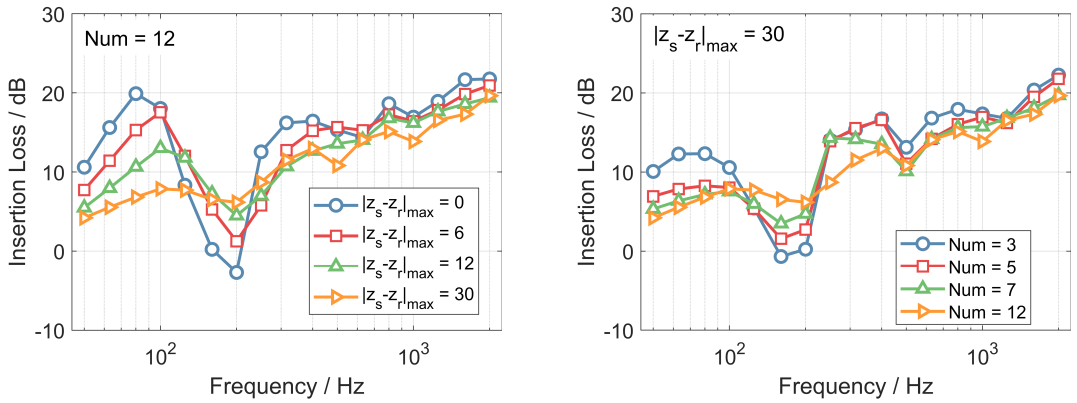

(a) The same number of point sources, different maximum source-receiver longitudinal distances

(b) The same maximum source-receiver longitudinal distance, different numbers of point sources

Fig 4.13.: The spectra of insertion loss in the fields radiated by different incoherent point sources, case 3

diated by multiple incoherent point sources is basically the same as that in the field radiated by a single point source. It is due to the too small longitudinal distances between the sources and the receiver. In Figure 4.12(a), the insertion loss spectra in the field radiated solely by each point source are marked by red dotted lines. Due to the excessive density, they are zoomed at the lower right corner. It can be seen that these spectra are almost unchanged with the increased source-receiver longitudinal distance since each longitudinal distance (see Table 4.1 is of the same order as the source-receiver distance in the cross section (2.67 m). Meanwhile, the insertion loss spectrum for incoherent point sources has a mean characteristic, which results from the incoherence of multiple point sources. Therefore, the insertion loss spectrum for incoherent point sources should be consistent with that for a single point source. This explanation is in agreement with the results observed in the scale model test of case 3, verifying the noise reduction mechanism of a barrier for multiple incoherent point sources: the incoherence of point sources gives a mean characteristic to the insertion loss spectrum, which is almost equivalent to the average of those in the fields radiated solely by each point source. Due to the differences between each two source-receiver longitudinal distances are too small in case 3, the mean characteristic of the insertion loss for multiple incoherent point sources cannot be effectively observed.

However, a set of urban rail transit vehicles is usually composed of 6 sections, with a total length of 120-150 meters. The total length is always significantly higher than the source-receiver distance in the cross section. Figure 4.14 shows the insertion loss spectra in the field radiated solely by each point source measured in case 4. It can be clearly seen that the spectrum moves from low frequencies to high frequencies with the increased source-receiver longitudinal distance. Meanwhile, the incoherence of multiple point sources causes a linear superposition of these insertion loss spectra, resulting in the smoothness of the insertion loss spectrum for the multiple point sources, as shown in Figure 4.10(b).

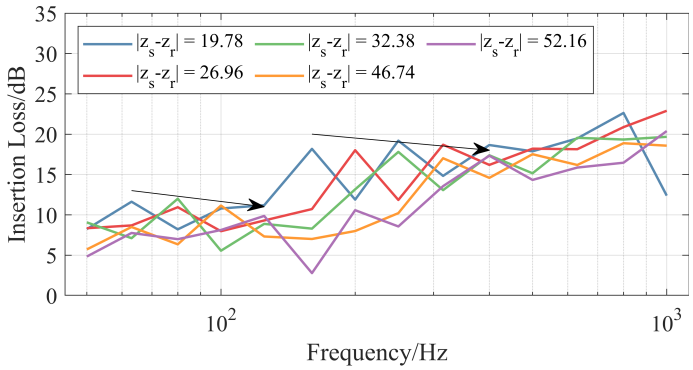

Fig 4.14.: The insertion loss spectra in the field radiated solely by each point source measured in case 4

It also suggests that the differences between each two bogie source-receiver longitudinal distances in urban rail transit are sufficient, the minimum longitudinal distance equal to zero and the maximum equal to 60 meters, to cover the variation of the insertion loss with the longitudinal distance. Hence it is easily to find a significant effect of the incoherence of sources on the insertion loss spectrum of an urban rail transit barrier. Therefore, it is necessary to consider the influence of the incoherence of sources on the insertion loss spectrum in the research of urban rail transit noise barriers.

4.4.2 Incoherent and coherent line sources

Figure 4.2 also shows the insertion loss spectra of case 1-3 for the coherent line source and the incoherent line source, compared with those for the point source with a source-receiver longitudinal distance of zero (hereinafter, the point source). In Figure 4.2, each dotted curve represents the barrier attenuations in the frequency spectrum whereas the solid curve in the same colour corresponds to the results in one-third-octave bands from 50 Hz to 5000 Hz. Thus, the latter appears to be much smoother than the former. In case 1, the solid curve for each kind of source is basically identical to the dotted curve. But in case 2 and case 3, it is only in the bands of 50-200 Hz that the solid curves for the point source and the coherent line source are almost consistent with those dotted curves, respectively. At high frequencies, the 1/3 octave spectra for the point source and the coherent line source are much smoother than the frequency spectra. However, in these two cases, the 1/3 octave spectra of the insertion loss for the incoherent line source are identical to the frequency spectra from the lowest to the highest, having a strong consistency. Therefore, when calculating the frequency spectrum of insertion loss in the field radiated by an incoherent line source, the calculation process can be simplified to only calculating the insertion losses at the centre frequencies for each 1/3 octave band.

By comparing the insertion loss spectra for the coherent line source and those for the point source, marked by red rectangular curves and blue circle curves, it can be found

that they have good agreements in the whole frequency range. This is consistent with the results obtained by DUHAMEL[176]. Meanwhile, DAUMAS[215] also found the agreements between the measured insertion losses for the point source and those for the coherent line source. Therefore, the insertion loss spectrum for a coherent line source can be used thoroughly estimate that for the corresponding point source.

By comparing the insertion loss spectra for the incoherent line source and those for the point source, marked by green triangle curves and blue circle curves, it can be found that it is only at low frequencies that they have good agreements, but the insertion losses for the incoherent line source are much lower than those for the point source at mid- and high frequencies. Assuming the field radiated by the incoherent line source as a linear superposition of the fields radiated by an infinite number of incoherent point sources arranged densely on the line, the insertion loss spectrum for the incoherent line source can be regarded as the average of the spectra for the point sources on this line. Since the insertion loss spectrum for the point source regularly changes with the source-receiver longitudinal distance, the insertion loss spectrum for the incoherent line source is therefore much smoother and lower than that for the point source.

Based on the tested and calculated results mentioned above, we can summarize the effect of line source type on the spectrum of insertion loss: when the line source is coherent, the insertion loss spectrum is approximate to that for the point source. When the line source is incoherent, the influence of the source-receiver longitudinal distance and the incoherence of the source makes the insertion loss spectrum show a steady increase. The spectra of insertion loss for the coherent line source and the incoherent line source are significant different: the former is higher than the latter and the difference increases significantly with frequency. If the insertion loss spectrum for the incoherent line source is analyzed by the model for the coherent line source, the insertion loss spectrum will be overestimated. Therefore, the determination of the line source type is of critical importance to the insertion loss spectrum in the research of the noise reduction mechanism of noise barriers. For urban rail transit systems, the noise source is always simplified as the incoherent line sources at the positions of wheel-rail interactions. Hence the incoherence of the line source must be fully considered in the subsequent study of the nearly-enclosed barrier in terms of reducing urban rail transit noise.

Except for the frequency spectrum, the equivalent insertion loss within a frequency range of interest is always used to analyze the barrier performance. Chapter 3 introduced the equivalent insertion loss rating named as "insertion loss"(IL) by using time histories of sound pressure. Here the equivalent insertion loss is calculated by the frequency spectrum of sound pressure, given as

$$\mathrm{IL} = 10 \log \frac{\int_{f_{\min}}^{f_{\max}} p_{\mathrm{wo}}^2(f)\, df}{\int_{f_{\min}}^{f_{\max}} p_{\mathrm{w}}^2(f)\, df} \tag{4.7}$$

where $f_{\min}$ and $f_{\max}$ are the lower and upper limits of the frequency range, respectively.

According to the norm ISO 10847:1997[153], the frequency range for the railway traffic noise is recommended to range from 50 Hz to 5000 Hz. To compare the equivalent insertion losses for the one-point source between the two calculation methods, we find from Table 4.3 that the results predicted by the 2.5-D BEM were 2-3 dB higher than those obtained

Tab 4.3.: Insertion losses for three configurations for different types of sources (frequency range: 50-5000 Hz)

IL / dB	Analytical solution	Predicted results by BEM		
	One-point	One-point	Coherent line	Incoherent line
Case 1	19.7	22.9	11.7	14.2
Case 2	21.3	24.1	14.8	15.2
Case 3	17.7	19.7	13.4	13.0
Case 4		20.5	13.7	11.8

from the analytical solutions, which were the results of the assumed thin barriers in the analytical model. Notably, by comparing the equivalent insertion loss predicted by the 2.5-D BEM program for different source types, the results for the coherent line source are in good agreement with those for the incoherent line source but much lower than those predicted for the one-point source. This result is why many studies considered the sound field radiated by a coherent line source to be that for an incoherent line source, although the results observed in the frequency spectrum are completely contrary to each other. Hence, it is indicated that the equivalent insertion loss for the coherent line source can be used to estimate the value for the incoherent line source to reduce the computational time. However, the equivalent insertion losses for a coherent line source are significantly lower than those for a one-point source, which are completely contrary to those observed in the frequency spectrum analysis. This opposite trend can be due to the low-frequency characteristics of the equivalent insertion loss for a coherent line source. An elaborate explanation will be presented in Appendix A.

Based on the calculated results mentioned above, we can summarize the effect of line source type on the equivalent insertion loss: when the line source is incoherent, the sound pressure at a given receiver remains unchanged in the whole frequency range of interest, which is the same as that in the field of the corresponding point source. When the line source is coherent, the sound pressure at a given receiver decreases linearly with the increase of logarithmic frequency, governed mainly by the low-frequency component. Therefore, the equivalent insertion loss at a given receiver for the incoherent line source is approximately equal to that for the coherent line source, but both of them are much lower than that for the corresponding point source.

4.5 Conclusion

In this chapter, the attenuations of a rigid straight barrier on the rigid ground and a double-straight barrier on a rigid viaduct generated from different types of sources have been investigated. A first comparison has been achieved by the analytical solution proposed by MacDonald and the 2.5-D BEM predictions by SAMRAY, able to achieve the ground reflection effects on the insertion loss spectrum of straight barriers. Then, a measurement procedure using several loudspeakers radiating incoherent sounds simultaneously with two scale models has been presented to verify the 2.5-D BEM calculations for different numbers of incoherent point sources. From the 2.5-D BEM results, it has been possible to determine the source type effects on the insertion loss spectrum of noise barriers. In addition, the equivalent insertion loss for the frequency range of interest has also been analysed for all configurations.

The following conclusions can be drawn from the predictions and measurements:

1. The ground reflection directly affects the sound pressures at a given receiver on the site without and with the barrier, causing both the real and the imaginary parts of the sound pressure to show the periodic changes of two simple harmonics. Therefore, the influence of the ground reflection on the insertion loss of noise barriers is significant. Since the viaducts used in urban rail transit are commonly approximated as totally reflecting, the influence of the viaduct reflection on the insertion loss of noise barriers is also significant.

2. The tested results of the scale model for the straight barrier are basically in agreement with the numerical simulation results, which not only verifies the validity of the scale model, but also confirms the reliability of the test technology devices. The set of the devices and the materials used to build the scale model can be used to study the noise reduction mechanism of the nearly-enclosed barriers in urban rail transit later.

3. The spectrum of the insertion loss for the point source varies significantly with the source-receiver longitudinal distance: the path length of the direct and the reflected waves increases with the source-receiver longitudinal distance, resulting in the monotonic decrease of the low-frequency insertion loss. Meanwhile, the increased source-receiver longitudinal distance makes the decrease of the path difference between the direct and the reflected waves, causing the rest of the spectrum moves to the higher frequencies.

4. The insertion loss spectrum for a coherent line source is approximate to that for the corresponding point source, but the insertion loss spectrum for an incoherent line source shows a steady increase due to the influence of the source-receiver longitudinal

distance and the incoherence of the source. The spectra of insertion loss for the coherent line source and the incoherent line source are significant different: the former is higher than the latter and the difference increases significantly with frequency. Therefore, the determination of the line source type is of critical importance to the insertion loss spectrum in the research of the noise reduction mechanism of noise barriers.

5. The determination of the line source type is also of critical importance to the equivalent insertion loss. The equivalent insertion loss at a given receiver for the incoherent line source is approximately equal to that for the coherent line source, the former governed by the low-frequency component whereas the latter considered as the average, but both of them are much lower than that for the corresponding point source.

6. There is a strong consistency between the 1/3 octave spectrum and the frequency spectrum of the insertion loss for the incoherent line source. Therefore, when calculating the frequency spectrum of insertion loss in the field radiated by an incoherent line source, the calculation process can be simplified to only calculating the insertion losses at the centre frequencies for each 1/3 octave band.

5 Scale model experiments and 2.5-D BEM modelizations for reflective nearly-enclosed barriers

5.1 Introduction

The aim of this chapter is to analyze the acoustic performance of a reflective nearly-enclosed barrier using 2.5-D BEM methods and scale modelling tests. Based on the conclusion of the last chapter, the 2.5-D BEM program SAMRAY would probably come in useful to evaluate the acoustic performance of a reflective nearly-enclosed barrier. Its reliability was validated by comparing predictions with measured results from scale model tests. The scale modelling technique is more efficient and more accurate to investigate barrier performance. By using scale experiments and 2.5-D BEM approach the efficiency of noise reduction of constructed panels and the number effect of incoherent point sources are also studied.

This chapter is organized as follows. Section 5.2 presents a 2.5-D BEM model obtained from the real prototype measured in-situ in Chapter 3. The resonance effect of acoustic modes on the barrier performance is also described by a preliminary investigation in this section. Section 5.3 validates the numerical model by a series of scale measurements. As a result of the measured results much lower than the predictions, the sound insulation property of transparent materials is discussed in this section. Then a series of remeasurement on the modified model is described and the results give confidence in the subsequent predictions. Section 5.4 predicts the acoustic performance of a nearly-enclosed barrier by using a 2.5-D BEM modelling. The attenuation of the barrier for several receiver positions in the near and far fields comparing different source types are discussed in detail, and all the predicted results are summarized. Section 5.5 gives a brief conclusion in this chapter.

5.2 2.5-D Boundary element modelling

Last chapter discussed the effects of the source characteristics to the acoustic performance of a rigid straight barrier on the rigid ground and the acoustic performance of a reflective double-straight barrier on a viaduct, and found the barrier attenuations were significantly different in the acoustic fields of coherent line sources, point sources, and incoherent line

sources. P. Jean et al.[175] emphasized the importance of the source type in the numerical modelling based on calculations with 2.5-D BEM approaches. This section continues to discuss the acoustic performance of a reflective nearly-enclosed barrier on a viaduct in the acoustic fields of coherent line sources and a one-point source. Based on the numerical method proposed in [176], the 2.5-D existing program SAMRAY was used to carry out 3-D boundary element calculations from solutions of problems defined in two-dimensional domains outside the associated cross-section. At the beginning of 2.5-D calculations, the source is assumed as a coherent line source perpendicular to the cross-section at first, which maintains the two-dimensional nature of the model. Subsequently by Fourier-like transformations referred to in Chapter 4, the sound pressure fields created by the coherent line source for the whole frequency spectrum will be converted into those radiated by a point source in three dimensions. Besides, the nearly-enclosed prototype had a negative effect on the barrier attenuation at the 1/3 octave band of 100 Hz, which will be studied in the next chapters.

5.2.1 The model of a reflective nearly-enclosed barrier

The 2.5-D model of a nearly-enclosed barrier was obtained from the real prototype located on the viaduct of Metro 1 in Ningbo city, China, as shown in Figure 1.2. The noise barrier and the viaduct were assumed infinite uniform in construction along their length. In reality the barriers are installed on the viaducts so that there is no gap between the barriers and viaducts. However, on the basis of the BEM principle the distance between these two independent boundaries is at least larger than the element size[216]. Thus, this requires the geometry removal of the connections between them and therefore the boundaries of the viaduct and the barrier were integrated as a whole. These changes in the model are illustrated in Figure 5.1. The shape of source vehicle was simplified as a rectangle based on

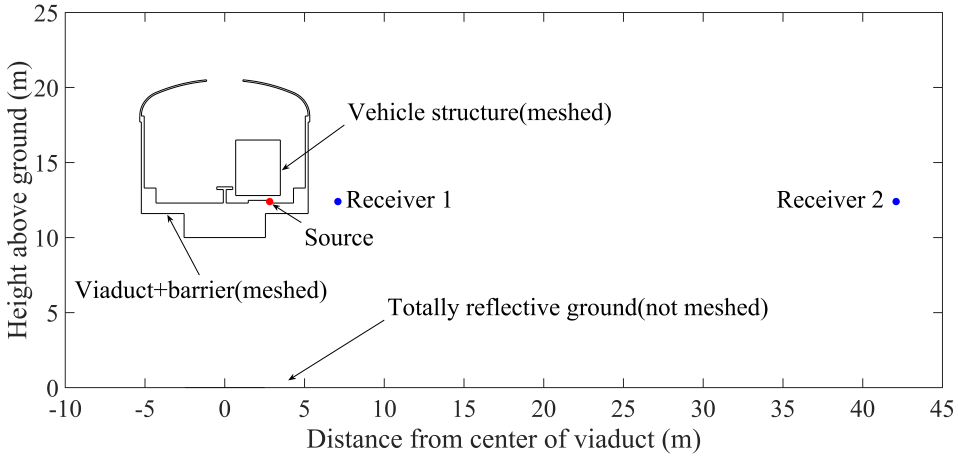

Fig 5.1.: Numerical model for nearly-enclosed barriers on urban railway viaducts solved by 2.5-D BEM program

measurements of the stock Type B of China Railway Rolling Stock. The height assumed was

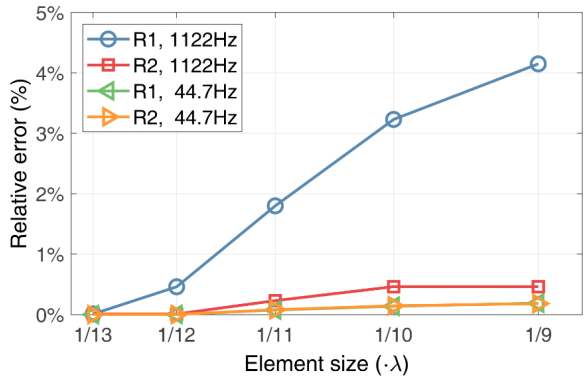

Fig 5.2.: A grid convergence of the 2.5-D BEM model for the nearly-enclosed barrier

3.7 m and the width was 2.8m. It can be seen from Figure 5.1 that the source was placed at the outside wheel-rail interaction position, and the distance between the source and the boundaries were required to be at least larger than the element size. All the boundaries of the vehicle structure were assumed to be acoustically rigid. The height of the viaduct above ground was 10 meters. In the BEM model, the ground was assumed to be acoustically rigid. Hence the effective sound pressure can be calculated by adding the separate intensity contributions due to the source and its image source in the perfectly reflecting plane[217].

Numerical predictions were calculated at third octave frequencies from 50 Hz to 1000 Hz. Figure 5.2 shows a grid convergence study for the specific geometry. For the receiver R1 at 44.7 Hz, R2 at 44.7 Hz and R1 at 1122 Hz, the relative errors of sound pressure are all less than 1% when the element size is no more than one ninth of the wavelength of 1122 Hz. Whereas for the receiver R1 at 1122 Hz, the relative errors of sound pressure are less than 5%. The results of grid convergence meet the need of our research. Hence to improve the precision requirement, the size of quadratic order element was defined as one tenth of the minimum wavelength.

5.2.2 Acoustic resonance effects of the open cavities

A preliminary investigation was performed with the BEM predictions to understand the mechanism of the multiple reflections inside a nearly-enclosed barrier. Figure 5.3 shows the BEM prediction results for Receiver 1(R1) and 2(R2) shown in Figure 5.1. It can be found that there are a great deal of significant peaks and valleys at many frequencies (some peaks are marked by red circles), and the number of them increases considerably with the increased frequency. In the fields radiated by the two types of sources, these peaks and valleys result in the distortions of sound pressure distributions, directly weakening the noise reduction performance of the reflective nearly-enclosed barrier. To simplify the calculation process, this section will find the reasons only for the occurrence of these peaks and valleys in the field radiated by the coherent line source.

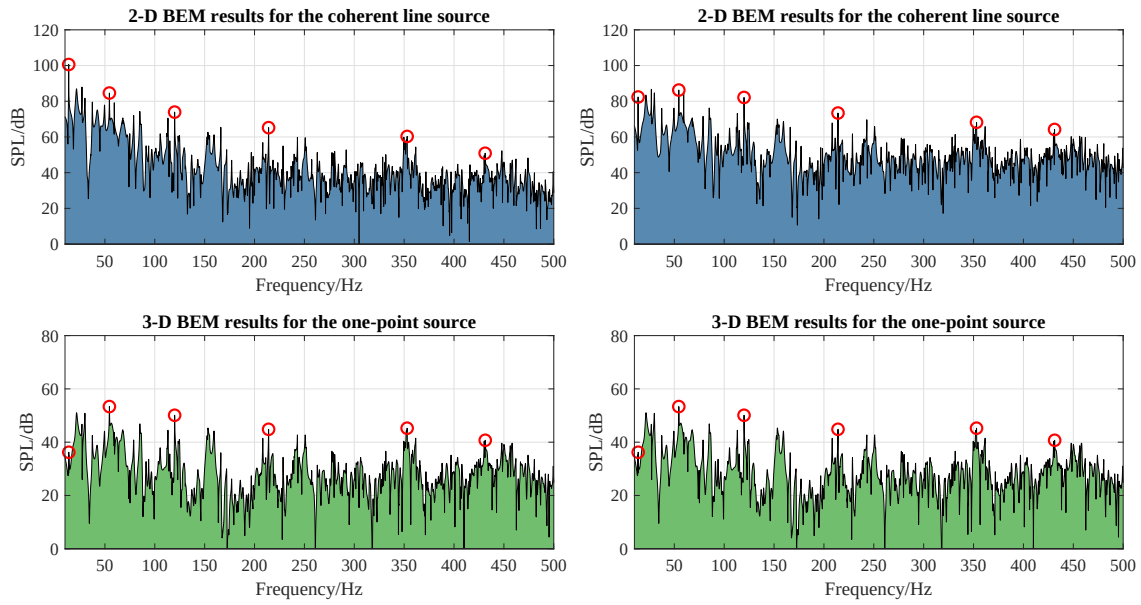

(a) Receiver 1 (R1)

(b) Receiver 2 (R2)

Fig 5.3.: The spectrum of sound pressure levels in the near and far field governed by the nearly-enclosed barrier(the receivers are positioned at the height of source)

Figure 5.4 shows the sound pressure distributions inside the nearly-enclosed barrier at peak frequencies marked by red circles in Figure 5.3. The peak frequencies were selected since the peak values of the sound pressure on the site with the barrier directly reduced the performance of the nearly-enclosed barrier compared with the valley values. It can be seen from Figure 5.4 that a spatial model distribution can be clearly identified at each peak frequency. Since the source is located inside the two inverted L-shaped structures, the sound waves are reflected by the surface of the structures for many times. The multiple-reflected waves are superimposed on the direct waves, interfering with each other. When the frequency of these sound waves approaches to the modal frequency of the open cavity, these sound waves form a resonant response at the resonant frequency. Therefore, the sound pressure distributions corresponding to these peak frequencies are governed by the modes of the open cavity.

These modes can be considered as trapped modes[57], that is, modes with local variations of geometries or materials in infinite space. The trapped modes can be also found in many systems, like local resonance modes formed by the fluid under gravity bounded by a fixed surface and an infinite free surface[218], floating breakwaters[219], electromagnetic hyper-surface[220] and etc. The trapped modes converge most of the acoustic energy into the local area inside the open cavity, and the energy density decreases with the increased distance from the source. From a mathematical perspective, the trapped mode can be considered as the eigenvalues of the homogeneous Helmholtz equation with the specific boundary conditions[221]. In order to identify the trapped modes of the nearly-enclosed barrier, the two-dimensional acoustic modes of the cavity was calculated by the finite element method (FEM, ABAQUS). Since the finite element method can only be used to solve finite-space

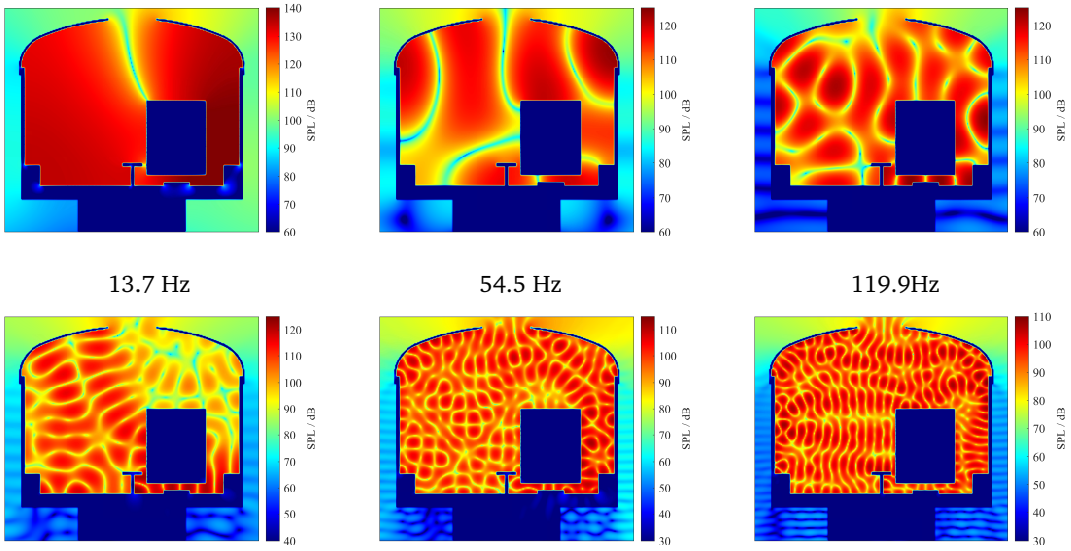

Fig 5.4.: Examples of pressure level distributions at the peak frequencies in the 2-D BEM model of the nearly-enclosed barrier

problems, and the width of the top opening is much smaller than the size of the whole barrier, the top opening was ignored and only the modes of the fully-enclosed cavity were calculated by using the FEM. Figure 5.5 shows the spatial distributions of sound pressure for

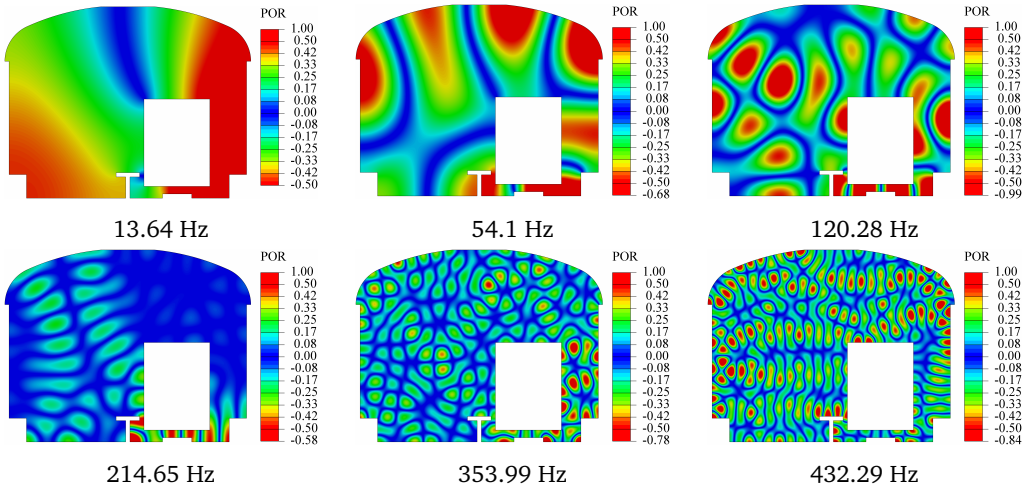

Fig 5.5.: Examples of acoustic modes of the fully-enclosed air cavity calculated by a 2-D FEM method

the fully-enclosed barrier at the modal frequencies which are close to the peak frequencies shown in Figure 5.4. It can be seen that the spatial distribution at each modal frequency for the fully-enclosed cavity is basically consistent with that at the similar peak frequency for the nearly-enclosed barrier, but there is a slight difference between the modal frequency and the peak frequency.

The spatial distributions of the sound pressure inside the nearly-enclosed barrier depend

strongly on the trapped modes of the open cavity, and the peak frequencies are close to the modal frequencies. Therefore, it can be concluded that the peaks in the spectrum of sound pressure at the receiver outside the barrier are caused by the acoustic resonance effect of the open air-cavity. The open cavity causes the superposition of the directed and the multiple reflected waves, resulting in the acoustic resonance responses at the resonant frequencies. The open cavity cannot capture all the sound energy, resulting in the overflow of the energy from the top opening to the external shadow area. Hence the insertion loss of the nearly-enclosed barrier at the resonant frequencies are weakened. From the number of the modes for the fully-enclosed cavity in different frequency bands (as shown in Figure 5.6), it can be found that the number of the mode increases significantly with the frequency,

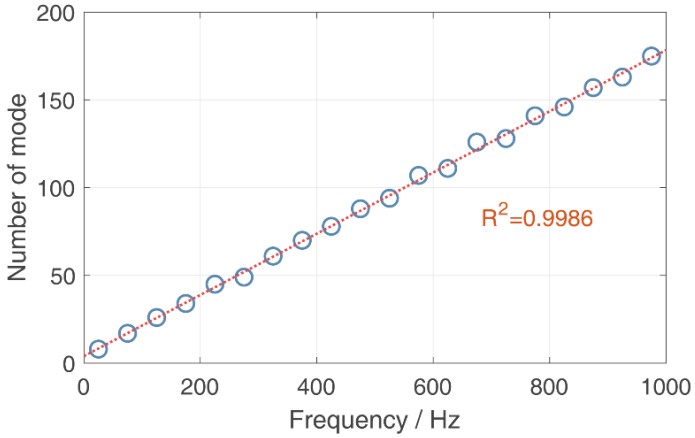

Fig 5.6.: The variation of the mode number with the frequency for the fully-enclosed cavity

with a linear relationship (linear fitting $R^2 = 0.9986$). This corresponds to the change law that the number of the peak increases profoundly with frequency, which indicates that it is in the whole frequency range that the acoustic resonance effect caused by the open cavity has a negative influence on the noise reduction performance of the barrier. The negative influence at low frequencies mainly depends on the amplitude of the peak, while that for high frequencies mainly depends on the number of the peak.

To clearly understand the relationship between the peak frequency and the modal frequency for the fully-enclosed cavity, the complex geometry of the nearly-enclosed barrier was simplified to a rectangular open cavity with a cross section of 9 meters wide and 7 meters high, the width of the opening being 2 meters. The simplified open cavity is shown in Figure 5.7, compared with a fully-enclosed cavity of the same size. For a totally-reflecting cavity with a rectangular cross section, its modal wave number is commonly expressed as,

$$k_{mn} = \sqrt{\left(\frac{\pi m}{b}\right)^2 + \left(\frac{\pi n}{d}\right)^2} \tag{5.1}$$

where b and d represents the width and the height of the rectangular cross section, respectively. m and n represents the modal order corresponding to the width and the height of the rectangular cross section, respectively. All the modal frequencies were calculated by

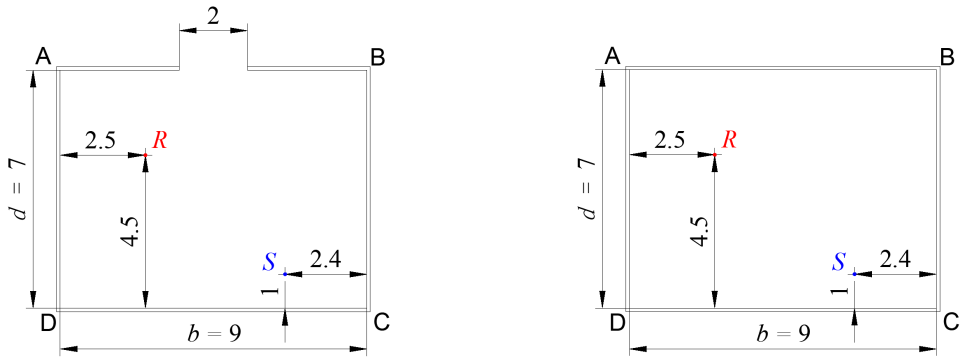

The rectangular cavity with an opening

The fully-enclosed rectangular cavity

Fig 5.7.: The cross sections of the simplified models for the nearly-enclosed barrier and the fully-enclosed cavity

$k = 2\pi f/c$, those below 100 Hz being shown in Table 5.1.

Tab 5.1.: The modal frequencies for the fully-enclosed cavity (below 100 Hz)

Modal frequency		m ($b = 9$)					
		0	1	2	3	4	5
n ($d = 7$)	0	0.00	19.06	38.11	57.17	76.22	95.28
	1	24.50	31.04	45.31	62.20	80.06	98.38
	2	49.00	52.57	62.08	75.29	90.61	-
	3	73.50	75.93	75.29	93.11	-	-
	4	98.00	99.84	-	-	-	-

The sound pressure level spectra at a given receiver (receiver R shown in Figure 5.7) inside the cavity with an opening and the fully-enclosed cavity were solved by the boundary element method respectively, as shown in Figure 5.8. It can be seen that in the sound

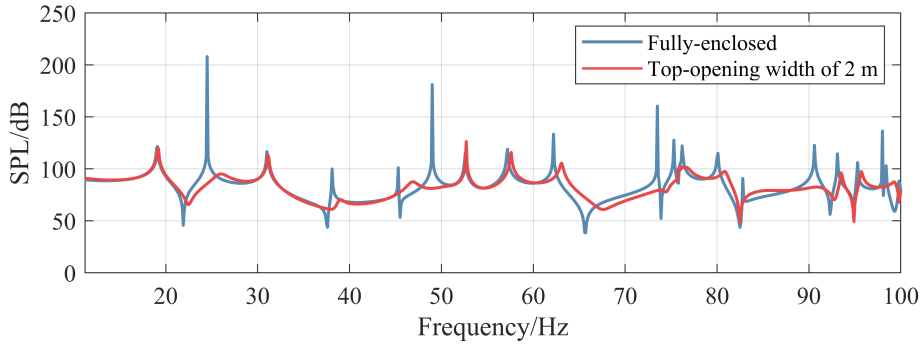

Fig 5.8.: The sound pressure level spectra at a given receiver inside the cavity with an opening and the fully-enclosed cavity

pressure spectrum at the receiver inside the fully-enclosed cavity (Figure 5.7(b)), there are significant peaks at each of the modal frequencies listed in Table 5.1. However, in the spectrum at the receiver inside the cavity with an opening (Figure 5.7(a)), the peaks are visible at the frequency corresponding to only part of the modal frequencies listed in

Table 5.1, each peak frequency slightly higher than the corresponding modal frequency. Close to other modal frequencies, there are no peaks. This is caused by the opening of the cavity, of which the existence on the boundary AB causes a reduction in the multiple reflections of sound waves between the boundary AB and the boundary CD. Therefore, the peak values near the modal frequencies corresponding to the height of the cavity can be significantly decreased. For example, the peak value near 24.50 Hz for the cavity with an opening is much lower than the corresponding peak value of the first-order vertical mode $(m = 0, n = 1)$ for the fully-enclosed cavity. Besides, the presence of the opening also results in an inconsistency of the sound distributions between these two cavities, and therefore the peak frequencies corresponding to the width of the open cavity are close to the modal frequencies for the fully-enclosed cavity but not exactly the same.

With the increased width of the opening, the cavity with an opening gradually approaches to the cavity with a fully-opening. By changing the opening width of the boundary AB, its influence on the characteristic parameters of the peaks is analyzed. Figure 5.9 compares the

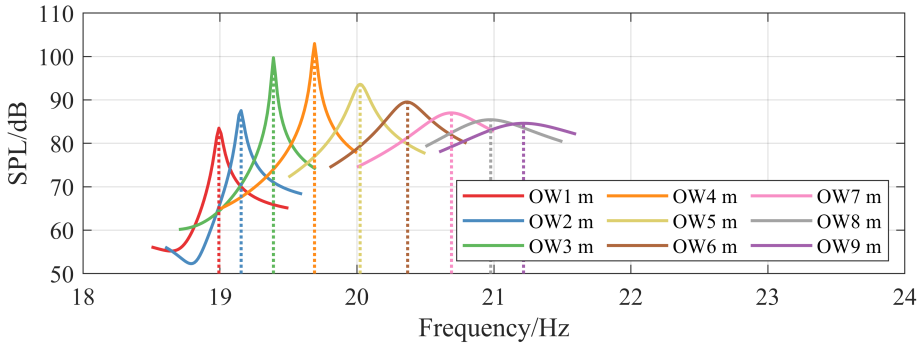

The peak corresponding to the first-order horizontal trapped mode

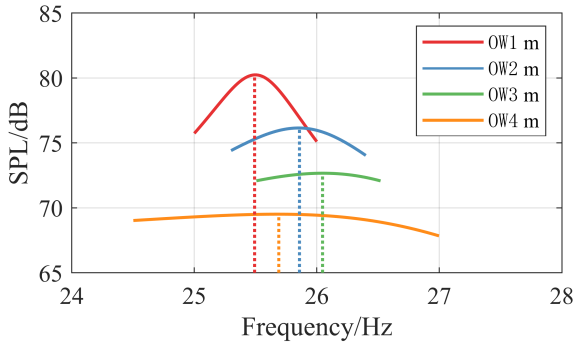

The peak corresponding to the first-order vertical trapped mode

Fig 5.9.: The variation of the peak value and the peak frequency with the opening width

peaks of the sound pressure level at a given receiver outside the cavities with openings of different widths, at the frequencies corresponding to the first-order trapped modes. It can be seen that the peak frequency of the first-order horizontal mode increases with the opening width, and the relationship between the peak frequency and the opening rate (the ratio of the opening width to the length of the boundary) can be fitted by Fourier series(determination coefficient $R^2 = 0.998$); The peak value first increases and then decreases, and the maximum appears at the opening rate of about 50%; The damping coefficient ξ first decreases and then

increases significantly, calculated by the half-power bandwidth method. From Figure 5.9(b), it can be seen that the peak value of the first-order vertical mode appears significantly when the opening width is only 1 meter. With the increased width of the opening, the peak value decreases significantly until it disappear. Therefore, when one boundary of a cavity (i.e. boundary AB) is fully open, that is, only one pair of opposite boundaries (i.e. boundary AD and boundary BC) are available, all the peaks in the spectrum of the sound pressure can be highly corresponding to all the horizontal trapped modes.

The noise reduction mechanism of the double-straight barrier which can be considered as the nearly-enclose barrier without the top arched PC sheets (see Chapter 4 Figure 4.8(b)), can be further analyzed based on the fully-open cavity. A comparison of the sound pressure level spectrum at a given receiver outside the barrier is made between the nearly-enclosed and the double-straight models, being shown in Figure 5.10. It can be seen that the peak

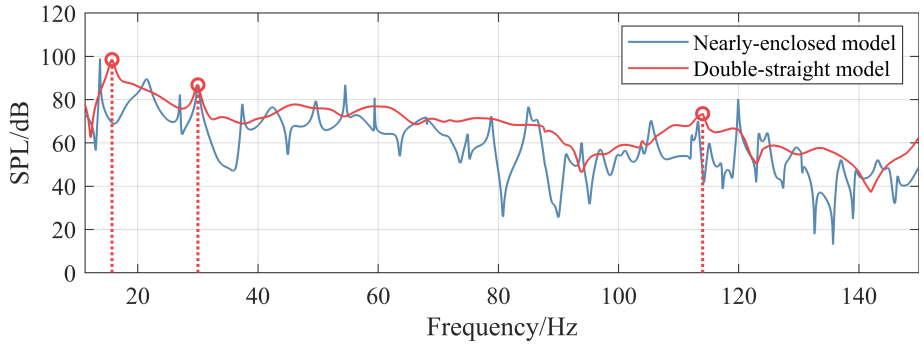

Fig 5.10.: The spectra of sound pressure level at a given receiver outside the barrier for the nearly-enclosed and the double-straight barriers

number for the double-straight model is relatively small, which is because the top opening is completely open, resulting in only the peaks caused by the acoustic resonance effects of horizontal trapped modes appearing.

In Figure 5.10, the frequencies of the first three peaks for the double-straight barrier are 15.7 Hz, 30 Hz and 114 Hz, respectively (marked by the red circles). And there is also a peak for the nearly-enclosed barrier close to each of them. Figure 5.11 shows the sound distribution at each peak frequency of the three for these two models. It can be found that the three peaks marked by red circles in Figure 5.10 are mainly caused by the acoustic resonance effects of the first-order horizontal modes for the region A, the region B and the region C shown in Figure 5.11, respectively. The three peak frequencies for the double-straight model are slightly higher than those for the nearly-enclosed model, and the peak values for both two models are approximately consistent with each other. The trapped mode of 30 Hz for the nearly-enclosed model has not only the first-order horizontal trapped mode for the region B, but also the second-order horizontal trapped mode for the region A. Hence the peak frequency for the double-straight model is the same as that for the nearly-enclosed model.

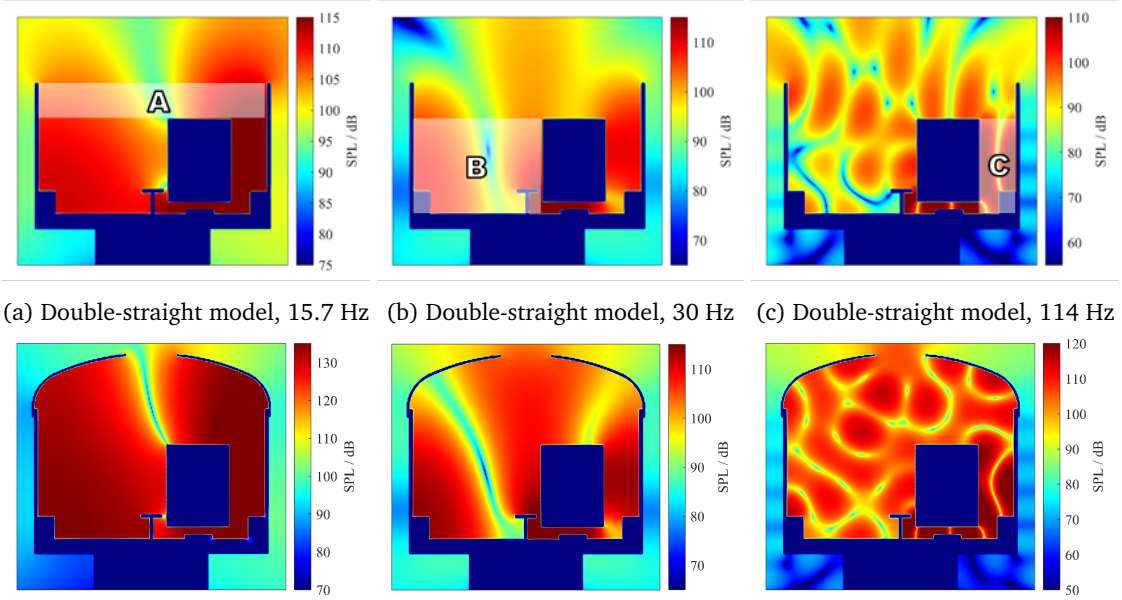

(a) Double-straight model, 15.7 Hz (b) Double-straight model, 30 Hz (c) Double-straight model, 114 Hz

(d) Nearly-enclosed model, 13.7 Hz (e) Nearly-enclosed model, 30 Hz (f) Nearly-enclosed model, 113.2 Hz

Fig 5.11.: Examples of pressure level distributions at the peak frequencies in the 2-D BEM model of the nearly-enclosed barrier

Given the above, it can be concluded that it is with different degrees that the geometries of the noise barriers with top openings of different widths have influences on the noise reduction effects. Nevertheless, the noise reduction mechanisms of all the noise barriers with top openings can be reasonably explained by the acoustic resonance effects of open cavities.

5.2.3 Multiple-reflection effects of the vehicle boundaries

It can be found from the discussion of the noise reduction mechanism of the double-straight barrier that even if there are only one pair of opposite boundaries on a cavity, that is, the top of the cavity is completely open, there are still many peaks in the sound pressure spectrum at the receivers outside the barrier. These peaks are caused by the multiple-reflection effects of the barriers on two sides, as well as the multiple reflections between the vehicle boundaries and the barrier on each side. Acoustic resonance effect of the open cavity can be used to explain the multiple reflections caused by the double-straight model, also the multiple-reflection effects of the vehicle boundaries. Therefore, it can be used to explain the multiple reflections between the vehicles and the viaducts. Taking example for the site without a barrier, it can be observed from Figure 5.12 that with the help of the vehicle structure, a micro-opening cavity is formed by the vehicle, the T-shape passageway, the top and the side panels of the viaduct. While in the model without the vehicle (see Figure 5.12(b)), there is only a fully-open cavity formed by the T-shape passageway, the top and the side of the viaduct. Figure 5.13 compares frequency spectra and one-third octave spectra

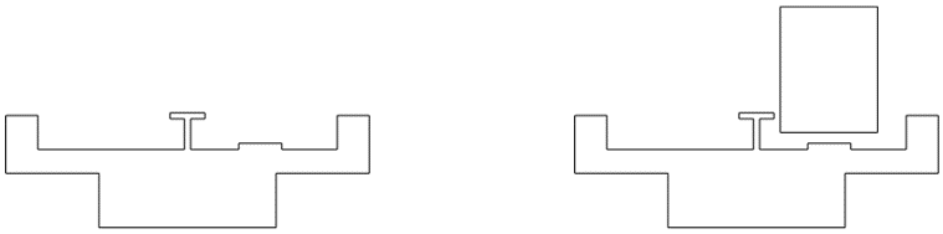

(a) The model without the vehicle structure (b) The model with the vehicle structure

Fig 5.12.: The models on the site without a barrier

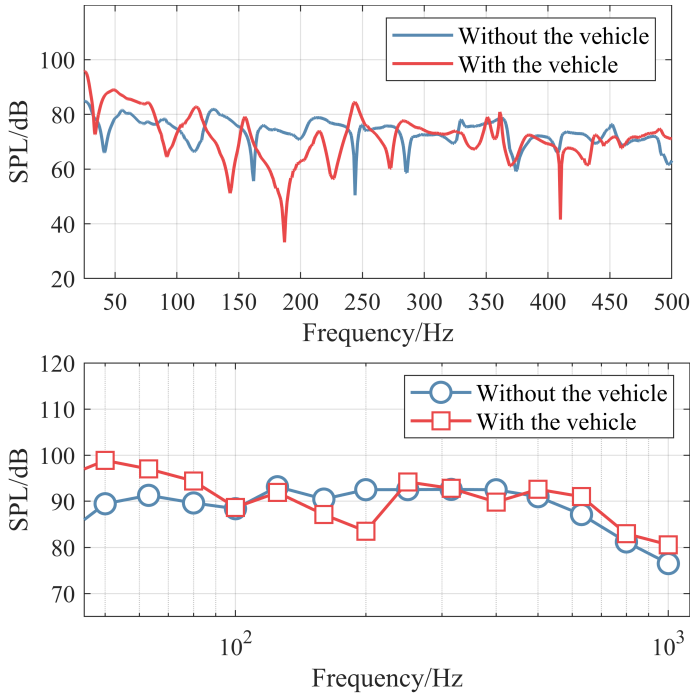

Fig 5.13.: A comparison of sound pressure frequency spectra and one-third octave spectra at a given receiver between the models with and without the vehicle structure

at a given receiver between the models with and without the vehicle structure. It can be seen that there are more peaks and valleys in the frequency spectrum for the model with the vehicle structure, causing the levels higher than those for the model without the vehicle in the one-third octave bands below 100 Hz, and the levels lower than those for the model without the vehicle in the bands of 160 Hz, 200 Hz and 400 Hz.

Similar to study the acoustic resonance effect of the open cavity, a fully-enclosed cavity model formed by the vehicle, the T-shape passageway, the top and the side of the viaduct, was established (see Figure 5.14) and calculated. The spectrum result of sound pressure at the receiver inside the cavity is drawn by a blue curve in Figure 5.15. It is obvious that there are many peaks (marked by red stars) and valleys (marked by red crosses) in the spectrum, definitely dependent on the acoustic modes of the fully-enclosed cavity. Based on the conclusion given above, the trapped modes must be formed in the model with the vehicle structure, and the trapped-modal frequencies can be approximate to the modal

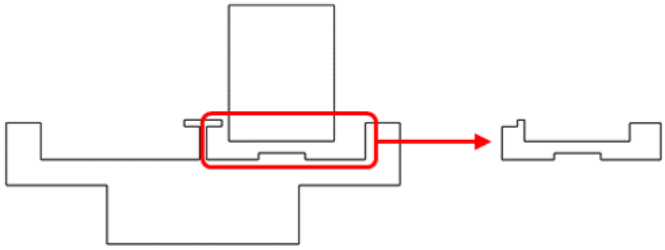

Fig 5.14.: A fully-enclosed cavity model formed by the vehicle, the T-shape passageway, the top and the side of the viaduct

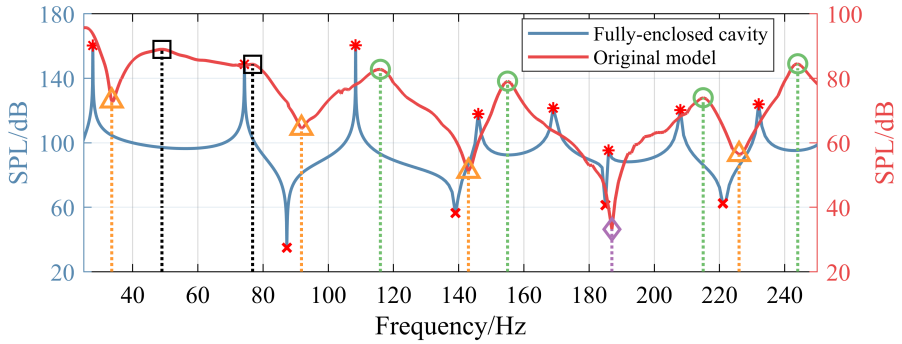

Fig 5.15.: A comparison of sound pressure spectrum between the fully-enclosed cavity model and the model with the vehicle structure

frequencies of the fully-enclosed cavity.

Figure 5.15 also shows the spectrum at a given receiver in the model with the vehicle structure, compared with that for the fully-enclosed cavity. It can be found that the peaks at 116 Hz, 155 Hz, 215 Hz and 244 Hz (marked by green circles) are governed by the trapped modes of the micro-open cavity, the sound distributions of the two models at these peak frequencies compared one-to-one and shown in Figure 5.16. Besides, the peaks at

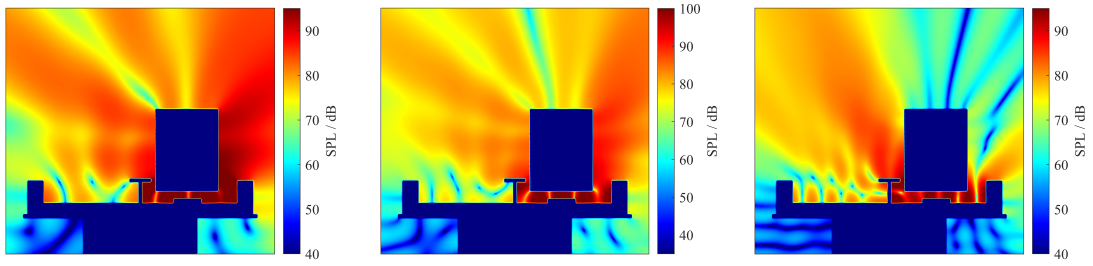

(a) The model with the vehicle structure, 116 Hz

(b) The model with the vehicle structure, 155 Hz

(c) The model with the vehicle structure, 215 Hz

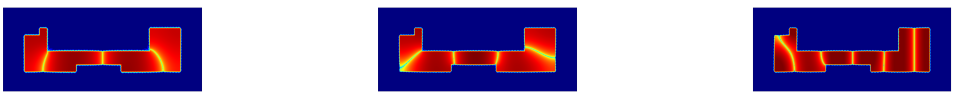

(d) The fully-enclosed cavity model 108.5 Hz

(e) The fully-enclosed cavity model 146 Hz

(f) The fully-enclosed cavity model 208 Hz

Fig 5.16.: A comparison of sound distributions at the peak frequencies between the model with the vehicle structures and the fully-enclosed cavity model

27.9 Hz and 74.3 Hz for the fully-enclosed cavity model can not be found in the spectrum curve for the model with the vehicle structure, which is because the opening formed by the right side of the vehicle and the side of the viaduct is too large, significantly reducing the multiple-reflection effects nearby, directly influence the effective constructions of these two modes. By observing the sound pressure distributions at 49 Hz and 76.8 Hz (relatively higher levels marked by black rectangles in Figure 5.15) for the model with the vehicle structure (shown in Figure 5.17), it can be seen that the sound pressure distribu-

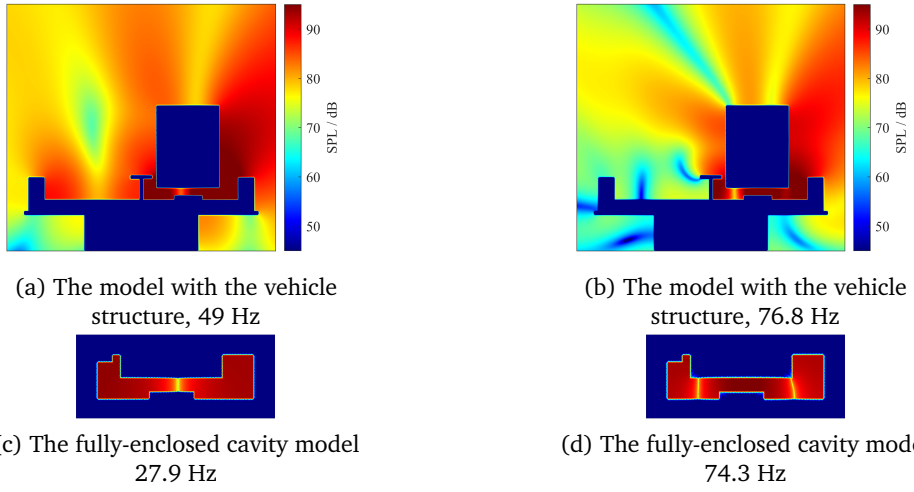

(a) The model with the vehicle structure, 49 Hz

(b) The model with the vehicle structure, 76.8 Hz

(c) The fully-enclosed cavity model 27.9 Hz

(d) The fully-enclosed cavity model 74.3 Hz

Fig 5.17.: A comparison of sound distributions at low frequencies between the model with the vehicle structure and the fully-enclosed cavity model

tions in most fields are still governed by the trapped modes except the area close to the opening on the right, resulting in considerably higher levels at the frequencies below 100 Hz.

The valleys at 33.6 Hz, 91.8 Hz, 143 Hz and 226 Hz (marked by orange triangles in Figure 5.15) are also governed by the trapped modes of the micro-open cavity, the sound distributions of the two models at these valley frequencies compared one-to-one and shown in Figure 5.18. However, it is at the valley frequencies of 187 Hz and 410 Hz for the model with the vehicle structure (marked by purple diamonds in Figure 5.15) that there are no valleys found in the spectrum curve for the fully-enclosed cavity. This is attributed to the receiver position in the destructive region of the direct and the reflected waves, marked by white dots in Figure 5.19. As a consequence, although there are two valleys for the model with the vehicle at the peak frequencies for the fully-enclosed cavity model, these two valleys are still governed by the acoustic resonance effect of the micro-open cavity.

Given the above, the frequency spectrum for the model with the vehicle structure can be reasonably explained by the acoustic resonance effect of the micro-open cavity, although the peak and the valley frequencies are not completely corresponding to the trapped modal frequencies. Hence it suggests that the multiple-reflection effects of the vehicle boundaries must be considered seriously in the study of the noise radiation problems from urban rail transits or high-speed railways.

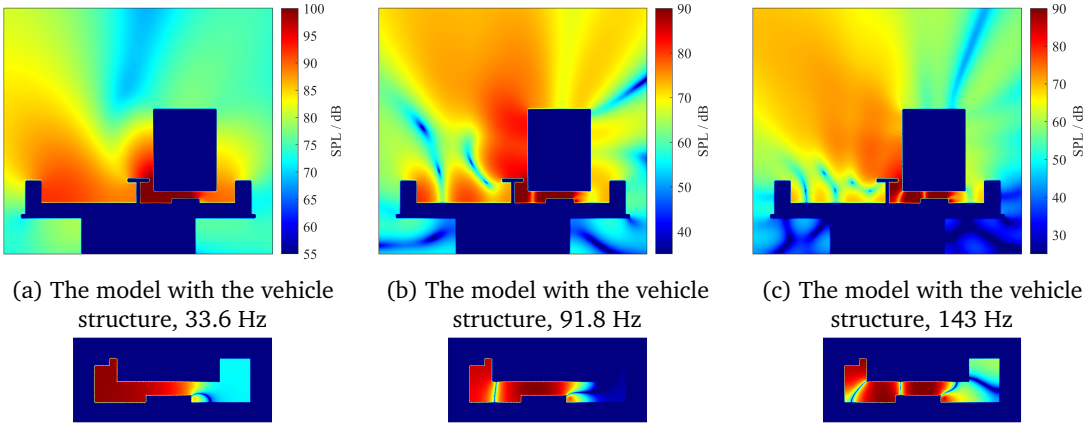

(a) The model with the vehicle structure, 33.6 Hz

(b) The model with the vehicle structure, 91.8 Hz

(c) The model with the vehicle structure, 143 Hz

(d) The fully-enclosed cavity model 22.3 Hz

(e) The fully-enclosed cavity model 87.3 Hz

(f) The fully-enclosed cavity model 140 Hz

Fig 5.18.: A comparison of sound distributions at the valley frequencies between the model with the vehicle structures and the fully-enclosed cavity model

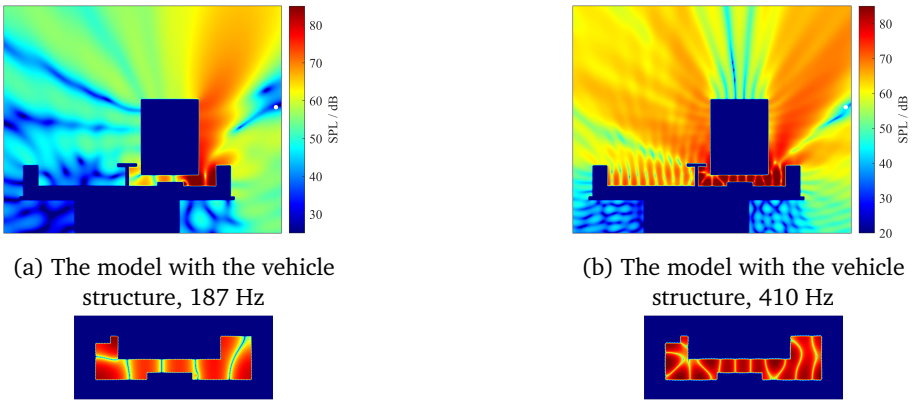

(a) The model with the vehicle structure, 187 Hz

(b) The model with the vehicle structure, 410 Hz

(c) The fully-enclosed cavity model 186 Hz

(d) The fully-enclosed cavity model 410 Hz

Fig 5.19.: A comparison of sound distributions at the frequencies where the receiver is positioned at the destructive region

5.3 Scale model measurement

To validate the predicted results for a nearly-enclosed barrier, the method of acoustic scale modelling was introduced. Scale model measurement has strict request to measurement environment. The test site has to be deliberately left as open as possible in order to emphasize the diffraction sound generated by the barrier model and prevent reflection sound caused by any reflecting surface close to the model from affecting the measured results. The site was finally selected as shown in Figure 5.20(a), which fully met the requirement specified previously. Considering the site limitations, the scale of the barrier model in our case was determined as 1:20.

5.3.1 Measurement apparatus

Generally loudspeakers and microphones are the indispensable transducers in an acoustic experiment. In order to send the electrical audio signal to the loudspeaker and receive it from the microphone synchronously, a collection of electronic apparatus was prepared. Miniature speakers with the size of less than 1 mm^3 were chosen in our study since the space where the speaker was located was less than 10 cm^3(approximately the size of an eraser). Commonly a normal-sized loudspeaker has a diameter of at least 30 mm, which is too large to be placed inside this model. The spectrum of the speaker was measured at several angles. It was found to be omni-directional when towards the microphone. During the formal measurement for each test several employed loudspeakers emitted simultaneously white noise with one of the third octave spectrum from the signal output module. For these miniature loudspeakers the amplifiers and the power supply were selected accordingly. On the other hand, the highly sensitive B&K microphones 4189-A-021 satisfy the requirements of such high-precision, free-field measurement. They were powered from the supply offered by the DAQ signal output module. All the electronic apparatus were put under the model above ground, which did not appear in the transmitting path between the loudspeakers and the microphones affecting the measured results.

A VI project was designed in the LabVIEW development environment to transmit\receive electric signals, shown in Appendix B. Figure 5.20(b) illustrates the signal flow graph of the measurement. It can be seen clearly that the original source signal was generated by the VI project from the laptop, transmitting to the output module, via the amplifier to the loudspeaker. In the meantime, sound pressure signal was received and preamplified by the microphone, via the input module back to the laptop, finally saved by the VI project. It is worth emphasizing that the VI project did not only play a role as a signal generator for activating the loudspeaker, it also undertook that of receiving, saving and analysing the signals from the receivers.

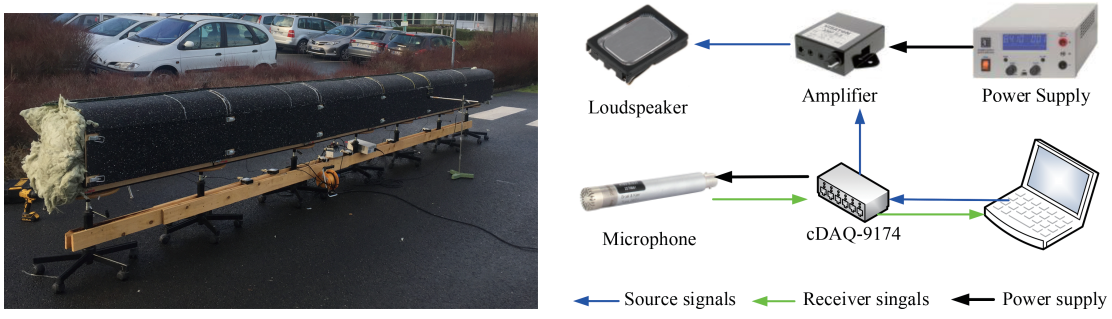

(a) Measurement site (b) Electronic apparatus

Fig 5.20.: Scale measurement preparation

5.3.2 Scale model measurements

All barriers used in the experiment were a twentieth of the full scale numerical models. It was necessary to build simplified models for the complex structure so that sound diffraction towards the barrier top would dominate attenuation measurements, facilitating comparison with the predictions from the BEM model which is 2.5-D in the space with infinitely long barriers. The tests were made in six configurations, of which the cross-sections were shown in Figure 5.21,

- Tests with viaducts and nearly-enclosed barriers(Figure 5.21(a1)(a2)).
- Tests with viaducts and double-straight barriers(Figure 5.21(b1)(b2)).
- Tests with viaducts(Figure 5.21(c1)(c2)).

The blue parts represent PC panels with a thickness of 5 mm and the brown parts are 9-mm-thick assembled wood planks. Unlike the simplification in the BEM model that the connection between the viaduct and the barrier were removed, in the scale model the viaduct and the barrier were two independent and complete components. Screws were used to fix these two components together, as shown in Figure 5.21(a1). Tests were made with and without vehicle structures which were one twentieth the practicable 3.7x2.8 m^2 in full scale.

The 1:20 scale model was an assembly of six sections the length of each section being defined as 1 m since the metro vehicle is 19 m long and each train has six vehicles in reality. However, sound transmitting over the two ends of the model to the microphone must affect sound pressure levels at the receivers. In order to reduce the end effect as much as possible, both barrier ends were filled with mineral wool to absorb the sound diffracted by the ends(shown in Figure 5.20(a)). This way can be equated with the infinitely long barrier in the BEM model, aiming to eliminate the sound diffracted by the two ends.

There were twelve loudspeakers arrayed along the length of the six-section model. Each section of the model had two sources placed exactly at the position of each vehicle wheel in reality. The position in the cross section was close to the location of the wheel-rail interaction, in accord with that of the point source in the 2.5-D BEM model. A time-history signal of white noise was taken as the input of the sound source to the loudspeaker. The white-noise signals were mutually incoherent to each other. Figure 5.22 and Table 5.2 present these co-ordinates and the numbers of loudspeakers. The sampling position for the microphone was placed exactly at the cross-section where the 7th loudspeaker was positioned.

Two sets of tests were taken to determine the third octave sound pressure levels outside the barriers. Tests were completed with the viaduct but without barriers(Figure 5.21(c1)(c2))

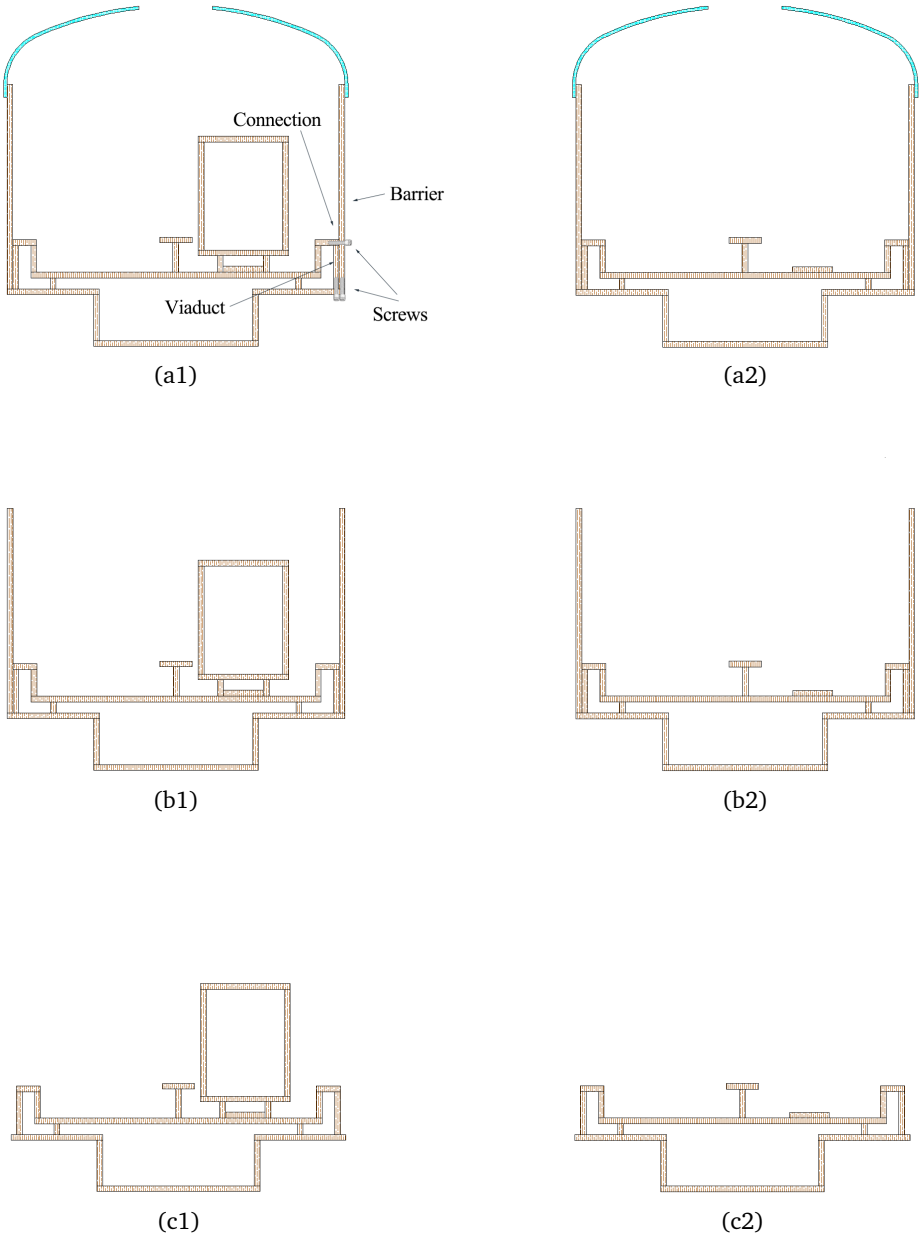

Fig 5.21.: All the configurations of tested models. The left row shows the models with vehicle structures and the right row shows the models without vehicle structures.

so that the attenuation could be calculated as the difference between the sound pressures measured in the presence and absence of barriers. Tests with viaducts and double-straight barriers(Figure 5.21(b1)(b2)) were completed as well in order to understand the sound insulation property of the PC panels. In addition, the attenuations at the third octave band frequency from 1000 Hz to 20 kHz were tested to validate the 2.5-D BEM predictions from 50 Hz to 1000 Hz.

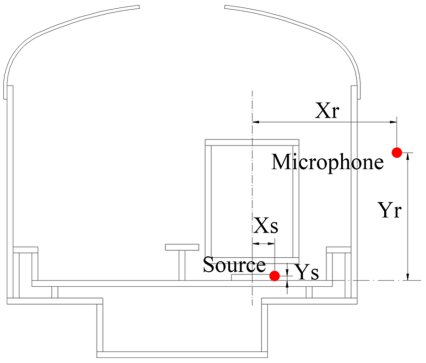

(a) Cross-section of the scale model

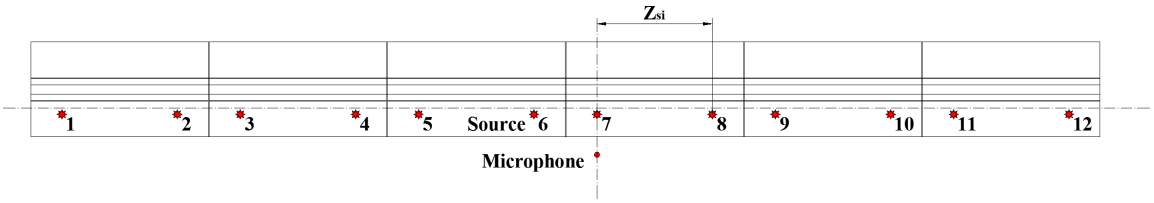

(b) Plan view of the scale model

Fig 5.22.: Experimental arrangement for the nearly-enclosed scale barrier

Tab 5.2.: Positions of loudspeakers and microphone in three co-ordinates(cm)

Loudspeaker			Microphone		
X_s	Y_s	Z_{si}(i=1,2,...,12)	X_r	Y_r	Z_r
3.6	0.5	-296.7, -233.7, -197.8, -134.8, -98.9, -35.9, 0, 63.0, 98.9, 161.9, 197.8, 260.8	25.6	19.0	0

5.3.3 Comparisons with BEM predictions

Predictions were carried out for the nearly-enclosed and double-straight barriers using the 2.5-D BEM program SAMRAY. The measured results were obtained by the differences of the sound pressure levels at the site without a barrier and at the site with a barrier, while the predicted results were obtained by using the calculation method shown in Chapter 4. There were four comparisons of models in the acoustic field of the one-point source:

- The nearly-enclosed barrier on the viaduct with the vehicle.
- The nearly-enclosed barrier on the viaduct without the vehicle.
- The double-straight barrier on the viaduct with the vehicle.
- The double-straight barrier on the viaduct without the vehicle.

The model of the double-straight barrier on the viaduct with the vehicle was the one measured in Chapter 4, which was measured and predicted again to compare its acoustic performance with that of the nearly-enclosed barriers. Figure 5.23 shows these four

comparisons between the predicted and the measured results. The predicted third octave source spectra was adjusted in the analysis so that the effective source spectra used in the BEM and scale models were identical. Note that further frequencies in Section 5.3 will be given in the scale 1:20 from 1000 Hz to 20 kHz for the sake of clarity.

For one point source facing the microphone, Figure 5.23(a) shows plots of measured and predicted attenuations by the third octave band in the case of the double-straight barriers on the viaduct with and without vehicles. It is clear that as expected there is good agreement for each comparison between the measured results and those predicted by the 2.5-D BEM approach. The small deviation between the measured and predicted results is normal and permissible due to the non-idealised point source used for measurements.

Figure 5.23(b) shows the compared results for the nearly-enclosed barrier on the viaduct. It is worth noting that the measured attenuations are much lower than those predictions regardless of the vehicle structures present, especially for high frequencies. And these measured results are as high as those measured for the double-straight type. With the finding of these significant differences between the measured and predicted results for the nearly-enclosed barrier, a strong argument can be made that the PC panels on the top were not considered to be acoustically rigid. This finding might be due to the sound insulation properties of the PC panels and wood planks which were not sufficiently high to reduce sound transmission through the nearly-enclosed barrier. Hence, the sound insulation performance of the employed PC panels would be studied in the next section.

5.3.4 Sound insulation problem

In terms of energy transfer, attenuation of the sound barrier(also known as Insertion Loss) depends precisely on the energy distribution of sound diffraction over the top, transmission through the barrier and reflection bounced off its surface. Considering the effect of ground absorption, the practical attenuation of the sound barrier is given as[154],

$$Att = IL = A_d - C_t - C_r - C_G \tag{5.2}$$

where A_d denotes diffraction attenuation of the top edges of a single barrier on the acoustically rigid ground, which is the most important physical phenomenon in the noise reduction process. C_t is the correction value for sound transmission through the barrier. Typically, the diffraction attenuation A_d is much lower than the TL of high-density materials employed in the construction of the barrier, at least 10 dB. In such case, the correction for sound transmission C_t is negligible in the overall performance of the barrier. Otherwise, the correction C_t must be taken into account. When there are parallel barriers on the roads or railways, the multiple reflection will reduce the barrier attenuation. The reduction induced by the multiple reflection wave is considered as the correction for the sound reflection, denoted by

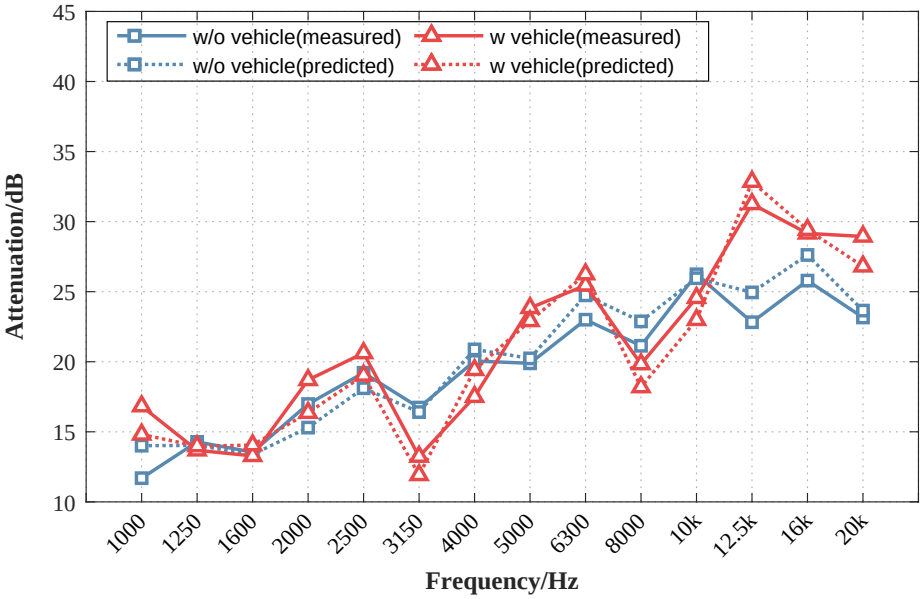

(a) Double-straight barrier on the viaduct

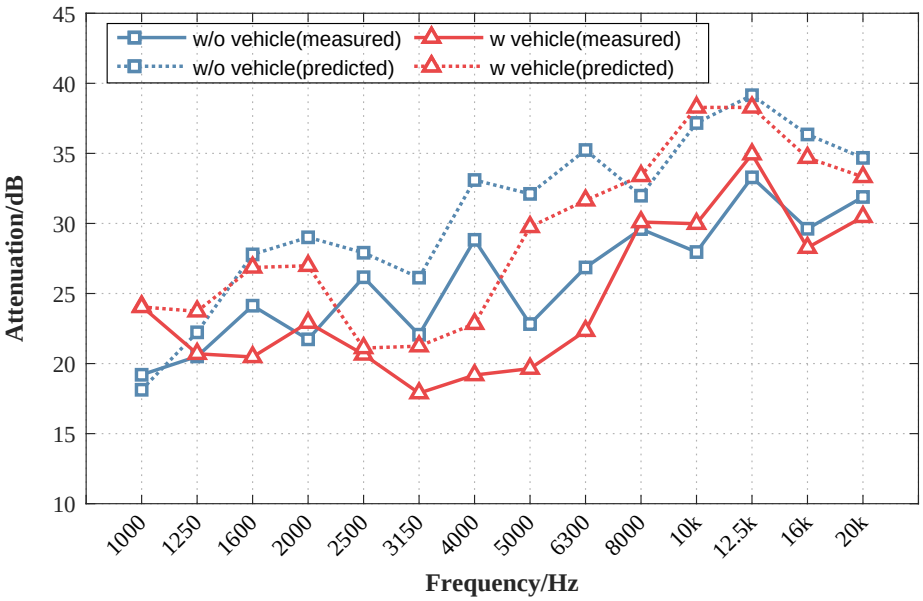

(b) Nearly-enclosed barrier on the viaduct

Fig 5.23.: Measured and predicted attenuations for the model(a) double-straight barrier(Figure 5.21(b1)(b2)); (b) nearly-enclosed barrier(Figure 5.21(a1)(a2))

C_r. C_r mainly depends on the distance between two parallel barriers, the distances between the source and the barriers and the absorption coefficient of the barrier close to the source. C_G denotes the correction for ground absorption. If the ground is not perfectly reflecting, it will absorb a lot the transmitting sound waves, resulting in the reduction of the barrier attenuation. This reduction is considered as the correction for ground absorption C_G in the calculation of the barrier attenuation.

In the BEM model, the parallel barriers and the vehicle structure had been meshed. Therefore, the multiple reflection induced by them had been considered in the predictions so that the correction for the sound reflection $C_{r,\text{enclosed}}$ could be neglected. Since the ground was assumed acoustically rigid, there was no correction for ground absorption $C_{G,\text{enclosed}}$. As a consequence, the attenuation of the nearly-enclosed barrier was dependent on the diffraction attenuation A_d and the correction for sound transmission C_t. In the context, the C_t can be ignored only when the A_d is lower than the TL of the employed materials at least 10 dB. In such case, the barrier attenuation Att will be approximately to A_d. Figure 5.23 shows that the predicted attenuations of the nearly-enclosed barrier(Att_{enclosed}) are greatly higher than 20 dB over the frequency range of 1000 Hz-20 kHz. These values might be extremely close to those for the TLs of the employed materials so that the correction $C_{t,\text{enclosed}}$ could not be ignored in the calculation of the insertion loss. According to Equation (5.2), the measured attenuations were therefore lower than our expectations.

Since the barrier attenuation is frequency dependent and so is the impact of transmission loss, to better understand their relationship, the comparisons for high frequencies between the predicted attenuations for the nearly-enclosed and the double-straight barrier and the measured TLs for the PC panels are illustrated in Figure 5.24. The blue and red curves without symbols represent the TLs for PC panels measured by Woo-Mi Lee et al.[222] with a thickness of 4 mm and 8 mm, respectively. On account of the thickness of the PC panel in our test being 5 mm, its TL curve must be sensibly lying in the region between these two curves. At the frequency higher than 4000 Hz, the value of TL theoretically tends to increase 6 dB per octave band. As a consequence, the approximated transmission loss of the employed PC panels in our test was estimated reasonably for each third-octave band of interest according to the discussion above, which is represented by the green dotted line shown in Figure 5.24. The blue and red curves with rectangular symbols in Figure 5.24 represent the predicted attenuations for the nearly-enclosed and double-straight barrier, respectively. It is obvious that at frequencies from 1000 Hz to 2000 Hz and from 4000 Hz to 12.5 kHz the approximated TLs are quite close to the predicted attenuations for the nearly-enclosed type, but much higher than those for the double-straight type by at least 10 dB. Hence the correction term of sound transmission must be taken into account and in such case the boundary condition of two arched PC panels cannot be considered as totally reflected in the BEM model for the nearly-enclosed barrier. Therefore, we can conclude that the insufficient insulation property of the PC panels must be the foremost reason for the considerable differences between the predicted and measured results mentioned previously for the nearly-enclosed barrier.

To improve the sound insulation property of the arched parts for the nearly-enclosed barrier so that better measured attenuations could be tested, a kind of material that provides good sound insulation as well as flexibility was needed. The transmission loss of a typical single-layer material is theoretically divided into three distinct performance regions developed from the frequency range: I. stiffness and resonance region, II. mass region and III. coincidence

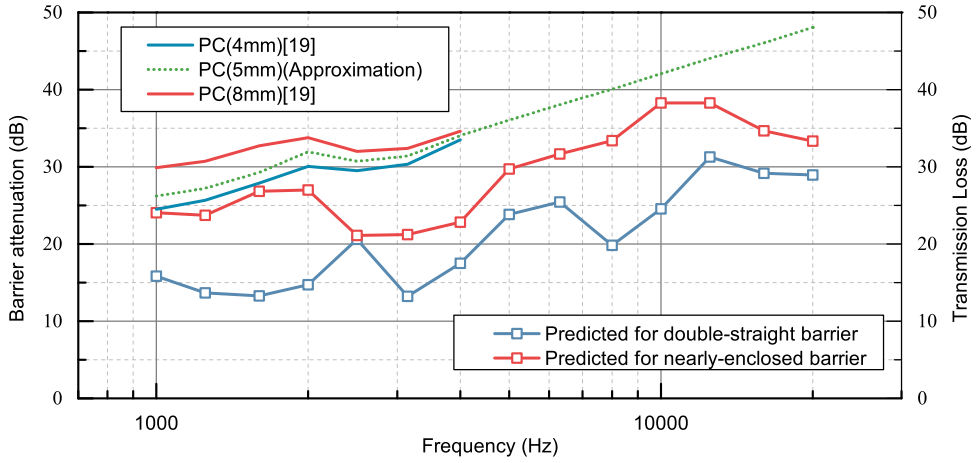

Fig 5.24.: Comparison between the predicted attenuations of barriers and the TLs of PC panels

region. Region I typically ranges below 200 Hz[223] where the TL is controlled by the stiffness and the resonance frequency of the material. In Region II the relationship between TL and frequency is mainly controlled by the mass of material, which is known as the mass law: each time the mass is doubled the TL increases 6 dB. This law continues to meet the critical frequency f_c at which sound waves incidents are able to efficiently transfer energy to the panel. This phenomenon is called the "coincident effect" which severely influences the sound insulation performance of the material. The critical frequency for a single-layer isotropic homogenous material is defined as,

$$f_c = \frac{c^2}{2\pi t}\sqrt{\frac{12\rho_m\left(1-\sigma^2\right)}{E}} \tag{5.3}$$

where c denotes sound speed, t is the thickness of material and ρ_m is mass of the panel per unit surface area. E and σ are Young's modulus and Poisson's ratio of the material, respectively.

Taking for instance the 5-mm-thick PC panel with an average density of 1.2 g/cm^3 employed in the scale measurement, the TL fluctuates violently in Region I, then increases by 6 dB per octave in Region II and suddenly declines significantly when approaching critical frequency. At higher frequencies the TL continues to increase by 6 dB per octave again in Region III. The value of critical frequency is in the range of interest, which means the employed PC panels in the scale measurement showed their sound insulation performance not only in Region II but also in Region III. Recall from Figure 5.24 that in Region II the differences between the TLs and the predicted attenuations for the nearly-enclosed model were less than 10 dB, and in Region III the loss of TL caused by the coincident effect leads the TL much closer to the increased attenuation with increasing frequency. Once more, the further analysis based on the sound insulation theory proves that the PC panels employed in our test were not able to sufficiently insulate the traffic noise.

From these findings we can summarize that the material with high density has a good sound insulation property due to the mass law. On the other hand, with high critical frequency the material shows its TL performance in the test almost in Region II to avoid the coincident effect. Hence it is better to select a kind of transparent material with high density, high critical frequency and high flexibility for the arched shape. According to this description, the 10-millimetre-thick rubber was chosen. The TL of the arched parts must be improved considerably by the heavy mass owing to the high thickness of rubber. Although the density can be expected to be between 0.96 g/cm^3 and 1.3 g/cm^3f only as large as that for the PC panels, with a low Young's Modulus(0.001-0.0022 GPa) its critical frequency can be up to over 40 kHz so that its TL performs only by the mass law in the scale model measurement. Furthermore, it is quite easy to reshape. Thus, it was possible to reduce the differences between measured and predicted results by the rubber covering with no need to worry about the transparency of the material.

For the sake of comparison between the scale model with and without rubber, the rubber was only applied to coat the whole model of barrier, not to act as the alternative to any existing materials constructing the barrier. Figure 5.20(a) shows its application in our scale model measurement.

5.3.5 Scale model tests with rubber coverings

In order to improve the sound insulation, repeated scale tests with additional 10-mm-thick rubber covering on the outer surface of the model were carried out. Figure 5.25 illustrates all the configurations of the tested models with the rubber covering. The black parts represent the rubber coating on all the outer surfaces of the barrier. In addition, to test the effect to the nearly-enclosed barrier(Figure 5.25(d1)(d2)), a comparison for the double-straight barrier between the model with and without the rubber covering was made as well. The same as that in the previous scale model tests, the 7th loudspeaker(as shown in Figure 5.22) was used to emit one-point white noise source. And the measured and the predicted results for the models with rubber coverings were calculated by using the same method presented in Section 5.3.3.

Figure 5.26 compares the measured results with the corresponding BEM predictions for the double-straight model and the nearly-enclosed barrier, respectively. Identically to the previous observations, the measured results for the double-straight barrier with the rubber covering correspond to the 2.5-D BEM predictions, and the differences between the measured results and the predictions are a little smaller than those for the case without the rubber covering(Figure 5.23(a)). This proves the employed wood planks were sufficiently thick to insulate sound when the barrier shape was straight. And with the help of the rubber covering the improvement was negligible. Then to compare with the nearly-enclosed barrier it is encouraging that with the addition of the rubber covering the agreement between the

measured and predicted results was obviously improved comparing with that shown in Figure 5.23(b) . This agreement provides very strong evidence that the employed PC panels cannot be assumed to be totally reflective panels to preventing sound from transmitting through when the barrier has a nearly-enclosed shape, and adding a cover of material with good sound insulation to the surface of the PC panels is a practicable way to improve the barrier attenuation, to bring it close to the expectation of 2.5-D BEM model.

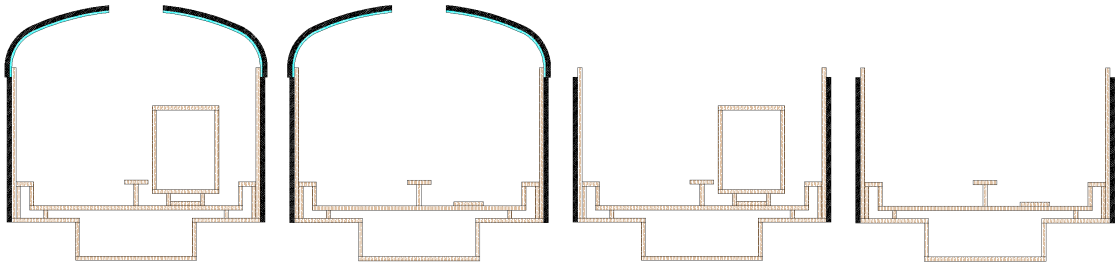

Fig 5.25.: The configurations of the tested models with the rubber covering

On the basis of the agreement between the measured results and predictions for the nearly-enclosed barrier in the acoustic field of a one-point source, the number effect of incoherent point sources on the barrier attenuation was analyzed. In order to validate the 2.5-D BEM predictions with several incoherent point sources the number of loudspeakers was changed as mentioned previously. Figure 5.27 provides the information about the results for different numbers of incoherent point sources for the nearly-enclosed barrier. Before the discussion on the number effect of incoherent point sources, it is necessary as a starting point to verify the predictions by the measured results. Apparently each comparison shows good agreement, as our expectation. Then, we found that the curves in Figure 5.27 vary widely with increased frequency: some are extremely fluctuating, while others tend to smooth.

In Figure 5.27, it is easy to understand that the growth of attenuation fluctuates seriously with frequency for one point source(blue curves). And yet it is interesting that the attenuation tends to become smoother as the number of incoherent point sources increases to four(red curves). When increased to the maximum number of sources(green curves), the attenuations have a visible decline at each frequency band in comparison with those of four-point source. In addition, the comparison of the results between the model with and without the vehicle structures was also considered. The frequency-attenuation curves with the vehicle structures(Figure 5.27(b)) fluctuate much more than those without the vehicles(Figure 5.27(a)), even for the smoothest curves corresponding to the twelve incoherent point sources. This is due to the multiple reflections between the vehicle structure and the inner surface of the barrier, which can be reduced by treating the inner surface with absorbent materials. The last two chapters will discuss the absorptive nearly-enclosed barriers.

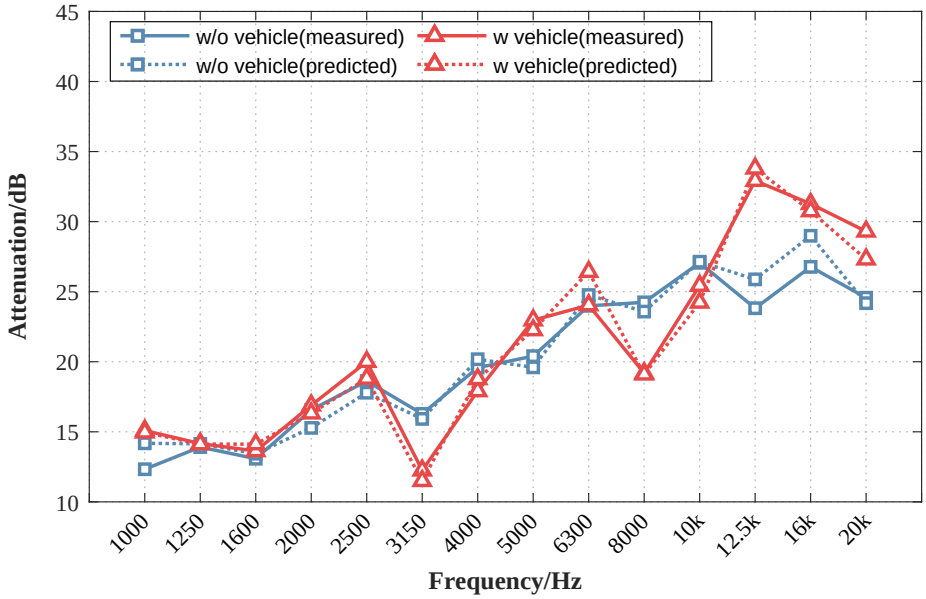

(a) Double-straight barrier on the viaduct

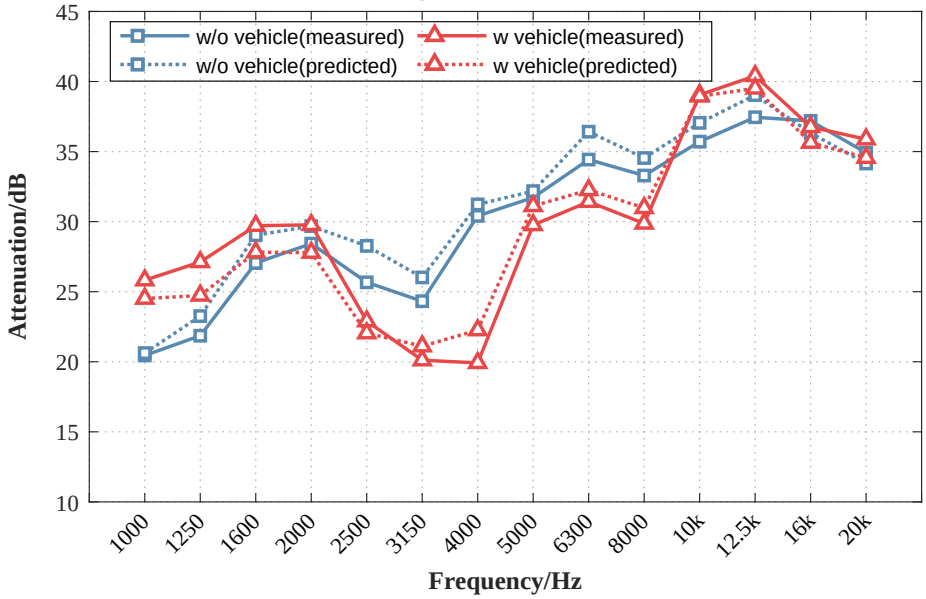

(b) Nearly-enclosed barrier on the viaduct

Fig 5.26.: Measured and predicted attenuations for the model with the rubber covering(a) double-straight barrier(Figure 5.25(e1)(e2)); (b) nearly-enclosed barrier(Figure 5.25(d1)(d2))

All the findings in the scale measurement for the nearly-enclosed model with a rubber covering demonstrate good agreement with those predicted by the 2.5-D BEM approach for each third octave band from 1000 Hz to 20 kHz. To summarize, it can be assumed that the acoustic performance of the nearly-enclosed barrier investigated by the 2.5-D BEM predictions for incoherent point sources are reliable.

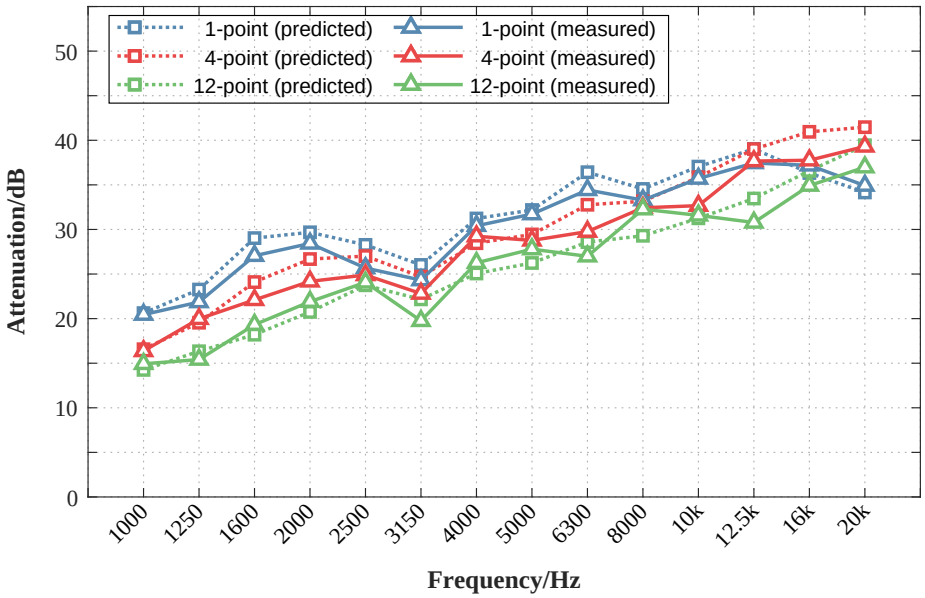

(a) Without vehicle

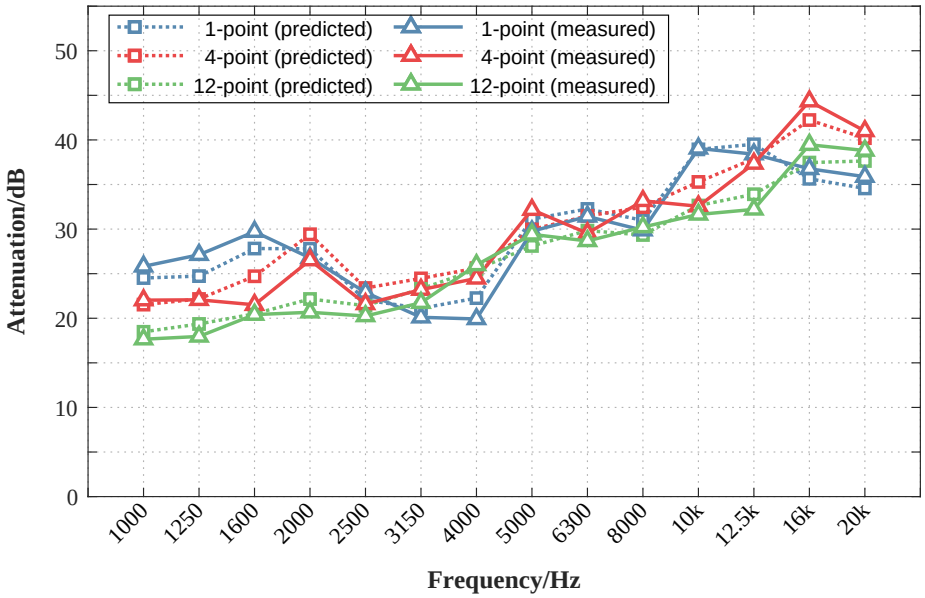

(b) With vehicle

Fig 5.27.: Measured and predicted attenuation for the nearly-enclosed barrier: (a) without vehicle(Figure 5.25(d2)); (b) with vehicle(Figure 5.25(d1))

5.4 2.5-D BEM predictions

The 2.5-D BEM program was used to make predictions of attenuations by the nearly-enclosed barrier in order to identify its acoustic performance in the surroundings. Run times with the complex geometry of the nearly-enclosed barrier and railway vehicle simulation were excessive. In order to reduce calculation times only the model with viaducts and nearly-enclosed barriers but without rubber coverings(Figure 5.21(a1)) was calculated for

the whole frequency spectrum. Identically to the measurement, the calculation was also completed without barriers(Figure 5.21(c1)) for attenuation analysis.

5.4.1 Rearrangement of source and receiver positions

As discussed in chapter 2, based on the diffraction theory the receiver positions need to be in all six significant acoustic areas: bright zone, transition zone and shadow zone in the near field and far field, respectively. Due to the special shape of the top of the nearly-enclosed barrier, the bright zone and transition zone were elongated and extremely high as shown in Figure 5.28. The rest is therefore the shadow zone covering most of the acoustic field. Considering that it is impossible to develop any construction projects at the two former zones, our observation in this section is focused on the performance at the shadow zone. Within this zone the receiver positions were in the near field and far field separately. The acoustic far field is defined as beginning at a distance of two wavelengths away from the sound source. For the frequency range of interest(50 Hz- 1000 Hz in the full scale) the boundary between the near field and far field is located at around 14 meters away from the source, as shown in Figure 5.28. Notice that further frequencies in Section 5.4 will be given in the full scale from 50 Hz to 1000 Hz. Consequently, by the grid-form method referred to in Chapter 2, predictions were made at receivers placed at the four receiver distances(5, 10, 20 and 40 m from the centre of the track) on the horizontal axis and at the three receiver heights(1.5 m above, 1.5 m below and at the height of the track) on the vertical axis. Figure 5.28 illustrates these receiver positions. Given the large number of receiver positions, it was important to assign a name to each receiver. The naming rules were the same as those in the in-situ measurements presented in Chapter 3. The name of each receiver begins with "M". The first number represents the column number which is smaller as the receiver gets closer to the source, whereas the second number represents the row number which is larger as the receiver gets closer to the ground. A symbol like "M1-" "M -1" which will be seen in later sections represents, for example, all the receivers in the first column or the first row, respectively. Unlike only one point source simulated on the cross-section of the scale model in the measurement, the noise sources were modelled as two incoherent point sources on the cross-section positioned at the approximate height of two rail-wheel interaction positions(represented by two dots in Figure 5.28). Note that the source to receiver distance discussed below represents the distance horizontally away from centre of track(also the centre of two incoherent point sources on the cross-section). Identically to the previous calculation, the predictions for different numbers of sources(1, 4 and 12 incoherent point sources arrayed along the length of barrier) were made as well for all the receivers mentioned above. Each distance perpendicular to the cross-section between the source and receiver is also the same as that in the previous calculations.

In the 2.5-D calculations, sound pressure was predicted for several individual frequencies with a linear spacing of 0.1 Hz per third octave band ranging from 50 Hz to 1000 Hz.

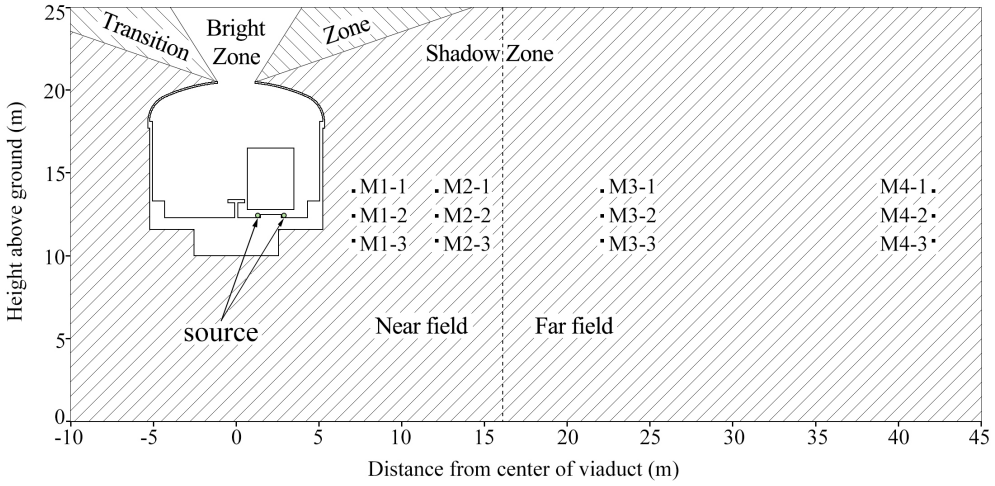

Fig 5.28.: Source and receiver positions in the 2.5-D BEM calculation

The energy for all the incoherent point sources in the model was summed within each band yielding the third octave band spectrum. Eventually the attenuation spectrum was calculated by the logarithmic ratio of the energy obtained between the model without and with the barrier.

5.4.2 Performance in the near field

Figure 5.29&5.31 show the predicted attenuations for the receivers in the near field for different numbers of incoherent point sources. For the source to receiver distance of 5 m there is a consistent pattern in the results obtained, with the attenuation varying with the third-octave band for a given number of sources, but to different degrees as observed in Figure 5.29. Among them receiver M1-1 is the most greatly affected by changes in the band for a given number of sources while there is the least effect for M1-3. And it can be seen more obviously that the attenuation obtained with the highest receiver M1-1 is significantly greater than that obtained with the lowest receiver M1-3 for all the third-octave bands of interest. That means the attenuation increases with the increased height of receivers for all the cases examined in M1- and the effect is very considerable, which are similar to the in-situ measured results obtained in Chapter 3. A good explanation for this is the barrier effect of the viaduct. In the case without the barrier(shown in Figure 5.30(a)), the structure of the viaduct can be considered as a low-height barrier that attenuates a lot the sound pressure levels for M1-1, M1-2 and M1-3. Hence the reduction effect of the viaduct on M1-3 is the most significant. And the sound pressure level for M1-1 can be the highest and affected the most from the sources. In the case with the barrier(shown in Figure 5.30(b)), the nearly-enclosed barrier separates the sources and the receivers in two nearly-disconnected fields. Because of this, the sound pressure levels for M1-1, M1-2 and M1-3 are almost on the same level. In this context, the attenuation for M1-1 can be the highest.

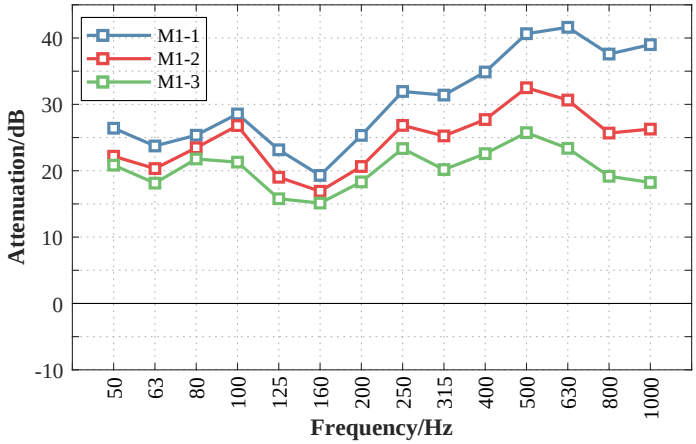

(a) one-point source

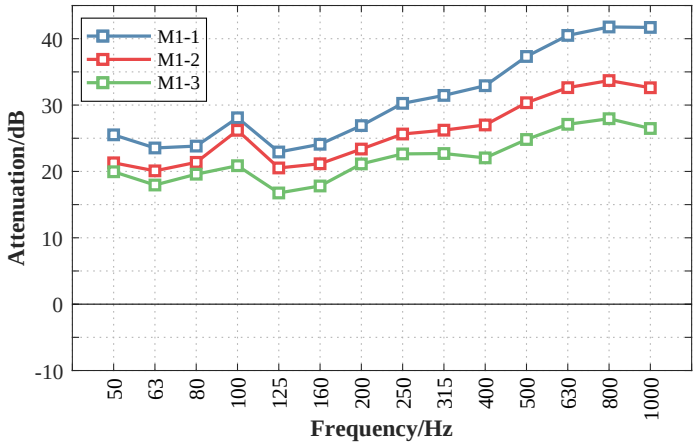

(b) four-point source

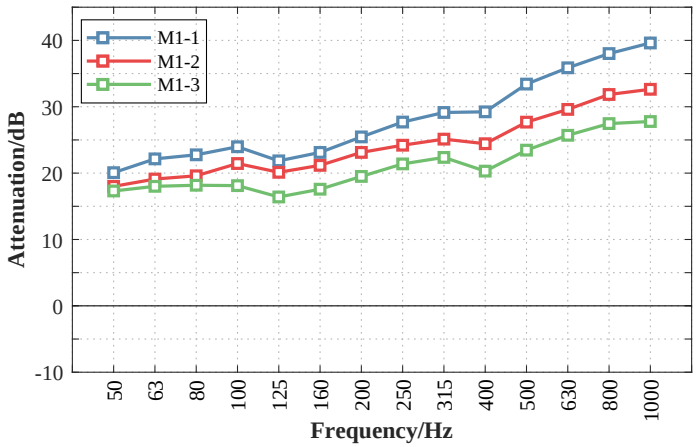

(c) twelve-point source

Fig 5.29.: Predicted attenuations for the source to receiver distance of 5 meters

However, with the increased number of sources, attenuation always decreases for a given receiver, and more importantly, it tends to fluctuate less. Taking an example for receiver M1-1, the global maximum of attenuation for one-point source is 41.61 dB at 630 Hz, while

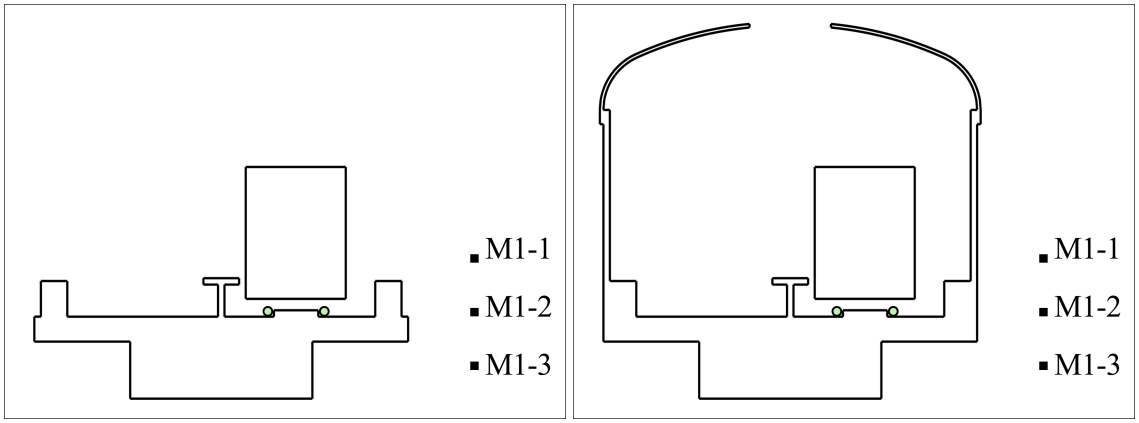

(a) Without the barrier (b) With the barrier

Fig 5.30.: Two sketches for part of the cross-sections of the 2.5-D BEM model without and with the barrier

there are two local maximums, 31.94 dB and 28.56 dB at 250 Hz and 100 Hz, respectively. For the four-point source the increase of attenuation from 630 Hz, to 1000 Hz is positive but slow so that the global maximum is located at the maximum band of interest, i.e. 41.83 dB at 1000 Hz. And obviously there is only one local maximum: 27.89 dB at 100 Hz. For the twelve-point source the attenuation increases smoothly with the increased band and therefore it is difficult to find a local maximum. Again, the global maximum is located at the maximum band of interest, i.e. 39.34 dB at 1000 Hz.

The attenuation for the source to receiver distance of 5 meters in general is higher than 13 dB for each band, and from 400 Hz to 1000 Hz it is even higher than 20 dB. While for the source to receiver distance of 10 m the attenuation is on average higher than 10 dB, and from 400 Hz to 1000 Hz it is even higher than 15 dB. Figure 5.31 shows the attenuation achieved for the source to barrier distance of 10 m for all configurations examined. Again, it can be observed that there is a similar pattern in the results obtained with the attenuation varying with the third-octave band for a given number of source. However, unlike the predictions for receiver in M1- the attenuations for the receiver in M2- are not greatly affected by changes in the height of the receiver for a given third-octave band ranging from 50 Hz to 400 Hz, although there is a small effect on attenuation from 500 Hz to 1000 Hz.

For the source to receiver distance of 10 m with the increased number of source attenuation decreases again and tends to fluctuate less for a give receiver. There is a similar trend for each receiver in M2- that the attenuation ranging from 400 Hz to 1000 Hz firstly increases and then decreases for one-point source, then increases slowly when the number increases to four, and finally increases linearly for the twelve-point source. Because of this, the associated frequency of the global maximum increases with the increased number of sources, i.e. the global maximum for M2-1 is 25.33 dB, 28.13 dB and 27.2 dB at 630 Hz, 800 Hz and 1000 Hz for the one-point, four-point and twelve-point source respectively. On the other hand

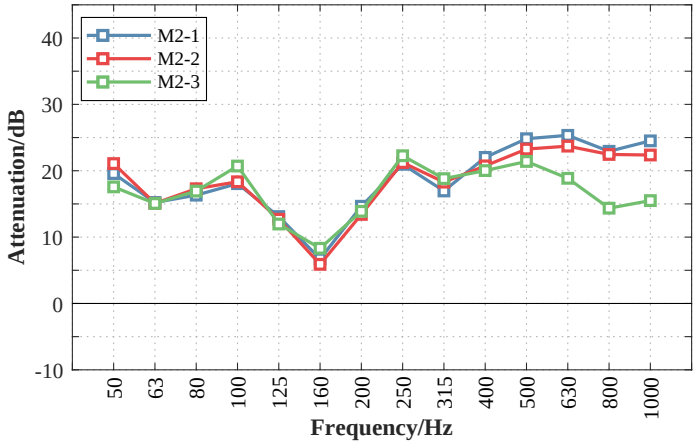

(a) one-point source

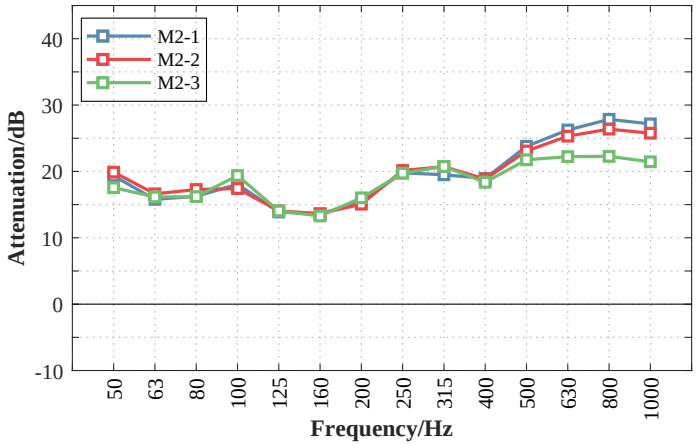

(b) four-point source

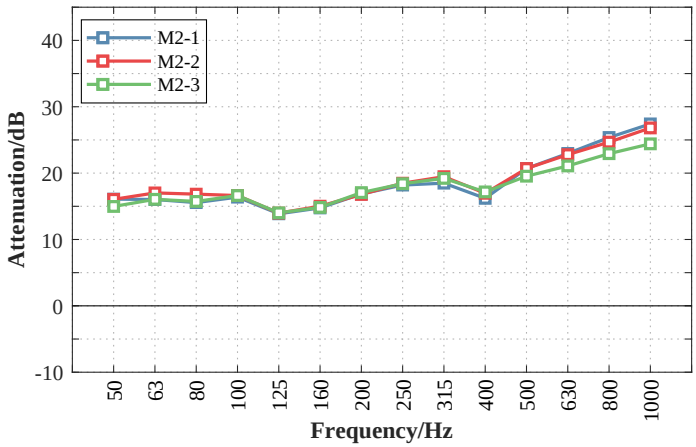

(c) twelve-point source

Fig 5.31.: Predicted attenuations for the source to receiver distance of 10 meters

the global minimum of attenuation for the one-point source for the receiver in M2- can be seen clearly at 160 Hz with the value of approximately 6 dB, and it is the most distinct

trough in Figure 5.31. Nevertheless, this trough gradually disappears for the four-point and twelve-point sources.

The following general conclusions can be drawn from the above: first, the attenuation with an average of approximately 15 dB can be achieved in the near field; secondly, the height effect of the receiver on attenuation is significant for the source to receiver distance of 5 m while that for the source-receiver distance of 10 m is almost invisible; thirdly, the increased number of source can result in a smoother and lower attenuation.

5.4.3 Performance in the far field

Figure 5.32 &5.33 show the predicted attenuations for the receivers in the far field for different numbers of incoherent point sources. For the source to receiver distance of 20 m there is again a similar trend in the results obtained, with the attenuation varying with the third-octave band for the whole frequency range for a given number of sources(as observed in Figure 5.32). However, an opposite trend for the height effect of receivers can be observed in M3- that attenuation decreases with the increased height of receivers for a given number of sources but the effect is very small.

With the increased number of sources, the attenuation decreases for a given receiver. A similar noticeable trough can be observed at 160 Hz in Figure 5.32 for one-point source, but it is surprising that it is a negative value and its magnitude increases with decreased height for the receiver in M3- with the lowest value of -2.46 dB. However, for all cases of the other two source types the magnitudes of attenuations are always positive since the attenuation is more stable with smaller fluctuations. For a given receiver there is also a peak at 250 Hz for the one-point source but less obviously for the four-point source, and it finally disappears for the twelve-point source. The attenuation for the twelve-point source for the receiver in M3- fluctuates within a small range of 6-13 dB ranging from 50 Hz to 400 Hz, and it increases slowly from 400 Hz to 1000 Hz.

The attenuation for the source to receiver distance of 20 m on average is lower than 20 dB for each band, while for the source to receiver distance of 40 m the attenuation is on average lower than 10 dB. Figure 5.33 shows the attenuation achieved for the source to barrier distance of 40 m for all configurations examined. Again, it can be observed that there is a similar pattern in the results obtained, with the attenuation varying with the third-octave band for a given number of sources. And similar to those in Figure 5.32 attenuation decreases with the increased height of the receiver for a given number of sources, but the effect is quite small.

Unlike the negative value of global minimum for all the receivers in M3- for the one-point source, there is a negative attenuation as the global minimum only at 160 Hz for M4-2 for

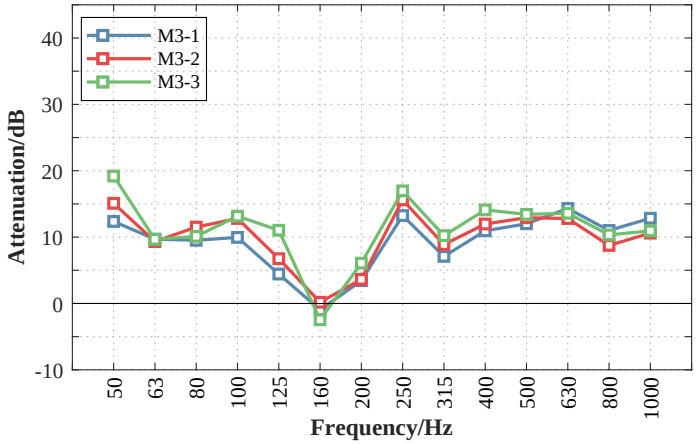

(a) one-point source

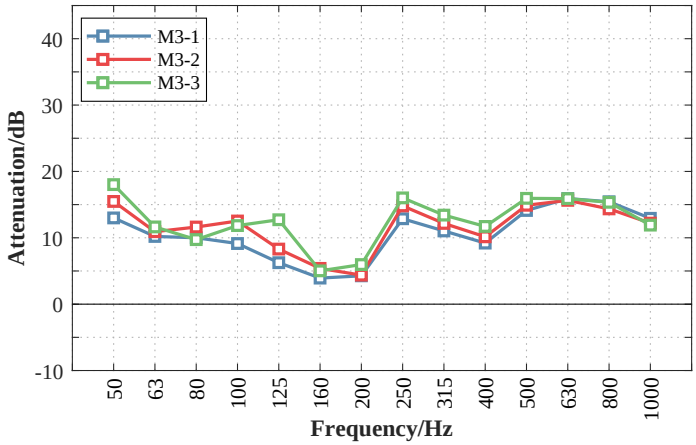

(b) four-point source

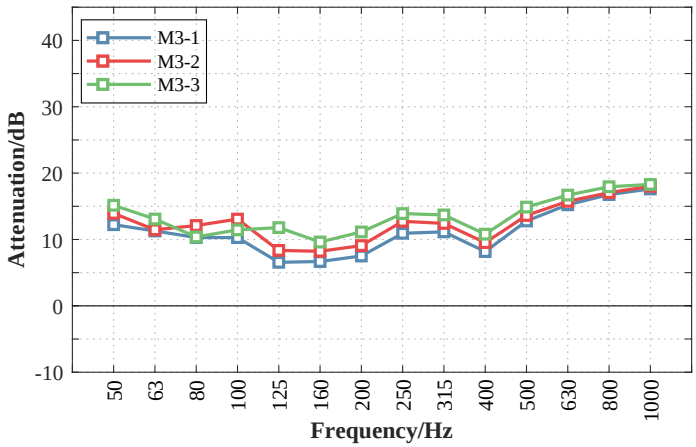

(c) twelve-point source

Fig 5.32.: Predicted attenuations for the source to receiver distance of 20 meters

the one-point and the four-point source. Apart from that, for the source to receiver distance of 40 m with increased number of sources, attenuation for the receiver in M4- decreases and fluctuates less again for a given receiver. For the global maximum, the associated

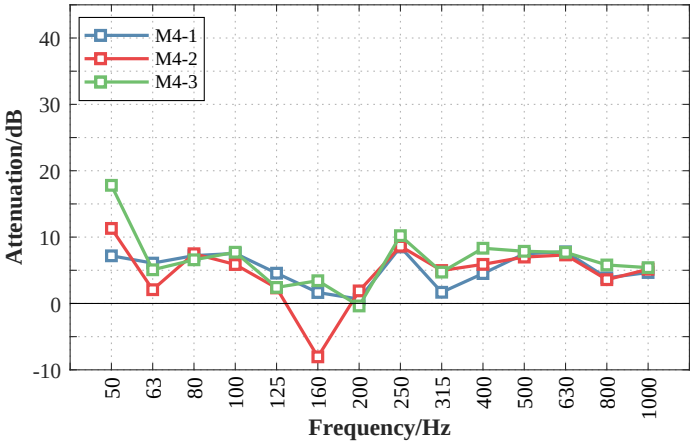

(a) one-point source

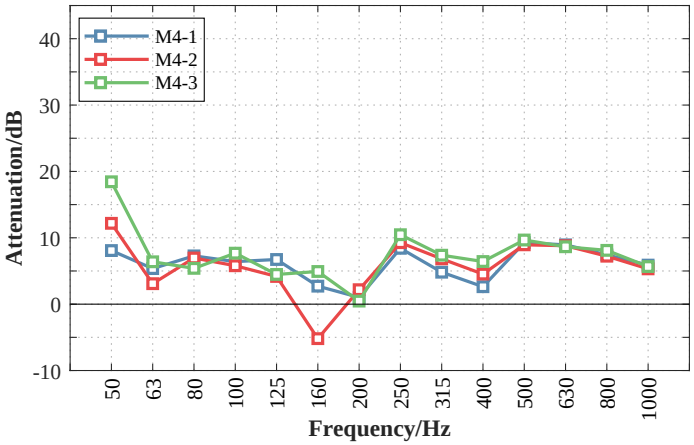

(b) four-point source

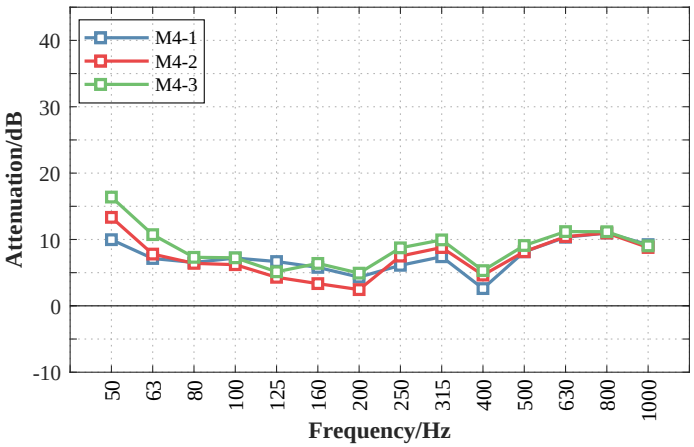

(c) twelve-point source

Fig 5.33.: Predicted attenuations for the source to receiver distance of 40 meters

frequency is unchanged with the value of 50 Hz. And the magnitude firstly increases and then decreases with increasing number of sources, i.e. for M4-1 it is 17.80 dB, 18.58 dB and 16.10 dB for the one-point, four-point and twelve-point sources, respectively.

The following general conclusions can be drawn from the above: first, the attenuation with an average of approximately 10 dB can be achieved in the far field; secondly, the performance in the far field reduces with increasing height of receivers but the effect is very small, in other words, the performance is relatively unaffected by the height of receivers; thirdly, the increased number of sources can result in the attenuation being much smoother and lower, especially eliminating the negative value induced by the small number of sources.

5.5 Discussion and conclusions

The 2.5-D BEM program developed for incoherent point source calculations was used to solve the practical problem of assessing the acoustic performance outside a nearly-enclosed barrier with infinite length. The results of a preliminary investigation calculated by the 2.5-D BEM program showed that there were many peaks in the frequency domain of sound pressure in the surroundings of the nearly-enclosed barrier. With good agreement between the sound pressure distributions at the peak frequencies and the corresponding acoustic modes of the air cavity inside the barrier, a reasonable explanation of these peaks was given that when the shape of the barrier was nearly-enclosed, the acoustic resonance effect generated by the open air cavity could result in extremely high levels at the resonance frequencies, directly deteriorating the barrier performance. To suppress the resonance effect additional absorptive treatments on the inner surface of the barrier are proposed for further researches.

To validate the predictions a series of scale model measurements were made since the scale modelling technique allowed the effect of the employed material on the barrier performance to be more realistic. It was shown from the comparison that there was a significant deviation between the measured and predicted results for the nearly-enclosed barrier, but good agreement for the double-straight barrier. Measured attenuations for the nearly-enclosed barrier were obviously higher than those for the double-straight type in the mid-frequency range, while at high frequencies, attenuations for the nearly-enclosed barrier were almost the same as those for the double-straight type. More importantly, the measured results for the nearly-enclosed barrier were much lower than those predicted by the BEM, which may result from the insufficient sound insulation of the PC panels.

Based on the sound insulation theory and the measured TLs in [222], the transmission loss of the 5-mm-thick PC panels employed in the scale model was estimated. The comparisons show that the predicted attenuations for the nearly-enclosed type were quite close to the transmission loss of the PC panels in the frequency range of interest. According to the calculation of barrier attenuation in the form of energy transfer, the correction for sound transmission could not be ignored. Therefore, the insufficient sound insulation of the PC

panels was identified to be the main cause of the differences between the measured and predicted attenuations for the nearly-enclosed barrier. As mentioned in Chapter 1, the PC panels, employed for the arched parts in the full-scale prototype of the nearly-enclosed barrier in China, have a thickness of only 6.5 mm, a little thicker than those employed in the scale model in our test. Thus, the sound insulation of the PC panels in the actual project are considered to be not sufficient as well. The need for transparent material with better sound insulation and high flexibility was long ignored and urgent for the arched parts, both in the scale model tests and the actual projects.

With the help of 10-mm-thick rubber, a supplementary measurement was developed for solving the difficulty. The predictions of one-third octave band levels using the 2.5-D BEM program were shown to be comparable with the 1:20 scale measurements by fully coating all surfaces with rubber so that confidence can be given in the BEM predictions for the whole field. The compared results also reconfirmed the insulation problem of the PC panels for the nearly-enclosed barrier. In addition, the predictions for the four-point and twelve-point sources were shown to be comparable with the measured results, which provides us the opportunity to discuss the number effect of incoherent point sources.

Considering the complex sound field distribution caused by the specific structure of a nearly-enclosed barrier, in order to understand thoroughly the barrier performance, the receiver positions were rearranged according to Chapter 2[208]. The rearrangement approach based on the diffraction theory was used to estimate the performance of the sound barrier in each area with different acoustic features.

As expected, the attenuation of the nearly-enclosed barrier averaged around 15 dB in the near field and around 10 dB in the far field. This indicates that the nearly-enclosed type has a more effective and efficient performance on the premise that all the boundaries are acoustically rigid. This kind of barrier with high attenuation designed by the modification of shape requires the employed material with sufficiently high sound insulation property. Otherwise the design will not be performant nor economical for the practical use.

It was also shown that the attenuation decreased with increasing source-receiver distance, while it increased with increasing height of receivers only in the column which was the closest to the source in our study. For the other three source-receiver distances the height effect of receiver was almost negligible. The number effect of incoherent point sources was also taken into account for modelling railway traffic noise. Apparently, the increased number of source can result in much smoother and lower attenuations for all the areas, especially eliminating the negative value induced by the small number of sources. In addition, the resonance effect referred to previously can be the reasonable explanation of the negative values of the attenuations in the far field.

6 2.5-D BEM modelizations of the absorptive nearly-enclosed prototype

6.1 Introduction

Considering that the attenuations for the receivers at the site with a barrier resulted from the joint effect of the the nearly-enclosed barrier and the employment of Floating Slab Tracks, it is possible that the measured results overestimated the acoustic performance of the nearly-enclosed barrier. Nevertheless, it is difficult to find a suitable site to take measurements on existing lines. And to simulate incoherent-line sources is another difficulty in the scale model tests. Thus, it is required to seek a method to study the single effect of the nearly-enclosed barrier on a viaduct on rail traffic noise. A 2.5-D BEM approach, proposed by Duhamel[176, 178], is appropriate for this purpose. The main idea of this approach is to solve the sound pressure fields created by point or incoherent line sources by using a Fourier-type formulation to transform the 2-D BEM results. With the help of the 2.5-D BEM method, the barrier attenuation can be predicted, though with large computational cost.

6.2 Acoustic models

6.2.1 Acoustic models for absorption panels

The performance of the nearly-enclosed barrier can be enhanced by the application of absorbent treatment applied to either the top of the barrier or the inner face of the additional edges. As shown in Chapter 3, the prototype employed on the existing line has two realistic absorption treatments: glass wool panels and aluminium foam panels. In this section, the two absorption treatments are modelled by two different acoustic models.

Glass wool panels

Glass wool is a typical porous fibrous material used in noise control engineering. Considering its complicated structure, the prediction of the acoustic properties of porous material is usually performed using empirical formulae instead of analytical solutions. Delany and

Bazley[123] proposed an empirical formula to predict the characteristic impedance and absorption coefficient of fibrous absorbent materials. This formula has been widely used to predict sound propagation in absorption treatments, though it is not suitable for very low and very high frequencies[224]. In this 2.5-D BEM model, the glass wool panels could be achieved by assigning the value of the characteristic impedance of a hard backed layer of porous material of a thickness with a flow resistivity as the normal impedance of the treated surface. The normal acoustical impedance of this treatment as a function of frequency was calculated by employing the Delany-Bazley model ("DB model" in short) and in the remainder of this chapter will be denoted by $\mathrm{DB}_{\mathrm{gw}}$. The flow resistivity of fibre glass R_{gw} can be given by[225],

$$R_{\mathrm{gw}} = Kd^{-2}\rho_{\mathrm{B}}^{-1.53} \tag{6.1}$$

where K has the constant value of 3.18×10^{-9}, d denotes the fibre diameter in metres, the bulk density, ρ_{B}, is in kg/m^3. Since the absorption panels, jagged and filled with $48kg/m^3$ glass wool, have a thickness of $60mm$, the flow resistivity R_{gw} is approximately $25000\mathrm{rayl/m}$ when the fibre diameter is given as $7\mu m$.

As can been seen in Figure 6.1, the glass wool panels have the typical absorption characteristics of a hard backed porous material of this thickness where the coefficient of absorption approaches 1.0 for frequencies above 1 kHz but falls rapidly for lower frequencies. The absorption characteristics are sufficiently effective against rail traffic noise since the noise was measured predominantly in the frequency range of 315-1000 Hz and 2000-4000 Hz, as presented in Chapter 3.

Open-celled aluminium foam panels

Aluminium foams show great sound absorption properties. Many authors[226–229] have proposed that porous metals are a good alternative to non-metallic porous materials like urethane foam and glass wool, etc. in noise control engineering applications since they have relatively higher mechanical strength and stiffness, and resistance to heat, corrosion, and climatic conditions[230]. Compared with closed-celled structures, Han et al.[226] noted that open-celled aluminium foam which is manufactured using an infiltration process, showed a significant improvement in sound absorption capacity. This advantage of open-celled aluminium foam can be understood simply as the sound wave propagating easily into the material.

The DB model is mainly used to predict the sound propagation in fibre porous materials with high porosities. However, to model the open-celled aluminium foam it has limitations at very low and very high frequencies. With the gradual maturity of studies on porous metals, many researchers[231] have tried to use microstructure models to predict absorption coefficients

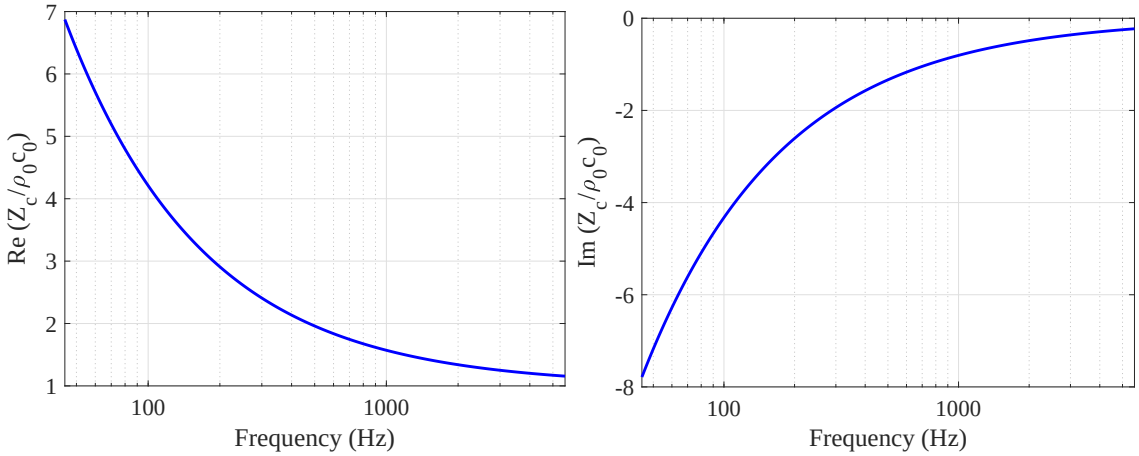

(a) The real part of the characteristic impedance (b) The imaginary part of the characteristic impedance

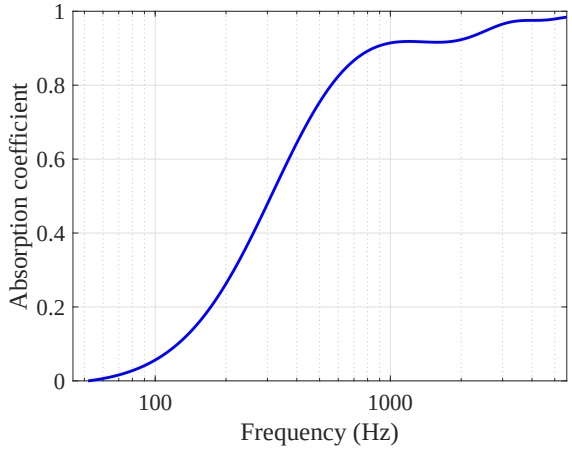

(c) Absorption coefficient

Fig 6.1.: Absorption properties of $\mathrm{DB_{gw}}$ absorbent treatment calculated using the Delany-Bazley model[123] for $48kg/m^3$, $60mm$ panels of glass fibrous wool

of porous metals in comparison with laboratory test results. Based on the Zwikker-Kosten's microstructure model[119], it can be found that the air viscous resistance and the frictions of air molecules and pore walls could only affect the sound wave equation, whereas thermal effects could only affect the continuity equation. Inspired by this, H. LI[231] deduced a simplified theoretical model for predicting absorption capabilities of open-celled metal foams. In his model, taking into account visco-inertial effects and thermal effects, the complex effective density $\rho(\omega)$, the effective bulk modulus $K(\omega)$ and the characteristic impedance Z_c of metal foams were given by[231],

$$\begin{aligned}
\rho(\omega) &= \rho_0 \left[1 + \frac{1}{\sqrt{3^2 + \frac{4\omega\rho_0}{\sigma\phi}}} - j\frac{\sigma\phi}{\omega\rho_0}\sqrt{1 + \frac{\omega\rho_0}{4\sigma\phi}}\right] \\
K(\omega) &= \frac{\gamma P_0}{\gamma - (\gamma - 1)\left(1 - \frac{Nu}{j8\omega\rho_0 \mathrm{Pr}/\sigma\phi + Nu}\right)} \\
Z_c &= \sqrt{\rho(\omega) K(\omega)}
\end{aligned} \tag{6.2}$$

where the angle frequency is ω, the flow resistivity is σ, the porosity is ϕ, the specific heat ratio is γ. Nu and Pr denote Nusselt number and Prandtl number, respectively. ρ_0 and P_0 denote the density of the air and the static pressure, respectively.

To know the absorption coefficients of the open-celled aluminium foam panels backed by a air cavity of a thickness of 50 mm, the normal impedance can be calculated using a transfer-matrix approach[232] and Equation (6.2), and is given by[231],

$$Z_N = \frac{Z_c}{\phi} \frac{-\phi \cot(kd) \cot(k_0 D) Z_0 + Z_c}{-j\phi \cot(k_0 D) Z_0 - j \cot(kd) Z_c}$$
$$k = \omega\sqrt{\rho/K} \qquad k_0 = \omega/c_0 \qquad Z_0 = \rho_0 c_0 \tag{6.3}$$

where k and k_0 denotes the wavenumber in the material and in the air, respectively. d is the thickness of the material whereas D is the thickness of the cavity.

The predictions by using this model had good agreements with the laboratory test results in his thesis. However, J. Zhang[233] found this model ignored the effect of the complicated pore structure on the sound wave propagation. Then, on the basis of this model, J. Zhang introduced the independent tortuosity factor α_∞[234] and the shape factor s_p[120] to modify this microstructure model. In the modified model, the angle and the shape of pores in the material was taken into consideration. The rigorous derivation process of the modified model has been discussed and embodied in [233] and is not repeated here. Finally, better agreements were observed between the modified model predictions and the test results in his thesis.

Thanks to their studies on the sound absorption behaviour of metal foam, the modified microstructure model was introduced to model the absorption properties of the open-celled aluminium foam panels in the 2.5-D BEM model of the nearly-enclosed barrier. The relevant parameters of the absorption properties of the open-celled aluminium foam panels are shown in Table 6.1. As can be seen in Figure 6.2, the open-celled aluminium foam panels have relatively poor absorption characteristics owing to the very thin materials inside the panels. The coefficient of absorption has two peaks for frequencies about 1500 Hz and 4400Hz with values of less than 0.6, and falls rapidly for lower frequencies and the frequencies between the two peaks. In spite of the poor absorption properties, the open-celled aluminium foam panels, as a supplement to noise barriers, contribute somewhat to the improvement of noise control for rail traffic.

Tab 6.1.: Relevant parameters of the absorption coefficients of the open-celled aluminium foam panels

σ (rayl/m)	ϕ (%)	ρ_0 (kg/m^3)	γ	P_0 (Pa)	Nu
14000	75	1.213	1.40	1.013×10^5	4.36
Pr	c_0 (m/s)	D (m)	d (m)	α_∞	s_p
0.71	343	0.05	0.004	1.44	0.5

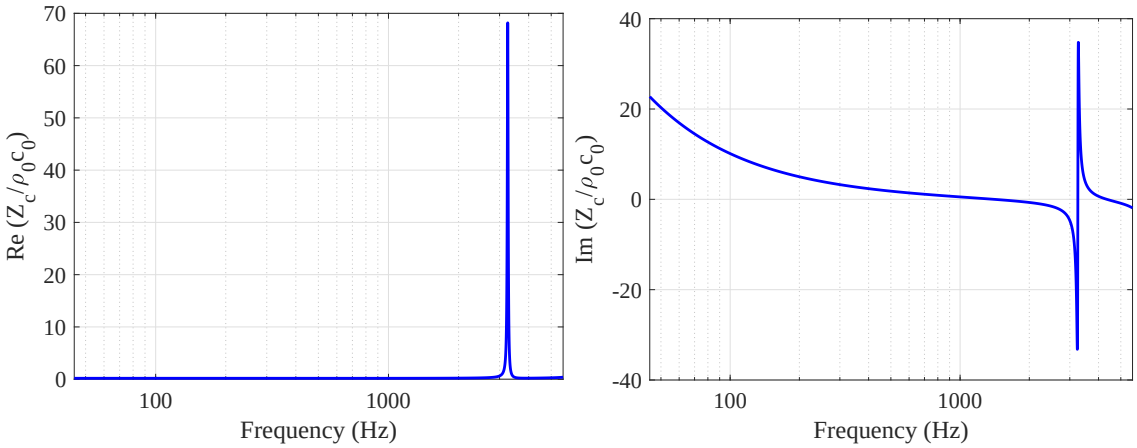

(a) The real part of the characteristic impedance (b) The imaginary part of the characteristic impedance

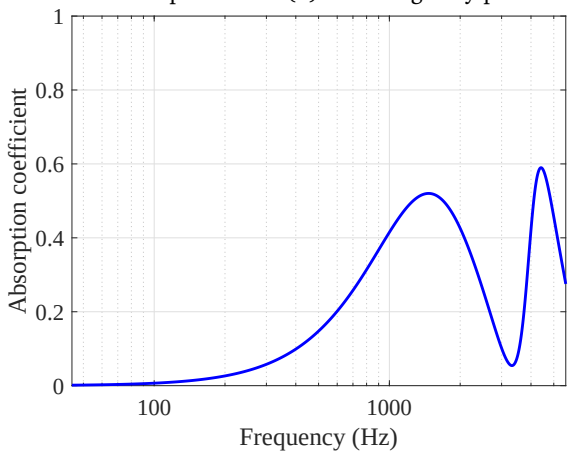

(c) Absorption coefficient

Fig 6.2.: Absorption properties of open-celled aluminium foam panels calculated using a microstructure model[233]

6.2.2 Acoustic model for sites with and without absorptive nearly-enclosed barriers

The geometries of 2.5-D BEM models were obtained from the configurations examined in the in-situ measurements shown in Chapter 3, with two cross-sections of the site without a barrier and the site with nearly-enclosed barriers. As concluded in Chapter 5, the 5-mm-thick PC panels employed in the scale model tests did not have sufficient insulation capabilities to reduce the sound transmission. In this circumstance, a BEM model modelling the site with barriers without the part of the 6.5-mm-thick PC panels was established and the barriers were named double-straight barriers. The model of the site with double-straight barriers was built not only to test the sound insulation effect of the PC panels, but also to make a comparison with the site with nearly-enclosed barriers.

Figure 6.3 shows the cross-sections of the three models. In the model of the site without a barrier (Figure 6.3(a)), the boundaries of the viaduct, the safe passage and the vehicle,

denoted by black curves, were assumed to be acoustically rigid by using the Neumann boundary conditions. The ground was assumed totally reflecting as well, by using an image source technique[217]. The vehicle bottom and the surface of the track were assumed to be acoustically soft in order to eliminate multiple reflections between them. There were assumed two sources located at the positions of the wheel-rail interactions, marked by red dots. Because rail traffic noise is generally considered as having incoherent line sources, whereas coherent line sources are always used in evaluating the performance of barriers, two types of sound sources, including coherent line sources and incoherent line sources, were used and compared. On the basis of the model for the site without barrier, two straight barriers with a height of 4.5 meters were added in the model of the site with double-straight barriers (Figure 6.3(b)). Each of them consisted of a one-meter-long glass-wool panel, a 1.5-meter-long PMMA sheet and a two-meter-long glass-wool panel from bottom to top. The employment of the glass-wool panels was to absorb the rolling noise so that the boundaries on the side facing the vehicles were assigned the value of the normal impedance of the DB model $\mathrm{DB}_{\mathrm{gw}}$, highlighted by blue curves. The PMMA sheets had a thickness of $20mm$. Besides that, there were open-celled aluminium-foam panels employed on the two insides of the flanges of the viaduct and on the two sides of the safe passage, illustrated by green curves. Its normal impedance was modelled as a function of frequency detailed in Section 6.2.1. Then, in the model with nearly-enclosed barriers (Figure 6.3(c)), two arched PC panels were added to the top of the straight barriers. The PC panels had a thickness of $20mm$ with the acoustically rigid boundaries although the PC panels employed on the existing line in China have a thickness of $6mm$.

Numerical predictions were calculated at third octave frequencies from 50 Hz to 5000 Hz. For the acoustic element size in BEM models, a common rule in engineering practice is formulated as six linear elements per wavelength[235]. Instead of using linear elements, using three quadratic elements per wavelength was found to provide similar error limits as ten linear elements did[236]. To solve these three models, a quadratic mesh was used with three node elements. Hence, the element size L was limited to less than a third of the wavelength of the maximum frequency f_{max},

$$L \leqslant \frac{c}{3f_{\mathrm{max}}} \approx 0.020\,(m) \quad (c = 343m/s, f_{\mathrm{max}} = 5623\mathrm{Hz}) \tag{6.4}$$

A compromise was made between model precision and computation time by verifying whether the relative error exceeded a given tolerance. The tolerance for sound pressure e is given by the relative error of the residuum,

$$e = \frac{\|p - p_{\mathrm{fine}}\|}{p_{\mathrm{fine}}} \times 100\% \tag{6.5}$$

where p and p_{fine} denote the pressure of the element size L and the pressure of the highest precision, respectively. Since the results were denoted in level, the tolerance in our study was controlled within 1.0dB. The tolerances of 0.1dB, 0.5dB and 1dB, and the corresponding

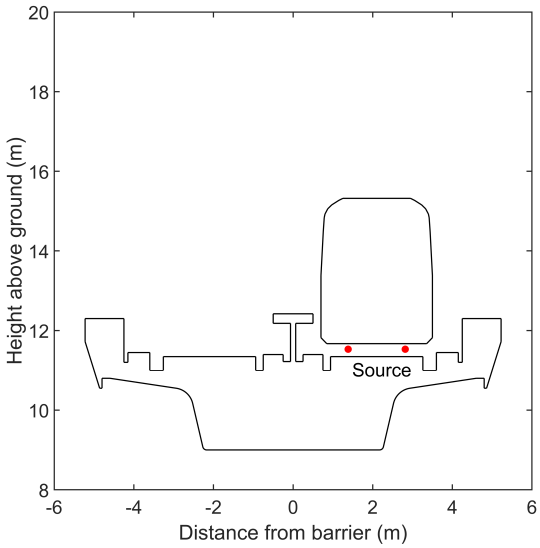

(a)The site without barrier

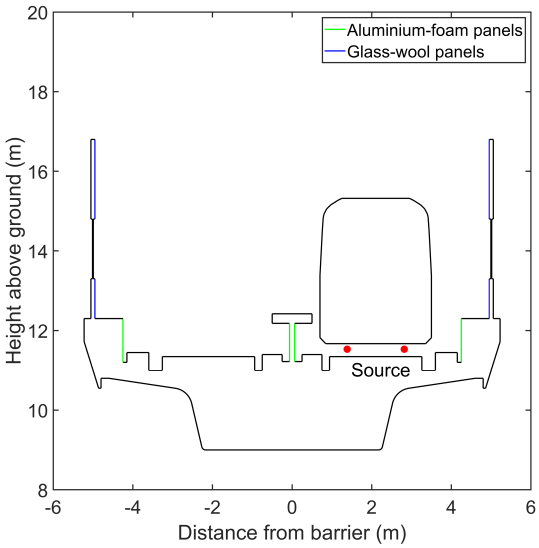

(b) The site with double-straight barriers

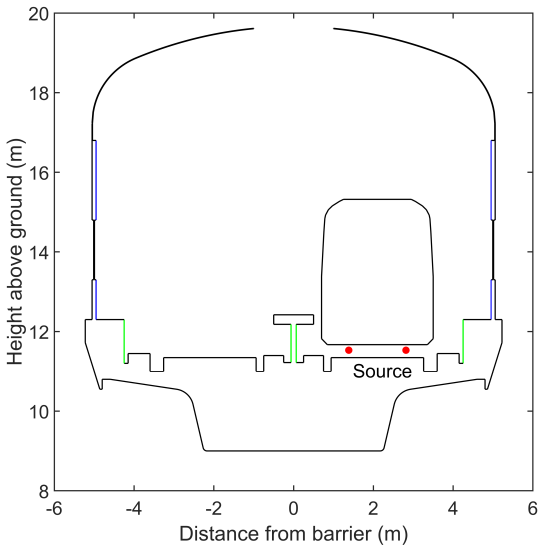

(c) The site with nearly-enclosed barriers

Fig 6.3.: Cross-sections of three 2.5-D BEM models calculated in the comparison with in-situ measured results

relative errors are shown in Table 6.2. Hence, the relative error of each 2.5-D BEM model was less than 6%.

Tab 6.2.: The tolerances of BEM models and the corresponding relative errors

	Tolerance in level		
	0.1dB	0.5dB	1.0dB
e	1.16%	5.93%	12.20%

Figure 6.4 shows a grid convergence study for these three models with specific geometries. It can be seen that with the element size of 0.02 m, the relative error of sound pressure at 5623Hz for the model without a barrier, the model with double-straight barriers and the

model with nearly-enclosed barriers are less than 1.2%, 5.9% and 12.2%, respectively. This means the precision of these three models was 0.1dB, 0.5dB and 1.0dB, respectively. As a result, the convergence investigation limited to the frequency range of $50\text{Hz} - 5000\text{Hz}$ essentially confirmed that three quadratic elements per wavelength were sufficient to obtain a solution of less than 12.2% error. Finally, the element size was determined as 0.02m and the number of nodes and elements are presented in Table 6.3.

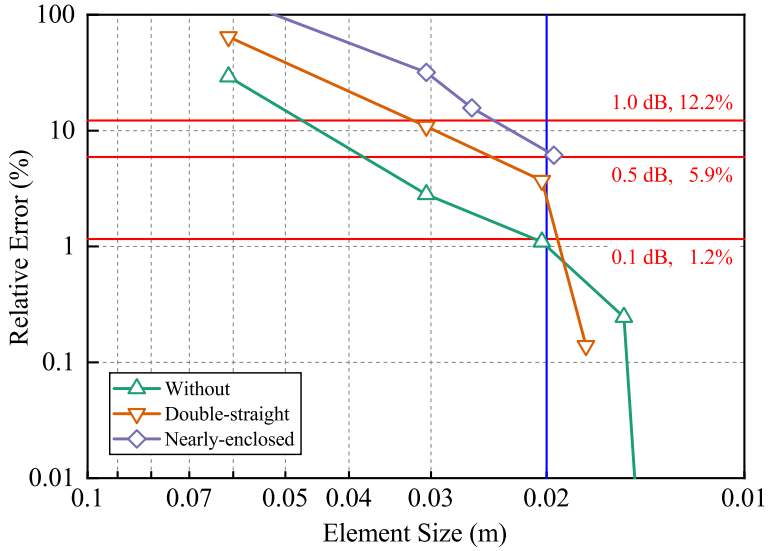

Fig 6.4.: A grid convergence study for the three models with specific geometries

Tab 6.3.: The number of nodes and elements for the three models

Model	Without barrier	Double-straight	Nearly-enclosed
Node	4934	6770	9014
Element	2467	3385	4507

Besides the limitation of calculated frequencies, to avoid the singularity existing in the singular boundary integral equation, the distance between each two nodes l_n and the distance between each source position and node r_n must also be larger than the minimum of element size L. And because of this$(l_n \geqslant L, r_n \geqslant L)$, the minimum length of each geometry for the models was required to be no less than one element size. This rule is the reasonable explanation for the PC panels in the BEM models with a thickness of 20 mm rather than 6 mm. The distance between each source position and the closest node $min\,[r_n]$ was 0.14 m, larger than 0.02 m.

The calculations for each model were made with the following values for the frequencies (all in Hz): $f_0 = 0.00001$, $f_1 = 0.0001$, $f_2 = 0.001$, $f_3 = 0.01$ between $f_4 = 0.1$ and $f_{1124} = 112$ in steps of 0.1, and between $f_{1125} = 113$ and $f_{\max} = f_{6635} = 5623$ in steps of 1. For coherent line sources, the pressures of the models in two dimensions was calculated at each frequency, while for incoherent line sources, the pressures were calculated only at central frequencies of one-third octave bands from 50 Hz to 5000 Hz. It has been addressed in Chapter 4

that when considering incoherent line sources, the estimation results calculated for central frequencies of one-third octave bands are sufficient to show an accurate spectrum. For an example of calculating sound pressure at 500 Hz, the calculations for each model were made with the above lists of frequency values at the beginning, by changing the maximum value to 500 Hz and defining the 3-D frequency to 500 Hz for the calculation of the 2-D to 3-D transform for the models with absorbent treatments. The calculations for imaginary frequencies were made as well. Then, by using a Fourier-like transformation[178], the pressures of the models in 2.5 dimensions were calculated as a numerical integral of 2-D results from $f_0\,(0.0001\text{Hz})$ to the maximum $f_{\text{max}}\,(500\text{Hz})$.

6.3 Comparison with the in-situ measured results

6.3.1 Coherent line sources

The models for coherent line sources and incoherent line sources were solved with these complex boundary conditions including absorbent treatments. Since the two coherent line sources in each model were incoherent to each other, the sound pressure for each model was a combination result radiated from two incoherent sources. Hence, the predicted attenuations for coherent line sources were calculated by rewriting Equation (3.5), given as,

$$Att\,(f_c) = IL\,(f_c) = 10\log\left(\frac{\sum_{f_1}^{f_u} p_{\text{wo},1}^2\,(f) + \sum_{f_1}^{f_u} p_{\text{wo},2}^2\,(f)}{\sum_{f_1}^{f_u} p_{\text{w},1}^2\,(f) + \sum_{f_1}^{f_u} p_{\text{w},2}^2\,(f)}\right) \tag{6.6}$$

where $p_{\text{wo},1}\,(f)$ and $p_{\text{wo},2}\,(f)$ denote the pressure at the frequency f of the model without a barrier radiated from two incoherent sources, respectively. And $p_{\text{w},1}\,(f)$ and $p_{\text{w},2}\,(f)$ denote the pressure of the model with double-straight barriers or nearly-enclosed barriers radiated from two incoherent sources, respectively.

To compare with the measured results in each one-third octave band, the predicted and measured attenuations are shown together in Figure 6.5. The blue curves with circles, the red curves with squares and the black curves with triangles denote the predicted attenuations for the site with double-straight barriers, the predicted attenuations for the site with nearly-enclosed barriers, and the in-situ measured results, respectively. The arrangement of sub figures in Figure 6.5 follows twelve receiver positions in the field measurements. It can be seen that the predicted attenuation in general fluctuates violently with frequency for the sites with double-straight barriers and nearly-enclosed barriers. Compared with the predictions, the measured attenuation changes relatively more smoothly. For the receiver column M1-, the predicted attenuations for nearly-enclosed barriers are higher than those for double-straight barriers at almost all the frequencies of interest. And the predictions for

two cases at low frequencies of 50-400 Hz and 1000-2500 Hz significantly overestimate the measured results. For the receiver column M2-, the differences between predictions and measured results are less than those between other pairs except for M2-1. The predicted result for M2-1 changes sharply with the increased frequency, and at high frequencies the prediction decreases more seriously compared with the measured results. For the receiver column M3-, the predicted attenuations at low and mid- frequencies of 50-800 Hz agree well with the measured results, but at high frequencies the differences between the predicted and the measured attenuations become large, like those for column M1-.

As a consequence, the models for coherent-line source can not predict the acoustic performance of the nearly-enclosed barriers well. Nevertheless, the comparison between double-straight barriers and nearly-enclosed barriers can be predicted for coherent line source by Figure 6.5. The gain of the arched PC panels can be achieved only for the receiver column M1-(source-receiver distance: 7.5m) at low frequencies from 50 Hz to 500 Hz. But at high frequencies above 2500 Hz the gains of the arched PC panels for all the receiver positions are negative. In the frequency range of 500-2000 Hz, the attenuations for double-straight barriers and nearly-enclosed barriers are almost the same for all the receiver positions. Hence, the nearly-enclosed barriers can enhance the performance at low frequencies in the near field, but aggravate a little the noise reduction effect for high frequencies.

6.3.2 Incoherent line sources

Since the pressure was calculated only for the central frequency f_c of each one-third octave band, the predicted attenuation for incoherent line sources in each one-third octave band could be calculated by,

$$Att\left(f_c\right) = IL\left(f_c\right) = 10\log\left(\frac{p_{\mathrm{wo},1}^2\left(f_c\right) + p_{\mathrm{wo},2}^2\left(f_c\right)}{p_{\mathrm{w},1}^2\left(f_c\right) + p_{\mathrm{w},2}^2\left(f_c\right)}\right) \tag{6.7}$$

Figure 6.6 compares the predicted and measured attenuations in order of frequency, from lowest to highest. In Figure 6.6, at low frequencies the measured results are higher than those predicted by the 2.5-D BEM models. This can be due to the effect of the FST, which has been addressed in Chapter 3. The values of the predicted attenuations are almost equal to zero, or even negative, which confirms a previous thought that the nearly-enclosed barrier has a negative but small effect on low-frequency noise. The next section will give a detailed analysis on the acoustic resonance effects of the open absorption cavities. In the range of 125-400 Hz, the predicted attenuations for the nearly-enclosed barrier overestimate the measured results but good agreements are observed between the predicted attenuations for the double-straight barrier and the measured results. And it is only in the range of 125-400 Hz that the predicted attenuations for the nearly-enclosed barrier are higher than those for the double-straight barrier for each receiver position. Since the PC sheets employed on

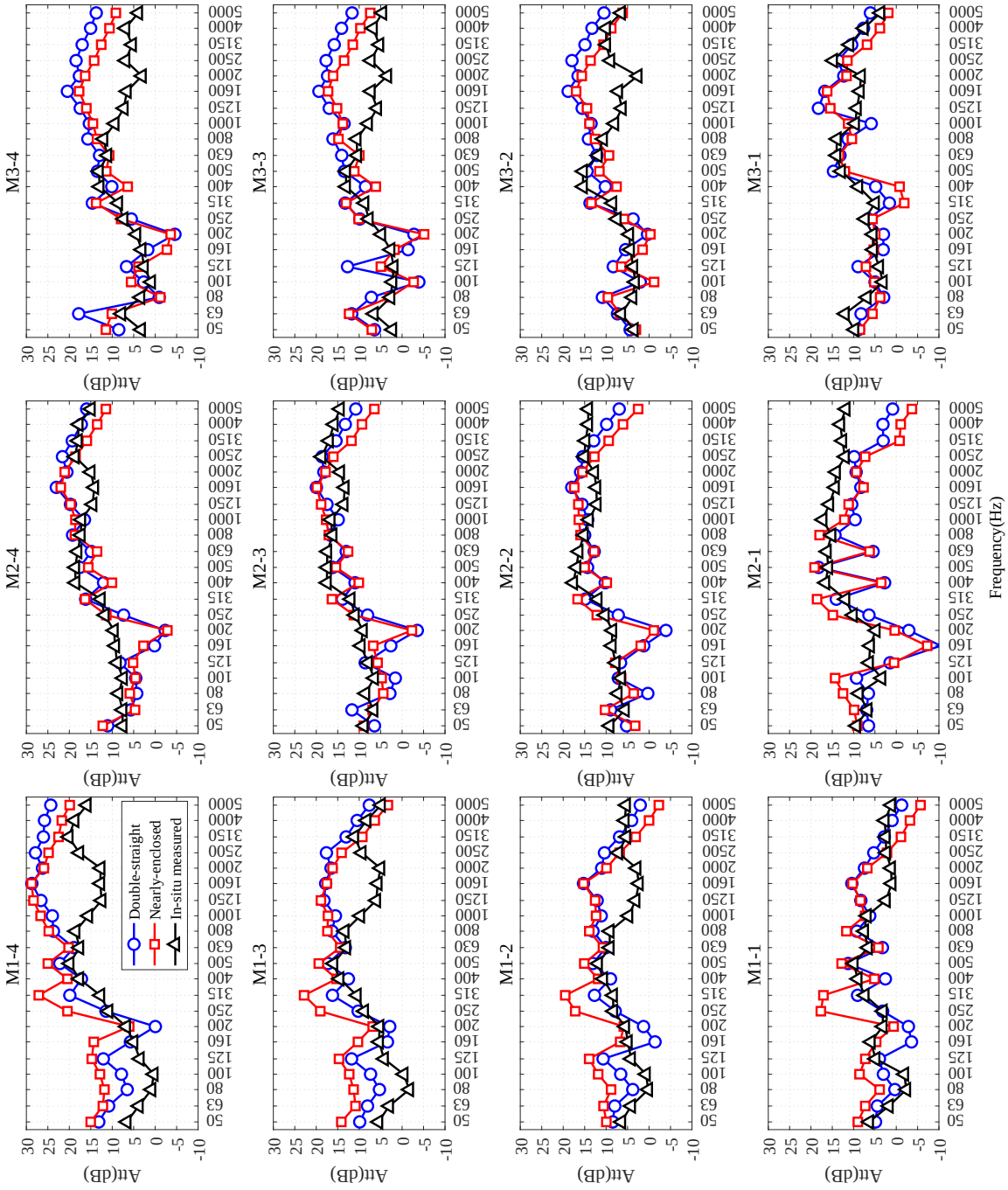

Fig 6.5.: Predictions radiated from coherent line sources versus in-situ measured results (blue curves with circles: predicted results for the nearly-enclosed barrier; red curves with squares: predicted results for the double-straight barrier; black curves with triangles: in-situ measured results)

the top of the barrier have a thickness of 6.5 mm, the sound isolation property may not be sufficient. A previous work[211] using scale model experiments and the 2.5-D BEM approach concluded that the top PC sheets with a thickness of 6mm could not be regarded as perfectly reflecting boundary conditions when the transmission loss of the employed PC sheets was close to the barrier attenuation. Figure 6.7 shows the comparison between them for receiver M1-4. It shows clearly that the differences at 125-400 Hz are all less than 5 dB.

Thus, the PC sheets on the top can only play a role on an arch shape with a high flexibility but have no significant effect on the sound insulation for rail traffic noise, resulting in the overestimations from 125 Hz to 400 Hz.

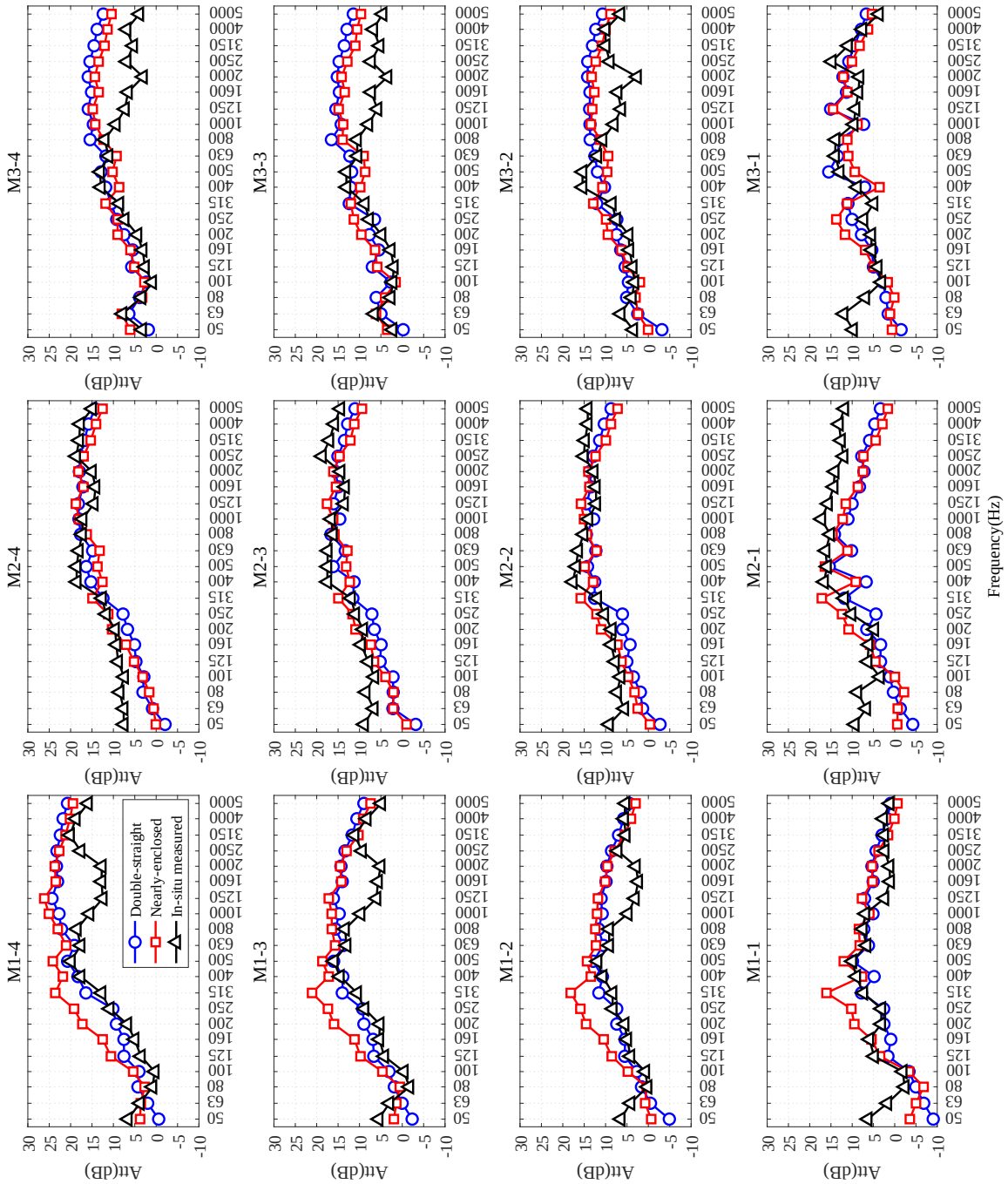

Fig 6.6.: Predictions radiated from incoherent line sources versus in-situ measured results(blue curves with circles: predicted results for the nearly-enclosed barrier; red curves with squares: predicted results for the double-straight barrier; black curves with triangles: in-situ measured results)

In the range of 500-800 Hz there are good agreements between two of the three curves for each receiver position. However, at frequencies from 1000 Hz to 2500 Hz, there are

remarkable differences between the predicted and measured results, especially for the receivers at a height close to that of the source (M-2, M-3, M-4). Based on the theory of sound insulation, these differences are probably from the coincident effect of the employed PMMA sheets which is of great importance in the consideration of transmission loss[217]. According to Equation (8.3) in [217], the critical frequency for the employed PMMA sheets is calculated as about 2000Hz. Therefore, at the frequency of about 2000Hz, the PMMA sheets would be strongly driven by the incident sound, and would radiate a corresponding acoustic wave well. Hence, the transmission loss of the employed PMMA sheets is markedly reduced in this range and they can be considered as "transparent" sheets allowing exposure to rail traffic noise. Figure 6.7 also shows the comparison between them for receiver M1-4. It shows clearly that the transmission loss of PMMA sheets at 2000 Hz is extremely low, below 0 dB. And the differences at about 2000 Hz between the transmission losses of PMMA and the attenuations for the nearly-enclosed barrier and the double-straight barrier are all less than 5 dB. Then, at frequencies above 2000Hz, the transmission loss rises again, approaching an extension of the original curve, in accordance with the good agreements observed in Figure 6.6 between the predicted and measured results for each receiver position. As a consequence, the attenuations predicted by the 2.5-D BEM model have good agreement with the measured results. And the 2.5-D BEM approach for incoherent line sources is suitable for predicting the acoustic performance of a noise barrier on a viaduct for an urban rail traffic system. Finally, based on the measured and predicted results in this chapter, one

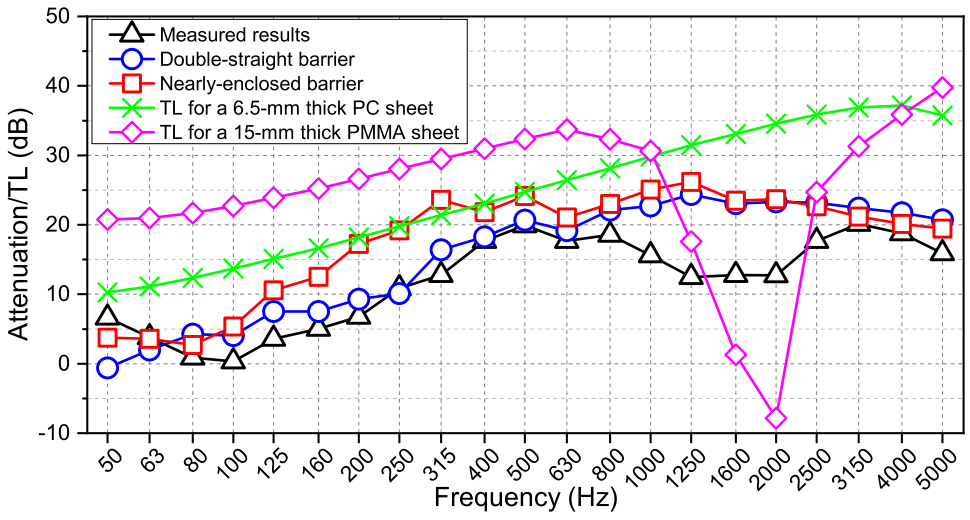

Fig 6.7.: One-third octave spectra for a comparison between measured and predicted attenuation, and transmission loss of a 6.5-mm-thick PC sheet

can state that the predictions for incoherent line sources have better agreements with the measured results presented in Chapter 3, than those for coherent line sources.

6.4 Acoustic resonance effects of the open absorption cavities

Figure 6.8 presents the spectra of sound pressure level at the receivers in M1-, calculated by the BEM model of the absorptive nearly-enclosed prototype. It can be found that there

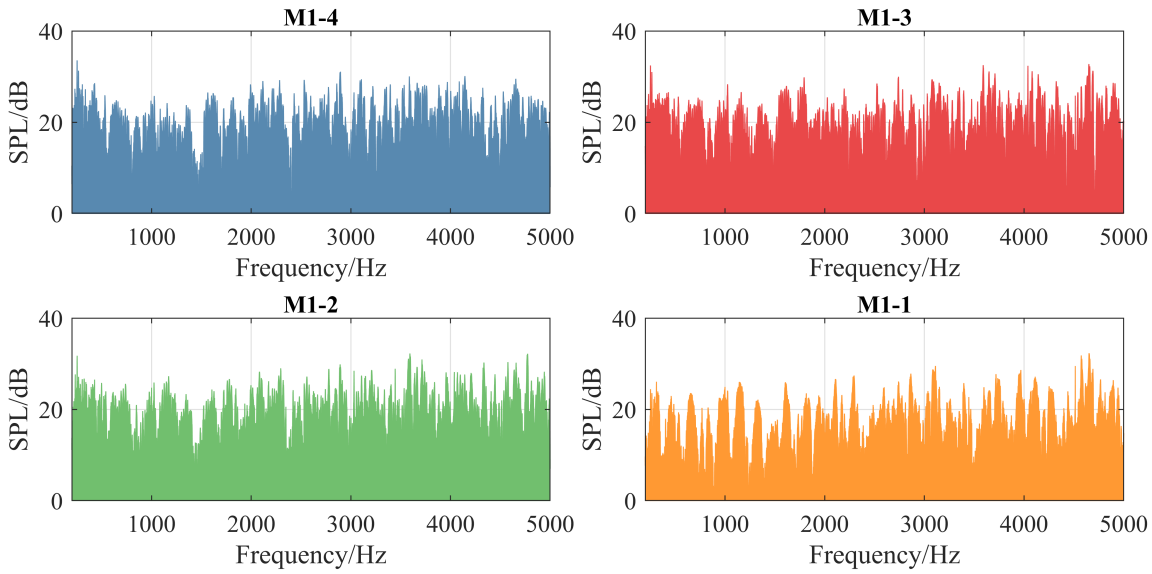

Fig 6.8.: The spectra of sound pressure level at the receivers in M1-, calculated by the BEM model of the absorptive nearly-enclosed prototype

are still significant peaks and valleys at many frequencies, covering the whole frequency range of the interest. The sound pressure distributions at part of the peak frequencies were calculated and compared with the modes of a similar fully-enclosed reflective cavity at similar frequencies, as shown in Figure 6.9 and Figure 6.10. It can be seen that each sound

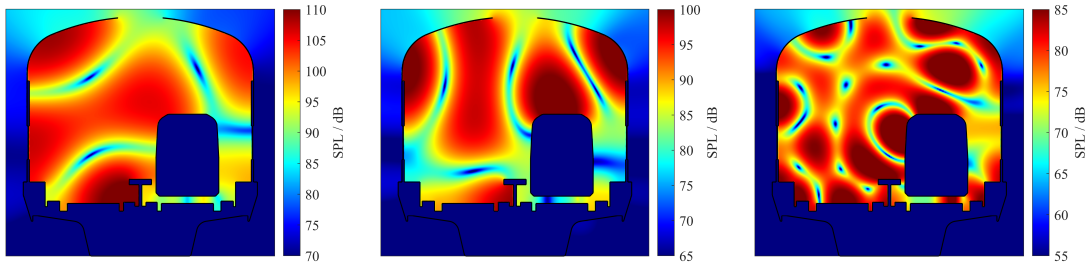

(a) 43.9 Hz (b) 55.1 Hz (c) 98.1 Hz

Fig 6.9.: Sound pressure distributions of the absorptive nearly-enclosed barrier model at part of the peak frequencies

pressure distribution of the absorptive nearly-enclosed barrier model at the peak frequency is basically consistent with the mode of the fully-enclosed reflective cavity, and each peak frequency is slightly higher than the corresponding modal frequency. Therefore, the peak values are still caused by the acoustic resonance effect of the open absorption cavity. The

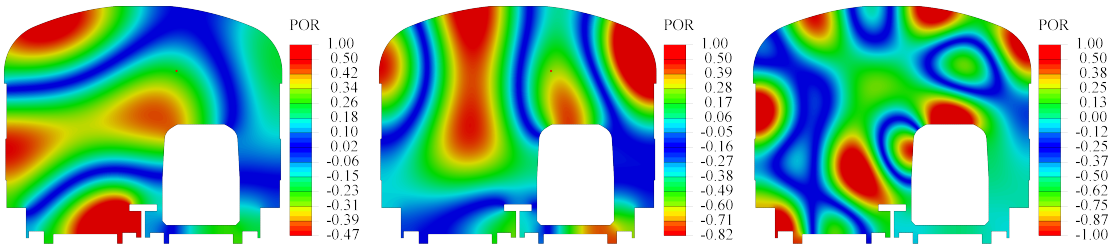

(a) 43.798 Hz (b) 54.869 Hz (c) 97.847 Hz

Fig 6.10.: Modes of a similar fully-enclosed reflective cavity at the modal frequencies corresponding to the peak frequencies

presence of these peaks and valleys also indicates that the acoustic resonance effect of the open absorption cavity still exists even if the nearly-enclosed barrier partly consists of sound absorption panels. However, by comparing the sound pressure level distribution at the peak frequency of 253 Hz with the mode of the fully-enclosed cavity at the frequency near 253 Hz (Figure 6.11) , it is found that they are not strictly consistent with each other, and the

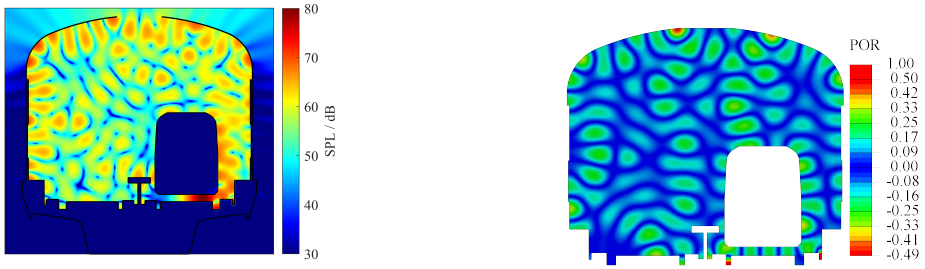

(a) The sound distribution of the absorptive nearly-enclosed barrier model, 253 Hz

(b) The mode of the fully-enclosed cavity model, 253.48 Hz

Fig 6.11.: The sound distribution at the peak frequency of 253 Hz is inconsistent with the mode of the fully-enclosed reflective cavity at the modal frequency close to 253 Hz

peak frequency is slightly lower than the modal frequency.

The absorption nearly-enclosed barrier can be regarded as an open cavity with sound absorption characteristics on the boundary surfaces. To reasonably explain the acoustic resonance effect of the open absorption cavity, the effect of the fully-enclosed absorption cavity was firstly studied, by analysing the influence of the sound absorption characteristics on the peak characteristic parameters (frequency, amplitude and damping coefficient) caused by the acoustic resonance effect. Then the influence of the top opening on the acoustic resonance effect of the open absorption cavity was studied in order to further explain the noise reduction mechanism of the absorptive nearly-enclosed barrier.

6.4.1 The fully-enclosed absorption cavity

Similar to the simplification used in Section 5.2.2, a fully-enclosed rectangular cavity with a cross section of 9 meters wide and 7 meters high was taken as an example. Sound absorption materials were added on one side and two opposite sides, respectively, as shown in Figure 6.12. For the cavity with absorption materials on one side, the boundary BC

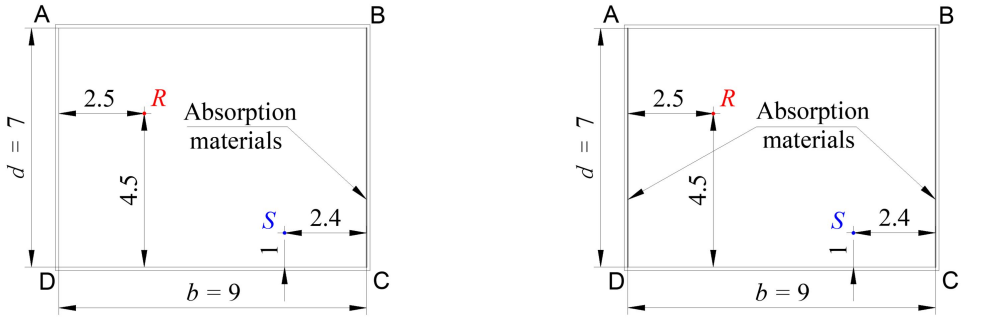

(a) A cavity with absorption materials on one side (BC)

(b) A cavity with absorption materials on two opposite sides (AD & BC)

Fig 6.12.: Different types of fully-enclosed absorption cavities

was absorptive. Whereas the boundaries AD and BC were absorptive for the cavity with absorption materials on two opposite sides. The ratio of each surface impedance and the air characteristic impedance was assumed to be $Z_s/\rho_0 c_0 = 0.001 + 0i$, that is, the absorption coefficient of each absorptive surface was $\alpha = 0.004$.

Sound pressure spectra at the same receiver inside these two fully-enclosed absorption cavities were calculated, and compared with the spectrum for the fully-enclosed reflective cavity. It can be seen from Figure 6.13 that the peaks at the resonant frequencies for the

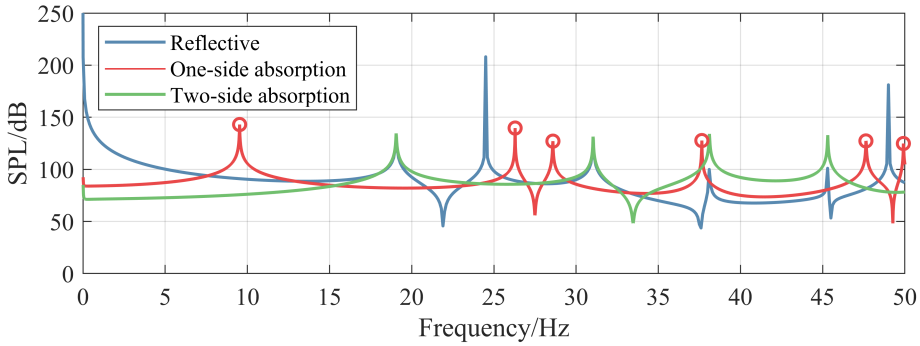

Fig 6.13.: Sound pressure spectra at the same receiver inside these two fully-enclosed absorption cavities, compared with the spectrum for the fully-enclosed reflective cavity

reflective cavity completely disappear in the results for the cavity with one-side absorption materials, and are replaced by the peaks at the new frequencies (marked by red circles). However, in the results of the cavity with two-side absorption materials, there are still many peaks at part of the resonant frequencies for the reflective cavity.

Sound distributions at the peak frequencies for these two absorption cavities were calculated, as shown in Figure 6.14 and Figure 6.15. It can be observed that a spatial modal

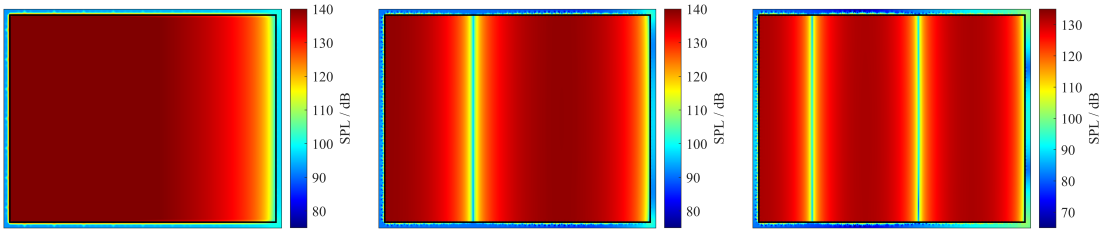

(a) 9.53 Hz (b) 28.58 Hz (c) 47.64 Hz

Fig 6.14.: Sound distributions at the peak frequencies for the cavity with one-side absorption materials

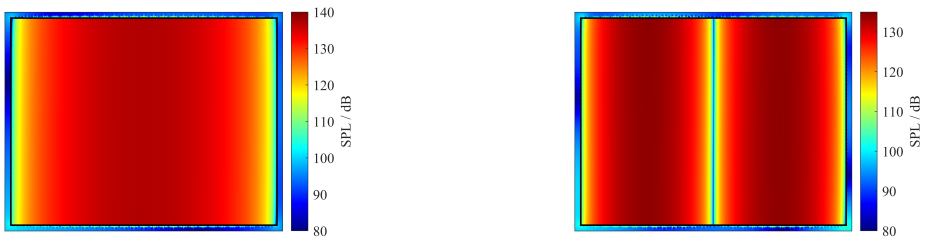

(a) 19.06 Hz (b) 38.11 Hz

Fig 6.15.: Sound distributions at the peak frequencies for the cavity with two-side absorption materials

distribution can be identified at each peak frequency: for the cavity with one-side absorption materials, the level at the absorptive boundary BC is always the minimum in the whole field whereas that at the opposite boundary AD has the maximum characteristics. Such sound pressure distributions can be viewed as part of the odd-order modes of a reflective cavity whose height is the same as that of the absorptive cavity but whose width is twice (Figure 6.14(a) can be viewed as the first-order mode, (b) as the third-order mode, (c) as the fifth-order mode). For the cavity with two-side absorption materials (Figure 6.15), although the peak frequencies are consistent with part of the resonant frequencies for the reflective cavity, the sound distribution at each peak frequency is completely different from the corresponding mode of the reflective cavity: the minimum of the level in the whole field is always located on the opposite absorptive boundaries BC and AD. Therefore, the sound distributions can be also regarded as part of the non-zero even-order modes of a reflective cavity with the same height but twice the width (Figure 6.15(a) can be viewed as the second-order mode, (b) as the forth-order mode).

The modal frequencies of the reflective cavity with the same height and twice the width were calculated by using Equation 5.1, those below 50 Hz being shown in Table 6.4. It can be seen that the odd-order modal frequencies are completely consistent with the peak frequencies for the cavity with one-side absorption materials, while the non-zero even-order

Tab 6.4.: The modal frequencies for the reflective cavity (below 50 Hz)

Modal frequency		m ($b' = 2b = 18$)					
		0	1	2	3	4	5
	0	0.00	9.53	19.06	28.58	38.11	47.64
	1	24.50	26.29	31.04	37.65	45.31	-
n ($d = 7$)	2	49.00	49.92	-	-	-	-

modal frequencies are completely consistent with the peak frequencies for the cavity with two-side absorption materials. Hence it can be concluded that when a reflective cavity has one absorptive boundary or two opposite absorptive boundaries, and their absorption coefficients are very low, the acoustic resonance effect caused by the cavity still exists and the peaks will not disappear due to the addition of the absorption materials. The absorptive boundaries cause the peak frequencies to appear at the modal frequencies of the double-spaced reflective cavity, changing the sound distributions at the peak frequencies. Nevertheless, these sound distributions at the peak frequencies are still governed by the acoustic modes, but the modes of the double-spaced reflective cavity.

The sound absorption capability of the absorptive boundary is always determined by the sound absorption coefficient α. The stronger the absorption capability of the absorptive boundary is, the closer the absorption coefficient α is to 1, and the closer the ratio of the acoustic impedance of the boundary surface and the air characteristic impedance $Z_s/\rho_0 c_0$ is to $1 + 0i$. Therefore, the influence of the sound absorption capability of the absorptive boundaries on the peak characteristics parameters (frequency, amplitude and the damping coefficient) can be discussed by changing the surface impedance ratioof the absorptive boundaries for the cavities with one-side absorption boundary and two-side absorption boundaries, respectively.

By changing the surface impedance ratio $Z_s/\rho_0 c_0$ of the absorptive boundary BC, the influence of the sound absorption on the peak characteristics parameters for the cavity with one-side absorption boundary can be observed in Figure 6.16. Assuming that the imaginary part of the acoustic impedance ratio equals zero, as seen in Figure 6.16(a), with the increase of the real part from 0.001 to 1 (black arrow(1)), the frequencies of the peaks at 9.53 Hz, 26.29 Hz and 28.58 Hz are unchanged, the peak amplitudes decreasing and the damping coefficients increasing gradually. When the real part of the surface impedance ratio reaches to 1 (the orange curve), all the peaks at the resonant frequencies associated with the horizontal modes disappear, and only the peaks at the resonant frequencies associated with the vertical modes (26.29 Hz) were retained with small amplitudes. Then, as the impedance ratio increases from 1 to 100 (black arrow(2)), there are new peaks at 19.06 Hz and 24.50 Hz, with the increased amplitude and the decreased damping coefficient. These new peaks are attributed to the transition from the absorptive cavity to the reflective cavity. When the real part of the surface impedance ratio increases to infinity, the absorptive boundary can

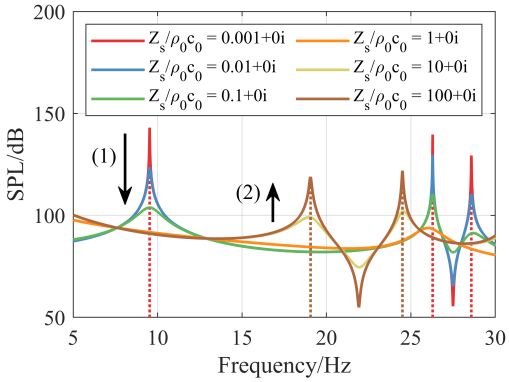

(a) The real part of the surface impedance ratio $Z_s/\rho_0 c_0$ increases positively

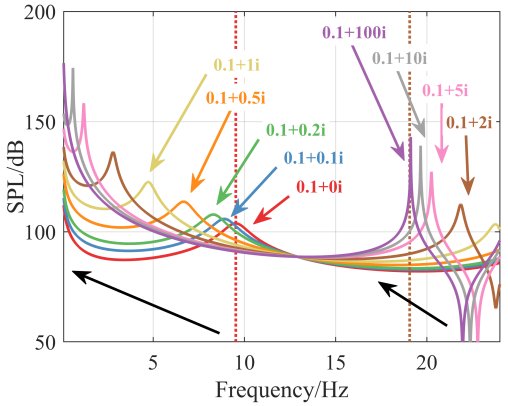

(b) The imaginary part of the surface impedance ratio $Z_s/\rho_0 c_0$ increases positively

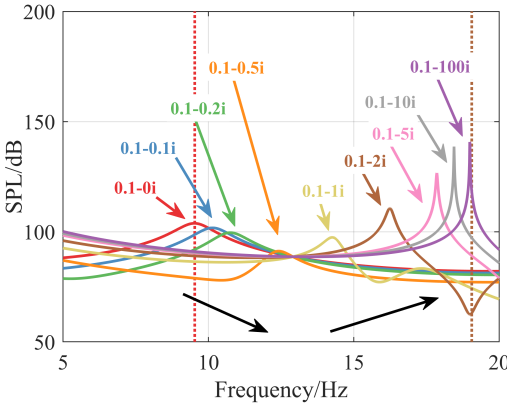

(c) The imaginary part of the surface impedance ratio $Z_s/\rho_0 c_0$ increases negatively

Fig 6.16.: The change law of the peaks with the increase of the surface impedance ratio for the cavity with one-side absorption materials

be regarded as the reflective boundary, and therefore the peaks at the original frequencies disappear, while the peaks at the resonant frequencies of the reflective cavity appear.

Assuming that the real part of the acoustic impedance ratio equals 0.1, as seen in Figure 6.16(b), when the imaginary part increases positively, the peak at 9.53 Hz moves to the lower frequency zone, with the increased amplitude and the decreased damping coefficient. When the imaginary part of the surface impedance ratio increases to infinity, the peak at 9.53 Hz moves to the resonant frequency of the reflective cavity, the peak amplitude and the damping coefficient being close to those of the reflective cavity. when the imaginary part increases negatively from 0 to -1, as seen in Figure 6.16(c), the peak at 9.53 Hz moves to the higher frequency zone, with the decreased amplitude and the increased damping coefficient. When the imaginary part of the surface impedance ratio reaches to -1, the peak close to 9.53 Hz disappears, and a new peak near 19.06 Hz (a resonant frequency of the reflective cavity) appears. Then, as the imaginary part of the surface impedance ratio decreases from -1 to -100, the peaks continue to move to the higher frequency zone, with the increased amplitude and the decreased damping coefficient. When the imaginary part of the surface impedance ratio decreases to negative infinity, the peaks move to the resonant frequencies

of the reflective cavity, the peak amplitudes and the damping coefficients being close to those of the reflective cavity.

By changing the surface impedance ratios $Z_s/\rho_0 c_0$ of the absorptive boundary BC and AD simultaneously, the influence of the sound absorption on the peak characteristics parameters for the cavity with two-side absorption boundaries can be observed in Figure 6.16. Assuming that the imaginary part of the acoustic impedance ratio equals zero, as seen in

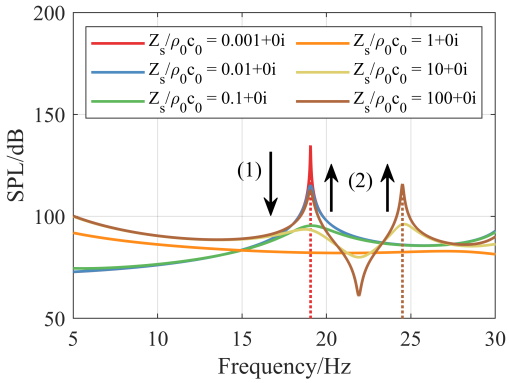

(a) The real part of the surface impedance ratio $Z_s/\rho_0 c_0$ increases positively

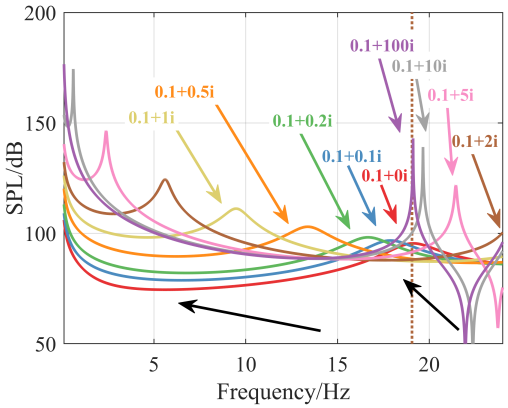

(b) The imaginary part of the surface impedance ratio $Z_s/\rho_0 c_0$ increases positively

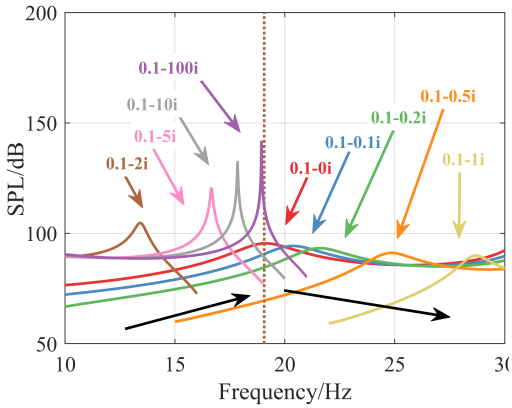

(c) The imaginary part of the surface impedance ratio $Z_s/\rho_0 c_0$ increases negatively

Fig 6.17.: The change law of the peak with the increase of the surface impedance ratio for the cavity with two-side absorption materials

Figure 6.17(a), with the increase of the real part from 0.001 to 1 (black arrow(1)), the frequency of the peak at 19.06 Hz is unchanged, the amplitude decreasing and the damping coefficients increasing gradually. When the real part of the surface impedance ratio reaches to 1 (the orange curve), all the peaks at the resonant frequencies disappear. Then, as the real part of the impedance ratio increases from 1 to 100 (black arrow(2)), the amplitude of the peak at 19.06 Hz increases whereas the damping coefficient decreases gradually. Meanwhile, there is a new peak at 24.50 Hz, with the increased amplitude and the decreased damping coefficient. The new peak is also attributed to the transition from the absorptive cavity to the reflective cavity.

Assuming that the real part of the acoustic impedance ratio equals 0.1, as seen in Figure 6.17(b), when the imaginary part increases positively, the peak at 19.06 Hz moves to the lower frequency zone, with the increased amplitude and the decreased damping coefficient. When the imaginary part of the surface impedance ratio increases to infinity, the peak at 19.06 Hz moves to the resonant frequency of the reflective cavity, the peak amplitude and the damping coefficient being close to those of the reflective cavity. When the imaginary part increases negatively from 0 to -1, as seen in Figure 6.17(c), the peak at 19.06 Hz moves to the higher frequency zone, with the decreased amplitude. When the imaginary part of the surface impedance ratio reaches to -1, the peak close to 19.06 Hz disappears, and a new peak at the frequency lower than 19.06 Hz appears. Then, as the imaginary part of the surface impedance ratio decreases from -1 to -100, the peaks continue to move to the higher frequency zone, with the increased amplitude and the decreased damping coefficient. When the imaginary part of the surface impedance ratio decreases to negative infinity, the peaks move to the resonant frequencies of the reflective cavity, the peak amplitudes and the damping coefficients being close to those of the reflective cavity.

To summarize the influence of sound absorption characteristics of the absorptive boundaries on the peak characteristic parameters at the resonant frequencies, it can be found that the variation of the real part of $(Z_s/\rho_0 c_0 - 1)$ only affects the peak amplitude rather than the peak frequency. While the change in the sign of the real part of $(Z_s/\rho_0 c_0 - 1)$ directly determines the peak frequency: when the real part of $Z_s/\rho_0 c_0$ is greater than 1, the peaks will appear at the resonant frequencies of the reflective cavity. The amplitudes of the peaks increase with $|Z_s/\rho_0 c_0 - 1|$ and the damping coefficients decrease accordingly, until these peaks approach those of the reflective cavity; when the real part is less than 1, the peaks will appear at the resonant frequencies of the original absorptive cavity. The amplitudes of the peaks increase with $|Z_s/\rho_0 c_0 - 1|$ and the damping coefficients decrease accordingly; when the real part is equal to 1, the peaks at the resonant frequencies related to the absorptive boundaries will disappear, and there will be no peaks appearing at the resonant frequencies of the reflective cavity.

However, the variation of $Z_s/\rho_0 c_0$ in the imaginary part affects not only the peak amplitude, but also the peak frequency. While the change of the sign in the imaginary part determines the peaks to move to the lower or the higher frequency zone. When the imaginary part is greater than 0, the peaks move to the lower frequency zone with the increase of the absolute value of the imaginary part, and the peak amplitudes increase accordingly, until these peaks are close to those of the reflective cavity; when the imaginary part is less than 0, the original peak move to the higher frequency zone, with the increase of the absolute value of the imaginary part, and the peak amplitudes gradually decrease accordingly; when the imaginary part is less than -1, there are new peaks appearing at the lower frequencies near the resonant frequencies of the reflective cavity. With the increase of the absolute value of the imaginary part, the peaks move to the higher frequency zone, and the peak amplitudes gradually increase accordingly, until these peaks are close

to those of the reflective cavity. When the imaginary part is equal to 0, the characteristic parameters of these peaks are determined by the real part of the impedance ratio $Z_s/\rho_0 c_0$.

In summary, when the ratio of the surface impedance and the air characteristic impedance is close to $1 + 0i$, that is, the absorption coefficient is close to 1, the peak amplitudes caused by the resonance effects will decrease significantly. However, when the impedance ratio is not equal to 1, the peaks caused by the resonance effects will still exist, but the frequencies, the amplitudes and the damping coefficients of the peaks will be determined by the locations, the lengths, and the impedance ratios of the absorptive boundaries. That is the main reason why there are still hundreds of resonant peaks in the sound pressure spectrum at the receivers inside the fully-enclosed absorption cavity.

6.4.2 The open absorption cavity

To analyze the variation law of the peak characteristic parameters with the opening width, the cavities with one-side and two-side absorption materials shown in Figure 6.12 are opened at the top, respectively, with the widths of 1 m, 2 m, 4 m, 6 m and 8 m. For the cavity with one-side absorption materials, the sound pressure spectra at a given receiver outside the cavities with the openings of different widths were calculated and are shown in Figure 6.18. It can be seen that the peaks associated with the trapped modes formed

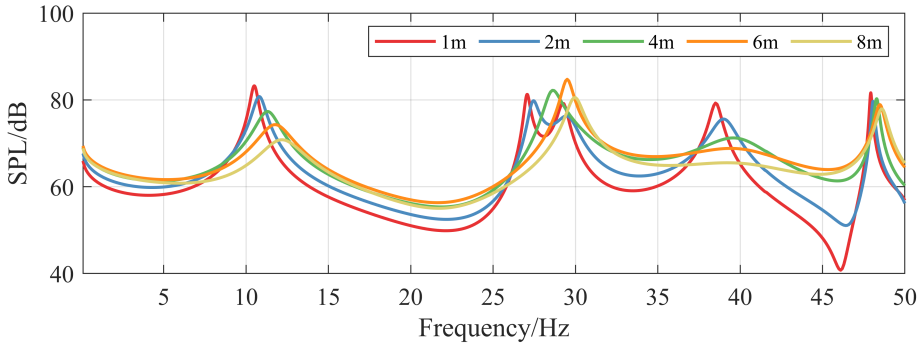

Fig 6.18.: The variation law of the sound pressure spectra with the opening width, for the cavity with one-side absorption materials

by the opening side (boundary AB) move to the higher frequency zone with the increase of the opening width, and their amplitudes approach to disappear gradually, such as the peaks at around 26.29 Hz and 37.65 Hz. On the other hand, some peaks associated with the trapped modes independent of the opening side also move to the higher frequency zone, and their amplitudes gradually decrease, but they do not disappear, such as the peaks at around 9.53 Hz and 47.64 Hz. Moreover, we can also find that the amplitudes of the peaks of the low-order modes decrease more significantly with the increase of the opening width, than those of the high-order modes. For example, for the absorption cavity with the 8-meter-width opening (the yellow curve), the peak amplitude at around 9.53 Hz is much lower than that at around 47.64 Hz. This is because the resonance regions of the

low-order modes are quite large, vulnerable to the width of the opening. While those of the high-order modes are quite small, the local resonance being not susceptible to the opening width. Hence, the amplitudes of the peaks associated with the high-order modes are less affected by the opening width.

For the other peaks associated with the trapped modes independent of the opening side, such as the peak at around 28.58 Hz, the characteristic parameters vary in two phases with the increase of the opening width, being shown in Figure 6.19: when the opening width

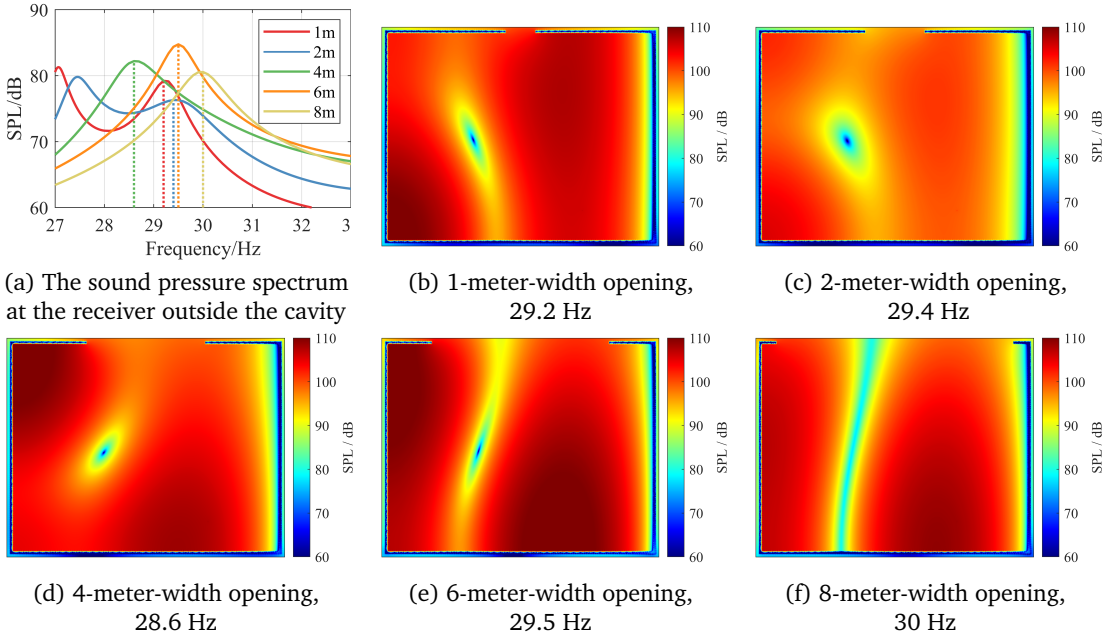

(a) The sound pressure spectrum at the receiver outside the cavity

(b) 1-meter-width opening, 29.2 Hz

(c) 2-meter-width opening, 29.4 Hz

(d) 4-meter-width opening, 28.6 Hz

(e) 6-meter-width opening, 29.5 Hz

(f) 8-meter-width opening, 30 Hz

Fig 6.19.: The relationship between the sound distribution at around 28.58 Hz and the opening width of the cavity with one-side absorption materials

increases from 1 m to 2 m, the peak frequency increases and the amplitude decreases; when the opening width increases from 4 m to 8 m, the peak frequency increases and the peak amplitude first increases and then decreases. This variation law is directly caused by the sound distributions of the trapped modes. By observing the sound pressure distributions of the cavities at the peak frequencies (see Figure 6.19(b)-(f)), it can be found that when the opening width is less than 3 meters, only the right resonance region is connected with the external field, resulting in the increased peak frequency and the decreased peak amplitude; when the opening width is greater than 3 meters, both the left and the right resonance regions are connected with the external field, causing the peak frequency to increase and the peak amplitude to increase first and then decrease. The variation law in the second phase is also consistent with the change rule of the peak characteristic parameters of the reflective open cavity with the opening width discussed in Chapter 4.

For the cavity with two-side absorption materials, the sound pressure spectra at a given receiver outside the cavities with the openings of different widths were calculated and are shown in Figure 6.20. It can be found that the change rule of the peak characteristic

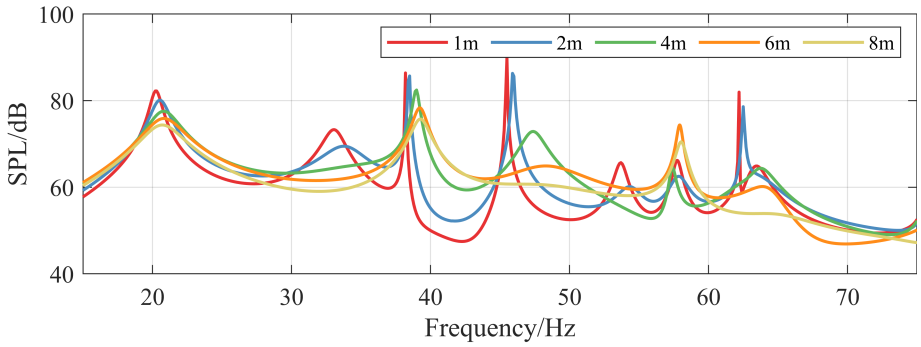

Fig 6.20.: The variation law of the sound pressure spectra with the opening width, for the cavity with two-side absorption materials

parameters is the same as that for the cavity with one-side absorption materials: the peaks associated with the trapped modes formed by the opening side move to the higher frequency zone with the increase of the opening width, and their amplitudes approach to disappear gradually, such as the peaks at around 31.04 Hz and 45.31 Hz; some peaks associated with the trapped modes independent of the opening side also move to the higher frequency zone, and their amplitudes gradually decrease, but they do not disappear, such as the peaks at around 19.06 Hz and 38.11 Hz. Moreover, we can also find that the amplitudes of the peaks of the low-order modes decrease more significantly with the increase of the opening width, than those of the high-order modes. For example, for the absorption cavity with the 8-meter-width opening (the yellow curve), the peak amplitude at around 19.06 Hz is much lower than that at around 38.11 Hz, and the damping coefficient of the former is higher than that of the latter.

For the other peaks associated with the trapped modes independent of the opening side, such as the peak at around 57.17 Hz, the characteristic parameters also vary in two phases with the increase of the opening width, and the variation law is more obvious than that for the cavity with one-side absorption materials, being shown in Figure 6.19: when the opening width is less than 3 meters, only the middle resonance region is connected with the external field, resulting in the increased peak frequency and the decreased peak amplitude; when the opening width is greater than 3 meters, all the two sides and the middle resonance regions are connected with the external field, causing the peak frequency to increase and the peak amplitude to increase first and then decrease.

From the simulated results for the open cavities with one-side and two-side absorption materials, it can be summarized that the peaks associated with the trapped modes formed by the opening side move to the higher frequency zone with the increase of the opening width, and their amplitudes approach to disappear gradually; whereas the relationship between the opening width and the peaks associated with the trapped modes independent of the opening side is directly dependent on the sound distributions at the peak frequencies: when the variation of the opening width does not affect the connections between the resonance

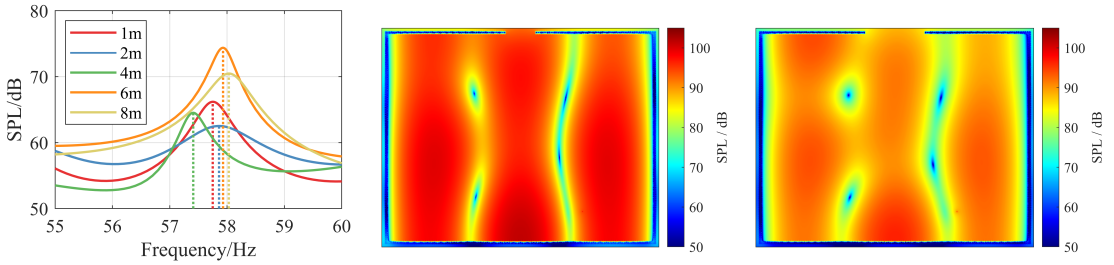

(a) The sound pressure spectrum at the receiver outside the cavity

(b) 1-meter-width opening, 57.75 Hz

(c) 2-meter-width opening, 57.86 Hz

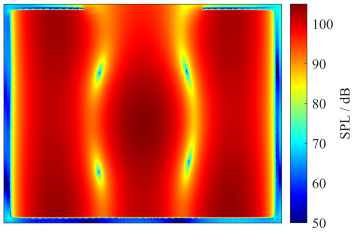

(d) 4-meter-width opening, 57.41 Hz

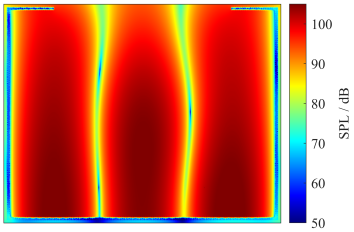

(e) 6-meter-width opening, 57.93 Hz

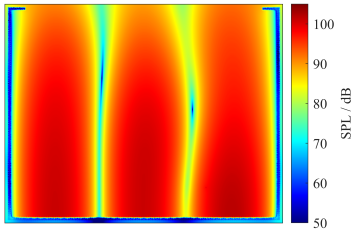

(f) 8-meter-width opening, 58.03 Hz

Fig 6.21.: The relationship between the sound distribution at around 57.17 Hz and the opening width of the cavity with two-side absorption materials

regions and the external field, the peaks move to the higher frequency zone with the increase of the opening width, and the peak amplitudes increase first and then decrease gradually. Moreover, the peak amplitudes of the low-order modes decrease more significantly with the increase of the opening width, than those of the high-order modes.

By reviewing the geometry and the absorption characteristics of the absorptive nearly-enclosed prototype considered previously, it can be found that an open cavity with two-side absorption materials is formed by the sound absorption panels at the top of the barriers located on both sides of the viaduct, and two open cavities with one-side absorption materials are formed by the vehicle boundaries and the sound absorption panels at the bottom of the barriers located on each side of the viaduct. Hence, the sound distributions at some peak frequencies for the nearly-enclosed prototype must be changed due to the absorption characteristics. The comparison presented in Figure 6.11 validates that the sound distribution at the peak frequency of 253 Hz for the nearly-enclosed prototype is inconsistent with that at the corresponding modal frequency of 253.48 Hz for the reflective fully-enclosed model. Besides, the glass-wool absorption panels with the imaginary parts of the impedance ratio less than 0 in the whole frequency range, can cause the peaks to move to the higher frequency zone; the open-cell aluminium panels with the imaginary parts of the impedance ratio greater than 0 at high frequencies, can cause the peaks to move to the lower frequency zone; the opening with the width of 2 meters can also cause the variation of the peak frequencies. As a result of these three major causes, the resonant peak frequencies can be slightly higher or slightly lower than the modal frequencies of the fully-enclosed reflective nearly-enclosed model. The comparisons presented in Figure 6.9 and Figure 6.10 validate that the resonant frequencies are slightly higher than the modal frequencies, while

the comparison presented in Figure 6.11 validates that the resonant frequencies are slightly lower than the modal frequencies.

In summary, it can be concluded that when the nearly-enclosed barrier has absorptive panels, there are still many peaks in the spectrum at resonant frequencies induced by the trapped modes of the open absorptive cavity, since the absorption coefficients of the panels are significantly low. These peaks are different from those for the reflective type because the surface absorption characteristics of the panels not only change the whole sound distributions at peaks' frequencies, but also cause regular changes of the characteristic parameters of these peaks. When the ratio of surface acoustic impedance to air characteristic impedance is close to $1+0i$, that is, the absorption coefficient is close to 1, the acoustic resonance of the open absorptive cavity can be effectively reduced. Besides, the increase of the top opening width changes the characteristic parameters of the peaks as well, but at the same time it also leads to the increase of the sound pressure level at the external field in the non-peak frequency band. Therefore, the influence of the top opening width on the sound absorption cavity should be considered comprehensively based on the frequency spectrum of the noise source.

6.5 The effect prediction of the nearly-enclosed prototype

In this section, the transmission loss of topped PC panels for each one-third octave band was assumed sufficiently higher than the attenuation of nearly-enclosed barriers. Hence, the acoustic performance of nearly-enclosed barriers could be discussed without the disturbance of acoustic properties of employed materials, in two cases: vehicles situated near and far from receiver positions (shown in Figure 6.22).

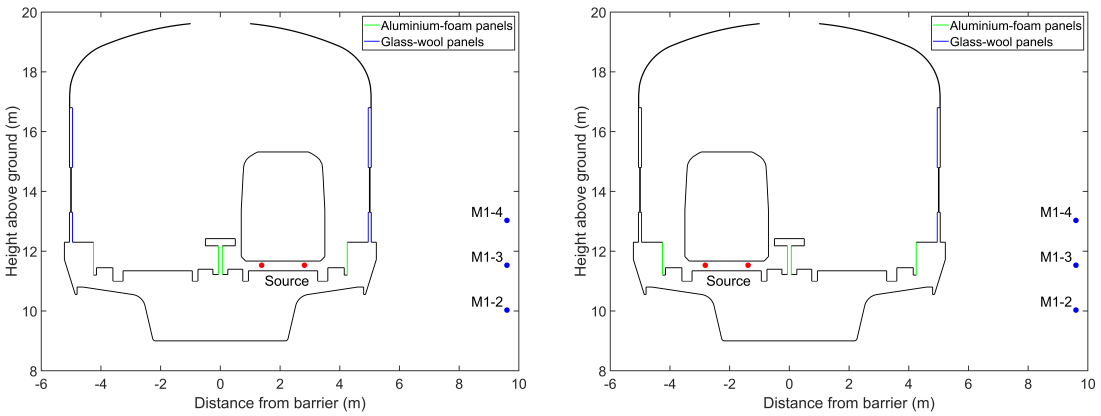

(a) Near receiver positions (b) Far from receiver positions

Fig 6.22.: The sites of vehicles situated near and far from receiver positions for nearly-enclosed barriers

6.5.1 Vehicles situated near receiver positions

Figure 6.6 shows the predicted attenuations for vehicles situated near receiver positions (shown in Figure 6.22(a)). For the source to receiver distance of 7.5 m (receiver column M1-), the attenuations at low frequencies below 100 Hz are less than 5 dB for all four receiver positions, even negative at M1-1. Then there is a consistent pattern in the results obtained, with the attenuation increasing with the third-octave band from 100 Hz to 315 Hz. The localized maximums for receiver positions at 315 Hz are 24 dB, 21 dB, 18 dB and 16 dB, respectively. Subsequently, the attenuation at M1-4 stabilizes around 20-25 dB in the range of 315-5000 Hz, while the attenuations at M1-3, M1-2 and M1-1 in the range of 315-5000 Hz have a similar pattern: the attenuation decreases with the increased frequency. And this pattern becomes more significant with the increased distance between the sources and the receiver position. Finally, at 5000 Hz, the attenuations for M1-3, M1-2 and M1-1 are 7 dB, 3 dB and 1dB, respectively. For the source to receiver distance of 22m (receiver column M2-), with the increased frequency from 100-315 Hz the attenuation increases again, but the localized maximums are about 15 dB rather than 20 dB for each receiver in column M1-. At low frequencies below 100 Hz the attenuations are less than 5 dB as well. From 315 Hz to 5000 Hz the attenuation stabilizes around 10-20 dB for M2-4, M2-3 and M2-2, while the attenuation at M2-1 fluctuates violently at 315-800 Hz and then decreases with the increased frequency from 1000Hz to 5000 Hz. The value of the attenuation at 5000 Hz for M2-1 is only 2 dB. For the source to receiver distance of 55 m (receiver column M3-), at low frequencies below 125 Hz the attenuations are still less than 5 dB. In the range of 125-315 Hz, the attenuation increases with frequency again with the localized maximums of around 13 dB. Subsequently, the attenuation in the column M3- stabilizes around 5-15 dB in the range of 315-5000 Hz.

6.5.2 Vehicles situated far from receiver positions

Figure 6.23 shows the predicted attenuations for vehicles situated far from receiver positions (shown in Figure 6.22(b)). For the source to receiver distance of 7.5 m (receiver column M1-), the attenuations at low frequencies below 125 Hz are less than 5 dB for M1-4, M1-3 and M1-2, even for M1-1 the values are less than zero decibels. In the range of 50-315 Hz there is a consistent pattern in the results obtained, with the attenuation increasing with the third-octave band. The localized maximums at 315 Hz for M1-4, M1-3, M1-2 and M1-1 are 14 dB, 11 dB, 10 dB and 6 dB, respectively. Subsequently, the attenuation continues to increase and finally stabilizes around 15-20 dB. The global maximum for M1-4 is 19 dB at 1000 Hz, while the attenuations in the range of 315-1000 Hz remain around 5-10 dB at M1-3 and M1-2, and around 0-5 dB at M1-1. Then, the attenuations from 1000-5000 Hz at M1-3, M1-2 and M1-1 have a similar pattern that the attenuation decreases with the increased frequency. Finally, at 5000 Hz, the attenuations for M1-3, M1-2 and M1-1 are 1 dB, -2 dB and -3 dB, respectively. For the source to receiver distance of 22m (receiver

column M2-), with the increased frequency from 50-315 Hz the attenuation increases again. At low frequencies below 160 Hz the attenuations are less than 5 dB as well. From 315 Hz to 5000 Hz the attenuation for M2-4 continues to increase and finally stabilizes around 5-15 dB, while for M2-3 and M2-2 the attenuation stabilizes around 0-10 dB. The attenuation for M2-1 decreases gradually from 315 Hz to 5000 Hz, with a value of -3 dB at 5000 Hz. For the source to receiver distance of 55 m (receiver column M3-), at low frequencies below 200 Hz the attenuations are still less than 5 dB. In the range of 125-5000 Hz, the attenuation stabilizes around 5-10 dB at M3-4 and around 0-5 dB at M3-3 and M3-2. For M3-1 the attenuation increases significantly from 125 Hz to 250 Hz, and then sharply decreases to 400 Hz with the localized minimum of 1 dB. Subsequently, the attenuation stabilizes around -5-5 dB.

6.5.3 Discussion

As mentioned in Section 6.3.2, for the case of vehicles situated near the receiver positions, effectively the only significant difference between the prediction for nearly-enclosed barriers and double-straight barriers is the extra attenuations Att_{ex} in the range of 160-315 Hz. And the value of the extra attenuations decreases considerably with the increased source to receiver distance (Att_{ex}(M1-)=4-10dB, Att_{ex}(M2-)=2-7 dB, Att_{ex}(M3-1)=0-4 dB). For the case of vehicles situated far from the receiver positions, the extra attenuations in the range of 160-315 Hz can be seen again in Figure 6.23. But only in the receiver column M1- the extra values are around 1-4 dB, whereas for the other two receiver columns there is no significant extra attenuation. Another noticeable difference in the case of vehicles situated far from the receiver positions shown in Figure 6.23 can be seen at low frequencies from 50 Hz to 100 Hz. Without the top arched PC panels, the double-straight barriers can result in the increased pressure level in this frequency range in the case of the vehicles situated far from the receiver positions, leading to the large negative values of the attenuations (even lower than -10 dB), while for the nearly-enclosed barriers, although the attenuations in the range of 50-100 Hz are small, most of these values are not negative. There is one more thing worth noting: at high frequencies above 1000 Hz the attenuations for double-straight barriers are a little higher than those for nearly-enclosed barriers, with values of less than 2 dB.

A single rating analysis was performed in the study of in-situ measured results. It can also be used to predict the acoustic performance of nearly-enclosed barriers. The single rating analysis is not only related to the attenuations caused by barriers but also dependent on the pressure levels for the site without a barrier. Hence, the measured pressure levels for the

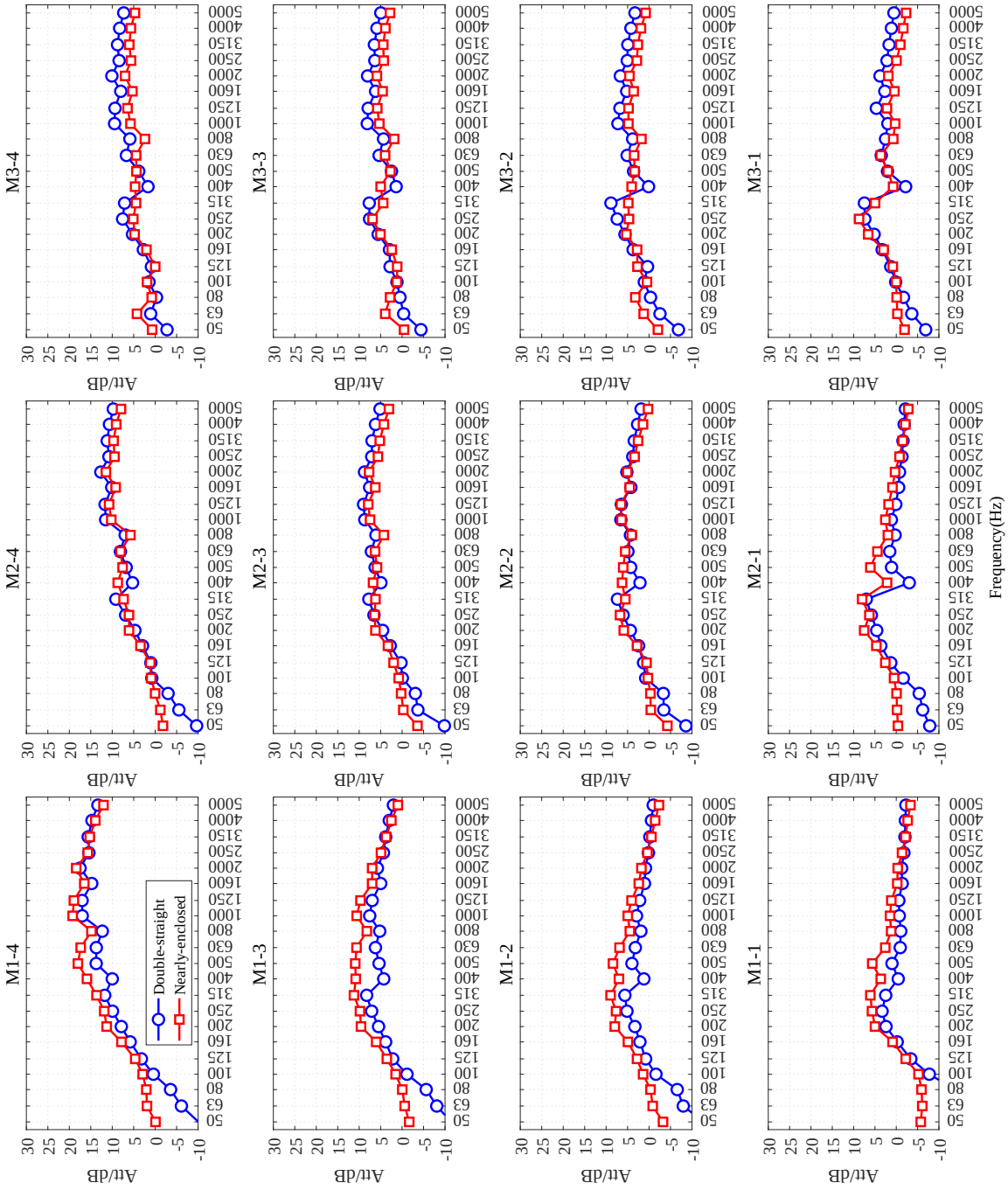

Fig 6.23.: Predictions radiated from incoherent line sources for the vehicles situated far from receiver positions (blue curves with circles: predicted results for the nearly-enclosed barrier; red curves with squares: predicted results for the double-straight barrier)

site without a barrier were introduced into the calculations. The A-weighted single rating in the range of 50-5000 Hz for each type of barrier is given as,

$$Att_{\mathrm{A},50-5000} = \frac{\sum_{i=1}^{n} 10^{((\mathrm{SPL}_{\mathrm{wo},i}+\mathrm{A}_i)/10)}}{\sum_{i=1}^{n} 10^{((\mathrm{SPL}_{\mathrm{wo},i}-Att_{\mathrm{ty},i}+\mathrm{A}_i)/10)}} \quad (i = 1, 2, 3, ...n = 21) \tag{6.8}$$

where $SPL_{wo,i}$ denotes the sound pressure level for the site without a barrier at the ith one-third octave band. A_i denotes the weighted value in level of A-weighting at the ith one-third octave band. $Att_{ty,i}$ denotes the attenuation in level for the site with double-straight barriers or nearly-enclosed barriers at the ith one-third octave band.

Due to a lack of measured results for the sites of the vehicles far from receiver positions, we could merely solve the single ratings for the sites of the vehicles near receiver positions, as shown in Table 6.5, at all twelve receiver positions for both double-straight barriers and nearly-enclosed barriers. For the receiver column M1-, the single ratings for nearly-enclosed barriers are higher by only 2-3 dB than those for double-straight barriers, while for the receiver column M2- the attenuations in level for both kinds of barrier are almost the same. However, for the receiver column M3- the attenuation for nearly-enclosed barriers are less than those for double-straight barriers by about 2-3 dB. Based on the single rating analysis, we propose that compared with double-straight barriers, nearly-enclosed barriers have a better effect on reducing the level at receiver positions in the near field (source to receiver distance: 7.5 m), almost no effect in the medium field (source to receiver distance: 22 m) and an even worse effect in the far field (source to receiver distance: 55 m).

Tab 6.5.: The A-weighted single rating in the range of 50-5000 Hz for double-straight barriers and nearly-enclosed barriers on the site of the vehicles situated near receiver positions

$Att_{A,50-5000}$(dB(A))	Double-straight barriers			$Att_{A,50-5000}$(dB(A))	Nearly-enclosed barriers		
	M1-	M2-	M3-		M1-	M2-	M3-
M-4	19	15	12	M-4	22	14	10
M-3	14	13	13	M-3	16	13	10
M-2	10	12	12	M-2	12	13	10
M-1	5	10	11	M-1	7	11	9

6.6 Conclusion

This chapter firstly presented a Delany-Bazley model with only two parameters (thickness of panel and flow resistivity) to model the acoustic behaviour of glass wool panels. Then, to model open-celled aluminium foam panels, a microstructure model proposed by H. Li and J. Zhang was introduced. By using these models for absorbent treatments, the BEM models for coherent line sources and incoherent line sources were solved, respectively. In a comparison with the in-situ measured results discussed in Chapter 3, the predictions for incoherent line sources have much better agreements than those for coherent line sources, which illustrates the conclusions in Chapter 4 once again that the source type is one of the most important parameters in the numerical modelling of urban rail transit noise and the acoustic performance of barriers. 2.5-D BEM modelling is an effective method to model the acoustic performance of noise barriers for urban rail traffic noise, since the calculations

allow the use of incoherent-line sources. 2.5-D BEM models for incoherent line sources are preferred to predict the noise barriers employed in rail traffic systems.

In terms of the acoustic performance of the nearly-enclosed prototype, it was effective against the measured rolling noise for urban rail traffic in the range of 315-1000 Hz and 2000-4000 Hz. However, compared the predictions and the measured results, the economic benefits of the nearly-enclosed barriers were not satisfactory since the only significant gains compared with the double-straight barriers could not be obtained due to the poor sound isolation properties of the top PC sheets. Moreover, the coincidence effect of the employed PMMA sheets also degraded the barrier performance in the range of 1000-2500 Hz. In conclusion, it is definitely important to consider the sound insulation capability of employed transparent panels when developing nearly-enclosed barriers in the engineering projects.

Although the 2.5-D BEM predictions of the acoustic performance were not the same as those measured results, a discussion of predictions for different receiver positions and different configurations of vehicles was performed yet. For the cases of vehicles situated near receiver positions, the high attenuations above 15 dB are focused in the range of 315-5000 Hz. However, for the cases of vehicles situated far from receiver positions, the attenuations from 315 to 5000 Hz are around 5-15 dB. Compared with double-straight barriers, the attenuations for nearly-enclosed barriers are significantly higher for the cases of vehicles situated near receiver positions, while for the cases of vehicles situated far from receiver positions, there is no significant gain in the range of 315-5000 Hz but a considerable benefit can be obtained at frequencies below 100 Hz. In addition, a single rating analysis was also performed to assess the 2.5-D BEM predicted results. Based on the single rating analysis, we can conclude that compared with double-straight barriers, nearly-enclosed barriers have a better effect (1-2 dB) on reducing the level at receiver positions in the near field (source to receiver distance: 7.5 m), almost no effect in the medium field (source to receiver distance: 22 m) and an even worse effect ((-1)-(-2) dB) in the far field (source to receiver distance: 55 m).

7 Parametric investigations of absorptive nearly-enclosed barriers

7.1 Introduction

In the last chapter, advantages and disadvantages of the absorptive nearly-enclosed prototype have been found and studied thoroughly. To optimize the acoustic performance of absorptive nearly-enclosed barriers and increase its economic benefits, a parametric investigation will be presented in this chapter. First of all, there is an assumption here, that needs to be made explicit. That assumption is that all the panels employed in the optimization of the nearly-enclosed barriers have sufficient sound insulation capacities: the transmission loss(TL) of the given panel at each 1/3 octave band is higher than the insertion loss of the barriers by at least 10 dB. This chapter will introduce the optimization of the acoustic performance of nearly-enclosed barriers on the premise of this assumption. All the models are based on the absorptive nearly-enclosed barrier model on the viaduct presented in the last chapter.

To clearly understand the effects of any changes of the BEM model introduced in this chapter, an excess attenuation for each 1/3 octave band is introduced and defined as the ratio of the quadratic sum of the sound pressure in the field of the modified model and in the field of the reference model, given by,

$$\mathrm{Ex\_att}\left(f_{\mathrm{oct}}\right)=10\log_{10}\left(\frac{\sum_{i}^{N}\left|p_{\mathrm{modi},1}\left(f_i\right)\right|^2+\left|p_{\mathrm{modi},2}\left(f_i\right)\right|^2}{\sum_{i}^{N}\left|p_{\mathrm{ref},1}\left(f_i\right)\right|^2+\left|p_{\mathrm{ref},2}\left(f_i\right)\right|^2}\right) \tag{7.1}$$

where $p_{\mathrm{modi,i}}$ and $p_{\mathrm{ref,i}}$ denote the sound pressure at the given receiver radiated from the ith source of the modified model and that of the reference model, respectively.

The first parameter investigated is the width of the opening on the top, to balance the acoustic resonance effect and the acoustic performance of the nearly-enclosed barriers. Secondly, to investigate the effect of different sound absorptive treatments to the acoustic performance, the investigation will be discussed in Section 7.3. Section 7.4 will present a comprehensive discussion on the parametric investigation of the nearly-enclosed barriers, and give a brief conclusion of this chapter.

7.2 The width of the opening on the top

The width of the opening in the model presented in Chapter 6 is 2 meters. To investigate its effect on the acoustic performance, the openings on the top with widths of 2 m, 4 m, 6 m and 8 m were chosen. Figure 7.1(a)-(d) shows these models with different opening widths. The model of the double-straight barrier was chosen as the reference model, shown in Figure 7.1(e). All the calculated models were almost the same, only with different opening widths. In Figure 7.1, the green curves denote the open-celled aluminium foam panels using the microstructural model proposed by H. LI[231] and improved by J. Zhang[233], whereas the blue curves denote the glass-wool panels using the Delany-Bazley model[123]. Two incoherent line sources were located at the places where wheels and rails interacted. While receiver positions were determined the same as those presented in the in-situ measurements: 7.5 m, 22 m, 55 m horizontally away from the centre of the nearest track; -1.5 m, 0 m, 1.5 m vertically above the height of the source, and 1.2 m above the ground. All the names of the receiver positions were the same as those presented in the in-situ measurements, shown in Figure 3.1. Figure 7.2-7.6 show 1/3 octave spectra of the excess attenuation calculated by using the 2.5-D BEM modelling and Equation (7.1).

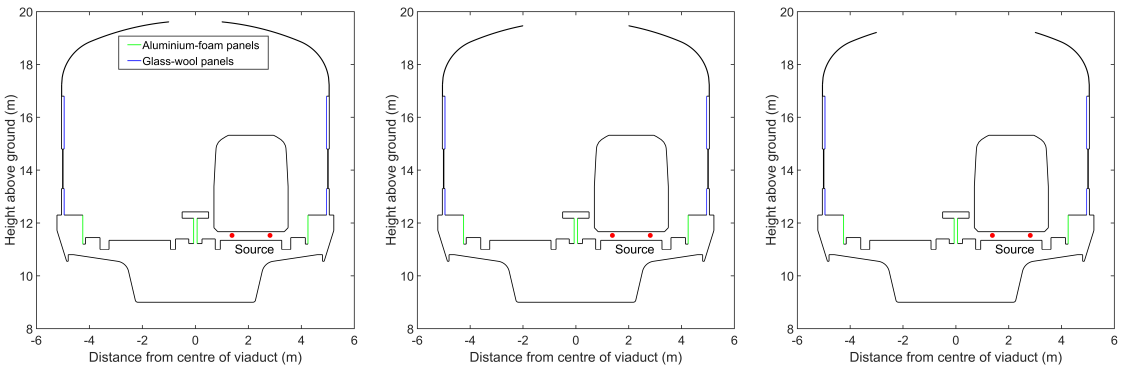

(a) opening width: 2 m (b) opening width: 4 m (c) opening width: 6 m

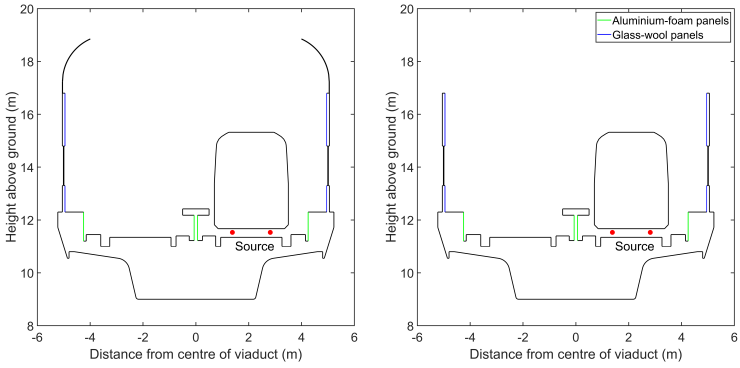

(d) opening width: 8 m (e) The double-straight barrier(ref. model)

Fig 7.1.: Cross-sections of models in the investigation of opening widths

In Figure 7.2, all the curves represent the excess attenuations at the receiver positions 7.5 m horizontally away from the centre of the nearest track. The purple curves represent the

excess attenuations for the model of the double straight barriers. The values are all equal to zero since the reference model was also the double-straight barriers. With the additions of

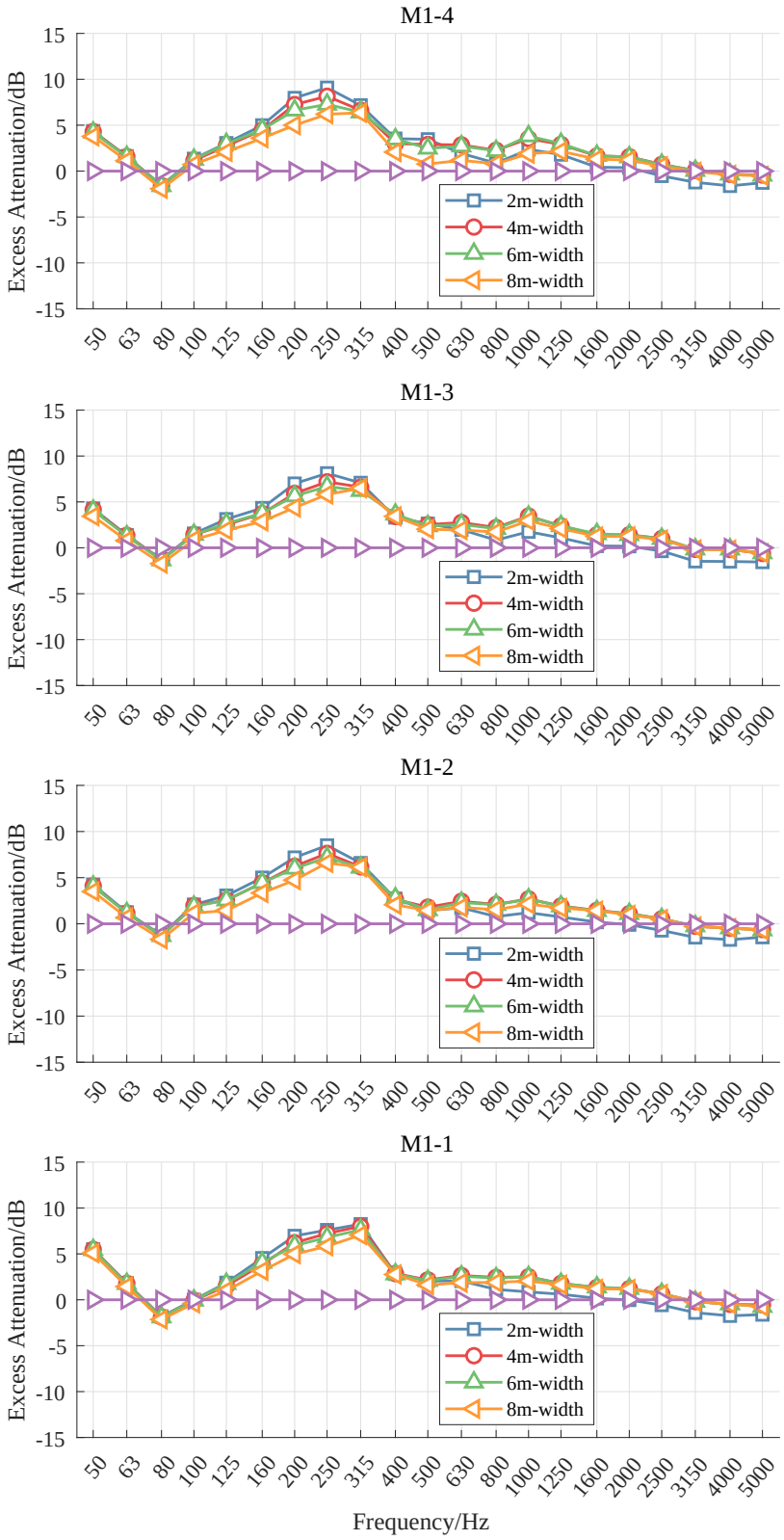

Fig 7.2.: 1/3 octave spectra of excess attenuations at receiver positions 7.5 m horizontally away from the centre of the nearest track, in the investigation of opening widths

two arched parts, the excess attenuations for the nearly-enclosed barriers are significantly higher than 5 dB at the 1/3 octave bands of 200 Hz, 250 Hz and 315 Hz. Besides, the excess attenuations at the 1/3 octave bands of 50 Hz and 160 Hz are about 5 dB. But at the 1/3 octave band of 80 Hz, the excess attenuations are negative due to the acoustic resonance effects induced by the air cavity inside the nearly-enclosed barriers. From 400 Hz to 2000 Hz, the excess attenuations are positive but lower than 5 dB. The negative excess attenuations at the 1/3 octave bands over 2000 Hz are very small(less than 1 dB), which can be explained by the numerical calculation convergence. The mesh convergence is much more difficult with the increased sound frequency, and the computation time also becomes much longer. Since the BEM program was classic and serial, the precisions of the nearly-enclosed barrier models at the 1/3 octave bands above 2000 Hz were 1 dB(see Section 6.2.2 in Chapter 6). Hence the negative excess attenuations at the 1/3 octave bands over 2000 Hz are not due to the addition of the arched parts on the top.

With the increased width of the opening on the top, the excess attenuation decrease significantly at the 1/3 octave bands of 200 Hz-315 Hz. While at the 1/3 octave bands of 800 Hz-1250 Hz, the excess attenuation increases firstly and then decreases with the increase of the opening width. Figure 7.3 shows clearly these two different variations of the excess attenuations at the receiver position M1-4. Hence, it can be concluded that the acoustic performance of the nearly-enclosed barrier is improved with the decreased opening width for low frequencies(200-315 Hz); But for mid-frequencies(800-1250 Hz), the maximum improvement is achieved by the opening on the top with a optimized width, between 4 and 6 metres. There is no significant effect of the opening width on the acoustic performance of the nearly-enclosed barrier at high frequencies at the receiver column of M1-.

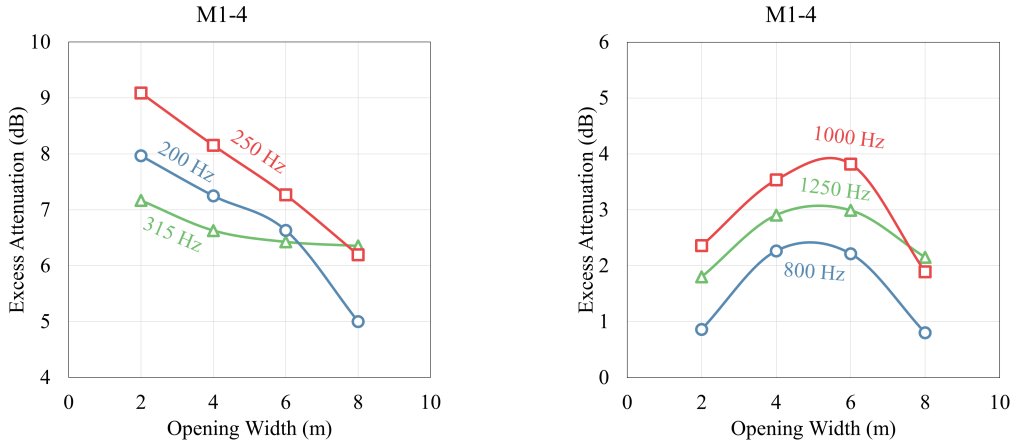

(a) 200-315 Hz (b) 800-1250 Hz

Fig 7.3.: Different variations of the excess attenuations with the increased opening widths

Figure 7.4 shows the excess attenuations at receiver positions 22 m horizontally away from the centre of the nearest track. It can be seen that the excess attenuation shows

significant gains of nearly 5 dB in the range of 200-315 Hz. Unlike the variations in this range mentioned above, the excess attenuation seems to be little affected by the change of the opening width. On this column of the receiver positions, the change of the opening width affects the excess attenuation mainly at the 1/3 octave bands of 400-1000 Hz. Figure 7.5 shows parts of the variations of the excess attenuations with the increased opening widths at the receiver position M2-4 and M2-3. The opening width can be optimized again since the excess attenuation increases firstly and then decreases with the increase of the opening width. And if the opening width is too small or too large, the excess attenuation is negative. Hence for the receiver positions in this column, the opening width is better designed to be 4-6 metres.

Figure 7.6 shows the excess attenuations at receiver positions 55 m horizontally away from the centre of the nearest track. Compared with the results for the previous two receiver columns, the excess attenuations for the receiver positions in this column are relative smaller. The gains of nearly 5 dB can be found at the 1/3 octave band of 50 Hz at these four receiver positions, 200 Hz at M3-1, and 250 Hz at M3-3 and M3-1. Besides these benefits achieved by the arched parts, there are serious unpleasant effects in the range of 400-800 Hz in this column. Figure 7.7 shows the variations of the excess attenuations with the opening widths in the range of 400-800 Hz at the receiver positions in this column. It can be seen that the excess attenuations vary almost the same as those at M2-4: increasing firstly and then decreasing with the increase of the opening width. And the excess attenuation is negative whether the opening width is too large or too small. Thus, the conclusion is reached again that the opening width is better designed to be 4-6 metres in this column.

Apparently, the excess attenuation is not a linear function of the opening width at each 1/3 octave band at each receiver position. And by the investigation of the opening width effect on the nearly-enclosed barrier performance, it can be found that the 2-metre-wide opening is not the best design, especially for the receiver positions far away from the source. Hence, it is necessary to design the optimized width of the opening, which depends on the actual situation of the urban rail transit system and the highly protected area.

7.3 The absorptive treatments

Besides the design of the opening, the absorptive treatments on the inner surface of the absorptive nearly-enclosed barrier can be also investigated, in order to improve the acoustic performance of the barrier. Inspired by the discussion on the absorptive treatments in Chapter 1, the ideal absorptive treatments can be divided into two groups: perfect absorptive surfaces where the characteristic impedance matches the product of the air density and the sound speed in air, and soft surfaces where the pressure equals to zero. Although these ideal absorptive treatments cannot be obtained in existing markets, to investigate their effects can

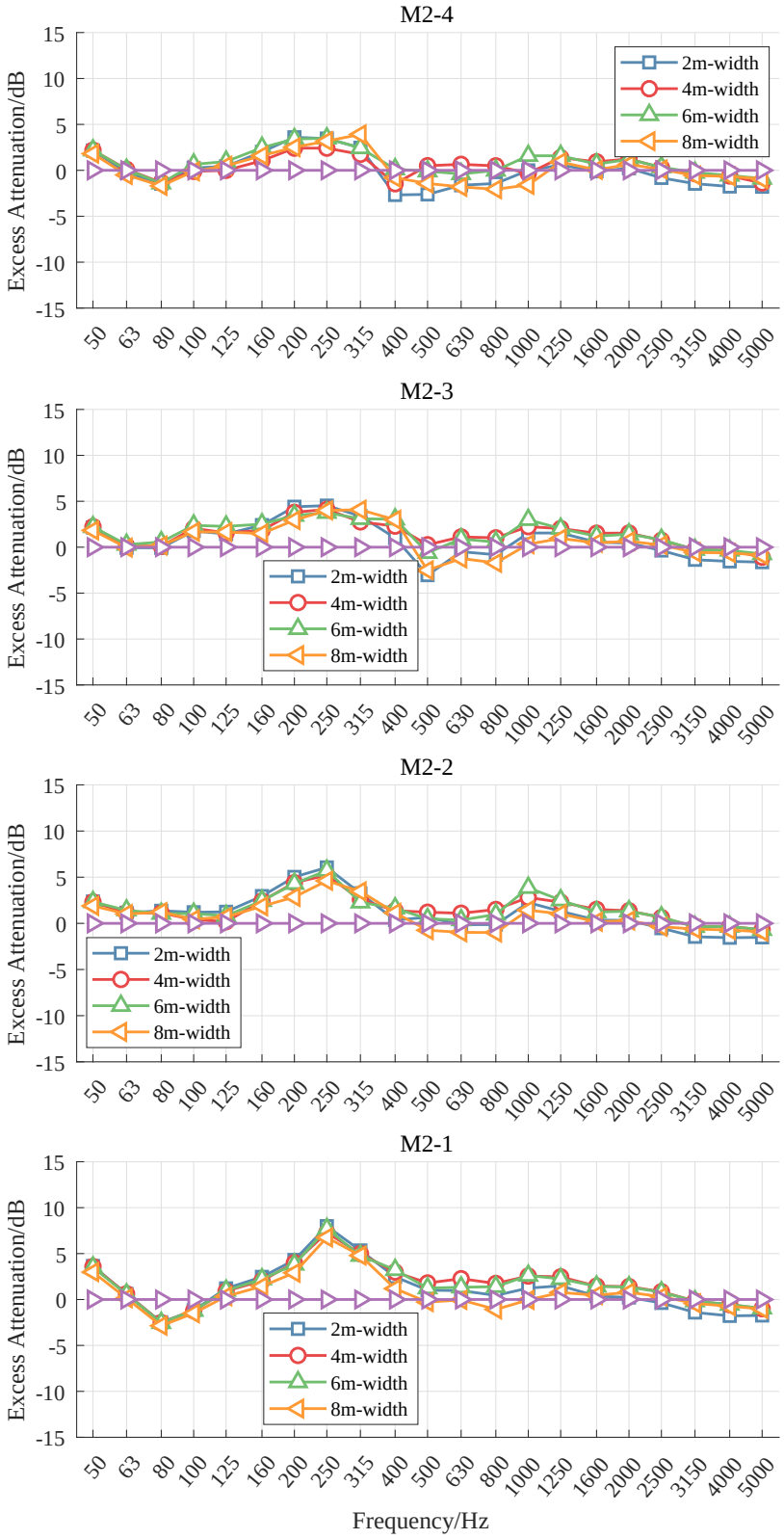

Fig 7.4.: 1/3 octave spectra of excess attenuations at receiver positions 22 m horizontally away from the centre of the nearest track, in the investigation of opening widths

become a guide to seek a suitable absorptive treatment for the improvement on the acoustic

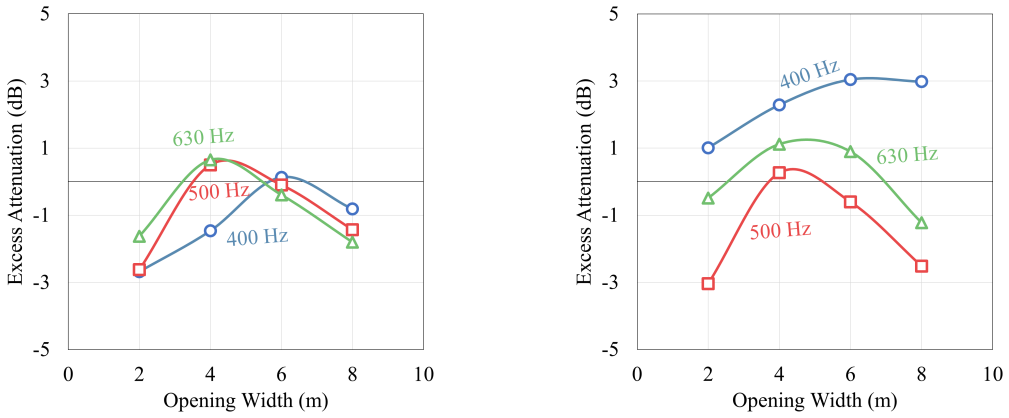

(a) M2-4 (b) M2-3

Fig 7.5.: Different variations of the excess attenuations with the increased opening widths in the range of 400-630 Hz in the column M2-

performance of the nearly-enclosed barrier. Hence, the investigation of these two kinds of absorptive treatments will be discussed separately.

7.3.1 Perfect absorptive surfaces

The absorptive nearly-enclosed barrier mentioned previously in Chapter 6 was chosen as the reference model in this section. There are two kinds of sound absorption panels in the reference model. Hence the perfect absorptive surface, with a characteristic impedance matching the impedance of air, was used as the alternative to each kind of panels in the 2.5-D BEM models. Figure 7.8 shows the cross sections of these two models with perfect absorptive surfaces and the reference model. Two incoherent line sources were located at the places where wheels and rails interacted. And the receiver positions were unchanged, the same as those presented in Section 7.2. Figure 7.9-7.11 show 1/3 octave spectra of the excess attenuation for these three models calculated by using the 2.5-D BEM modelling and Equation (7.1). The black curves presented in Figure 7.9-7.11 denote the excess attenuations for the reference model, which definitely equal to zero at each 1/3 octave band. The green curves and the blue curves denote the excess attenuations for the models shown in Figure 7.8(a) and Figure 7.8(b), respectively. For being well explained and easy to understand, the model shown in Figure 7.8(a) is named "AlZ1" whereas the model shown in Figure 7.8(b) is named "GWZ1".

In Figure 7.9, all the curves represent the excess attenuations at the receiver positions 7.5 horizontally away from the centre of the nearest track. It can be seen clearly that in the range of 50-160 Hz, the excess attenuations for two examined models are both extremely higher than those at mid- and high frequencies. The excess attenuations for the "GWZ1" model are even over 15 dB in the range of 50-100 Hz. While from 50 Hz to 100 Hz the excess attenuations for the "AlZ1" model are over 10 dB. Therefore, it is indicated that

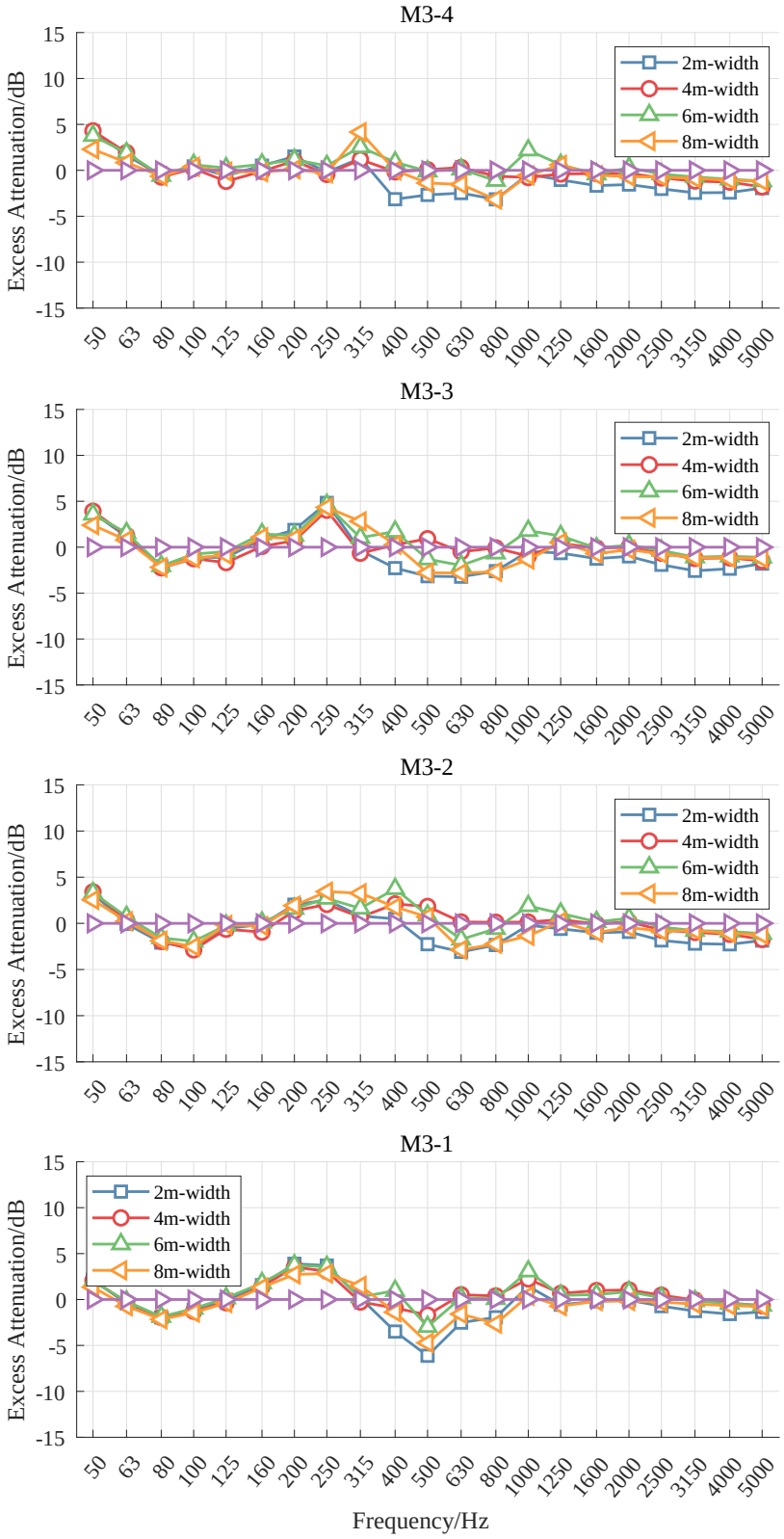

Fig 7.6.: 1/3 octave spectra of excess attenuations at receiver positions 55 m horizontally away from the centre of the nearest track, in the investigation of opening widths

the improvement of the absorptive materials at the position of the glass-wool panels is more effective on the barrier performance at low frequencies below 100 Hz(including 100

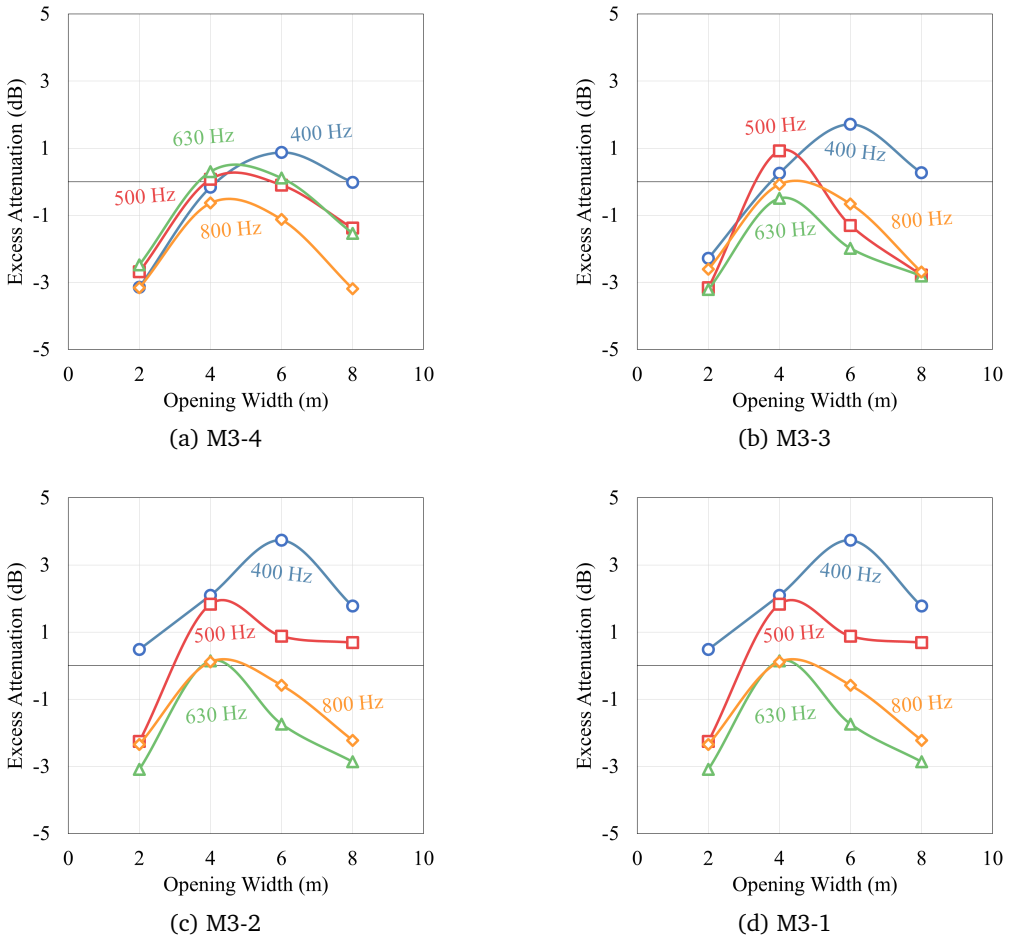

Fig 7.7.: Different variations of the excess attenuations with the increased opening widths in the range of 400-800 Hz in the column M3-

Hz). Then, at the 1/3 octave bands of 125 Hz and 160 Hz, the excess attenuations for two examined models are both at the same level, nearly 10 dB. In the range of 200-5000 Hz, the excess attenuations for the "GWZ1" model are almost zero, which means the perfect absorptive surfaces are of little use at the position of the glass-wool panels in the frequency range above 200 Hz. However, with the substitution of Aluminium-foam panels with the perfect absorptive surfaces, there are about 2-3 dB of the excess attenuations at high frequencies(1000-5000 Hz).

Figure 7.10 shows the excess attenuations at receiver positions 22 m horizontally away from the centre of the nearest track. There is a similar pattern to those for the receiver positions 7.5 m horizontally away from the source, with high excess attenuations below 200 Hz. But the differences of the excess attenuations between the "AlZ1" model and the "GWZ1" model are relative smaller than those for the receivers in the column M1-. Again, at the frequencies over 200 Hz, the excess attenuations for the "GWZ1" model are almost zero. However, the excess attenuations for the "AlZ1" model are significantly higher than zero in the range of 200-5000 Hz. At the 1/3 octave band of 500 Hz, the values of the excess attenuations for

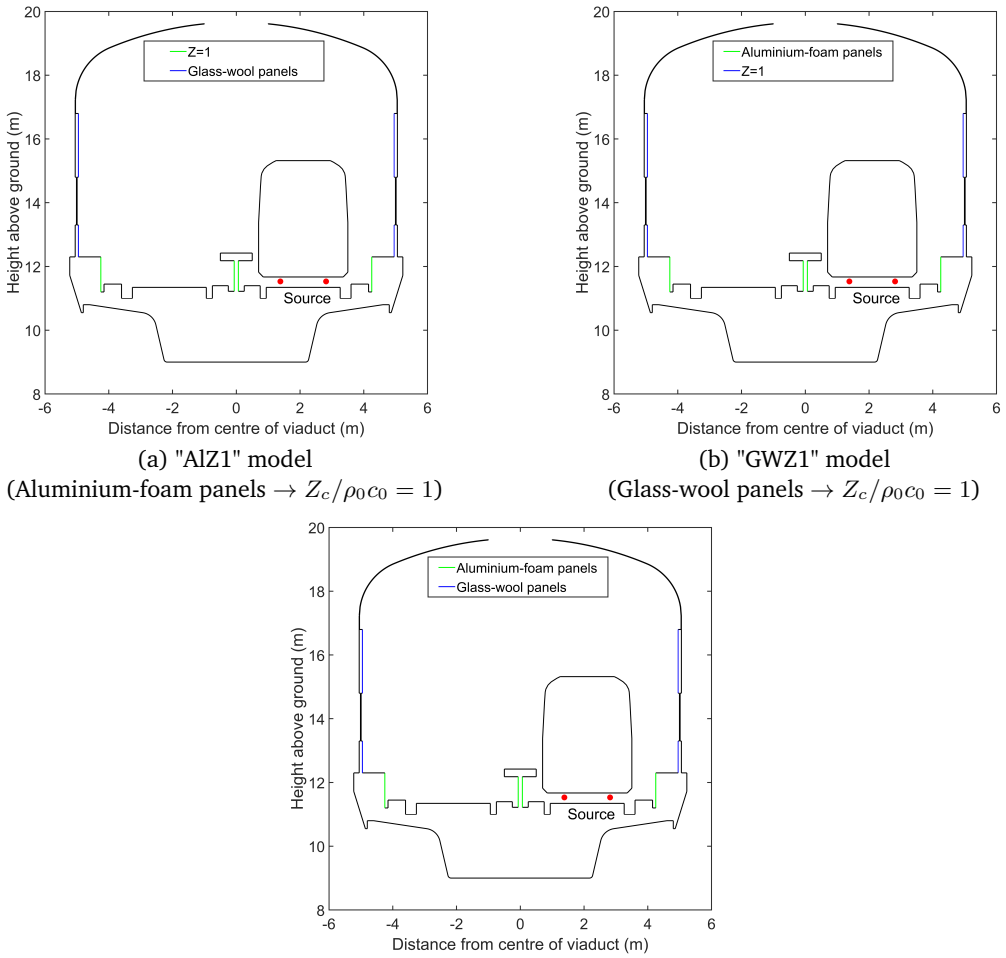

(a) "AlZ1" model
(Aluminium-foam panels $\rightarrow Z_c/\rho_0 c_0 = 1$)

(b) "GWZ1" model
(Glass-wool panels $\rightarrow Z_c/\rho_0 c_0 = 1$)

(c) Reference model

Fig 7.8.: Cross-sections of models in the investigation of perfect absorptive surfaces

the "AlZ1" model are even 5.5 dB, 5.2 dB, 2.5 dB and 2.3dB at the receiver position M2-4, M2-3, M2-2 and M2-1, respectively. There are again only small excess attenuations for the "GWZ1" model at high frequencies(1000-5000 Hz).

Figure 7.11 shows the excess attenuations at receiver positions 55 m horizontally away from the centre of the nearest track. Unlike the receiver positions in the previous two columns, the differences in excess attenuation between the "AlZ1" model and the "GWZ1" model are very little between 50 Hz and 200 Hz. The values of the excess attenuations at these low frequencies are around 10 dB. Then at the frequencies over 200 Hz, again, for the "GWZ1" model the excess attenuations approximate to be zero. While for the "AlZ1" model the excess attenuations are much higher than those at the receivers in the previous two columns, with local maximum values of about 5 dB at 500 Hz.

The following general conclusions can be deduced from the above: first, reasonable excess attenuations can be achieved at low frequencies below 200 Hz for both two models with the perfect absorptive surfaces. The values of these reasonable excess attenuation are over 10 dB

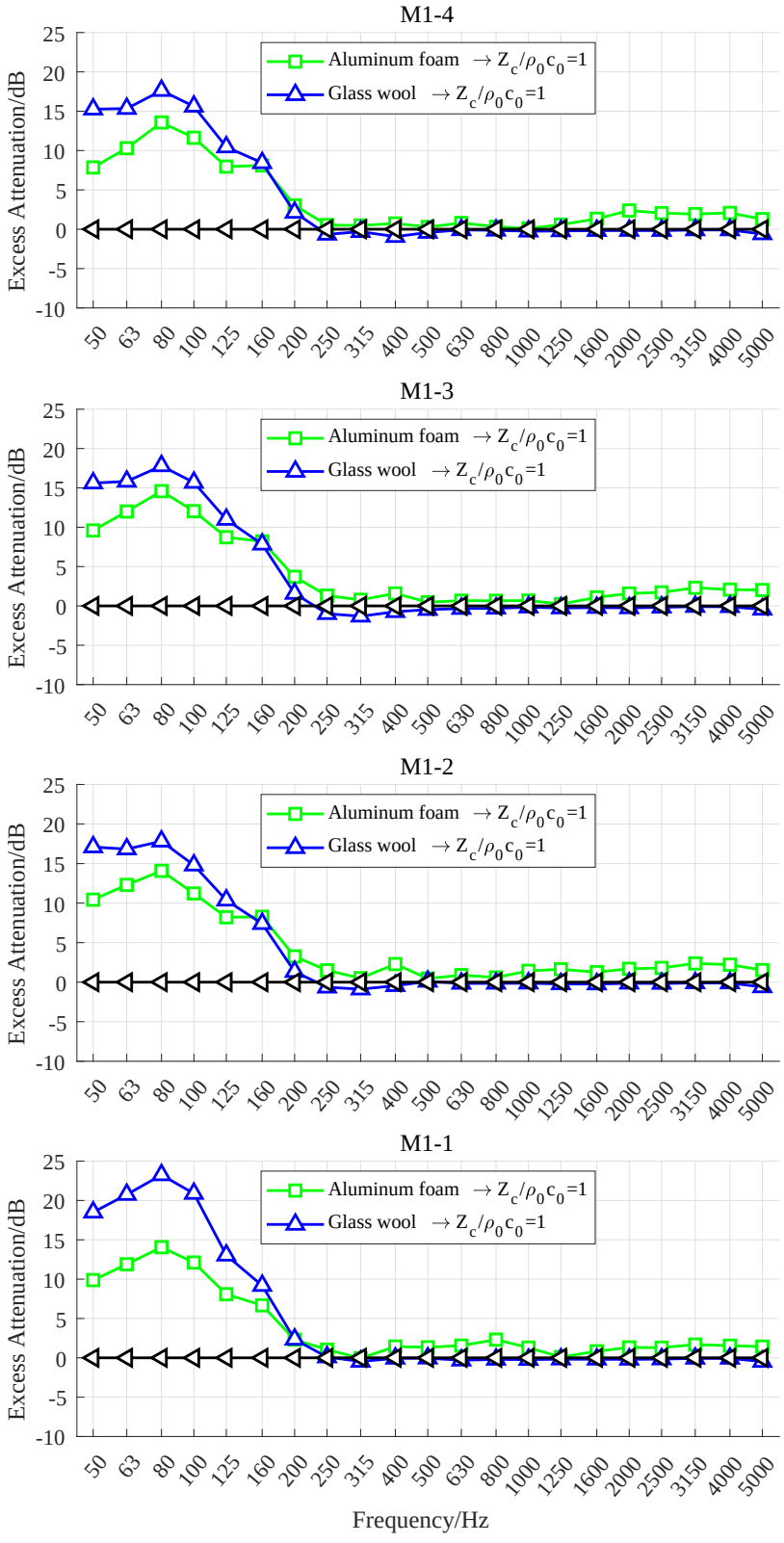

Fig 7.9.: 1/3 octave spectra of excess attenuations at receiver positions 7.5 m horizontally away from the centre of the nearest track, in the investigation of perfect absorptive surfaces

for each examined receiver position. With the increased horizontal distance from the source, the excess attenuation for the "AlZ1" model decreases a lot whereas that for the "GWZ1"

model decreases little; secondly, in the range of 400-630 Hz, the barrier performance can be significantly enhanced at the receiver positions in the last two columns, by the application of the perfect absorptive surfaces in the "AlZ1" model. And the enhancement increases a lot with the increasing horizontal distance from the source. The local maximum value is over 5 dB; thirdly, there would be a little gain of 2-3 dB to be achieved at frequencies over 2000 Hz in the "AlZ1" model. And the gain would not increase or decrease with the increased horizontal distance away from the source; fourthly, with the substitution of the perfect absorptive surfaces for the glass-wool panels, there would be no significant gain to be achieved at mid- and high frequencies from 250 Hz to 5000 Hz in the "GWZ1" model.

7.3.2 Soft surfaces

The absorptive nearly-enclosed barrier mentioned previously in Chapter 6 was chosen as the reference model in this section. There are two kinds of sound absorption panels in the reference model. Hence the soft surface, where the sound pressure equals to zero, was used as the alternative to each kind of panels in the 2.5-D BEM models. Figure 7.12 shows the cross sections of these two models with the soft surfaces and the reference model. Two incoherent line sources were located at the places where wheels and rails interacted. And the receiver positions were unchanged, the same as those presented in Section 7.2. Figure 7.13-7.15 show 1/3 octave spectra of the excess attenuation for these three models calculated by using the 2.5-D BEM modelling and Equation (7.1). The black curves presented in Figure 7.13-7.15 denote the excess attenuations for the reference model, which definitely equal to zero at each 1/3 octave band. The green curves and the blue curves denote the excess attenuations for the models shown in Figure 7.12(a) and Figure 7.12(b), respectively. For being well explained and easy to understand, the model shown in Figure 7.12(a) is named "Alp0" whereas the model shown in Figure 7.12(b) is named "GWp0".

In Figure 7.13, all the curves represent the excess attenuations at the receiver positions 7.5 horizontally away from the centre of the nearest track. There is a consistent pattern in the results obtained to those for the model with the perfect absorptive surfaces, with high values of the excess attenuations at low frequencies below 100 Hz(including 100 Hz). Unlike the cases with the perfect absorptive surfaces, in these cases the excess attenuations at low frequencies for the "Alp0" model are a little higher than those for the "GWp0" model at the receiver position M1-4, M1-3 and M1-2. At the 1/3 octave band of 125 Hz and 160 Hz, the excess attenuations for the "Alp0" model are about 5 dB, whereas those for the "GWp0" model are approximate zero. However, negative values of excess attenuations for the "GWp0" model can be seen from 200 Hz to 1000 Hz. The magnitude of the negative excess attenuation increases first and then decreases with the increased frequency, with a maximum of about -5 dB. For the "Alp0" model the negative values can be also seen but

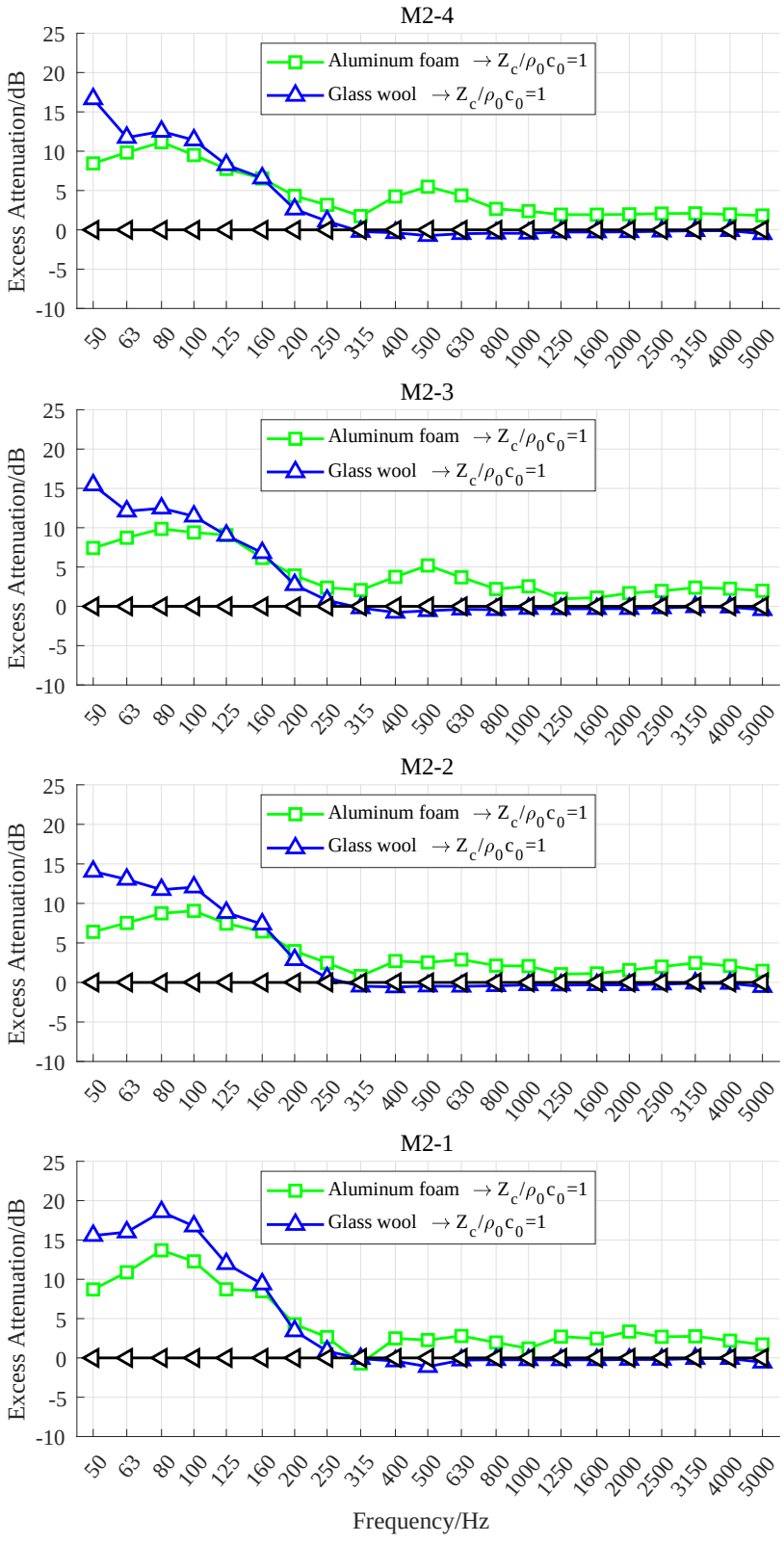

Fig 7.10.: 1/3 octave spectra of excess attenuations at receiver positions 22 m horizontally away from the centre of the nearest track, in the investigation of perfect absorptive surfaces

not significant in this frequency range. Then at high frequencies over 1000 Hz, the excess attenuations for both examined models are small.

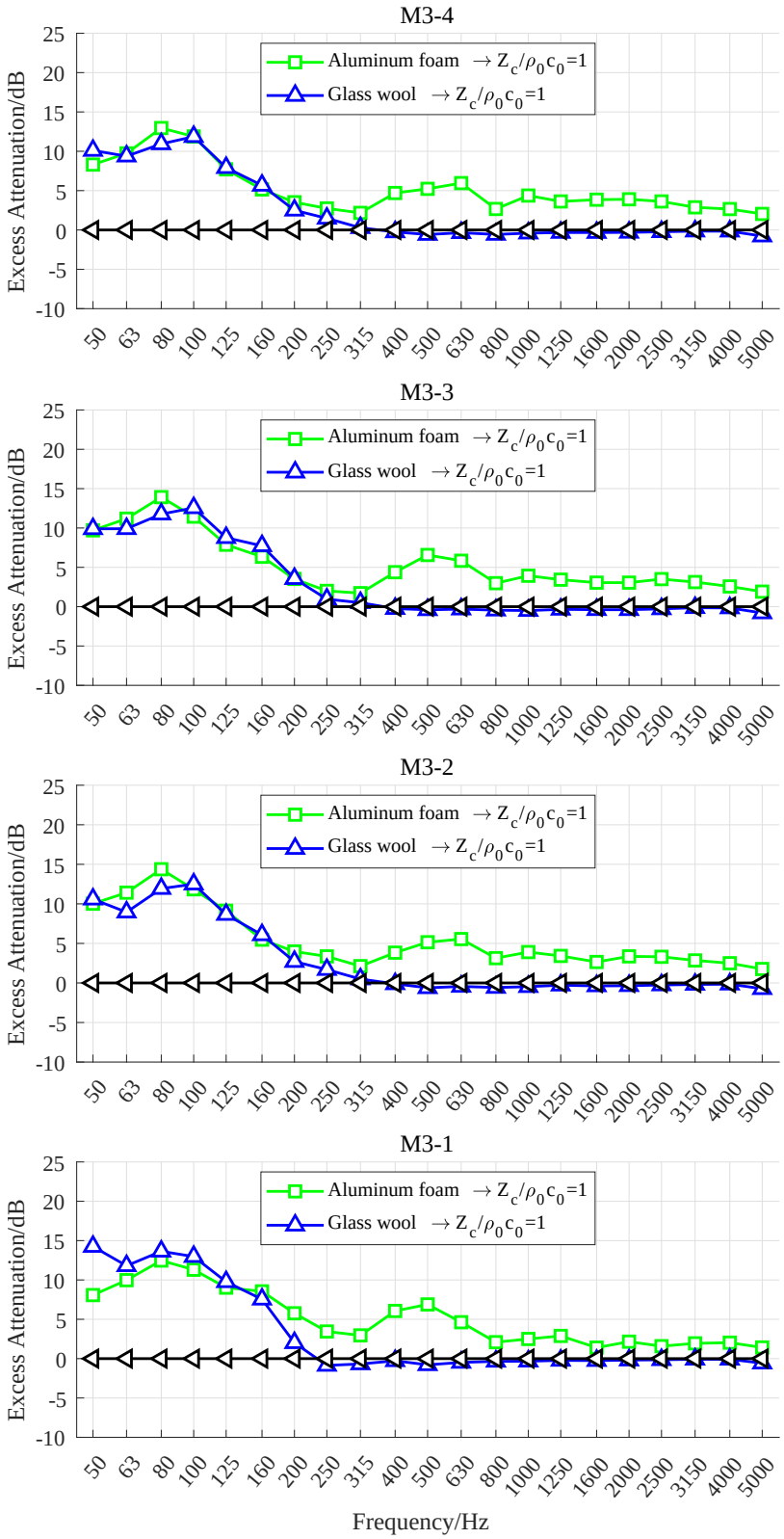

Fig 7.11.: 1/3 octave spectra of excess attenuations at receiver positions 55 m horizontally away from the centre of the nearest track, in the investigation of perfect absorptive surfaces

Figure 7.14 shows the excess attenuations at receiver positions 22 m horizontally away from the centre of the nearest track. Again, in the range of 50-100 Hz, the excess attenuations

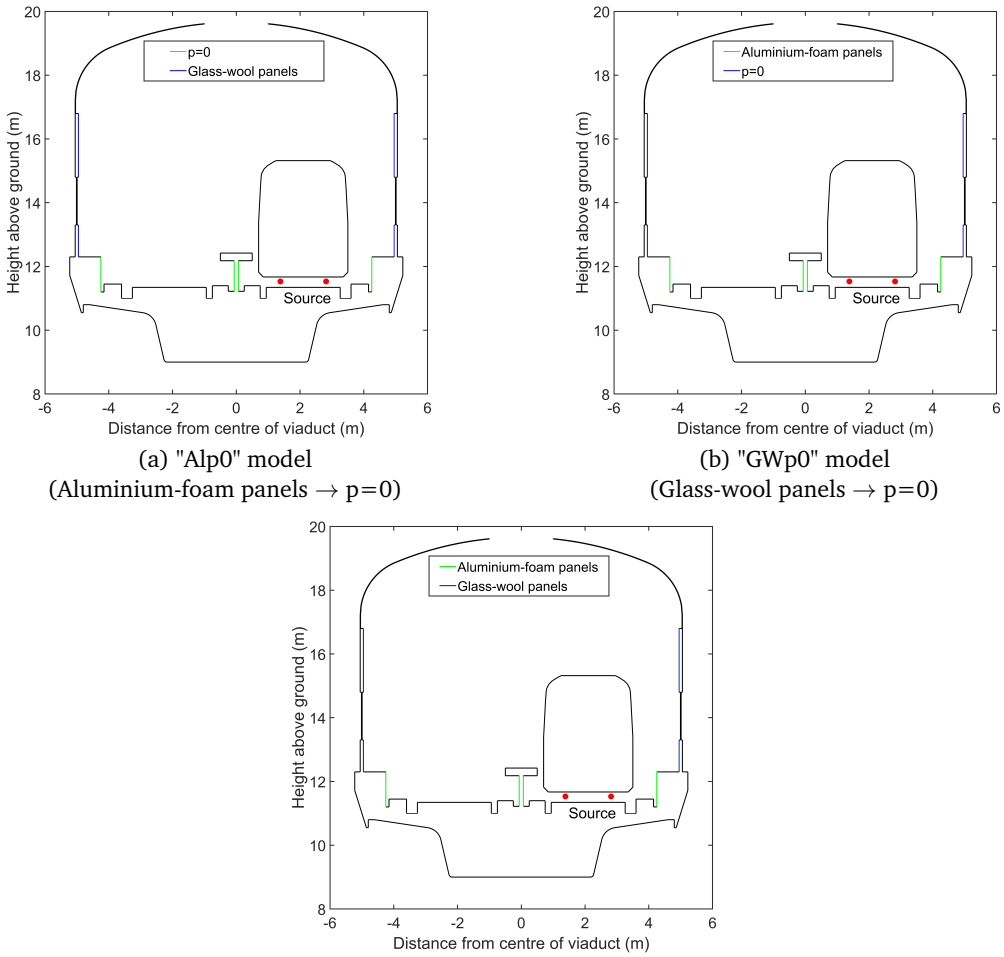

(a) "Alp0" model
(Aluminium-foam panels → p=0)

(b) "GWp0" model
(Glass-wool panels → p=0)

(c) Reference model

Fig 7.12.: Cross-sections of models in the investigation of soft surfaces

are over 5 dB for both the "Alp0" model and the "GWp0" model, but their differences are not significant. And at the 1/3 octave band of 125 Hz and 160 Hz, the excess attenuations for the "Alp0" model are about 5 dB, whereas those for the "GWp0" model are approximate zero. In the range of 200-1000 Hz, the excess attenuations for the "GWp0" model are negative again, and decreases more significantly(i.e. becomes more negative) compared with those at the receiver positions in the previous column. For example, the maximum magnitude of the negative excess attenuation at the receiver M2-4 is -8.4 dB at 250 Hz. The negative excess attenuation for the "GWp0" model at each receiver position decreases to the maximum firstly from 200 Hz to 250 Hz, and then increase to almost zero at 5000 Hz. While for the "Alp0" model, the excess attenuations in this frequency range are not significant.

Figure 7.15 shows the excess attenuations at receiver positions 55 m horizontally away from the centre of the nearest track. There is again a consistent pattern in the results obtained to those at the receivers in the previous two columns that the excess attenuations at low frequencies below 100 Hz are around 10 dB. And at the 1/3 octave band above 125 Hz(including 125 Hz), the variations of the excess attenuation with sound frequency

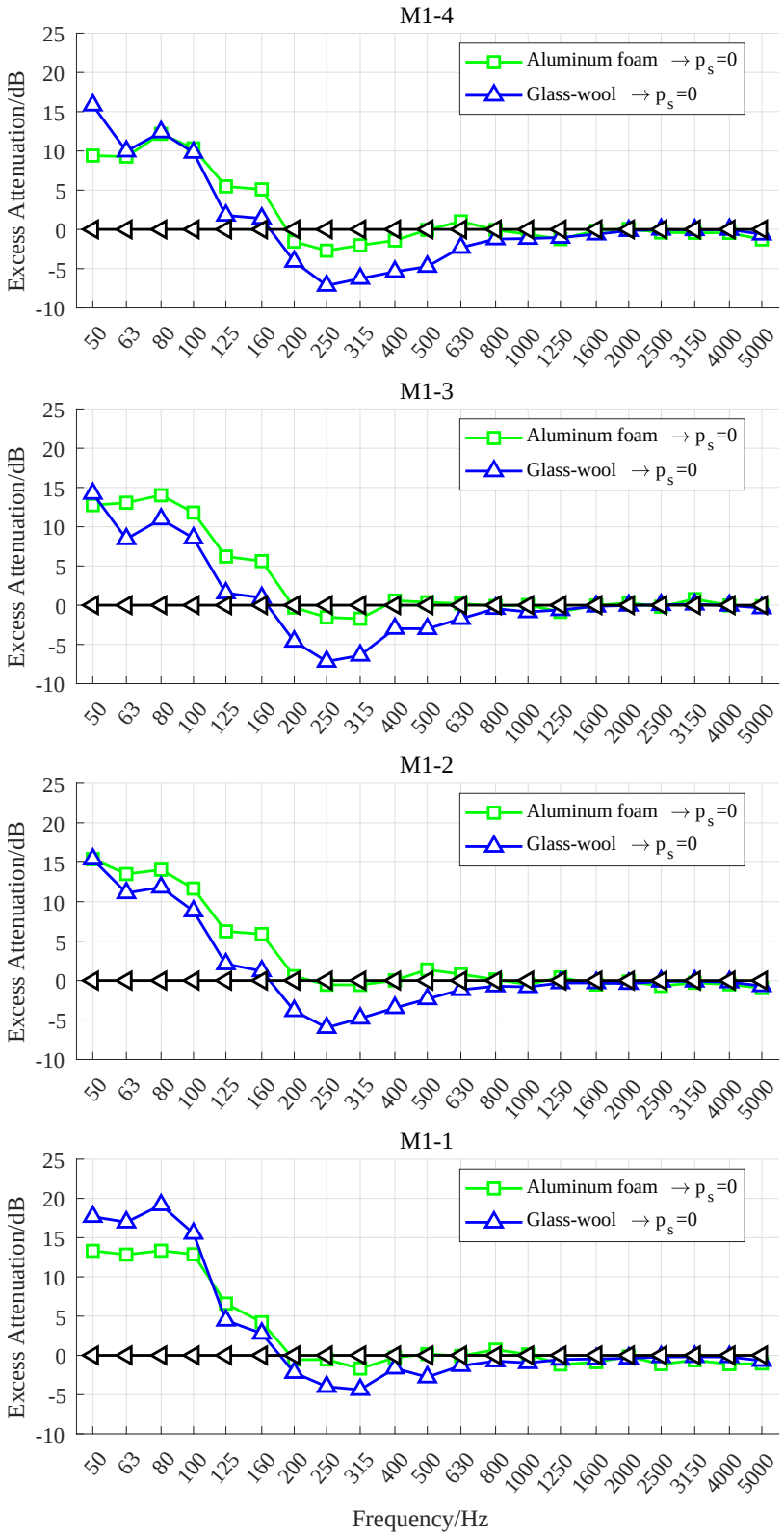

Fig 7.13.: 1/3 octave spectra of excess attenuations at receiver positions 7.5 m horizontally away from the centre of the nearest track, in the investigation of soft surfaces

for both the "Alp0" model and the "GWp0" model are similar to those found by the results obtained at the receivers in the previous two columns.

The following general conclusions can be deduced from the above: first, reasonable excess attenuation can be achieved at low frequencies below 100 Hz for both two models with the soft surfaces. The values of these reasonable excess attenuation are over 10 dB for the receivers in column M1-, and over 5 dB for other receivers; secondly, in the range of 125-160 Hz, there is no significant gain to be achieved from attempting to employ soft surfaces on the positions of glass-wool panels. While by the application of the soft surfaces in the "Alp0" model, the gains are about 5 dB; thirdly, at mid- and high frequencies over 200 Hz, the barrier performance can be severely reduced at each receiver position by the application of the soft surfaces in the "GWp0" model. And the reduction increases a lot with the increasing horizontal distance from the source. The maximum value of the negative excess attenuations is nearly -10 dB; fourthly, with the substitution of the soft surfaces for the Aluminium-foam panels, there would be no significant gain to be achieved at mid- and high frequencies from 200 Hz to 5000 Hz in the "Alp0" model.

7.4 Discussion and conclusions

This chapter is aimed at optimizing the acoustic performance of the absorptive nearly-enclosed barrier by changing the width of the opening on the top, and comparing two different absorptive treatments on the positions of the original sound absorption panels. By using 2.5-D BEM modelling, it can be found that compared with the model of double-straight barriers, the excess attenuation of the nearly-enclosed barrier would not monotonically increasing with the decreased width of the opening on the top, but have an optimum value with an optimal opening width at some 1/3 octave bands, especially in the range of 400-1000 Hz. In other low and high frequency ranges, the excess attenuations of the nearly-enclosed barrier are very slightly affected by changing the opening width on the top. The excess attenuations of the nearly-enclosed barrier with opening widths of 2 m, 4 m, 6 m and 8 m were compared. From the compared results it can be found the best design of the opening width is 4 meters or 6 meters.

The perfect absorptive surfaces where the characteristic impedance matches the air acoustic impedance were used to substitute for two kinds of the original absorption panels. It can be found that there were reasonable excess attenuations at low frequencies below 200 Hz in both the "AlZ1" model and the "GWZ1" model, and the values were over 10 dB for each examined receiver position. These extremely high excess attenuations at low frequencies are reasonable due to a relative lower level of the absorptive capacities of the original absorption panels and the low frequency diffract better than high frequencies by the top of a barrier on one hand. And on the other hand, with the help of the perfect absorptive surfaces, the huge amount of sound energy induced by the resonance effects of the air-cavity inside the nearly-enclosed barriers can be effectively absorbed. Then in the range of 250-5000 Hz, the excess attenuations for the "GWZ1" model are almost zero. As calculated in Chapter 6, the

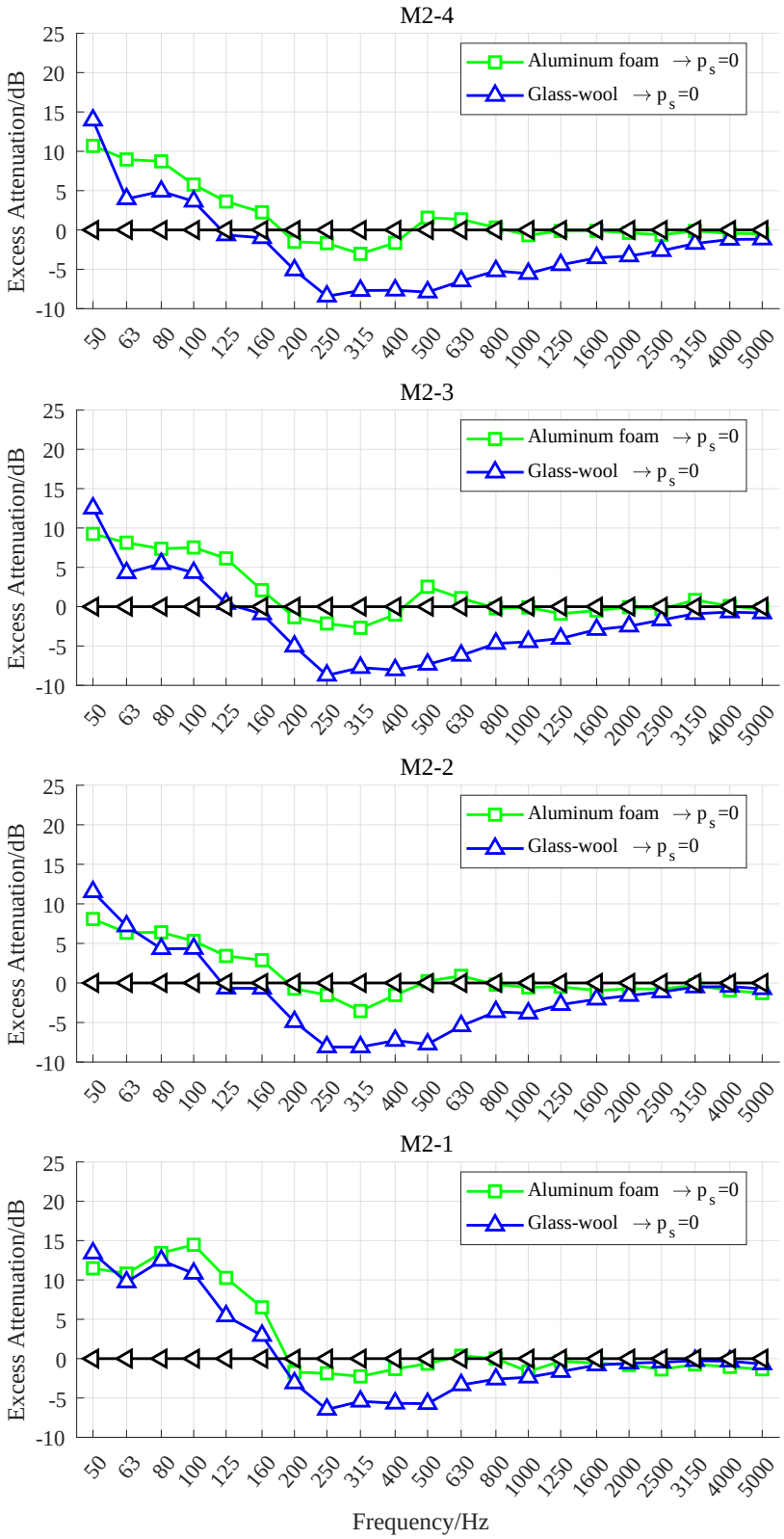

Fig 7.14.: 1/3 octave spectra of excess attenuations at receiver positions 22 m horizontally away from the centre of the nearest track, in the investigation of soft surfaces

absorption coefficients of the glass-wool panels are less than 0.9 in the range of 250-800 Hz. Therefore, to enhance the absorptive capabilities of the glass-wool panels in this range

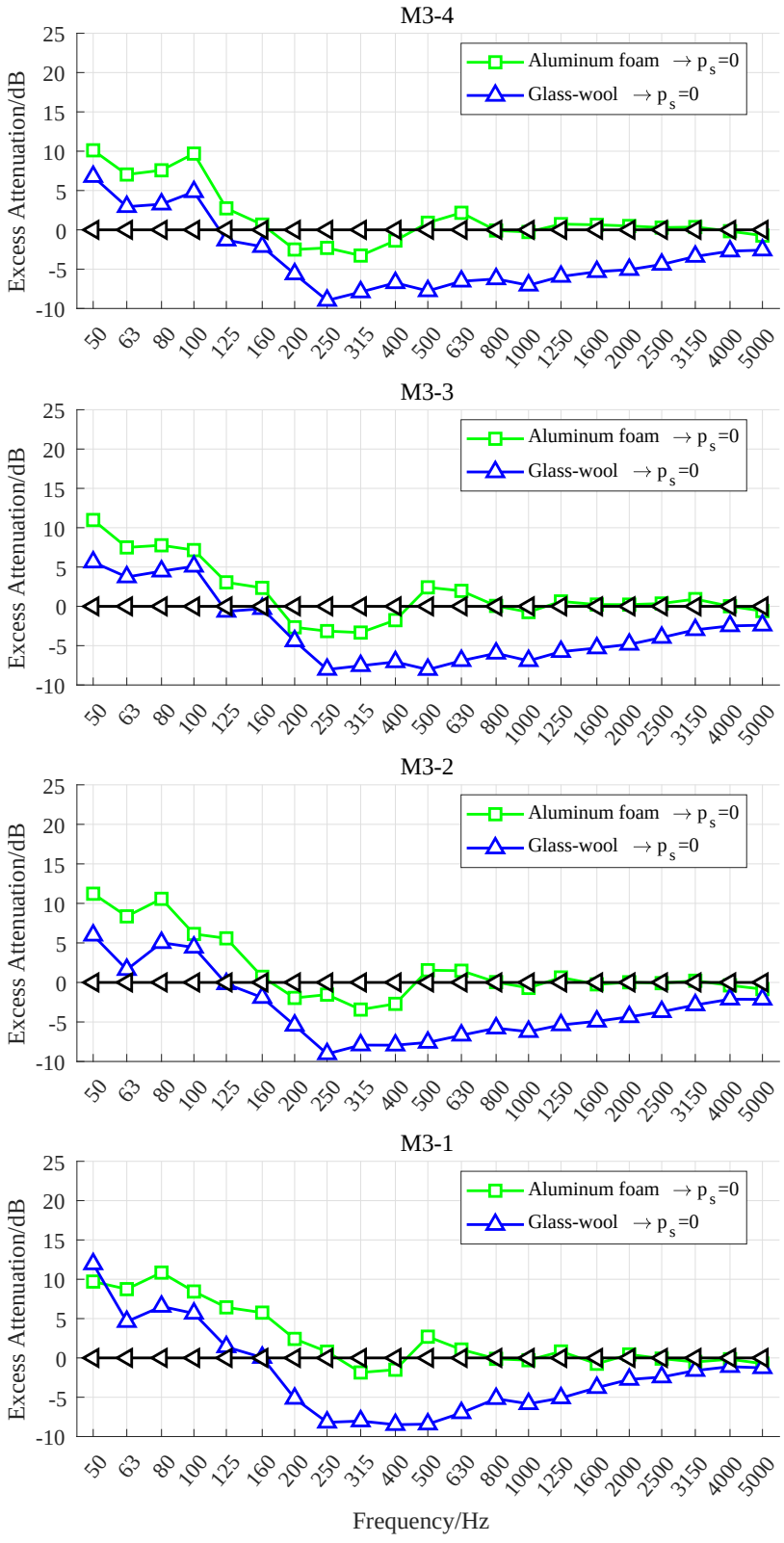

Fig 7.15.: 1/3 octave spectra of excess attenuations at receiver positions 55 m horizontally away from the centre of the nearest track, in the investigation of soft surfaces

would not improve effectively the acoustic performance of the nearly-enclosed barrier. A possible explanation for these results is the positions of the glass-wool panels far away from

the sources. When the Aluminium-foam panels, which were located close to the sources, were substituted by the perfect absorptive surfaces, significant excess attenuations can be achieved in the range of 250-5000 Hz, and the value increases a lot with the increased horizontal distance away from the source. Thus, to enhance the absorptive capabilities of the absorptive treatments at low frequencies is of great importance to the acoustic performance of the absorptive nearly-enclosed barriers, and for reducing the mid- and high frequency sound, it is better to enhance the absorptive capabilities of the absorptive treatments which locate much closer to the sources.

The soft surfaces where the pressures equal to zero were used to substitute for two kinds of the original absorption panels. It can be found that there were reasonable excess attenuations at low frequencies below 100 Hz in both the "Alp0" model and the "GWp0" model, and the values were over 5 dB for each examined receiver position. Then in the range of 250-5000 Hz, the excess attenuations for the "Alp0" model are almost zero. That means the acoustic performance of the absorptive nearly-enclosed barrier would not be affected by applying the soft surfaces close to the sources. And from the results for the "GWp0" model, it can be seen that the excess attenuations are negative in the range of 200-5000 Hz, and the value decreases(i.e. becomes more negative) significantly with the increased horizontal distance away from the sources. Thus, the substitution of the soft surfaces for the glass-wool panels would reduce the acoustic performance of the absorptive nearly-enclosed barrier, which should be not considered into the optimization and the design of the absorptive nearly-enclosed barrier in the future.

As concluded in Chapter 3, the urban rail transit noise was measured predominantly in the range of 315-1000 Hz and 2000-4000 Hz, of which the former covers the optimum response range of the opening width effect. Therefore, it is necessary to design the optimized width of the opening for the urban rail system, which depends on the actual situation and the highly protected area. Besides, by comparing two kinds of the absorptive treatments used in the 2.5-D BEM model of the absorptive nearly-enclosed barrier, we found the use of the perfect absorptive surfaces was better to improve the acoustic performance of the absorptive nearly-enclosed barrier. On one hand, the tremendous sound energy induced by the resonance effects can be effectively absorbed. On the other hand, for the receivers located close to the highly protected area(M3-1) in the in-situ case, it is necessary to improve the barrier performance in the predominant range(315-1000 Hz and 2000-4000 Hz) of the measured noise. And the substitution of the perfect absorptive surfaces for the Aluminium-foam panels can effectively solve this problem. So as a conclusion, to enhance the capabilities of the absorptive treatments located on the positions of th Aluminium-foam panels is the most effective way to improve the acoustic performance of the absorptive nearly-enclosed barrier.

8 Conclusion and Prospect

8.1 Conclusion

This thesis is aimed at understanding the acoustic performance of a nearly-enclosed barrier used in the urban rail transit system, and finding its optimization design specific to the urban rail transit noise:

1. Chapter 2 introduced two improved methods for measuring in-situ insertion losses of the noise barriers in urban rail transit systems. Based on the sound diffraction theory, a rearrangement of the receiver positions in the in-situ measurement was proposed. One-third octave analysis was chosen as the supplement to the underestimation of low-frequency sounds by using A-weighted indicators. To examine the improved methods, an in-situ measurement for testing the acoustic performance of a low-height noise barrier on a ground line was made. It could be concluded from the measured results that with the help of the improved arrangement method of receiver positions, the acoustic performance of a noise barrier could be obtained as comprehensively as possible in the half space behind the barrier. And combined with the one-third octave analysis, the acoustic performance could be obtained effectively in a specified frequency range. A-weighted indicators highlighted the acoustic performance of a noise barrier on the predominant frequency range of urban rail transit noise, and the additional one-third octave analysis could supplement the disadvantage of A-weighted indicators effectively in the measured results. Hence, these two improved methods would be suitably used in the formal in-situ measurements.

2. Chapter 3 introduced in-situ measurements of an absorptive nearly-enclosed noise barrier prototype on an existing line in a urban rail transit system. By using the improved arrangement of receiver positions mentioned previously in Chapter 2, twelve receiver positions were determined within the range of 55 metres away from the rail transit line on the site with the nearly-enclosed barrier and the site without the barrier. The train speed for each test was calculated through the time histories of the rail vertical vibration accelerations measured by a piezoelectric sensor when the train passed by. Since the differences between two measured sites were not only the presence or absence of the nearly-enclosed barrier but also different track structures(the track structure on the site without the barrier was a common ballastless track whereas that on the site with the barrier was a kind of floating slab track), the

effect on the rolling noise could be also investigated through the measured rail vertical vibration accelerations.

3. The measured results of the rail vertical vibration accelerations showed that the effect of the floating slab track structure on the rolling noise could be ignored. By using the dependence of the pass-by sound pressure level on the train speed, all the measured results were corrected. The speed-corrected results showed that on the site without the barrier, the viaduct had a barrier effect on the noise propagation, significantly reducing the sound pressure levels at the positions under the viaduct to a relative lower level; on the site with the nearly-enclosed barrier, the sound pressure levels for all the measured receiver positions were below the required limits of the Chinese standards, under the combined efforts of the viaduct, the floating track structures, and the nearly-enclosed barriers; The maximum of the insertion losses for all the receiver positions was 15 dB(A), and the minimum was 5 dB(A).

4. By using the one-third octave analysis, it can be concluded that the measured wheel-rail rolling noise was found predominantly in the range of 315-1000 Hz and 2000-4000 Hz, and the structural-borne noise induced by the pass-by of a train was found from 50 Hz to 200 Hz. The nearly-enclosed barriers could effectively reduce the measured rolling noise, with attenuation values of over 15 dB in the corresponding ranges. The low frequency noise was mostly reduced by the effects of the floating slab track structures. While the sound pressure levels at the 1/3 octave band of 100 Hz were enhanced a bit unexpectedly by the combined effects of the nearly-enclosed barrier and the floating slab track structures, which would be studied using scale model tests and 2.5-D BEM calculations.

5. Chapter 4 preliminarily investigated the use of a scale modelling method and a 2.5-D boundary element method to study the acoustic performance of noise barriers in the urban rail transit system. Since noise sources in urban rail transit systems were always considered as incoherent line sources, the attenuations of point sources, coherent line source, and incoherent line sources, induced by a common straight barrier on the rigid ground, and by a double-straight barrier on a rigid viaduct, were calculated using analytical solutions, a 2.5-D BEM modelling method and scale modelling tests. The comparisons, between the analytical solutions and the 2.5-D BEM predictions for a simple straight barrier on the rigid ground for a one-point source, indicated that the 2.5-D BEM modelling was more useful to model real barriers with non-zero thicknesses. Good agreements between the scale model tested results and the 2.5-D BEM calculations for incoherent point sources indicated that the 2.5-D BEM modelling could be generalised to predict the attenuation of the urban rail transit noise source induced by reflective nearly-enclosed barriers on a reflective viaduct.

6. Chapter 5 investigated the acoustic performance of the reflective nearly-enclosed barrier by using the scale modelling tests and the 2.5-D BEM calculations. It can be concluded from the predicted results for coherent line sources and point sources that under the radiation of the noise source inside the nearly-enclosed barrier, the sound pressures at the positions outside the barrier could be amplified at the resonance frequencies by the acoustic resonance effects induced by the open air cavity inside the barrier, directly deteriorating the barrier performance. To suppress the resonance effects, the absorptive treatments on the inner surface of the barrier must be added.

7. Comparing the 2.5-D BEM predictions with the measured results, we found that the insufficient sound insulation properties of the PC panels on the top was identified to be the main cause of the differences between the measured and predicted attenuations. As mentioned in Chapter 1, the PC panels, employed for the arched parts in the full-scale prototype of the absorptive nearly-enclosed barrier, have a thickness of only 6.5 mm, a little thicker than those employed in the scale modelling tests. Thus, the sound insulation of the PC panels in the actual project are considered to be not sufficient as well. The need for transparent materials with better sound insulation and high flexibility was long ignored and urgent for the arched parts, both in the scale model tests and the actual projects. With good sound insulation properties of the transparent panels on the top, as expected, the attenuations of the reflective nearly-enclosed barrier averaged around 15 dB in the near field and around 10 dB in the far field.

8. Chapter investigated the acoustic performance of the absorptive nearly-enclosed barrier by using the 2.5-D BEM calculations. For modelling the absorptive treatments, the glass-wool panels were modelled using a Delany-Bazley model, and the open-celled Aluminium-foam panels were modelled using a microstructure model proposed by H. Li and J. Zhang. It can be concluded that compared with the predictions for coherent line sources(2-D BEM predictions), there were better agreements between the predictions for incoherent line sources and the measured results presented in Chapter 3. The differences between the predictions for incoherent line sources and the measured results were due to the insufficient sound insulation properties of the PC panels and the PMMA panels.

9. In order to improve the acoustic performance of the absorptive nearly-enclosed barrier, assuming all the employed panels having sufficient sound insulation properties, Chapter 7 discussed the effects of the width of the opening on the top, and the absorption properties of the absorptive treatments by using 2.5-D BEM modelling calculations. From the compared results it can be found the best design of the opening width is 4 meters or 6 meters. By comparing the perfect absorptive surfaces and the soft surfaces used in the 2.5-D BEM model of the absorptive nearly-enclosed barrier, we found the use of the perfect absorptive surfaces was better to improve the acoustic performance of the absorptive nearly-enclosed barrier. And to enhance the capabilities of the ab-

sorptive treatments located on the positions of the Aluminium-foam panels is the most effective way to improve the acoustic performance of the absorptive nearly-enclosed barrier.

10. The economic benefits of the nearly-enclosed barriers were not satisfactory since the only significant gains compared with the double-straight barriers could not be obtained due to the poor sound isolation properties of the top PC sheets. Even though all the employed panels having sufficient sound insulation properties, compared with double-straight barriers, the absorptive nearly-enclosed barriers had a better effect (1-2 dB) on reducing the level at receiver positions in the near field (source to receiver distance: 7.5 m), almost no effect in the medium field (source to receiver distance: 22 m) and an even worse effect ((-1)-(-2) dB) in the far field (source to receiver distance: 55 m). Hence, it can be concluded that the economy and the efficiency of the nearly-enclosed barrier were both bad. New designs of noise barriers or more perfect acoustic solutions are being sought for reducing urban rail transit noise.

8.2 Further work

Although some achievements have been made in this study of noise reduction mechanism for nearly-enclosed noise barriers in urban rail transit, there are still many further studies to be done:

1. The 2.5-D BEM acoustic models of absorptive nearly-enclosed noise barriers in urban rail transit need to be further verified through a large number of field test data. Since their practical applications are near high-rise buildings in mega cities like Beijing, Shanghai, etc., it is necessary to measure acoustic performances of them at sites, so as to more widely verify the effectivenesses of models.

2. In this paper, only the opening width of the top arched parts were considered to be optimized. In the future, it is necessary to optimize the dimensions of other geometries based on the structural mechanics designs, to maximize the insertion losses of the absorptive nearly-enclosed barriers according to the source characteristics and spectra of urban rail transit noise.

3. Current studies showed that the actual noise reduction effects of the nearly-enclosed noise barriers were lower than the predicted results, which were mainly limited by the sound insulation properties of the panels. For this reason, the 2.5-D BEM acoustic model of noise barrier including sound insulation performances of sound panels should be further studied.

4. By combining with the latest acoustic metamaterial applications, new nearly-enclosed noise barriers in urban rail transit will be further investigated and developed.

Appendix A

An explanation on different insertion losses for different sources

As shown in Figure 4.2, for each case, the one-third octave spectrum of the attenuation for a one-point source is almost the same with that for a coherent line source. However, as illustrated in Table 4.3, for each case, the single rating for the former is significantly higher than the latter. These significant differences are due to different sources in which the proportions of sound energy are different at different frequencies.

When considering a coherent line source, it can be assumed to be a point source in 2-D BEM model. The corresponding Green function is given as,

$$G_{2d}\left(k, R^{'}\right) = \frac{\mathrm{i}}{4} H_0^{(1)}\left(kR^{'}\right) \tag{A.1}$$

where $R^{'}$ denotes the shortest source-edge-receiver path and k denotes wavenumber. $H_0^{(1)}$ denotes the zeroth Hankel function of the first kind.

When considering a one-point source, it can be assumed to be a point source in 3-D BEM model. The corresponding Green function is given as,

$$G_{3d}\left(k, R^{'}\right) = \frac{e^{\mathrm{i}kr}}{4\pi R^{'}} \tag{A.2}$$

For an instance, assuming the shortest source-edge receiver path $R^{'}$ equal to 1, from 50 Hz to 5000 Hz, the Green functions in level(reference pressure $20\mu\mathrm{Pa}$) for 2-D and 3-D BEM model were solved. The corresponding solutions are shown in Figure A.1. It can be seen that the sound pressure level for a coherent line source is inversely proportional to the logarithm of sound frequency, whereas that for a one-point source keeps constant. The results at low frequencies for a coherent line source are therefore much higher than those for a one-point source whereas at mid- and high frequencies the results for a coherent line source are significantly lower.

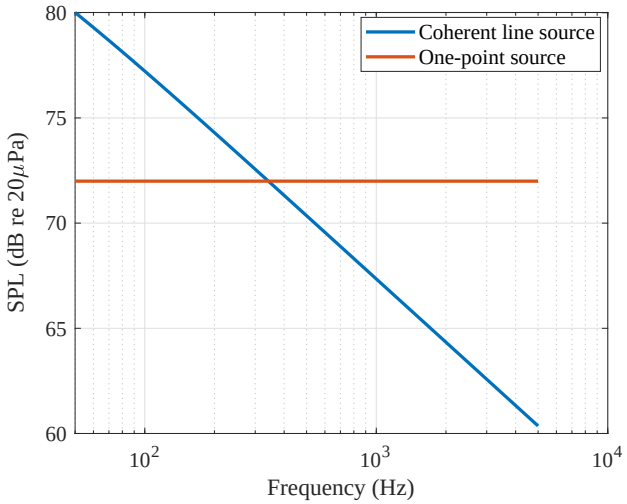

Fig A.1.: A comparison of solutions in frequency domain for a coherent line source and those for a one-point source

Taking for instance, Case 2 in Chapter 4, one source was located on the ground and one receiver was located above the rigid ground 1 meter (as shown in Figure 4.1(b)). The results on the site without a barrier for a coherent line source and those for a one-point source were solved separately using Green functions, as shown in Figure A.2(a). The sound pressure levels for a coherent line source are lower than those for a one-point source at low frequencies, whereas high than those for a one-point source at high frequencies. And the sound pressure level for a coherent line source is inversely proportional to frequency. We also find it again that the sound pressure level for a one-point source keeps constant in the frequency range of 50-5000 Hz. Under these circumstances, the attenuations in frequency domain of the simple straight barrier for these two kinds of sources were also solved by using McDonald's analytical method, as shown in Figure A.2(b). It can be seen that the

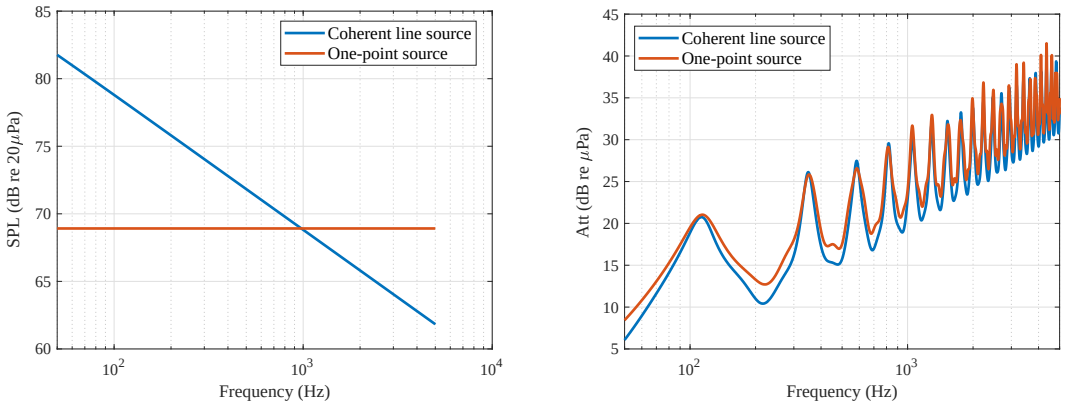

(a) The results of the site without a barrier

(b) The attenuations of the barrier

Fig A.2.: A comparison of solutions in frequency domain for a coherent line source and those for a one-point source in Case 2, Chapter 4

attenuation of the barrier in the sound field of a one-point source is almost identical to that in the field of a coherent line source at each frequency. Then with the help of Equation

(4.7), the insertion losses were obtained and are presented in Table 4.3. The insertion loss of the barrier for a coherent line source and that for a one-point source are 14.8 dB and 24.1 dB, respectively. Even though the spectrum for two types of sources are almost the same(shown in Figure A.2(b)), the single rating for a coherent line source is lower than that for a one-point source about 10 dB. This significant difference can be due to the different results for these two kinds of sources on the site without a barrier.

To verify this, a correction curve was proposed. This curve was used to adjust the sound pressure levels on the site without a barrier for a coherent line source to accord with the constant value for a one-point source. It means that the value of sound pressure for a one-point source at a given frequency will be multiplied by a correction coefficient. The coefficient at a given frequency is given as,

$$\gamma(f) = \sqrt{\frac{p^2_{\mathrm{wo,one-point}}(f)}{p^2_{\mathrm{wo,coherent_{l}ine}}(f)}} \tag{A.3}$$

With the help of these correction coefficients, the adjusted results of the site without a barrier were solved and are shown in Figure A.3(a). By using the correction curve, the sound pressure level for a coherent line source at each frequency is identical to that for a one-point source. Then the sound pressure levels on the site with a barrier for a coherent line source were thus multiplied by the correction coefficients. Because the sound pressure levels on the site without and with barrier were both multiplied by the same correction curve, the corresponding attenuations must be unchanged in the frequency domain, being shown in Figure A.3(b).

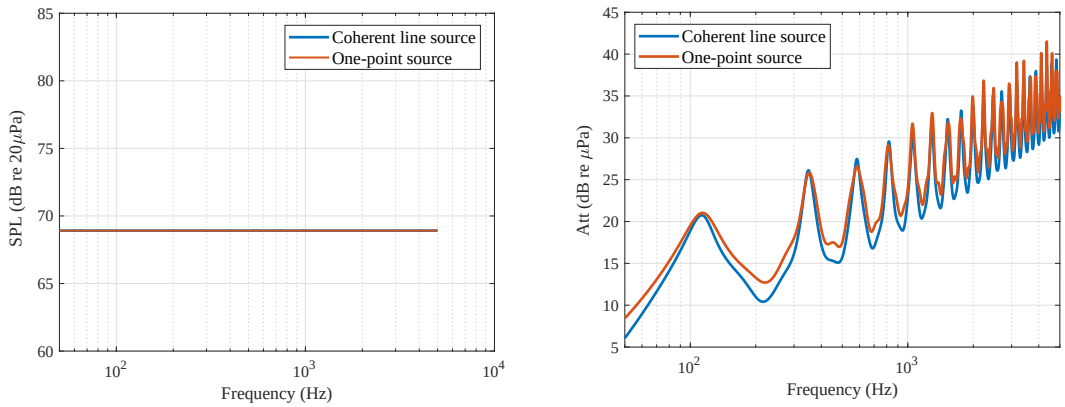

(a) The adjusted results of the site without a barrier

(b) The adjusted attenuations of the barrier

Fig A.3.: A comparison of adjusted solutions in frequency domain for a coherent line source and those for a one-point source in Case 2, Chapter 4

To try again to calculate the insertion losses of the barrier for these two kinds of sources. By using Equation (4.7), the insertion losses for a coherent line source was changed, with a much higher value of 22.5 dB. Table A.1 shows the variation of the insertion loss for the

coherent line source, compared with the results for a one-point source. It is indicated that

Tab A.1.: Insertion losses of Case 2 for two kinds of sources (frequency range: 50-5000 Hz)

IL / dB	Predicted results by BEM	
	One-point source	Coherent line source
Case 2	24.1	14.8 22.5(adjusted)

the insertion loss of a barrier for a coherent line source (2-D BEM results) is characterized by the importance of the attenuations at low frequencies, since the proportions of low-frequency energy are much higher than those at mid- and high frequencies. A conclusion is therefore obtained that the insertion loss of a barrier for a coherent line source can be almost identical to that for a one-point source, only on a premise that both kinds of sources have the same proportion of sound energy at each frequency. Since the insertion losses for incoherent line sources have frequency-averaged characteristics and longitudinal-distance-averaged characteristics, they can be almost at the same levels as those for coherent line sources with the low-frequency characteristics, as shown in Table 4.3.

Appendix B

Panel designs of the VI projects in scale model tests

Please see panel designs of the VI projects in scale model tests on the next page.

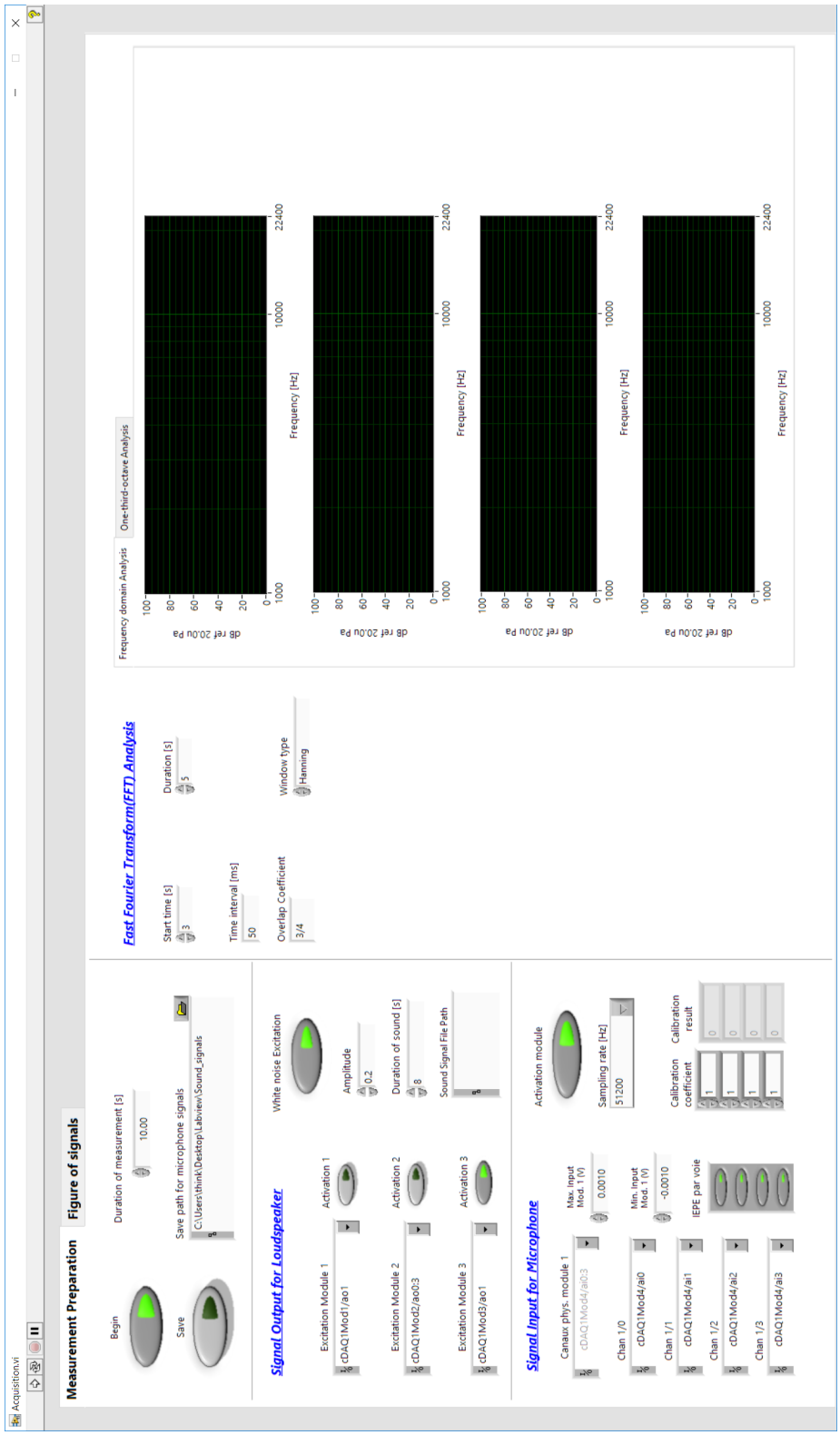

Fig B.1.: Measurement preparation panel

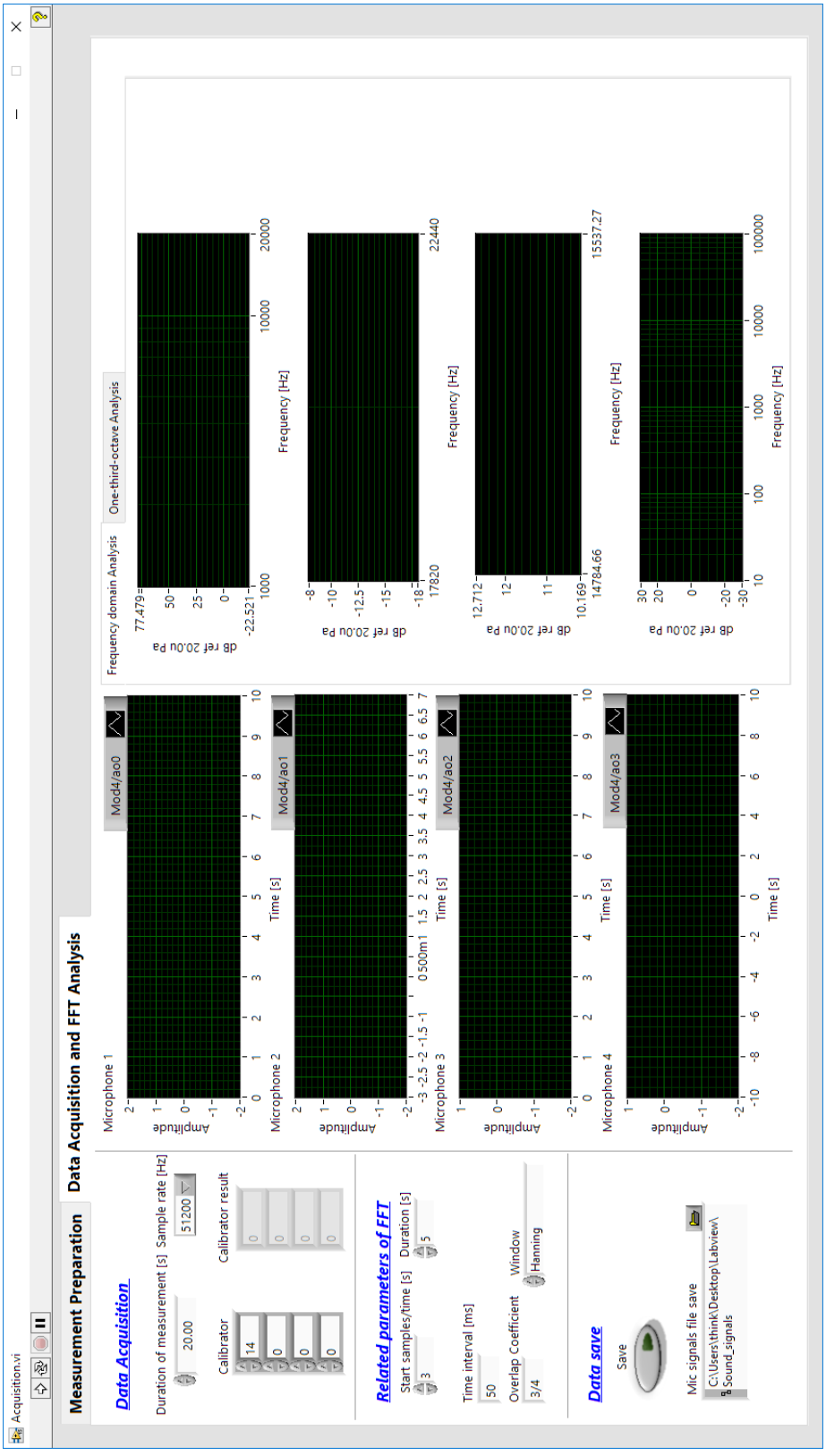

Fig B.2.: Data Acquisition and FFT Analysis panel

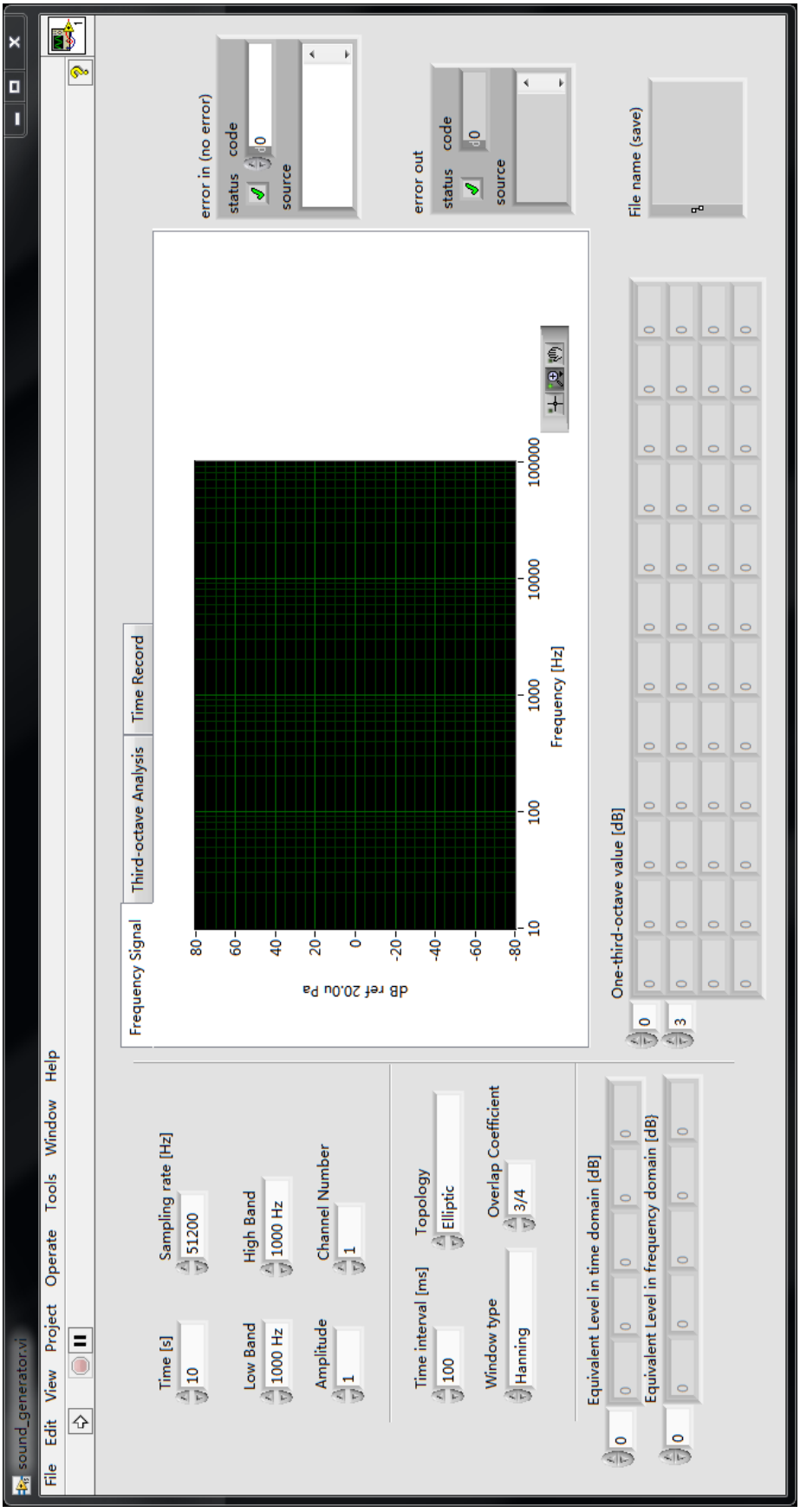

Fig B.3.: The front panel of the VI project for the sound generator

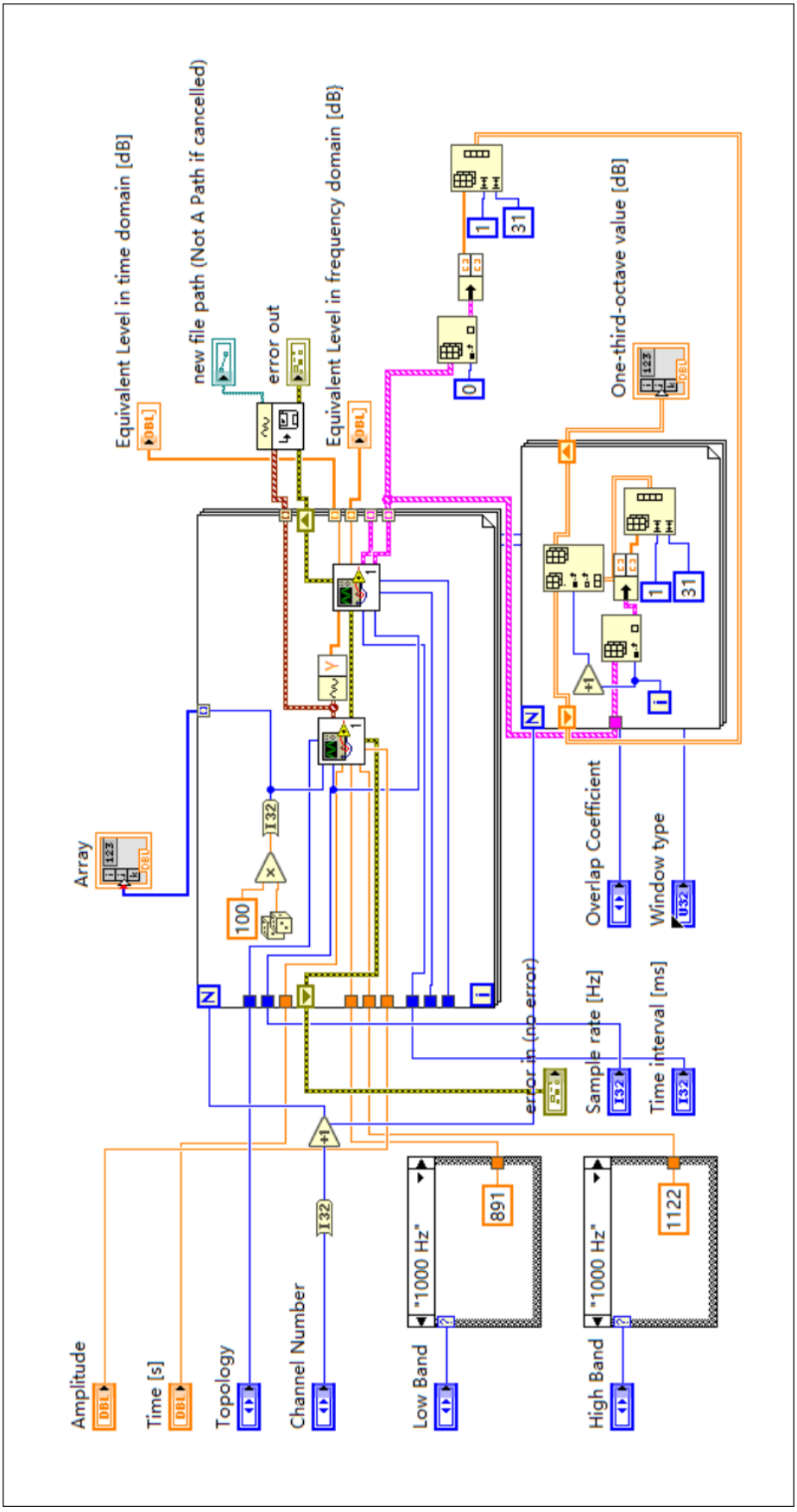

Fig B.4.: The back panel of the VI project for the sound generator

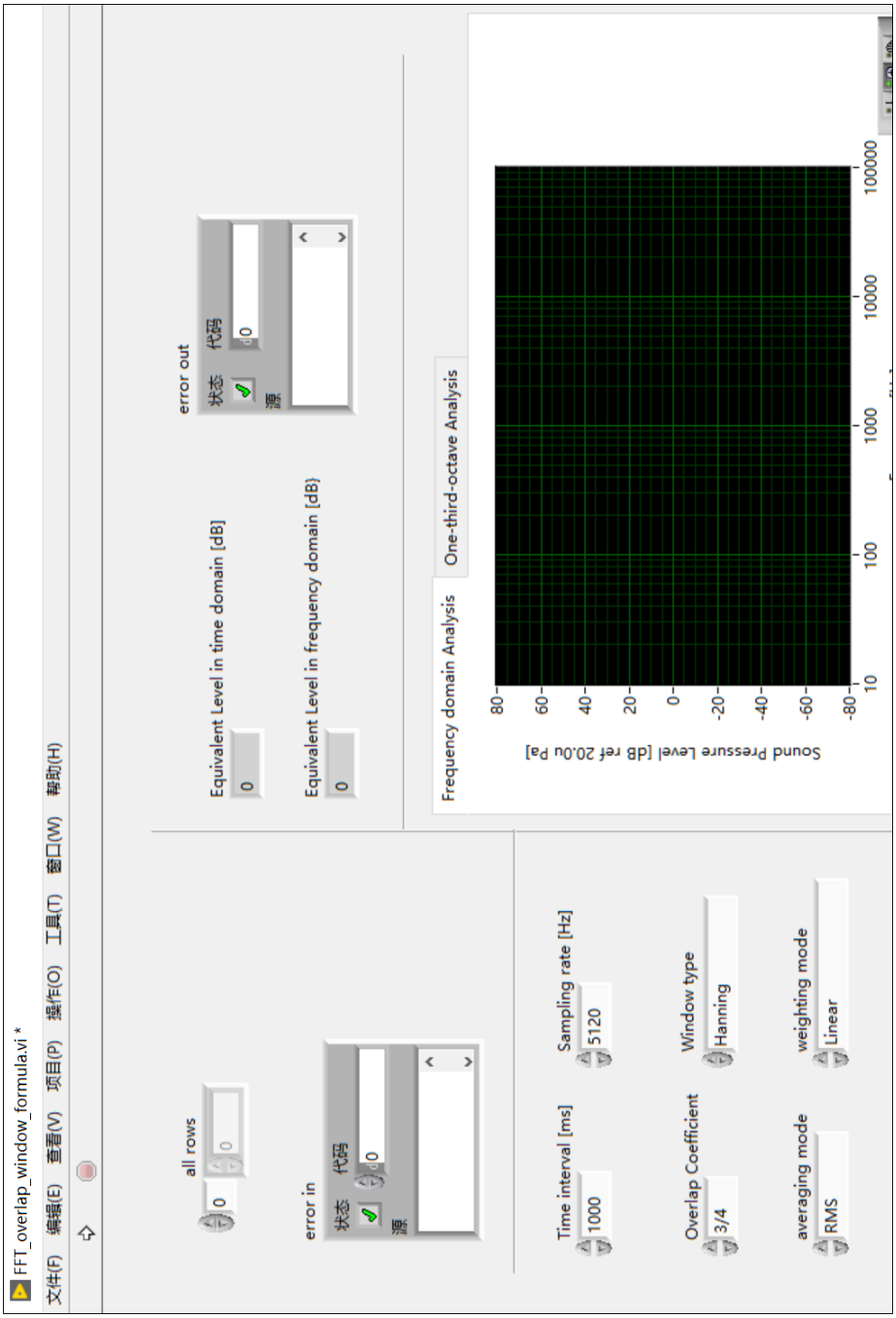

Fig B.5.: The front panel of the VI project for the FFT formula

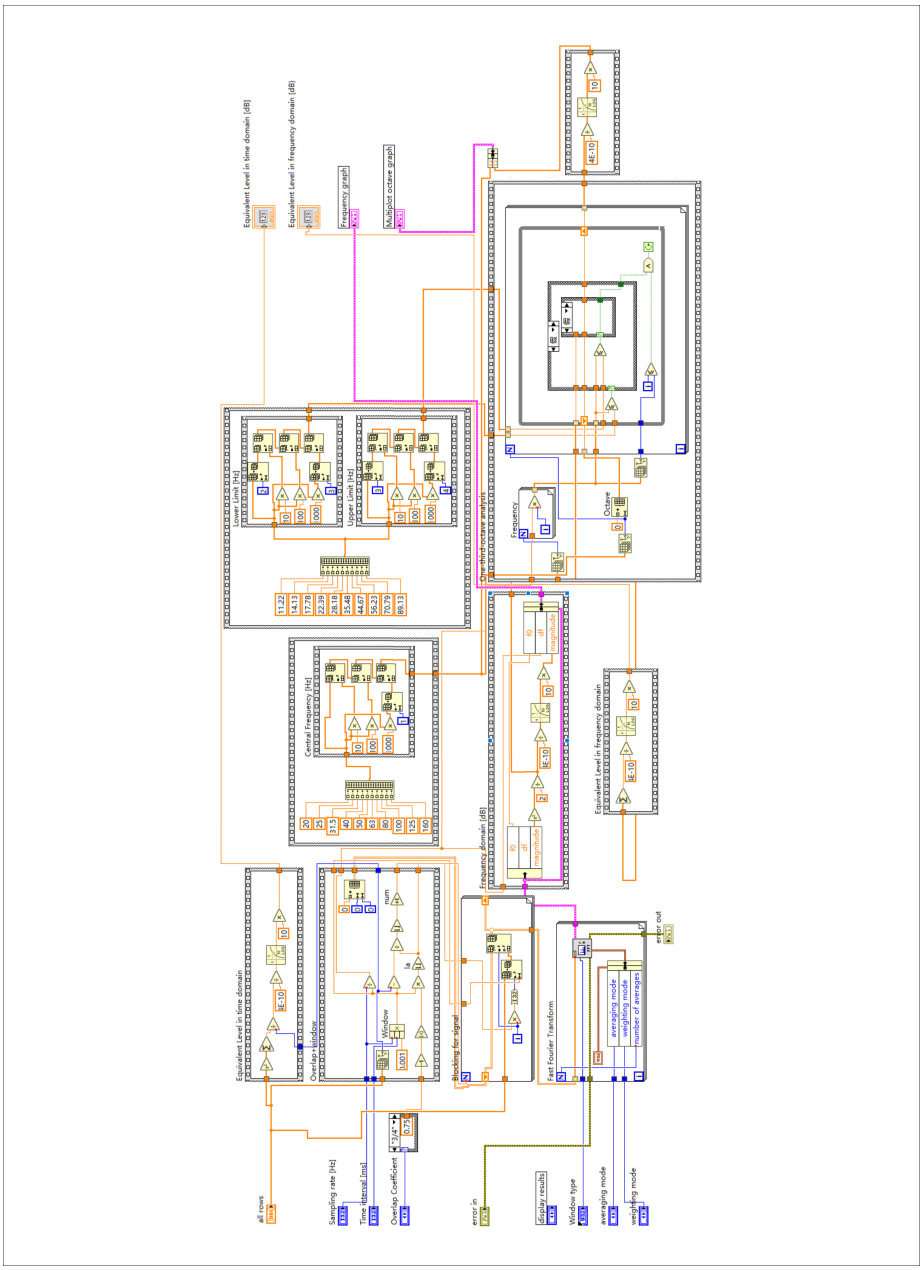

Fig B.6.: The back panel of the VI project for the FFT formula

References

[1]Liu, Y. and Dong, L. „The Pollution Control of Urban Elevated Railway Traffic Noise“. In: *Proceedings of the 10th European Congress and Exposition on Noise Control Engineering*. Netherlands: European Acoustics Association, 2015, pp. 1683–1687 (cit. on p. 1).

[2]Zhang, D. and Jiao, J. „How Does Urban Rail Transit Influence Residential Property Values? Evidence from An Emerging Chinese Megacity“. In: *Sustainability* 11.2 (2019), p. 534 (cit. on p. 1).

[3]Cui, R., Gao, L., and Cai, X. „Study on Vibration and Noise Reduction Properties of Damping Rail for High-speed Railway(in Chinese)“. In: *Journal of The China Railway Society* 37 (2015), pp. 78–84 (cit. on p. 1).

[4]Jiang, W., Wan, Q., and Yan, L. „Constrained Damping Dynamic Absorber Stuck on a Rail of Urban Transits(in Chinese)“. In: *Journal of Vibration and Shock* 28 (2009), pp. 78–80 (cit. on p. 1).

[5]Wang, A., Bewes, O. G., Cox, S. J., and Jones, C. J.C. „Measurement and Modelling of Noise from the Arsta Bridge in Stockholm“. In: *Noise and Vibration Mitigation for Rail Transportation Systems*. Berlin, Heidelberg: Springer Berlin Heidelberg, 2008, pp. 172–178 (cit. on p. 1).

[6]Xia, H., Deng, Y., Zou, Y., De Roeck, G., and Degrande, G. „Dynamic Analysis of Rail Transit Elevated Bridge with Ladder Track“. In: *Frontiers of Architecture and Civil Engineering in China* 3.1 (2009), pp. 2–8 (cit. on p. 1).

[7]Xiao, X. and Shen, H. „Vibration and the TMD Control of Bridges under Moving Loads(in Chinese)“. In: *Journal of Vibration and Shock* 24 (2005) (cit. on p. 1).

[8]Gu, P., Wang, M., and Wu, D. „Damping Suppression of Lateral Vibration of the Existing Steel Truss Railway Bridges Using TMD(in Chinese)“. In: *Journal of The China Railway Society* 27.02 (2005), pp. 85–89 (cit. on p. 1).

[9]Wang, H., Liu, H., Tao, T., Zong, Z, and He, X. „Vibration Control of Long-span Steel Truss Bridge Subjected to Train Loadings Using TMD(in Chinese)“. In: *Journal of Vibration Engineering* 03 (2014), pp. 385–391 (cit. on p. 1).

[10]Lin, C. C., Wang, J. F., and Chen, B. L. „Train-induced Vibration Control of High-speed Railway Bridges Equipped with Multiple Tuned Mass Dampers“. In: *Journal of Bridge Engineering* 10.4 (2005), pp. 398–414 (cit. on p. 1).

[11]Li, X., Yang, D., Chen, G., Li, Y., and Zhang, X. „Review of Recent Progress in Studies on Noise Emanating from Rail Transit Bridges“. In: *Journal of Modern Transportation* 4 (2016), pp. 237–250 (cit. on p. 1).

[12]Ekici, I. and Bougdah, H. „A Review of Research on Environmental Noise Barriers“. In: *Building Acoustics* 10.4 (2003), pp. 289–323 (cit. on pp. 1, 5).

[13]Oldham, David J. and Egan, Christopher A. „A Parametric Investigation of the Performance of T-Profiled Highway Noise Barriers and the Identification of a Potential Predictive Approach“. In: *Applied Acoustics* 72.11 (2011), pp. 803–813 (cit. on pp. 1, 41).

[14]Oldham, David J. and Egan, Christopher A. „A Parametric Investigation of the Performance of Multiple Edge Highway Noise Barriers and Proposals for Design Guidance“. In: *Applied Acoustics* 96 (2015), pp. 139–152 (cit. on pp. 1, 10).

[15]Ishizuka, T. and Fujiwara, K. „Performance of Noise Barriers with Various Edge Shapes and Acoustical Conditions“. In: *Applied Acoustics* 65.2 (2004), pp. 125–141 (cit. on pp. 1, 23, 24).

[16]Jolibois, A., Defrance, J., Koreneff, H., et al. „In Situ Measurement of the Acoustic Performance of a Full Scale Tramway Low Height Noise Barrier Prototype“. In: *Applied Acoustics* 94 (2015), pp. 57–68 (cit. on pp. 2, 9, 23, 42, 43, 46).

[17]Bérengier, M. C., Gauvreau, B., Blanc-Benon, Ph., and Juvé, D. „Outdoor Sound Propagation: a Short Review on Analytical and Numerical Approaches“. In: *Acta Acustica united with Acustica* 89 (2003), pp. 980–991 (cit. on p. 2).

[18]Makarewicz, R. „A Simple Model of Outdoor Noise Propagation“. In: *Applied Acoustics* 54.2 (1998), pp. 131–140 (cit. on p. 2).

[19]Fujiwara, K., Hothersall, D.C, and Kim, C. „Noise Barriers with Reactive Surfaces“. In: *Applied Acoustics* 53.4 (1998), pp. 255–272 (cit. on pp. 2, 6, 8).

[20]Hothersall, D.C., Crombie, D.H., and Chandler-Wilde, S.N. „The Performance of T-profile and Associated Noise Barriers“. In: *Applied Acoustics* 32.4 (1991), pp. 269–287 (cit. on pp. 3, 24).

[21]May, D. N. and Osman, N. M. „Highway Noise Barriers: New Shapes“. In: *Journal of Sound and vibration* 71.1 (1980), pp. 73–101 (cit. on pp. 3, 26).

[22]Zilvinas, V., Raimondas, G., and Albertas, V. „The Research on the Effectiveness of the Inclined Top Type of a Noise Barrier“. In: *Journal of Environmental Engineering and Landscape Management* 20.2 (2012), pp. 155–162 (cit. on p. 3).

[23]Watts, G. R., Crombie, D. H., and Hothersall, D. C. „Acoustic Performance of New Designs of Traffic Noise Barriers: Full Scale Tests“. In: *Journal of Sound and Vibration* 177.3 (1994), 289–305 (cit. on p. 4).

[24]Watts, G. R. „Acoustic performance of a multiple edge noise barrier profile at motorway sites“. In: *Applied Acoustics* 47.1 (1996), pp. 47–66 (cit. on p. 4).

[25]Ho, Steve S.T., Busch-Vishniac, Ilene J., and Blackstock, David T. „Noise Reduction by a Barrier Having a Random Edge Profile“. In: *The Journal of the Acoustical Society of America* 101.5 (1997), pp. 2669–2676 (cit. on p. 4).

[26]Menounou, P., Busch-Vishniac, Ilene J., and Blackstock, David T. „Jagged-edge Noise Barriers“. In: *The Journal of the Acoustical Society of America* 103.5 (1998), pp. 2759–2759 (cit. on p. 4).

[27]Shao, W., Lee, H.P., and Lim, S.P. „Performance of Noise Barriers with Random Edge Profiles“. In: *Applied Acoustics* 62.10 (2001), pp. 1157–1170 (cit. on p. 4).

[28]Nicolas, J. and Daigle, G.A. „Experimental Study of a Slow-waveguide Barrier on Finite Impedance Ground“. In: *The Journal of the Acoustical Society of America* 80.3 (1986), pp. 869–876 (cit. on p. 4).

[29]Watts, G.R. and Morgan, P.A. „Acoustic Performance of an Interference-type Noise-barrier Profile“. In: *Applied Acoustics* 49.1 (1996), pp. 1–16 (cit. on p. 4).

[30]Matsumoto, T., Yamamoto, K., and Ishikita, H. „Efficiency of Highway Noise Barrier With Horizontal Louver–A Study by Full Scale Model Experiment“. In: *INTER-NOISE and NOISE-CON Congress and Conference Proceedings, InterNoise00*. Nice, France: Institute of Noise Control Engineering, 2000, pp. 4665–4669 (cit. on pp. 5, 6).

[31]Watts, G. R., Hothersall, D. C., and Horoshenkov, K. V. „Measured and Predicted Acoustic Performance of Vertically Louvred Noise Barriers“. In: *Applied Acoustics* 62.11 (2001), pp. 1287–1311 (cit. on pp. 5, 11, 26).

[32]Wassilieff, C. „Improving the Noise Reduction of Picket Barriers“. In: *The Journal of the Acoustical Society of America* 84.2 (1988), p. 645 (cit. on p. 5).

[33]Martin, S. J. and Hothersall, D. C. „Performance of Median Noise Barriers“. In: *INTER-NOISE and NOISE-CON Congress and Conference Proceedings, InterNoise00*. Nice, France: Institute of Noise Control Engineering, 2000, pp. 4637–4642 (cit. on p. 5).

[34]Monazzam, Mohammad Reza and Fard, Samaneh Momen Bellah. „Impacts of Different Median Barrier Shapes on a Roadside Environmental Noise Screen“. In: *Environmental Engineering Science* 28.6 (2011), pp. 435–441 (cit. on pp. 5, 10).

[35]Wei, X. and Wang, Y. „The Study of Reducing Effect and Edge Diffraction Fields on Closed and Semi-closed Noise Barriers“. In: *Noise and Vibration Control* 30.S1 (2012), pp. 126–131 (cit. on p. 5).

[36]Zhang, C. „The Influence Analysis of the Opening Ratio of Fully-enclosed Barriers to the Micro-pressure Wave“. In: *Science & Technology Association Forum* 09 (2010), p. 97 (cit. on p. 5).

[37]Li, X., Yang, D., Gao, W., and Luo, Y. „Study on Vibration and Noise Reduction of Semi- or Fully- Enclosed Noise Barriers of High Speed Railways s(in Chinese)“. In: *Noise and vibration control* 38.s1 (2018), pp. 8–13 (cit. on p. 6).

[38]Waubke, H. and Kasess, C.H. „Simulation of the Noise Radiation and Shielding with the Boundary Element Method“. In: *Proceedings of the 23rd International Congress on Sound and Vibration*. Athens, Greece: International Institute of Acoustics and Vibrations, 2016, pp. 1–8 (cit. on p. 6).

[39]Hothersall, D. C., Horoshenkov, K. V., Morgan, P. A., and Swift, M. J. „Scale Modelling of Railway Noise Barriers“. In: *Journal of Sound and Vibration* 234.2 (2000), pp. 207–223 (cit. on p. 7).

[40]Daigle, Gilles A. „Technical Assessment of the Effectiveness of Noise Walls“. In: *Noise News International* 6.1 (1998), pp. 11–35 (cit. on p. 7).

[41]Amares, S., Sujatmika, E., Hong, T. W., Durairaj, R., and Hamid, H. S. H. B. „A Review: Characteristics of Noise Absorption Material“. In: *Journal of Physics Conference Series* 908.1 (2017) (cit. on p. 7).

[42]Bai, M. R., Lo, Y. Y., and Chen, Y. S. „Impedance Measurement Techniques for One-port and Two-port Networks“. In: *The Journal of the Acoustical Society of America* 138.4 (2015), pp. 2279–2290 (cit. on p. 7).

[43]Vorländer, M. *Auralization: Fundamentals of Acoustics, Modelling, Simulation, Algorithms and Acoustic Virtual Reality*. Berlin, Heidelberg: Springer, 2008 (cit. on p. 7).

[44] Okubo, T. and Fujiwara, K. „Efficiency of a Noise Barrier on the Ground with an Acoustically Soft Cylindrical Edge“. In: *Journal of Sosssund and Vibration* 216.5 (1998), pp. 771–790 (cit. on p. 8).

[45] Okubo, T. and Fujiwara, K. „Efficiency of a Noise Barrier with an Acoustically Soft Cylindrical Edge“. In: *Journal of the Acoustical Society of Japan (E)* 19.3 (1998), pp. 187–197 (cit. on p. 8).

[46] Schroeder, M. R. „Binaural Dissimilarity and Optimum Ceilings for Concert Halls: More Lateral Sound Diffusion“. In: *The Journal of the Acoustical Society of America* 65.4 (1979), pp. 958–963 (cit. on p. 8).

[47] D'Antonio, P. and Cox, T. „Two decades of sound diffuser design and development - Part 1: Applications and design“. In: *Journal of the Audio Engineering Society* 46.11 (1998), pp. 955–976 (cit. on p. 8).

[48] Cox, T. and D'Antonio, P. „Two Decades of Sound Diffuser Design and Development, Part 2: Prediction, Measurement, and Characterization“. In: *Journal of the Audio Engineering Society* 46.12 (1998), pp. 1075–1091 (cit. on p. 8).

[49] Fujiwara, K. and Miyajima, T. „Absorption Characteristics of a Practically Constructed Shroeder Diffuser of Quadratic Residue Type“. In: *Applied Acoustics* 35.2 (1992), pp. 149–152 (cit. on p. 8).

[50] Fujiwara, K. „A Study on the Sound Absorption of a Quadratic Residue Type Diffuser“. In: *Acta Acustica united with Acustica* 81.4 (1995), pp. 370–378 (cit. on p. 8).

[51] Kuttruff, H. „Sound Absorption by Pseudostochastic Diffusers (Schroeder Diffusers)“. In: *Applied Acoustics* 42.3 (1994), pp. 215–231 (cit. on p. 8).

[52] Mechel, F. P. „The Wide-angle Diffuser–A Wide-angle Absorber?“ In: *Acta Acustica united with Acustica* 81.4 (1995), pp. 379–401 (cit. on p. 8).

[53] Wu, T., Cox, T. J., and Lam, Y. W. „From a Profiled Diffuser to an Optimized Absorber“. In: *The Journal of the Acoustical Society of America* 108.2 (2000), pp. 643–650 (cit. on p. 8).

[54] Monazzam, M.R. and Lam, Y.W. „Performance of Profiled Single Noise Barriers Covered with Quadratic Residue Diffusers“. In: *Applied Acoustics* 66.6 (2005), pp. 709–730 (cit. on p. 8).

[55] Slutsky, S. and Bertoni, Henry L. „Analysis and Programs for Assessment of Absorptive and Tilted Parallel Barriers“. In: *Transportation Research Record* 1176 (1988), pp. 13–22 (cit. on p. 10).

[56] Watts, G. R. „Acoustic Performance of Parallel Traffic Noise Barriers“. In: *Applied Acoustics* 47.2 (1996), pp. 95–119 (cit. on pp. 10, 41).

[57] Yang, C., Pan, J., and Cheng, L. „A Mechanism Study of Sound Wave-trapping Barriers“. In: *The Journal of the Acoustical Society of America* 134.3 (2013) (cit. on pp. 10, 94).

[58] Bowlby, W. and Cohn, L. F. „A Model for Insertion Loss Degradation for Parallel Highway Noise Barriers“. In: *The Journal of the Acoustical Society of America* 80.3 (2005), pp. 855–868 (cit. on p. 10).

[59] Watts, G. R. and Godfrey, N. S. „Effects on Roadside Noise Levels of Sound Absorptive Materials in Noise Barriers“. In: *Applied Acoustics* 58.4 (1999), pp. 385–402 (cit. on p. 10).

[60] Zhao, J., Wang, X.-M., Chang, J.M., Yao, Y., and Cui, Q. „Sound Insulation Property of Wood–waste Tire Rubber Composite“. In: *Composites Science and Technology* 70.14 (2010), pp. 2033–2038 (cit. on p. 11).

[61]Vos, Paul de. *Railway noise in Europe*. Tech. rep. Paris, France, 2016 (cit. on pp. 11, 13).

[62]Thompson, D.J. „Wheel-rail Noise Generation, Part I: Introduction and Interaction Model“. In: *Journal of sound and vibration* 161.3 (1993), pp. 387–400 (cit. on pp. 11, 13, 14, 32).

[63]Van Leeuwen, Hans JA. „Railway Noise Prediction Models: a Comparison“. In: *Journal of Sound and Vibration* 231.3 (2000), pp. 975–987 (cit. on p. 12).

[64]Wang, Y. and Sun, J. „Design and Study on the Noise Barrier Applications on Line 5, Beijing.(in Chinese)“. In: *Railway Standard Design* 10 (2007), pp. 26–29 (cit. on p. 12).

[65]Peters, S. „The Prediction of Railway Noise Profiles“. In: *Journal of Sound and Vibration* 32.1 (1974), pp. 87–99 (cit. on p. 12).

[66]Hohenwarter, D. „Railway Noise Propagation Models“. In: *Journal of Sound and Vibration* 141.1 (1990), pp. 17–41 (cit. on p. 12).

[67]Morgan, P. A., Hothersall, D. C., and Chandler-Wilde, S. N. „Influence of Shape and Absorbing Surface—A Numerical Study of Railway Noise Barriers“. In: *Journal of Sound and Vibration* 217.3 (1998), pp. 405–417 (cit. on p. 12).

[68]Zhang, X. „The Directivity of Railway Noise at Different Speeds“. In: *Journal of Sound and Vibration* 329.25 (2010), pp. 5273–5288 (cit. on p. 12).

[69]Liu, Y., Wen, Z., and Cheng, M. „Research and Application of Noise Prediction Model for Urban Rail Transit(in Chinese)“. In: *Urban Rapid Rail Transit* 04 (1998), pp. 32–35 (cit. on p. 13).

[70]Zhai, G., Zhang, B., and Guo, C. „The Calculating Model of Sound Field Distribution Along the Urban Elevated Railway(in Chinese)“. In: *China Environmental Science* 24.3 (2004), pp. 65–68 (cit. on p. 13).

[71]Zhu, Y., Chen, G., and Lin, C. „Numerical Prediction and Analysis of Radiated Noise from Viaduct of City(in Chinese)“. In: *Noise and Vibration Control* 03 (2005), pp. 37–41 (cit. on p. 13).

[72]Xu, Yang. „Sound Environment Research and Analysis During the Operation Period of Beijing Metro Batong Line(in Chinese)“. MA thesis. Beijing Jiaotong University, China: Beijing Jiaotong University, Sept. 2006 (cit. on p. 13).

[73]Liu, H., Gong, F., Ou, Y., and Teng, H. „Shape Selection for Noise Barriers Located in Front of Suzhuang Street Station on Line Fangshan in Beijing.(in Chinese)“. In: *Railway Standard Design* 01 (2011), pp. 109–111 (cit. on p. 13).

[74]Wang, Q., Di, G., Zhu, Y., and Li, Z. „Study on Frequency Characteristics of Rail Traffic Noise on Different Running Conditions(in Chinese)“. In: *Noise and Vibration Control* 02 (2008), pp. 85–86+106 (cit. on p. 13).

[75]Bai, Ti., Jiang, W., Bi, Z., et al. „Comprehensive Technology of Vibration and Noise Reduction in Urban Rail Transit(in Chinese)“. In: *New Technologies in Urban Rail Transit of China*. Beijing, China: China Civil Engineering Society, 2009 (cit. on p. 13).

[76]Liu, P. and Yang, Y. „Design of Sound Barrier Based on Micro-perforated Panel Absorber for Urban Transit(in Chinese)“. In: *Noise and Vibration Control* Supplementary issue (2009), pp. 320–324 (cit. on p. 13).

[77]International union of railways. *Exploring Bearable Noise Limits and Emission Ceilings for the Railways, Part I: National and European Legislation and Analysis of Different Noise Limit Systems*. Tech. rep. Paris, France, 2011 (cit. on p. 13).

[78] Shield, B. M. and Roberts, J. P. „Acceptable Noise Levels for New Railways“. In: *Proceedings of the Institution of Mechanical Engineers, Part F: Journal of Rail and Rapid Transit* 206.2 (1992), pp. 93–97 (cit. on pp. 14, 15).

[79] Kuwano, S. „Advantages and Disadvantages of A-weighted Sound Pressure Level in Relation to Subjective Impression of Environmental Noises“. In: *Noise Control Engineering Journal* 33 (1989), pp. 107–115 (cit. on p. 14).

[80] Broner, N. and Leventhall, H. G. „A Criterion for Predicting the Annoyance Due to Higher Level, Low Frequency Noise“. In: *Journal of Sound and Vibration* 84.3 (1982), pp. 443–448 (cit. on pp. 14–16).

[81] Broner, N. and Leventhall, H. G. „Low Frequency Noise Annoyance Assessment by Low Frequency Noise Rating (LFNR) Curves“. In: *Journal of Low Frequency Noise, Vibration and Active Control* 2.1 (1983), pp. 20–28 (cit. on pp. 14, 16).

[82] Persson, K., Björkman, M., and Rylander, R. „Loudness, Annoyance and dBA in Evaluating Low Frequency Sounds“. In: *Journal of Low Frequency Noise, Vibration and Active Control* 9.1 (1990), pp. 32–45 (cit. on pp. 14, 15).

[83] Landström, U., Kjellberg, A., and Byström, M. „Acceptable Levels of Sounds with Different Spectral Characteristics During the Performance of a Simple and a Complex Non-Auditory Task“. In: *Journal of Sound and Vibration* 160.3 (1993), pp. 533–542 (cit. on pp. 14, 15).

[84] Pawlaczyk-Łuszczyńska, M., Dudarewicz A.and Waszkowska, M., and Śliwińska-Kowalska, M. „Assessment of Annoyance from Low Frequency and Broadband Noise“. In: *International Journal of Occupational Medicine and Environmental Health* 16 (2003), pp. 337–43 (cit. on pp. 14, 15).

[85] Leventhall, H. G. et al. „Low Frequency Noise and Annoyance“. In: *Noise and Health* 6.23 (2004), p. 59 (cit. on pp. 14, 15, 35).

[86] Ishac, N. „Low Frequency Noise and Environmental Assessment“. In: *Acoustics 2015 Hunter Valley*. Hunter Valley, NSW, Australia: NSW Division of the Australian Acoustical Society, 2005 (cit. on p. 14).

[87] Persson, K. and Björkman, M. „Annoyance Due to Low Frequency Noise and the Use of the dB (A) Scale“. In: *Journal of Sound and Vibration* 127.3 (1988), pp. 491–497 (cit. on pp. 14, 15).

[88] Kjellberg, A., Goldstein, M., and Gamberale, F. „An Assessment of dB (A) For Predicting Loudness and Annoyance of Noise Containing Low Frequency Components“. In: *Journal of Low Frequency Noise, Vibration and Active Control* 3.3 (1984), pp. 10–16 (cit. on p. 14).

[89] Swedish National Board of Health and Welfare. *Draft, Public Advise: Residential Noise(In Swedish)*. Tech. rep. Stockholm, Sweden: Stockholm: Swedish National Board of Health and Welfare, 1995 (cit. on p. 15).

[90], Swedish Royal Board of Building. *Low Frequency Noise from Ventilation Installations (In Swedish)*. Tech. rep. Stockholm, Sweden: Stockholm: Swedish Royal Board of Building, 1992 (cit. on p. 15).

[91] Kjellberg, A., Tesarz, M., Holmberg, K., and Landström, U. „Evaluation of Frequency-weighted Sound Level Measurements for Prediction of Low-Frequency Noise Annoyance“. In: *Environment International* 23.4 (1997), pp. 519–527 (cit. on p. 15).

[92] Stevens, S. S. „Perceived Level of Noise by Mark VII and Decibels (E)“. In: *The Journal of the Acoustical Society of America* 51.2B (1972), pp. 575–601 (cit. on p. 16).

[93]Higgins, Thomas H. *Human Response to Sound: The Calculation of Perceived Level, PLdB (Noisiness or Loudness) Directly from Physical Measures.* Tech. rep. Washington, DC United States, 1976 (cit. on p. 16).

[94]Broner, N. and Leventhall, H. G. „A Modified PNdB for Assessment of Low Frequency Noise". In: *Journal of Sound and Vibration* 73.2 (1980), pp. 271–277 (cit. on p. 16).

[95]Piorr, D. and Wietlake, K. H. „Assessment of Low Frequency Noise in the Vicinity of Industrial Noise Sources". In: *Journal of Low Frequency Noise Vibration and Active Control* 9.3 (1990), pp. 116–119 (cit. on pp. 16, 31).

[96]Persson, K. „Estimation of Environmental Low Frequency Noise-A Comparison of Previous Suggestions and the New Swedish Recommendation". In: *Proceedings of the 8th International Meeting on Low Frequency Noise and Vibration, Gothenburg*. Sweden: Gothenburg, 1997, pp. 135–141 (cit. on pp. 16, 31).

[97]Mirowska, M. „Evaluation of Low-Frequency Noise in Dwellings. New Polish Recommendations". In: *Journal of Low Frequency Noise, Vibration and Active Control* 20.2 (2001), pp. 67–74 (cit. on pp. 16, 31).

[98]Bérengier, M. C., Gauvreau, B., Blanc-Benon, Ph., and Juvé, D. „Outdoor Sound Propagation: A Short Review on Analytical and Numerical Approaches". In: *Acta Acustica united with Acustica* 89.6 (2003), pp. 980–991 (cit. on p. 17).

[99]Makarewicz, Rufin. „A simple model of outdoor noise propagation". In: *Applied Acoustics* 54.2 (1998), pp. 131–140 (cit. on p. 17).

[100]Sommerfeld, Arnold. *Über die Ausbreitung der Wellen in der Drahtlosen Telegraphie*. Germany: Verlag der Königlich Bayerischen Akademie der Wissenschaften, 1909 (cit. on p. 17).

[101]Rudnick, Isadore. „The Propagation of an Acoustic Wave Along a Boundary". In: *The Journal of the Acoustical Society of America* 19.2 (1947), pp. 348–356 (cit. on p. 17).

[102]Ingard, U. „On the Reflection of a Spherical Sound Wave from an Infinite Plane". In: *The Journal of the Acoustical Society of America* 23.3 (1951), pp. 329–335 (cit. on p. 17).

[103]Donato, R. J. „Propagation of a Spherical Wave Near a Plane Boundary with a Complex Impedance". In: *The Journal of the Acoustical Society of America* 60.1 (1976), pp. 34–39 (cit. on p. 17).

[104]Embleton, Tony F. W., Piercy, Joe E., and Olson, N. „Outdoor Sound Propagation over Ground of Finite Impedance". In: *The Journal of the Acoustical Society of America* 59.2 (1976), pp. 267–277 (cit. on p. 17).

[105]Thomasson, S. I. „Reflection of Waves from a Point Source by an Impedance Boundary". In: *The Journal of the Acoustical Society of America* 59.4 (1976), pp. 780–785 (cit. on p. 17).

[106]Chessell, C. I. „Propagation of Noise Along a Finite Impedance Boundary". In: *The Journal of the Acoustical Society of America* 62.4 (1977), pp. 825–834 (cit. on p. 17).

[107]Thomasson, S. I. „A Powerful Asymptotic Solution for Sound Propagation Above an Impedance Boundary". In: *Acta Acustica united with Acustica* 45.2 (1980), pp. 122–125 (cit. on p. 17).

[108]Attenborough, K., Hayek, S. I., and Lawther, J. M. „Propagation of Sound Above a Porous Half-space". In: *The Journal of the Acoustical Society of America* 68.5 (1980), pp. 1493–1501 (cit. on p. 17).

[109]Habault, D. and Filippi, P. J. T. „Ground Effect Analysis: Surface Wave and Layer Potential Representations“. In: *Journal of Sound and Vibration* 79.4 (1981), pp. 529–550 (cit. on p. 17).

[110]Habault, D. „Etude de l'influence des Sols sur la Propagation Sonore“. PhD thesis. Université Aix-Marseille I, 1984 (cit. on p. 17).

[111]Rasmussen, KB. „A note on the calculation of sound propagation over impedance jumps and screens“. In: *Journal of sound and Vibration* 84.4 (1982), pp. 598–602 (cit. on p. 18).

[112]Durnin, J. and Bertoni, H. L. „Acoustic Propagation Over Ground Having Inhomogeneous Surface Impedance“. In: *The Journal of the Acoustical Society of America* 70.3 (1981), pp. 852–859 (cit. on p. 18).

[113]Jong, Bo A. de, Moerkerken, A., and Van Der Toorn, J. D. „Propagation of Sound Over Grassland and Over an Earth Barrier“. In: *Journal of Sound and Vibration* 86.1 (1983), pp. 23–46 (cit. on p. 18).

[114]Koers, P. „Diffraction by an Absorbing Barrier or by an Impedance Transition“. In: *Proceedings - International Conference on Noise Control Engineering*. Edinburgh, SCOTLAND: Institute of Noise Control Engineering, 1983, pp. 311–314 (cit. on p. 18).

[115]Lam, Y. W. and Monazzam, M. R. „On the Modeling of Sound Propagation Over Multi-Impedance Discontinuities Using a Semiempirical Diffraction Formulation“. In: *The Journal of the Acoustical Society of America* 120.2 (2006), pp. 686–698 (cit. on p. 18).

[116]Boulanger, P., Waters-Fuller, T., Attenborough, K., and Kai, M. L. „Models and Measurements of Sound Propagation from a Point Source Over Mixed Impedance Ground“. In: *The Journal of the Acoustical Society of America* 102.3 (1997), pp. 1432–1442 (cit. on p. 18).

[117]Hamet, J. F. and Brengier, M. „Acoustical Characteristics of Porous Pavements: A New Phenomenological Model“. In: *Inter-noise 93: People Versus Noise*. Leuven, Belgium: Institute of Noise Control Engineering, 1993 (cit. on p. 18).

[118]Keith, D. „Relaxation-matched modeling of propagation through porous media, including fractal pore structure“. In: *The Journal of the Acoustical Society of America* 94 (1998), pp. 1136–1145 (cit. on p. 18).

[119]Zwikker, C. and Kosten, C. W. *Sound Absorbing Materials*. Netherland: Elsevier, 1949 (cit. on pp. 18, 129).

[120]Attenborough, K. „Acoustical characteristics of rigid fibrous absorbent and granular materials“. In: *The Journal of the Acoustical Society of America* 73.3 (1983), pp. 785–799 (cit. on pp. 18, 130).

[121]Biot, M. A. „Theory of Propagation of Elastic Waves in a Fluid-Saturated Porous Solid. I. Low-Frequency Range“. In: *The Journal of the Acoustical Society of America* 28.2 (2005), pp. 179–191 (cit. on p. 18).

[122]Allard, J. F. *Propagation of Sound in Porous Media*. Dordrecht: Springer, 1993 (cit. on p. 18).

[123]Delany, M. E. and Bazley, E. N. „Acoustical Properties of Fibrous Absorbent Materials“. In: *Applied Acoustics* 3.2 (1970) (cit. on pp. 18, 128, 129, 160).

[124]Attenborough, K. „Ground Impedance Models: A Review“. In: *8th International Congress on Acoustics*. Vol. 1. 10. Japan: Science Council of Japan, 2004, 4 pp.– (cit. on p. 18).

[125]Embleton, Tony F. W., Piercy, Joe E., and Daigle, Giles A. „Effective Flow Resistivity of Ground Surfaces Determined by Acoustical Measurements“. In: *The Journal of the Acoustical Society of America* 74.4 (1983), pp. 1239–1244 (cit. on p. 18).

[126]Rochat, Judith L. and Read, David R. „Effective Flow Resistivity of Highway Pavements“. In: *The Journal of the Acoustical Society of America* 134.6 (2013), p. 4710 (cit. on p. 18).

[127]Taraldsen, G. „The Delany-Bazley Impedance Model and Darcy's Law“. In: *Acta Acustica United with Acustica* 91.1 (2005), pp. 41–50 (cit. on p. 18).

[128]Noise, ISO/TC 43/SC 1. *ISO 9613-2:1996 Acoustics - attenuation of sound during propagation outdoors - part 2: general method of calculation*. Switzerland, 1996 (cit. on p. 19).

[129]Delaroche, F. „Sur l'influence que le Vent Exerce dans la Propagation du son, sous le Rapport de son Intensite“. In: *Annales de Chimie-Science des Materiaux* 1.176 (1816) (cit. on p. 19).

[130]Arago, D. F. J. „Resultats des Experiences Faites en 1822, par Ordre du Bureau des Longitudes, pour la Determination de la Vitesse du son dans l'atmosphere“. In: *Annales de Chimie et de Physique* 20.210 (1822) (cit. on p. 19).

[131]Stokes, S. G. G. *Mathematical and Physical Papers*. Cambridge, UK: Cambridge University Press, 1880 (cit. on p. 19).

[132]Reynolds, Osborne. „On the Refraction of Sound by the Atmosphere“. In: *Proceedings of the Royal Society of London* 22.148-155 (1874), pp. 531–548 (cit. on p. 19).

[133]Rayleigh, L. *The Theory of Sound*. New York, United States: Dover Publications Inc., 1945 (cit. on pp. 19, 20).

[134]Barton, Edwin H. „On the Refraction of Sound by Wind“. In: *Proceedings of the Physical Society of London* 17.1 (1899), p. 534 (cit. on p. 19).

[135]Kornhauser, E. T. „Ray Theory for Moving Fluids“. In: *The Journal of the Acoustical Society of America* 25.5 (1953), pp. 945–949 (cit. on p. 20).

[136]Ostashev, V. E. and Wilson, D. K. *Acoustics in Moving Inhomogeneous Media*. Boca Raton, FL, USA: CRC Press, 2015 (cit. on pp. 20, 21).

[137]Li, K. M. and Wang, Q. „Analytical Solutions for Outdoor Sound Propagation in the Presence of Wind“. In: *The Journal of the Acoustical Society of America* 102.4 (1997), pp. 2040–2049 (cit. on p. 20).

[138]Marburg, S. „Normal Modes in External Acoustics. Part III: Sound Power Evaluation Based on Superposition of Frequency-Independent Modes“. In: *Acta Acustica united with Acustica* 92.2 (2006), pp. 296–311 (cit. on p. 20).

[139]Wang, Q. and Li, K. M. „Sound Propagation over Concave Surfaces“. In: *The Journal of the Acoustical Society of America* 106.5 (1999), pp. 2358–2366 (cit. on p. 20).

[140]Rasmussen, K. B. „Outdoor Sound Propagation Under the Influence of Wind and Temperature Gradients“. In: *Journal of Sound and Vibration* 104.2 (1986), pp. 321–335 (cit. on p. 20).

[141]Franke, S. J. and Swenson, G. W. „A Brief Tutorial on the Fast Field Program (FFP) as Applied to Sound Propagation in the Air“. In: *Applied Acoustics* 27.3 (1989), pp. 203–215 (cit. on p. 20).

[142]Li, Y. L., White, M. J., and Franke, S. J. „New Fast Field Programs for Anisotropic Sound Propagation Through an Atmosphere with a Wind Velocity Profile“. In: *The Journal of the Acoustical Society of America* 95.2 (1994), pp. 718–726 (cit. on p. 20).

[143]White, M. J. and Gilbert, K. E. „Application of the Parabolic Equation to the Outdoor Propagation of Sound“. In: *Applied Acoustics* 27.3 (1989), pp. 227–238 (cit. on p. 20).

[144]Lihoreau, B., Gauvreau, B., Bérengier, M., Blanc-Benon, P., and Calmet, I. „Outdoor Sound Propagation Modeling in Realistic Environments: Application of Coupled Parabolic and Atmospheric Models“. In: *The Journal of the Acoustical Society of America* 120.1 (2006), pp. 110–119 (cit. on p. 20).

[145]Blumrich, R. and Heimann, D. „A Linearized Eulerian Sound Propagation Model for Studies of Complex Meteorological Effects“. In: *The Journal of the Acoustical Society of America* 112.2 (2002), pp. 446–455 (cit. on p. 20).

[146]Heimann, D. „Three-Dimensional Linearised Euler Model Simulations of Sound Propagation in Idealised Urban Situations With Wind Effects“. In: *Applied Acoustics* 68.2 (2007), pp. 217–237 (cit. on p. 20).

[147]Hornikx, M., Waxler, R., and Forssén, J. „The Extended Fourier Pseudospectral Time-Domain Method for Atmospheric Sound Propagation“. In: *The Journal of the Acoustical Society of America* 128.4 (2010), pp. 1632–1646 (cit. on p. 20).

[148]Gabillet, Y., Schroeder, H., Daigle, G. A., and L'Espérance, A. „Application of the Gaussian Beam Approach to Sound Propagation in the Atmosphere: Theory and Experiments“. In: *The Journal of the Acoustical Society of America* 93.6 (1993), pp. 3105–3116 (cit. on p. 20).

[149]Premat, E. and Gabillet, Y. „A New Boundary-Element Method for Predicting Outdoor Sound Propagation and Application to the Case of a Sound Barrier in the Presence of Downward Refraction“. In: *The Journal of the Acoustical Society of America* 108.6 (2000), pp. 2775–2783 (cit. on p. 20).

[150]Li, R., Zhao, J., Zhang, S., and Peng, Y.ss. „Influence of the Aerodynamic Force to Human Body Near High-speed Trains“. In: *China Railway Science* 28.5 (2007), pp. 98–104 (cit. on p. 20).

[151]Hidaka, T., Kageyama, K., and Masuda, S. „Sound Propagation in the Rest Atmosphere with Linear Sound Velocity Profile“. In: *Journal of the Acoustical Society of Japan (E)* 6.2 (1985), pp. 117–125 (cit. on p. 21).

[152]Geiger, R., Aron, R. H., and Todhunter, P. *The Climate Near the Ground*. Wiesbaden, Germany: Vieweg+Teubner Verlag, 1995 (cit. on p. 21).

[153]Noise, ISO/TC 43/SC 1. *ISO 10847:1997 Acoustics – In-situ Determination of Insertion Loss of Outdoor Noise Barriers of All Types*. Switzerland, 1997 (cit. on pp. 22, 23, 31, 32, 34, 36, 42, 44, 50, 58, 87).

[154], Ministry of Ecology Environment of People's Republic of China. *HJ/T 90-2004 Norm on Acoustical Design and Measurement of Noise Barriers*. China, 2004 (cit. on pp. 22, 23, 31, 109).

[155]UIC. *CEN/TS 16272-7:2015 Railway applications - Track - Noise barriers and related devices acting on airborne sound propagation - Test method for determining the acoustic performance - Part 7: Extrinsic characteristics - In situ values of insertion loss*. UIC, 2015 (cit. on pp. 22, 23, 31, 34, 44, 50).

[156]House, China Railway Publishing. *TB/T 3050-2002: Specifications for the Measuring Technique of Environmental Noise along Railway Lines(in Chinese)*. 2002 (cit. on pp. 22, 23, 31).

[157]Ecological Environment, Ministry of. *GB 12525-90: Emission standards and measurement methods of railway noise on the boundary alongside railway line(in Chinese)*. 1990 (cit. on pp. 22, 23, 31, 34).

[158]Sciences, Chinese Academy of. *GB/T 5111-2011: Acoustics. Measurement of noise emitted by rail bound vehicle(in Chinese)*. 2011 (cit. on pp. 22, 23, 31).

[159]Ecological Environment, Ministry of. *HJ 453-2008: Technical guidelines for environment impact-Assessment of urban rail transit(in Chinese)*. 2008 (cit. on pp. 22, 23, 31).

[160]Busch, T. A. and Nugent, R. E. „A Reduced-Scale Railway Noise Barrier's Insertion Loss and Absorption Coefficients: Comparison of Field Measurements and Predictions". In: *Journal of Sound and Vibration* 267.3 (2003), pp. 749–759 (cit. on p. 23).

[161]Li, X., Liu, Q., Pei, S., Song, L., and Zhang, X. „Structure-borne Noise of Railway Composite Bridge: Numerical Simulation and Experimental Validation". In: *Journal of Sound and Vibration* 353 (2015), pp. 378–394 (cit. on p. 23).

[162]Li, J. and He, J. „Acoustic modelling of Noise Barrier Design for Fangshang Line in Urban Rail Transit in Beijing(in Chinese)". In: *Railway Standard Design* 01 (2011), pp. 104–106 (cit. on p. 23).

[163]Zhao, Q., Li, M., Zhou, F., and Li, X. „Noise reduction effects of different sound barriers on rail transit bridge(in Chinese)". In: *World Transport Convention*. China Road Engineering Society, 2018, pp. 1526–1533 (cit. on p. 23).

[164]Shen, B. „Detailed Design Scheme of Traffic Acoustic Barrier Project for a Tunnel (in Chinese)". In: *Urban Roads Bridges and Flood Controlss* 240.04 (2019), pp. 25–26+244–250 (cit. on p. 23).

[165]Ma, N. „Design of Fully-closed Noise Barrier in Shanghai Rail Transit Line 6 (in Chinese)". In: *Modern Urban Transit* 5 (2010), pp. 38–39 (cit. on p. 23).

[166]Ma, N. „Design of Fully-Closed Sound-Barrier Work for Shanghai Mingzhu Rail Transit Line(in Chinese)". In: *Modern Urban Transit* 03 (2005), pp. 41–42+6 (cit. on p. 23).

[167]„Assessment of the Diffraction Efficiency of Novel Barrier Profiles Using an MLS-based Approach". In: *Journal of Sound and Vibration* 274.3-5 (2004), pp. 669–683 (cit. on pp. 23, 41).

[168]„Using a Boundary Eement Approach to Study Small Screens Close to Rails". In: *Journal of Sound and Vibration* 231.3 (2000), pp. 673–679 (cit. on p. 23).

[169]Sakamoto, S. and Aoki, A. „Numerical and Experimental Study on Noise Shielding Effect of Eaves/louvers Attached on Building Façade". In: *Building and Environment* 94.2 (2015), pp. 773–784 (cit. on pp. 23, 25, 26).

[170]Wu, X. „In-Situ Measurement on Noise Reduction Effect of Railway Fully-Enclosed Barrier (In Chinese)". In: *Railway Standard Design* (2019) (cit. on p. 24).

[171]Chandler-Wilde, S. and Langdon, S. *Boundary Element Methods for Acoustics*. Lecture Note. 2007 (cit. on p. 24).

[172]Baker, M. and Blelloch, P. „Comparison of BEM and FEM for Computation of Acoustic Resonant Response in a Laser Chamber". In: *The Journal of the Acoustical Society of America* 102.5 (1997), pp. 3113–3113 (cit. on p. 24).

[173]Baulac, M., Defrance, J., Jean, P., and Minard, F. „Efficiency of Noise Protections in Urban Areas: Predictions and Scale Model Measurements". In: *Acta Acustica united with Acustica* (2006) (cit. on pp. 24–26, 41).

[174]Koussa, F., Defrance, J., Jean, P., and Blanc-Benon, P. „Acoustic Performance of Gabions Noise Barriers: Numerical and Experimental Approaches“. In: *Applied Acoustics* 74.1 (2013), pp. 189–197 (cit. on pp. 24–26).

[175]Jean, P., Defrance, J., and Gabillet, Y. „The Importance of Source Type on the Assessment of Noise Barriers“. In: *Journal of Sound and Vibration* 226.2 (1999), pp. 201–216 (cit. on pp. 25, 92).

[176]Duhamel, D. „Efficient Calculation of the Three-Dimensional Sound Pressure Field Around a Noise Barrier“. In: *Journal of Sound and Vibration* 197.5 (1996), pp. 547–571 (cit. on pp. 25, 66, 67, 86, 92, 127).

[177]„Integration of the Efficiency of Noise Barrier Caps in a 3D Ray Tracing Method. Case of a T-Shaped Diffracting Device“. In: *Applied Acoustics* 64.8 (2003), pp. 765–780 (cit. on pp. 25, 26).

[178]Duhamel, D. and Sergent, P. „Sound Propagation over Noise Barriers with Absorbing Ground“. In: *Journal of Sound and Vibration* 218.5 (1998), pp. 799–823 (cit. on pp. 25, 66, 127, 135).

[179]Forssén, J., Estévez-Mauriz, L., Torehammar, C., and Jean, P.s. „A Low-height Acoustic Screen in a Setting with an Urban Road: Measured and Predicted Insertion Loss“. In: *Internoise*. Hamburg, Germany: German Acoustical Society (DEGA), 2016, pp. 6435 –6443 (cit. on pp. 25, 26).

[180]Hiroe, M., Kobayashi, T., and Ishikawa, S. „2.5-Dimensional Finite-Difference Time-Domain Analysis for Propagation of Conventional Railway Noise: Application to Propagation of Sound from Surface Railway and Its Verification by Scale Model Experiments“. In: *Acoustical Science and Technology* 38.1 (2017), pp. 42–45 (cit. on pp. 25, 26).

[181]Garai, M., Schoen, E., Behler, G., et al. „Repeatability and Reproducibility of In Situ Measurements of Sound Reflection and Airborne Sound Insulation Index of Noise Barriers“. In: *Acta Acustica united with Acustica* 100.6 (2014), pp. 1186–1201 (cit. on p. 26).

[182]Parnell, J., Samuels, S., and Tsitsos, C. „The Acoustic Performance of Novel Noise Barrier Profiles Measured at The Roadside“. In: *Acoustics Australia* 38.3 (2010), pp. 123–128 (cit. on p. 26).

[183]Wang, H., Luo, P., and Cai, M. „Calculation of Noise Barrier Insertion Loss Based on Varied Vehicle Frequencies“. In: *Applied Science* 8.1 (2018), p. 100 (cit. on p. 26).

[184]Garai, M. and Guidorzi, P. „In Situ Measurements of the Intrinsic Characteristics of the Acoustic Barriers Installed Along a New High-speed Railway Line“. In: *Noise Control Engineering Journal* 56.5 (2008), pp. 342–355 (cit. on p. 26).

[185]Jonasson, H. G. „Sound Reduction by Barriers on the Ground“. In: *Journal of Sound and Vibration* 22.1 (1972), pp. 113–126 (cit. on p. 26).

[186]Jones, H. W., Stredulinsky, D. C., and Vermeulen, P. J. „An Experimental and Theoretical Study of the Modelling of Road Traffic Noise and its Transmission in the Urban Environment“. In: *Applied Acoustics* 13.4 (1980), pp. 251–265 (cit. on p. 26).

[187]Delany, M. E., Rennie, A. J., and Collins, K. M. „A Scale Model Technique for Investigating Traffic Noise Propagation“. In: *Journal of Sound and Vibration* 56.3 (1978), pp. 325–340 (cit. on p. 26).

[188]Picaut, J. and Simon, L. „A Scale Model Experiment for the Study of Sound Propagation In Urban Areas“. In: *Applied Acoustics* 62.3 (2001), pp. 327–340 (cit. on p. 26).

[189]Okubo, T. and Yamamoto, K. „Procedures for Determining the Acoustic Efficiency of Edge-Modified Noise Barriers“. In: *Applied Acoustics* 68.7 (2007), pp. 797–819 (cit. on p. 26).

[190]Voropayev, S. I., Ovenden, N. C., Fernando, H. J. S., and Donovan, P. R. „Finding Optimal Geometries for Noise Barrier Tops Using Scaled Experiments“. In: *The Journal of the Acoustical Society of America* 141.2 (2017), pp. 722–736 (cit. on pp. 26, 45).

[191]Yamashita, M. and Yamamoto, K. „Scale Model Experiments for the Prediction of Road Traffic Noise and the Design of Noise Control Facilities“. In: *Applied Acoustics* 31.1-3 (1990), pp. 185–196 (cit. on p. 26).

[192]Mulholland, K. A. „The Prediction of Traffic Noise Using a Scale Model“. In: *Applied Acoustics* 12.6 (1979), pp. 459–478 (cit. on p. 26).

[193]Bhuripanyo, P., Voropayev, S. I., and Fernando, H. J. S. „Insertion Loss Spectrums Behind Straight Noise Barriers: Scaled Experiments“. In: *2015 International Conference on Sustainable Energy and Environmental Engineering*. Vol. 2. Paris, France: Atlantis Press, 2015, pp. 168–171 (cit. on p. 26).

[194]Qin, Q. and Attenborough, K. „Characteristics and Application of Laser-Generated Acoustic Shock Waves in Air“. In: *Applied Acoustics* 65.4 (2004), pp. 325–340 (cit. on p. 26).

[195]Pierce, A. D. „Diffraction of Sound Around Corners and Over Wide Barriers“. In: *The Journal of the Acoustical Society of America* 55.5 (2005), pp. 941–955 (cit. on p. 30).

[196]Kurze, U. J. and Anderson, G. S. „Sound Attenuation by Barriers“. In: *Applied Acoustics* 4.1 (1971), pp. 35–53 (cit. on p. 30).

[197]Beranek, L. L. and Mellow, T.s. *Acoustics: Sound Fields and Transducers*. Netherlands: Academic Press, 2012 (cit. on pp. 30, 32).

[198]Torija, A. J. and Flindell, I. H. „The Subjective Effect of Low Frequency Content in Road Traffic Noise“. In: *The Journal of the Acoustical Society of America* 137.1 (2015), pp. 189–198 (cit. on p. 31).

[199]Licitra, G. and Vorl*ä*Nder, M. „Noise Mapping in the EU, Models and Procedures“. In: *The Journal of the Acoustical Society of America* 133.4 (2013), p. 2506 (cit. on p. 32).

[200]Hellman, Rhona. „Why Can a Decrease in dB(A) Produce an Increase in Loudness?“ In: *The Journal of the Acoustical Society of America* 82.5 (1987), pp. 1700–1705 (cit. on p. 35).

[201]Anfosso-Lédée, F., Steimer, V., and Demizieux, P. „In Situ Methods for the Characterisation of Road Noise Barriers Efficiency“. In: *Inter-noise 2000*. USA: Institute of Noise Control Engineering, 2000 (cit. on p. 41).

[202]Poisson, F., Gautier, P. E., and Letourneaux, F. „Noise Sources for High Speed Trains: A Review of Results in the TGV Case“. In: *Noise and Vibration Mitigation for Rail Transportation Systems*. Berlin, Heidelberg: Springer Berlin Heidelberg, 2008, pp. 71–77 (cit. on pp. 43, 53).

[203]Mellet, C., Létourneaux, F., Poisson, F., and Talotte, C. „High Speed Train Noise Emission: Latest Investigation of the Aerodynamic/Rolling Noise Contribution“. In: *Journal of Sound and Vibration* 293.3 (2006), pp. 535–546 (cit. on p. 43).

[204]Thompson, D. *Railway Noise and Vibration: Mechanisms, Modelling and Means of Control*. Oxford: Elsevier, 2009 (cit. on pp. 43, 58).

[205]Dai, F., Thompson, D. J., Zhu, Y., and Liu, X. „Vibration Properties of Slab Track Installed on a Viaduct“. In: *Proceedings of the Institution of Mechanical Engineers, Part F: Journal of Rail and Rapid Transit* 230.1 (2016), pp. 235–252 (cit. on p. 43).

[206]Hui, C. K. and Ng, C. F. „The Effects of Floating Slab Bending Resonances on the Vibration Isolation of Rail Viaduct“. In: *Applied Acoustics* 70.6 (2009), pp. 830 –844 (cit. on p. 43).

[207]Wilson, G. P. „Use of Floating Slab Track to Control Noise from Rail Transportation Systems“. In: *The Journal of the Acoustical Society of America* 131.4 (2012), pp. 3263–3263 (cit. on pp. 43, 50).

[208]Li, Q., Duhamel, D., Luo, Y., and Yin, H. „Improved Methods for In-situ Measurement Railway Noise Barrier Insertion Loss“. In: *Transactions of Nanjing University of Aeronautics and Astronautics* 35.1 (2018), pp. 58–68 (cit. on pp. 44, 126).

[209], Ministry of Environmental Protection of the People's Republic of China. *GB 3096-2008 Environmental quality standard for noise(in Chinese)*. China, 2008 (cit. on p. 55).

[210]Sadeghi, J. and Hasheminezhad, A. „Correlation Between Rolling Noise Generation and Rail Roughness of Tangent Tracks and Curves in Time and Frequency Domains“. In: *Applied Acoustics* 107 (2016), pp. 10–18 (cit. on p. 58).

[211]Li, Q., Duhamel, D., Luo, Y., and Yin, H. „Analyzing the Acoustic Performance of a Nearly-Enclosed Noise Barrier Using Scale Model Experiments and a 2.5-D BEM Approach“. In: *Applied Acoustics* (2020) (cit. on pp. 62, 137).

[212]Li, K. M. and Wong, H.Y. „A Review of Commonly Used Analytical and Empirical Formulae for Predicting Sound Diffracted by a Thin Screen“. In: *Applied Acoustics* 66 (2005), pp. 45–76 (cit. on p. 65).

[213]Macdonald, H. M. „A Class of Diffraction Problems“. In: *Proceedings of the London Mathematical Society* 14.1 (1915), pp. 410–427 (cit. on p. 65).

[214]Bowman, J. J., Senior, T. B. A., and Uslenghi, P. L. E. *Electromagnetic and Acoustic Scattering by Simple Shapes (Revised Printing)*. Boca Raton, FL, USA: CRC Press, 1988 (cit. on p. 65).

[215]Daumas, A. „Etude de la diffraction par un ecran mince dispose sur le sol“. In: *Acta Acustica united with Acustica* 40.4 (1978), pp. 213–222 (cit. on p. 86).

[216]Bialecki, R.A., Dallner, R., and Kunhn, G. „Minimum Distance Calculation Between a Source Point and a Boundary Element“. In: *Engineering Analysis with Boundary Elements* 12.3 (1994), pp. 211–218 (cit. on p. 92).

[217]Bies, D. A., Hansen, C., and Howard, C. *Engineering Noise Control : Theory and Practice*. Boca Raton, FL, USA: CRC Press, 2009 (cit. on pp. 93, 132, 139).

[218]Ursell, F. „Trapping modes in the theory of surface waves“. In: *Mathematical Proceedings of the Cambridge Philosophical Society* 47.2 (1951), 347–358 (cit. on p. 94).

[219]Shi, Q., You, Y., and Liao, G. „Added mass and damping of a floating rectangular box in a two-layer fluid“. In: *The Ocean Engineering* 25.2 (June 2007), pp. 33–42 (cit. on p. 94).

[220]Deng, X., Fang, M., Ren, X., Huang, Z., and Wu, X. „Ultra-sensitive Bio-sensor Based on Trapped Mode All-dielectric Metasurface Coating with Graphene Layer“. In: *Acta Photonica Sinica* 48.12 (2019), p. 1248005 (cit. on p. 94).

[221]Hein, Stefan, Koch, Werner, and Nannen, Lothar. „Trapped modes and Fano resonances in two-dimensional acoustical duct–cavity systems“. In: *Journal of Fluid Mechanics* 692 (2012), 257–287 (cit. on p. 94).

[222]Lee, J. H., Park, J. R., Lee, W. M., et al. „Sound Insulation Properties of Polymer Soundproof Panels“. In: *Journal of Korean Society of Environmental Engineers* 35.8 (2014), pp. 592–597 (cit. on pp. 111, 125).

[223]Yang, Y., Li, B., Chen, Z., et al. „Acoustic Properties of Glass Fiber Assembly-filled Honeycomb Sandwich Panels“. In: *Composites Part B: Engineering* 96 (2016) (cit. on p. 112).

[224]Wang, C. N. and Torng, J. H. „Experimental Study of the Absorption Characteristics of Some Porous Fibrous Materials“. In: *Applied Acoustics* 62.4 (2001), pp. 447–459 (cit. on p. 128).

[225]Bies, D. A. and Hansen, C. H. „Flow Resistance Information for Acoustical Design“. In: *Applied Acoustics* 13.5 (1980), pp. 357–391 (cit. on p. 128).

[226]Han, F., Seiffert, G., Zhao, Y., and Gibbs, B. „Acoustic Absorption Behaviour of an Open-celled Aluminum Foam“. In: *Journal of Physics D Applied Physics* 36.3 (2003), pp. 294–302 (cit. on p. 128).

[227]Lu, T. J., Chen, F., and He, D. „Sound Absorption of Cellular Metals with Semi-open Cells“. In: *The Journal of the Acoustical Society of America* 108.4 (2000), pp. 1697–709 (cit. on p. 128).

[228]Hakamada, M., Kuromura, T., Chen, Y., Kusuda, H., and Mabuchi, M. „Sound Absorption Characteristics of Porous Aluminum Fabricated by Spacer Method“. In: *Journal of Applied Physics* 100.11 (2006), p. 573 (cit. on p. 128).

[229]Wang, X. F., Wei, X., Han, F. S., and Wang, X. L. „Sound Absorption of Open Celled Aluminum Foam Fabricated by Investment Casting Method“. In: *Materials Science and Technology* 27.4 (2013), pp. 800–804 (cit. on p. 128).

[230]Li, Y., Wang, X., Wang, X., et al. „Sound Absorption Characteristics of Aluminum Foam with Spherical Cells“. In: *Journal of Applied Physics* 110.11 (2011), p. 559 (cit. on p. 128).

[231]Li, Haibin. „Study on Sound Absorption Behavior of Metal Foam“. North China Electric Power University, 2009 (cit. on pp. 128–130, 160).

[232]Song, B. H. and Bolton, J. S. „A Transfer-matrix Approach for Estimating the Characteristic Impedance and Wave Numbers of Limp and Rigid Porous Materials“. In: *The Journal of the Acoustical Society of America* 107.3 (2000), pp. 1131–1152 (cit. on p. 130).

[233]Zhang, J. „Optimization on Sound Absorption Behaviour of Metal Foam and Numerical Simulation“. North China Electric Power University: North China Electric Power University, 2013 (cit. on pp. 130, 131, 160).

[234]Johnson, D. L., Koplik, J., and Dashen, R. „Theory of Dynamic Permeability and Tortuosity in Fluid-Saturated Porous Media“. In: *Journal of Fluid Mechanics* 176.176 (1987), pp. 379–402 (cit. on p. 130).

[235]Marburg, S. „Six Boundary Elements per Wavelength: Is That Enough?“ In: *Journal of Computational Acoustics* 10.01 (2002), pp. 25–51 (cit. on p. 132).

[236]Thompson, L. L. and Pinsky, P. M. „Complex Wavenumber Fourier Analysis of the P-Version Finite Element Method“. In: *Computational Mechanics* 13.4 (1994), pp. 255–275 (cit. on p. 132).

List of Figures

List of Tables